HERC4 as a Potential Radiosensitiser in Glioblastoma



Katherine Ferris

Department of Oncology

University of Oxford

Submitted for the degree of Doctor of Philosophy

Michaelmas Term 2025

Supervisors:

Professor Peter McHugh

Professor Alex Bullock

Acknowledgements

Firstly, I would like to thank my supervisors, Professors Peter McHugh and Alex Bullock, for helping me through the many challenges this project presented. I am particularly grateful to Peter for giving me the space and time to finish in Oxford when my previous lab group moved, and to Alex for accommodating my sudden requests for support amidst my otherwise patchy communication.

I would also like to thank Dr Paul Smith for his mentorship in the lab, and for guiding me through perhaps the most difficult part of my project. Without his patience and encouragement, I would never have finished. I am similarly grateful to Dr Lonnie Swift for taking over this role when I changed lab group, and for helping me rediscover my enthusiasm for the project. Similarly, Dr Hongbin Yang, Dr Varun Gopala-Krishna and the rest of both research groups offered countless hours of advice and support, all of which were invaluable and greatly appreciated. Dr Hongbin Yang was also extremely generous in sharing the data on which this project is based. Additionally, Professor Vincenzo D'Angiolella should be credited here for the inception of the project.

Chapter 3 in its entirety was made possible by Dr Iolanda Vendrell and Svenja Hester, alongside Dr Paul Smith, so I would like to extend deep thanks to them for facilitating this, and for the warmth with which this support was delivered. The work of the department facilities team was also a tremendous help in this project, and I am especially grateful to Caroline Fitchett and Andrew Mortimer for being so welcoming alongside their work.

Lastly in an academic context, I would like to thank my Director of Studies and College Advisors, Professors Eric O'Neill, Ester Hammond and Jane Barlow, for helping me to negotiate the challenges that this project posed away from the lab. I also include my undergraduate tutor, Professor Louis Mahadevan, for whose extended support I am intensely grateful. From application to submission, he has continued to answer questions, offer advice, and provide reassurance, and I feel incredibly fortunate to have had the benefit of his support throughout this endeavour.

Beyond the lab, I have had the privilege of being supported by a wonderful network of friends and family. I would like to thank my parents, sister and grandparents for their unwavering support, for clearing every obstacle they could and for helping me to overcome the remainder. I simply could not have done this without them and I am very grateful that they stuck by me for the whole journey.

This journey would also have ended prematurely without my amazing coach, Nic. There were so many occasions when I would have given up without her encouragement and advice. Nic, Tina and the rest of OUWLRC – thank you for giving me the escape I so desperately needed when work was overwhelming. Thank you for your patience and understanding, and for teaching me the resilience that this project demanded. I would also like to thank Allan, James, Zoe, Mark FH and especially Mark C for the confidence they have given me. Without Mark C in particular, this thesis would not exist.

Finally, I would like to thank Jackie for helping me to understand and overcome so many of the challenges that this project presented both in and outside the lab. I (and this project!) would still be well and truly stuck without you.

This section could be the length of a thesis in its own right, so to everyone, named here or not, that has pushed, supported and encouraged me, listened to me vent or ramble on about this project, or celebrated any scrap of progress, thank you.

Abstract

HERC4, a member of the HECT E3 ligase family, was previously identified as a potential radiosensitiser in a CRISPR screen. CRISPR editing was also used to generate knockout clones in 2 glioblastoma cell lines (DBTRG as used in the screen, and LN229), and these clones were used to test the effect of HERC4 loss on proliferation and DNA damage signalling after irradiation or treatment with compounds that induce similar damage types. Although the proliferation assays failed to give conclusive confirmation of this hypothesis, preliminary western blot data of the DNA damage response strengthened the hypothesis that HERC4 is involved in the cellular response to ionising radiation (IR). Additional assays were run to explore potential roles in processes known to influence radiosensitivity, including growth rate (proliferation assay), metabolism (resazurin assay), and cell cycle progression (flow cytometry and western blot). The resultant data did not identify a clear function for HERC4, but in combination with proteomic data from proximity labelling using overexpressed TurboID-tagged HERC4 and total proteome analysis of 2 knockout clones, they begin to uncover putative areas of involvement that could both explain the initial result of the CRISPR screen and provide further detail on the molecular function of HERC4. Of particular interest is its influence on the connection between the cell cycle and DNA repair, primarily through telomere length, senescence and apoptosis, and, tentatively, checkpoint signalling. Proteomic data also supports a role for HERC4 in antigen presentation to increase anti-tumour immune responses. This could supplement its intracellular effects on radiosensitivity at a patient level, and also facilitate use of existing immunotherapies to improve responses to radiotherapy, which is particularly relevant to glioblastoma due to its typically low immunogenicity. Given the poor survival outcomes associated with this disease, and the prominent role of radiotherapy in fighting it, the implication of HERC4 in multiple radiosensitivity mechanisms offers an exciting glimpse into a potential new therapeutic target for sensitising glioblastoma to ionising radiation.

Contents

1 – Introduction....1
Figures and Tables.... viii
Abbreviations....x
1.1 - Glioblastoma.... 1
1.1.1 - Glioblastoma definition.... 1
1.1.2 - Cell of origin and tumour heterogeneity.... 3
1.1.3 - Standard treatment and limitations.... 5
1.2 - Radiosensitivity mechanisms.... 8
1.2.1 - Repair.... 9
1.2.2 - Re-assortment....17
1.2.3 - Repopulation....17
1.2.4 - Reoxygenation....18
1.2.5 - Intrinsic mechanisms and cellular stress....19
1.2.5.1 - Reactive oxygen species (ROS)....19
1.2.5.2 - Metabolism....21
1.2.5.3 - Endoplasmic reticulum stress....21
1.2.6 - Reactivation of the immune response....22
1.3 - E3 ligases....25
1.3.1 - Definition....25
1.3.2 - RING E3s....25
1.3.3 – U-box E3s....26
1.3.4 - HECT E3s....26
1.3.5 - RBR E3s....27
1.3.5 - Function....28
1.3.6 - Roles in radiosensitivity and therapeutic potential....32
1.3.7 - Identification of HERC4 as potential radiosensitiser....34
1.3.8 - HERC4 – current knowledge....36
1.3.8.1 - Discovery....36
1.3.8.2 - Structure....36
1.3.8.3 - Interactors....37
1.3.8.4 - Expression....38
1.3.8.5 - Function....40
1.3.8.6 - Disease....41
1.4 – Objectives....44
1.5 - References....46
2 - Phenotypic changes after HERC4 loss....65
2.1 – Introduction....65
2.2 – Methods....72
2.2.1 – Tissue culture....72
2.2.2 – CRISPR knockouts....72
2.2.2.1 – CRISPR....72
2.2.2.2 – PCR validation....73
2.2.2.3 – Western blot validation....73
2.2.3 – Morphology imaging....74
2.2.4 – Resazurin assay....74

2.2.5 – Proliferation assays 75
2.2.6 – Cell cycle analysis 76
2.2.6.1 – Flow cytometry 76
2.2.6.2 – Western blot 77
2.2.7 – Colony formation assay 77
2.2.8 – DNA Damage Western Blots 78
2.3 – Results 79
2.3.1 – Cell Lines 79
2.3.1.1 – Selection of complementary glioblastoma cell lines 79
2.3.1.2 – Generation of HERC4 knockout clones 83
2.3.2 – HERC4 Knockout Clone Characterisation 87
2.3.2.1 – HERC4 loss has no consistent effect on cell morphology 87
2.3.2.2 – HERC4 loss may slow cell proliferation 92
2.3.2.3 – HERC4 loss has no significant effect on aerobic metabolic rate 95
2.3.2.4 – HERC4 loss does not significantly affect population distribution through the cell cycle 98
2.3.3 – Effect of HERC4 on DNA Damage Response 102
2.3.3.1 – Colony formation assays may not be suitable for assessing survival in DBTRG cells 102
2.3.3.2 – HERC4 loss does not affect cell proliferation after IR 104
2.3.3.3 – HERC4 loss may influence DNA damage signalling pathways 107
2.3.3.4 – HERC4 loss does not improve cell proliferation after chemically-induced DNA damage 111
2.4 – Discussion 116
2.5 – Conclusions and Future Directions 124
2.7 - References 125
2.8 - Appendices 130
Appendix 1 – sequences for HERC4 knockout guide RNAs 130
Appendix 2 - PCR primer sequences for HERC4 CRISPR amplicon 130
Appendix 3 – PCR parameters 130
Appendix 4 – antibodies 131
Appendix 5 – IncuCyte parameters 132
Appendix 6 – R scripts 133
Appendix 7 – CLARIOstar parameters 133
Appendix 8 – proliferation curve calculations 134
Appendix 9 – click reaction reagents 135
Appendix 10 – western blot validation of HERC4 knockout clones 136
Appendix 11 – PCR validation of HERC4 knockout clones 136
Appendix 12 – metabolic activity calculations 137
Appendix 13 – proliferation after DNA damage 138
Appendix 14 – plating efficiencies for colony formation assays 141
Appendix 15 – normalisation of western blots in Figure 9 142
3 – Proteomic changes associated with HERC4 145
3.1 – Introduction 143
3.2 – Methods 149
3.2.1 – Experiment Design 149
3.2.2 - Preparation of total proteome samples 150
3.2.3 – Processing of total proteome samples 150
3.2.4 – Preparation of proximity labelling samples 151

3.2.5 – Processing of proximity labelling samples 152
3.2.6 – Analysis of both datasets 153
3.3 - Results 156
3.3.1 - Total Proteome 156
3.3.1.1 - Significant hits shared by both clones show tentative connection to metabolism, cell growth, development and the immune system 156
3.3.1.2 - Combining significant hits from each clone produced more enriched terms, with some conflict between function and direction of change of proteins in the same term 160
3.3.1.3 - Differentially expressed proteins in Clone 3 show more similarity than those in Clone 1....165
3.3.1.4 - Terms in the combined dataset reinforce the putative role for HERC4 in cell proliferation and metabolism, and highlight several signalling pathways....169
3.3.1.5 - Analysis of each clone in isolation highlighted terms connected to previously published roles for HERC4 175
3.3.2 - Proximity Labelling....186
3.3.2.1 – Validation 189
3.3.2.2 - Protein processing....192
3.3.2.3 - Localisation and transport 195
3.3.2.4 - Metabolism and mitochondria 199
3.3.2.5 - Immune system....201
3.3.2.6 - Reproduction 203
3.3.2.7 - Cell cycle and telomeres 205
3.3.2.8 - DNA repair 208
3.3.2.9 - Signalling 210
3.3.3 – Combined analysis....212
3.3.3.1 - Neither experiment confirmed published HERC4 substrates and interactors 212
3.3.3.2 – Combined analysis identifies one shared hit between differentially expressed genes in both clones and putative HERC4 interactors 218
3.4 - Discussion....223
3.5 – Conclusions and Future Directions....229
3.6 – References 230
3.7 – Appendices 234
Appendix 1 – antibody catalogue numbers 234
Appendix 2 – code for analysis of mass spectrometry data....234
Appendix 3 – GOBP terms for differentially expressed genes shared by both clones 235
Appendix 4 – volcano plots for pathway analysis....239
Appendix 5 – STRING networks for Clone 1 and Clone 3 separately 242
Appendix 6 – proximity labelling analysis results....244
4 - Discussion....258
4.1 - DNA repair 260
4.2 - Cell cycle 262
4.3 - Proliferation 263
4.4 - Hypoxia and reoxygenation 264
4.5 - Metabolism....265
4.6 - ER stress....266
4.7 - Reactive oxygen species 266
4.8 - Immune responses....266
4.9 - References....268

5 - Conclusions and Future Directions.....272
5.1 – References 271

Figures and Tables

Chapter 1 – Introduction Page

Figure 1: *Non-homologous end joining pathway* 14
Figure 2: *Homologous recombination pathway* 16
Figure 3: *Ubiquitylation linkage types* 29
Figure 4: *Initial identification of HERC4 as a potential radiosensitiser* 35
Figure 5: *HERC4 mRNA and protein expression levels across cancer types* 39
Figure 6: *HERC4 structure as predicted by AlphaFold* 43

Table 1: *Effect of new glioblastoma definition on frequency of characteristic genetic changes* 3
Table 2: *Examples of different ubiquitylation patterns and their downstream functions* 30

Chapter 2 – Phenotypic changes after HERC4 loss

Figure 1: *DNA repair and cell cycle pathways are enriched in proteins associated with HERC4 in DNA damage responses* 69
Figure 2: *Morphology and cytogenetic properties of A) DBTRG and B) LN229 cells* 80
Figure 3: *HERC4 knockout clone generation* 85
Figure 4: *HERC4 loss does not significantly alter DBTRG cell morphology* 88
Figure 5: *HERC4 loss may alter LN229 cell morphology* 90
Figure 6: *HERC4 loss may slow proliferation in DBTRG (i) and LN229 cells (ii)* 93
Figure 7: *Analysis software could not identify DBTRG cell boundaries at high confluency* 96
Figure 8: *HERC4 knockout has no significant effect on metabolic rate in A) DBTRG and B) LN229 cells* 97
Figure 9: *HERC4 knockout has no significant effect on the distribution of A) DBTRG or B) LN229 cells through the cell cycle* 99
Figure 10: *HERC4 knockout has no significant effect on cyclin expression in A) DBTRG and B) LN229 cells* 101
Figure 11: *HERC4 loss has no detectable effect on DBTRG cell survival after IR (A) but colony formation assays may not be suitable for this cell type (B,C)* 103
Figure 12: *HERC4 loss has no significant effect on proliferation rate after IR in A) DBTRG and B) LN229 cells* 107
Figure 13: *HERC4 loss may alter cellular responses to DNA damage by IR* 109
Figure 14: *HERC4 loss may alter cellular responses to DNA damage by chemical agents* 110
Figure 15: *Mechanism of action of DNA-damaging drugs* 112
Figure 14: *Selected drug concentrations result in a range of proliferation rates* 113
Figure 15: *HERC4 loss has no significant effect on LN229 proliferation after different types of DNA damage* 115

Table 1: *Key cell line features* 81
Table 2: *Cell line classification by WHO criteria 2021* 82
Table 3: *Doubling times for DBTRG and LN229 cells with and without HERC4* 94

Chapter 3 - Proteomic changes associated with HERC4

Figure 1: *Differentially expressed proteins in LN229 HERC4 knockout clones* 157
Figure 2: *STRING analysis of common hits returns limited connections* 158
Figure 3: *Enrichment analysis of a combined dataset* 162
Figure 4: *Proteins contributing to enriched KEGG terms identified by pathway analysis of the combined total proteome dataset* 163
Figure 5: *Proteins contributing to enriched GO-BP terms identified by pathway analysis of the combined total proteome dataset* 164
Figure 6: *STRING analysis of the combined dataset* 166
Figure 7: *Significantly enriched terms in Clone 1* 167
Figure 8: *Significantly enriched terms in Clone 3* 168
Figure 9: *Enrichment analysis of the combined dataset with terms grouped by theme* 170
Figure 10: *GSEA results for Clone 1, grouped by theme* 176
Figure 11: *Pathway results for Clone 1, grouped by theme* 177
Figure 12: *KEGG terms identified for Clone 3 by GSEA, grouped by theme* 178
Figure 13: *GO-BP terms identified for Clone 3 by GSEA, grouped by theme* 179
Figure 14: *KEGG terms identified for Clone 3 by pathway analysis, grouped by theme* 180
Figure 15: *GO-BP terms identified for Clone 3 by pathway analysis, grouped by theme* 181
Figure 16: *Metabolism-associated terms identified for each clone* 183
Figure 17: *Immune system-associated terms identified for each clone* 185
Figure 18: *Proteins in close proximity to HERC4* 188
Figure 19: *Validation of proximity-labelling mass spectrometry results* 190
Figure 20: *Protein processing-related terms enriched in interactor and substrate datasets* 193
Figure 21: *Ubiquitin-related terms enriched in interactor and substrate datasets* 194
Figure 22: *Localisation-related terms enriched in interactor and substrate datasets* 196
Figure 23: *Transport-related terms enriched in interactor and substrate datasets* 198
Figure 24: *Mitochondria- and metabolism-related terms enriched in interactor and substrate datasets* 200
Figure 25: *Immune system-related terms enriched in interactor and substrate datasets* 202
Figure 26: *Reproduction-related terms enriched in interactor and substrate datasets* 204
Figure 27: *Cell cycle-related terms enriched in interactor and substrate datasets* 206
Figure 28: *DNA repair-related terms enriched in interactor and substrate datasets* 209
Figure 29: *Cell signalling-related terms enriched in interactor and substrate datasets* 211
Figure 30: *Published HERC4 interactors detected in mass spectrometry experiments* 215
Figure 31: *Published HERC4 substrates detected in mass spectrometry experiments* 216
Figure 32: *The number of proteins identified in each experiment and the overlap between them* 220
Figure 33: *HAUS1 was identified as a significant interactor that was also more abundant in the HERC4 knockout clones than wildtype cells* 221
Figure 34: *Predicted HERC4-HAUS1 interaction* 222

Table 1: *Published HERC4 interactors and substrates* 148
Table 2: *Categorisation of GO-BP terms for differentially expressed proteins common to both clones* 159

Chapter 4 – Discussion

Table 1: *Summary of and next steps for experiments presented in previous chapters* 259

Abbreviations

3D	3-dimensional
ADAM12	A disintegrin and metalloproteinase-12
AGE(R)	Advanced glycation end product (receptor)
AKR1	Aldo-keto reductase 1
AMPK	AMP-activated protein kinase
ANKRD10	Ankyrin repeat domain-containing protein 10
ANOVA	Analysis of variance
APC(/C)	Anaphase-promoting complex (/cyclosome)
ARF	ADP ribosylation factor
ARHGAP	Rho GTPase-activating protein
ARHGEF	Rho/Rac guanine nucleotide exchange factor
ATM	Ataxia telangiectasia mutated
ATP	Adenosine triphosphate
ATR	Ataxia telangiectasia and Rad3-related protein
ATRX	Alpha thalassemia/mental retardation syndrome X-Linked
BAK	Bcl-2-antagonist/killer
BCA	Bicinchoninic acid
BCL-2	B-cell lymphoma (protein)
BER	Base excision repair
BIRC3	Baculoviral IAP repeat-containing 3
BSA	Bovine serum albumin
C1	Clone 1
cAMP	Cyclic adenosine monophosphate
Cas9	CRISPR-associated protein 9
CCL	C-C motif chemokine ligand
CD	Cluster of differentiation (e.g. CD4)
CDK	Cyclin-dependent kinase
CDKN	Cyclin-dependent kinase inhibitor
cDNA	Complementary DNA
cGAS	Cyclic GMP-AMP synthase
cGMP	Cyclic guanosine monophosphate
PKG	Protein kinase G
CHK	Checkpoint kinase
Chr	Chromosome
cIAP	Cellular inhibitor of apoptosis
CIC	Capicua transcriptional repressor
circRNA	Circular RNA
CL	Confidence limits
CLUH	Clustered mitochondria homologue
CNS	Central nervous system
CoA	Coenzyme A
CPT	Camptothecin
CRABP	Cellular retinoic acid-binding protein
CRISPR	Clustered regularly interspaced short palindromic repeats
CRL	Cullin-RING ligase
CSC	Cancer stem cell
CTD	Carboxyl-terminal domain
CTSK	Cathepsin K
Cul	Cullin
CXCL	C-X-C motif chemokine ligand
DAMP	Damage-associated molecular pattern
DAPI	4',6-diamidino-2-phenylindole
dbcAMP	Dibutyryl cyclic-AMP
DCUN1D5	Defective in cullin neddylation 1 domain-containing 5
DDIT3	DNA damage-inducible transcript 3
dGMP	Deoxyguanosine monophosphate
DHODH	Dihydroorotate dehydrogenase (quinone)
DIA	Data-independent acquisition
DMEM	Dulbecco's modified eagle medium
DMSO	Dimethyl sulphoxide
DNA	Deoxyribonucleic acid
DRIL	Double RING finger-linked
DSB	Double-strand break
E6AP	HPV E6-associated protein
EBV	Epstein-Barr virus
ECM	Extracellular matrix
EdU	5-ethynyl-2'-deoxyuridine
EFR3A	EF-Tu receptor homologue 3A
EGF(R)	Epidermal growth factor (receptor)
eIF4A	Eukaryotic initiation factor 4A
EMT	Epithelial–mesenchymal transition
EPHB2	Erythropoietin-producing hepatoma amplified sequence receptor B2
ER	Endoplasmic reticulum
ERAD	Endoplasmic reticulum-associated degradation
ERK	Extracellular signal-regulated kinase 1/2 (MAPK)
ESCRT	Endosomal sorting complexes required for transport
FBS	Foetal bovine serum
FBXW7	F-box and WD repeat domain-containing 7
FHL1	Four and a half LIM domains 1
FLT1	Fms-related receptor tyrosine kinase 1
Foxe3	Forkhead box E3
FoxO	Forkhead box O
FT	Flow-through
FUBP1	Far upstream element binding protein 1

FZD6	Frizzled class receptor 6
GABA	Gamma-aminobutyric acid
GAPDH	Glyceraldehyde-3-phosphate dehydrogenase
GLDC	Glycine decarboxylase
GLUT1	Glucose transporter 1
GnRH	Gonadotropin-releasing hormone
GO-BP	Gene ontology - biological process
GPI	Glycosylphosphatidylinositol
GPT	Glutamic-pyruvic transaminase
GSEA	Gene set enrichment analysis
GSK	Glycogen synthase kinase
GTP	Guanosine triphosphate
HAUS1	HAUS augmin-like complex subunit
HCC	Hepatocellular carcinoma
HECT	Homologous to the E6AP carboxyl terminus
HERC	HECT and RCC1-like domain-containing proteins
HIF	Hypoxia-inducible factor
HNSCC	Head and neck squamous cell carcinoma
HPV	Human papilloma virus
HR	Homologous recombination
HSV	Herpes simplex virus
HUWE1	HECT, UBA and WWE domain-containing E3 ubiquitin protein ligase 1
IBR	In-between RING
IDH	Isocitrate dehydrogenase
IFN	Interferon
IGF	Insulin-like growth factor
Ig	Immunoglobulin (e.g. IgG)
IL	Interleukin
IP	Immunoprecipitation
IN	Input
ipTM	Interface predicted template modelling
IR	Ionising radiation
JAK	Janus kinase
STAT	Signal transducer and activator of transcription
JNK	c-Jun amino-terminal kinase
KEGG	Kyoto Encyclopedia of Genes and Genomes
KO	Knockout
KRT19	Keratin 19
KYNU	Kynureninase
LATS1	Large tumour suppressor kinase 1
MAF	Musculoaponeurotic fibrosarcoma
MAGEA10	Melanoma antigen family A10
MAPK(KK)	Mitogen-activated protein kinase (kinase kinase)
MCUR1	Mitochondrial calcium uniporter regulator 1
MDM2/4	Mouse double minute 2/4
METTL3	Methyltransferase 3, N6-adenosine-methyltransferase complex catalytic subunit
MGMT	O-6-methylguanine-DNA methyltransferase
MHC	Major histocompatibility complex
miRNA	microRNA
MM	Multiple myeloma
MOM	Mitochondrial outer membrane
MOPS	3-(N-morpholino)propanesulfonic acid
MPZ	Myelin protein zero
mRNA	Messenger RNA
MST	Synonym for STK (serine/threonine kinase). Hippo ortholog
mTOR	Mechanistic target of rapamycin kinase
N/n	Number of biological/technical replicates
NAD(H)	Nicotinamide adenine dinucleotide (hydrogen)
NBS1	Nijmegen breakage syndrome 1
ncRNA	Non-coding RNA
NDUFB	NADH dehydrogenase [ubiquinone] 1 beta subcomplex subunit
NEDD4	Neural precursor cell expressed developmentally down-regulated protein 4
NET	Neutrophil extracellular trap
NF1	Neurofibromin
NF90	Nuclear factor 90
NF-κB	Nuclear factor kappa-light-chain-enhancer of activated B cells
NHEJ	Non-homologou end joining
NIR	Non-irradiated
NKC	Natural killer cell
NLR	Nod-like receptor
NNMT	Nicotinamide N-methyltransferase
NOTCH1	Neurogenic locus notch homolog protein 1
NPC	Neural progenitor cell
NPRL	Nitrogen permease regulator-like
NRF2	Nuclear respiratory factor
ns	Non-significant (statistically)
NSC	Neural stem cells
NSCLC	Non-small cell lung carcinoma
NTD	Amino-terminal domain
OPC	Oligondendrocyte precursor cells
ORA	Over-representation analysis
OS	Overall survival
PAMP	Pathogen-associated molecular pattern
PAR(P)	Poly [ADP-ribose] (polymerase)
PATH	Pathway analysis
PBS	Phosphate-buffered saline
PCR	Polymerase chain reaction

PD-1	Programmed cell death protein 1
PDGFRA	Platelet-derived growth factor receptor A
PD-L1	PD ligand 1
Pen-Strep	Penicillin-streptomycin
PFA	Paraformaldehyde
PFS	Progression-free survival
PGR	Progesterone receptor
PI	Phosphatidylinositol
PI3K	Phosphatidylinositol-4,5-bisphosphate 3-kinase
pIDDT	Predicted local distance difference test
PIK3CD	Phosphatidylinositol-4,5-bisphosphate 3-kinase catalytic subunit delta
PITPNC1	Phosphatidylinositol transfer protein, cytoplasmic 1
DNA-PKcs	DNA-dependent protein kinase catalytic subunit
PKM2	Pyruvate kinase M2
PMF	Proton motive force
PPAR	Peroxisome proliferator-activated receptors
PROTAC	Proteolysis targeting chimera
PRPF19	Pre-mRNA-processing factor 19
PRR	Pattern recognition receptors
PRR11	Proline-rich protein 11
PT	Pathway topology
PTEN	Phosphatase and tensin homologue
pTERT	(Promoter of) telomerase reverse transcriptase
pTM	Predicted template modelling
PUMA	p53-upregulated modulator of apoptosis
PVDF	Polyvinylidene fluoride
RAGE	Receptor of AGE
RB	Retinoblastoma
RBR	RING between RING
RCC	Regulator of chromosome condensation
RING	Really interesting new gene
RIPA	Radioimmunoprecipitation assay buffer
RISC	RNA-induced silencing complex
RLD	RCC1-like domain
RNA	Ribonucleic acid
RNF	RING finger protein
ROS	Reactive oxygen species
RPE	Retinal pigment epithelium
rpS3	ribosomal protein S3
RRM2	Ribonucleotide reductase M2
RTK	Receptor tyrosine kinase
RUNX3	Runt-related transcription factor 3
SAV1	Salvador 1
SCD	Stearoyl-CoA desaturase
CF	Skp, Cullin, F-box
SDH	Succinate dehydrogenase
SDS	Sodium dodecyl sulphate
SEM	Standard error of the mean
SEMA3E	Semaphorin 3E
sgRNA	small guide RNA
siRNA	small interfering RNA
SMO	Smoothened
SMURF	SMAD ubiquitin regulatory factor
SNARE	Soluble N-ethylmaleimide-sensitive factor attachment protein receptor
snRNA	Small nuclear RNA
SPHK1	Sphingosine kinase
SQOR	Sulphide quinone oxidoreductase
SSB	Single-strand break
STING	Stimulator of interferon response cGAMP interactor
SVZ	Subventricular zone
TAZ	Transcriptional coactivator with PDZ-binding motif
TCA	Tricarboxylic acid
TCGA	The Cancer Genome Atlas
TCR	T-cell receptor
TEAD1	TEA domain-containing protein 1
TNF RI	Tumour necrosis factor receptor I
TGF	Transforming growth factor
TKI	Tyrosine kinase inhibitor
TKTL	Transketolase-like
TLR	Toll-like receptor
TORC1	Transducer of regulated CREB activity
TP53	Tumour protein 53
TREX1	Three prime repair exonuclease 1
TRIM	Tripartite motif-containing
tRNA	Transfer RNA
UALCAN	University of Alabama at Birmingham Cancer data analysis portal
Ub	Ubiquitin
UBE	Ubiquitin-conjugating enzyme
USP11	Ubiquitin-specific peptidase 11
UV	Ultraviolet
VEGF(R)	Vascular endothelial growth factor
VmpA	Variable membrane protein A
WHO	World Health Organisation
Wnt	Wingless-type
WT	Wildtype
YAP	Yes1-associated transcriptional regulator
ZFTRAF1	Zinc finger TRAF-type-containing 1

1 - Introduction

1.1 - Glioblastoma

Glioblastoma is a malignant primary brain tumour that is notable for its poor prognosis and slow research progress. Accounting for just over half of all malignant brain and central nervous system (CNS) tumours, it has a predicted incidence of ~3/100,000 person-years and a median survival of ~16 months with standard treatment [Price et al., 2025; Fabbro-Peray et al., 2018; Graus et al., 2013; Brown et al., 2022]. This treatment has seen little development since the addition of chemotherapeutic drug temozolomide in the early 2000s [Stupp et al., 2005; McCutcheon and Preul, 2021], despite extensive investigation of the mechanisms underpinning the development of glioblastoma and its resistance to therapy.

1.1.1 - Glioblastoma definition

Records of brain tumours date back to the early 1800s, with the first comprehensive description and use of the term 'glioma' appearing in 1867 [Virchov, 1867; Mitchell, 1883; Courville, 1936; Tooth, 1912]. By the turn of the century, brain tumour classification was being increasingly refined, and 'spongiblastoma multiforme' emerged for tumours whose histology deviated unrecognisably from typical glial cells, and this gradually evolved into 'glioblastoma multiforme' [Scherer, 1940]. The definition of this term has continued to evolve, with its most recent update by the World Health Organisation (WHO) in 2021, when it was reduced to 'glioblastoma' [Louis et al., 2021]. It remains a WHO CNS grade 4 diffuse glioma, reflecting its severity, lack of clear tumour boundary, and derivation from glial cells. However, the new definition excludes IDH1 mutations, which now result in a diagnosis of astrocytoma CNS WHO grade 4. This shifts the diagnostic emphasis away from histopathological features that are shared between the two new definitions (microvascular proliferation, and necrosis) towards molecular characterisation that will facilitate treatment optimisation. The key features of glioblastoma in the new classification

system are mutation of the *TERT* promoter, combined amplification of Chromosome 7 and deletion of Chromosome 10, and *EGFR* gene amplification.

While the new definition necessitates careful interpretation of previous studies, tumours previously classified as glioblastoma *IDH*-mutant were relatively rare compared to *IDH*-wildtype tumours, with mutations identified in 3.7-12% of primary glioblastoma tumours, depending on the study [Parsons et al., 2008; Ichimura et al., 2009; Nobusawa et al., 2009]. Reclassification of data in the TCGA low-grade glioma and glioblastoma datasets matched these percentages (5.9% of previous glioblastoma records reassigned) but also highlighted that not all samples will have adequate data for updated classification (20% in this study) [de Mendonça et al., 2025]. Assuming that the proportion of retained glioblastoma diagnoses remains the same among the unclassified cases, the effect of the new definition on metrics such as incidence and survival is likely to be minimal. Grade 4 astrocytoma has a much lower incidence (0.08 compared to 2.51 [Price et al., 2025]), meaning that incidence rates may be underestimates, but also that the impact on average survival times will be minimal. Since IDH1 mutations are associated with better prognosis, exclusion of such tumours from glioblastoma survival statistics will only reduce the already low figures further [Yan et al., 2009]. At a cellular level, it also seems unlikely that inclusion of *IDH*-mutant tumours will have significantly skewed published data, given their low abundance relative to *IDH*-wildtype glioblastoma. RTK/RAS/PI3K, p53 and RB signalling pathways have previously been implicated in glioblastoma development, and comparison of the 2008 TCGA glioblastoma dataset with a more recent study restricted to the latest glioblastoma definition shows few changes in the frequency of glioblastoma-associated genetic changes (Table 1) [The TCGA Research Network, 2008; Dundar et al., 2024]. Many studies divided glioblastoma tumours into subtypes, primarily pro-neural (PDGRFA amplification), classical (EGFR amplification) and mesenchymal (NF1 mutation or loss),[1] but these divisions remain

[1] The original version of this system included a fourth category (neural), but this has since been attributed to contamination by non-cancerous neural cells [Wang et al., 2017].

relevant regardless of IDH1 mutation, further limiting the reinterpretation required in response to the updated definition [Verhaak et al., 2010; Wang et al., 2017].

	TCGA, 2008	Dundar et al., 2024
RTK/RAS/PI3K pathway	**88%**	
EGFR mutation or amplification	45%	37.1% (35.4% amplification; 15.3% mutation; 13.7% both)
PTEN mutation or homozygous deletion	36%	31.4%
PI3K mutation	15%	7.2% (PIK3CA) + 5.6% (PIK3R1)
PDGFRA amplification	13%	12.2%
NF1 mutation or homozygous deletion	18%	16.1%
p53 signalling	**87%**	
$CDKN2A^{ARF}$ mutation or homozygous deletion	49%	62%*
TP53 mutation or homozygous deletion	35%	31.4%
MDM2 amplification	14%	8.9%
MDM4 amplification	7%	8.9%
RB signalling	**78%**	
$CDKN2A^{p16/INK2A}$ mutation or homozygous deletion	52%	62%*
CDKN2B homozygous deletion	47%	62%*
CDK4 amplification	18%	11.2%
RB1 mutation or homozygous deletion	11%	10.5%

*CDKN2A/B loss not separated for more recent dataset

Table 1: Effect of new glioblastoma definition on frequency of characteristic genetic changes

1.1.2 - Cell of origin and tumour heterogeneity

In addition to informing treatment decisions and survival time predictions, glioblastoma subtypes also underscore the intratumour heterogeneity that has been identified as a key feature of poor treatment outcomes in glioblastoma patients. Cells from the same tumour can display different driver mutations and hallmarks of different subtypes, and the dominant subtype often changes in response to treatment, especially if the primary tumour is more diverse [Sottoriva et al., 2013; Wang et al., 2017]. The mesenchymal subtype is the most consistent between primary and recurrent tumours, and it is the subtype to which pro-neural and classical tumours most commonly switch following treatment, reflecting its increased treatment resistance compared to the other subtypes [Wang et al., 2017; Segerman et al., 2016]. It is also the subtype for which an origin cell has proved most elusive, supporting the hypothesis that it is a secondary stage of tumour development that roughly corresponds to the epithelial-mesenchymal transition described for other tumours [Fedele et al., 2019].

Several models have been proposed for glioblastoma initiation, broadly clustering into transformation of stem or precursor cells, and dedifferentiation of astrocytes. Neural stem cells (NSCs) remote from the tumour were found to contain low levels of the driver mutations that were abundant in the corresponding tumour, and in mouse models in the same study, high-grade gliomas were produced by astrocyte-like NSCs with driver mutations that migrated from the sub-ventricular zone (SVZ) [Lee et al., 2018]. Additionally, tumour proximity to the SVZ has been associated with worse prognosis, and glioma cells in this region have been implicated in tumour regrowth after chemotherapy [Jafri et al., 2013; Chen et al., 2012]. However, when *TP53* and *NF1* mutations were added to NSCs in a separate study, only oligodendrocyte precursor cells (OPCs), a more specialised cell type produced from NSCs, were enriched in the resultant tumours [Liu et al., 2011]. Directly mutating OPCs had the same effect, indicating that this cell type can also give rise to glioblastoma. In an alternative approach, knockdown of the same genes (*TP53* and *NF1*) in differentiated astrocytes resulted in dedifferentiation, as indicated by expression of progenitor markers Nestin and Sox2 that were not otherwise expressed in these cells [Friedmann-Morvinski et al., 2012]. It seems likely, however, that this model is confined to astrocytes, since the transformative potential of *TP53* and *NF1* mutations declined in with increasing differentiation in neural cells.

Based on a model by Neftel et al., it is plausible that all of these proposed origin cells are correct [Neftel et al., 2019]. The study found 6 expression state clusters in glioblastoma cells, with 4 mimicking stages of neural development (astrocytic (EGFR-enriched), OPC-like (PDGFA-enriched) and 2 neural progenitor cell (NPC)-like clusters (CDK4-enriched) distinguished by presence or absence of overlap with the OPC group). The other two matched the mesenchymal glioblastoma subtype. All tumours contained cells from at least 2 clusters, with pro-neural tumours favouring NPC- and OPC-like expression states, while classical and mesenchymal tumours contained more astrocytic and mesenchymal cells respectively. Upregulation of EGFR or CDK4 in murine NPCs pushed the cells towards astrocytic and NPC-like states respectively,

indicating that one origin cell can produce multiple types of tumour cell. However, upregulation of CDK4 was more effective than EGFR at increasing proliferation in NPCs, whereas the reverse was true in murine astrocytes, suggesting that both cell types can be transformed and that each favours development of a different subtype. Neftel et al. also demonstrated that xenografts of a single cell type produce tumours with multiple expression states, highlighting the plasticity retained by tumour cells.

While these studies fail to identify a consistent mechanism for glioblastoma initiation, their breadth underscores the heterogeneous nature of these tumours, and the plasticity that makes them so adaptable.

1.1.3 - Standard treatment and limitations

Despite the high and rapid mortality rate for glioblastoma, very little progress has been made in treating it in the last 2 decades and the standard treatment protocol has scarcely changed since 2005. Surgical resection is followed, ideally within 3-6 weeks, by radiotherapy (60 Gy given in 30 2-Gy doses) and concomitant chemotherapy (75 mg/m^2/day temozolomide) [Stupp et al., 2005; Villanueva-Meyer et al., 2017]. Improved surgical techniques have increased the frequency of complete resection, which is associated with better treatment outcomes [Roder et al., 2014], and increasing radiation doses were also found to increase patient survival [Walker et al., 1979], but this improvement plateaued at 60 Gy [Graf et al., 2005]. Radiotherapy progress now focuses on improving the specificity with which the dose is delivered, and techniques such as volumetric-modulated arc radiation therapy (VMAT) and proton therapy (PT) increase patient survival and quality of life compared to older methods such as 3D-conformal radiotherapy [Xu et al., 2023; Brown et al., 2021]. VMAT allows radiation to be delivered in a 360° arc around the patient, converging on the tumour to maximise the dose to cancer cells while minimising the exposure of healthy tissue. PT also increases the difference in dose received by cancer and healthy tissues, but it does so by changing the distribution of energy release along the radiation beam. While

photons show relatively even release, impacting all tissues through which they pass, protons release most of their energy at a single point, which can be focused on the tumour. The sparing of healthy tissue can be further increased by use of protons in FLASH radiotherapy, in which doses are delivered at rates sometimes 6 orders of magnitude faster than in conventional radiotherapy [Hughes & Parsons, 2020]. Although the mechanisms are not fully understood, rapid dose delivery reduces damage to healthy tissue without compromising efficacy against the tumour.

The 3 approaches discussed above focus on improving external application of radiation, but the development of techniques such as boron neutron capture therapy (BNCT) facilitate radiation release only in tumour cells. The path length of the radioactive particles released in this method is <10 μm, confining radioactivity to the cell in which the particles are released and consequently, healthy cells are never exposed at all, in a way that cannot be achieved with external application [Coderre & Morris, 1999]. The premise of BNCT is that boron-10 is delivered specifically to tumour cells and then irradiated with neutrons which the boron captures to form boron-11. This isotope is highly unstable and decays into an alpha particle (^{4}He) and a lithium nucleus (^{7}Li), plus a small amount of gamma radiation [Wang et al., 2022]. Both particles are high-LET and deposit most of their energy at the end of their short path, ensuring maximum lethal DNA damage but only in the tumour cells. Since the neutron beam alone does not cause significant damage to healthy tissues, this results in highly localised radiotherapy. However, despite the exciting promise of this method and almost a century of research since its initial proposal in the 1930s, translation to the clinic remains limited [Wang et al., 2026]. The technological barriers to generating neutron beams have been significantly reduced, but the challenge of delivering adequate quantities of boron specifically to tumour cells remains [Krishnamoorthy & Prasad, 2026]. Glioblastoma was among the first cancer types on which this method was tested and it features frequently and optimistically in ongoing research [Wang et al., 2022; Farr et al., 1954; Goodwin et al., 1955; Zhang et al., 2025c; Rudawska et al., 2026]. One study from the early 2000s

showed a 50% increase in median survival time after BCNT compared to historical controls, while another reported a median survival time of 22.2 months, over the double the median for the historic controls used in the other study [Kawabata et al., 2009; Pellettieri et al., 2008]. More recently, glioblastoma models have been included in studies of new boron delivery mechanisms, bringing widespread clinical use another step closer [Hao et al., 2026; Rudawska et al., 2026].

While changes in radiotherapy protocols have driven incremental improvement in patient outcomes, the most substantial break-through was the addition of temozolomide, which more than doubled the 2-year survival rate from 10.6% to 26.4% in the initial trial [Stupp et al., 2005]. Temozolomide is a DNA-alkylating agent that is thought to increase the toxicity of radiotherapy by increasing the DNA damage load, particularly through double-strand breaks (DSBs). It is also cytotoxic in its own right, as demonstrated by the increase in 5-year survival rate from 1.9% (95% CL 0.6-4.4%) to 9.8% (95% CL 6.4-14.0%) when concomitant chemotherapy is supplemented by up to 6 rounds of adjuvant temozolomide (150-200 mg/m^2/day for 5 days every 4 weeks) [Stupp et al., 2009]. Additional rounds of chemotherapy, however, do not extend progression-free or overall survival (PFS, OS) [Balana et al., 2020].

Other treatment mechanisms have been explored, but so far none have been successful in altering the standard treatment protocol. Delivery of tumour-treating fields (alternating electric fields that impair cell division) during chemotherapy extends overall survival by roughly a third, but the practicality of this treatment is limited by its delivery time of 18 h per day [Stupp et al., 2015]. Angiogenesis inhibitor Bevacizumab has also shown clinical potential for recurrent glioblastoma, but it shows limited benefit in primary tumours so it has not resulted in an updated standard of care. Notably, it alleviates the effects of radiation necrosis, a serious adverse event associated with re-irradiation at recurrence [reviewed by Narita, 2015]. There are many other promising chemotherapy regimens currently in clinical trials, so it is to be hoped that this promise will be realised in order to tackle what is currently a highly treatment-resistant disease.

Glioblastoma derives its resistance primarily from its diffuse and heterogeneous nature. It is extremely challenging to achieve total surgical resection when tumour cells infiltrate surrounding healthy and essential tissue. Coupled with strong evidence for glioblastoma stem cells capable of regenerating the tumour, this results in a high likelihood of recurrence. Radiotherapy and chemotherapy protocols are intended to target cells outside resectable tumour margins, but the intratumoral genetic heterogeneity makes it almost inevitable that at least a subset of cells will be resistant to any given treatment. Chemotherapy options are further limited by delivery problems caused by the blood-brain barrier, which also contributes to the unique immune environment of the brain that impairs the efficacy of immunotherapies and the immune response that contributes to the tumour toxicity of radiotherapy. Radiation has the advantage of bypassing the obstacle of the blood-brain barrier, but its indiscriminate mechanism means its use is limited by the tolerance of the surrounding, non-tumour tissue. Just as for surgical resection, this limitation is particularly pronounced for glioblastoma given the intricate and essential nature of this tissue. Improvements in concentrating radiation on the tumour reduce off-target effects, and may eventually facilitate higher, more effective doses, but so far, this has not been achieved. An alternative approach would be to sensitise tumour cells to radiation, so that they would be eliminated at doses easily tolerated by healthy cells. This requires cancer-specific properties to be compared with mechanisms regulating radiosensitivity in order to identify tumour vulnerabilities.

1.2 - Radiosensitivity mechanisms

IR is used to treat over 50% of cancer patients, targeting cancer cells by location and the increased vulnerability to DNA damage compared to slower-proliferating normal tissue. The sensitivity of both cancerous and healthy tissue to the cytotoxic effect of IR is generally attributed to 6 factors, known as the “six Rs of radiobiology” [Boustani et al., 2019]:

1. Repair – specifically, DNA repair to prevent DNA damage-induced cell death

2. Re-assortment – the ability of a cell population to redistribute itself through the cell cycle after relatively radiosensitive phases, particularly mitosis, have been depleted
3. Repopulation – recovery of cell number by cell division
4. Reoxygenation – a better oxygen supply correlates with increased radiosensitivity
5. Radiosensitivity – intrinsic mechanisms that alter susceptibility to IR-induced damage
6. Reactivation of the immune response – increased immune visibility of damaged cells promotes an anti-tumour response, but IR can also upregulate immunosuppressive processes, such as macrophage differentiation into the pro-tumour M2 subtype.

1.2.1 - Repair

DNA damage is the primary mechanism by which radiotherapy kills cells, and the potency of this treatment is largely attributed to its induction of clustered DNA damage, in which at least 2 lesions (single- or double-strand break (SSB/DSB), or base oxidation or loss) form within 2 turns of the DNA helix [Lomax et al., 2002]. For radiation types with low linear energy transfer (LET) such as X-rays, ~70% of IR-induced damage occurs as isolated lesions, predominantly SSBs and base damage, and is easily repaired, and toxicity is mediated by the remaining 30% of lesions that form DSBs and damage clusters [O'Neill, 2001; Lomax et al., 2013]. For high-LET radiation such as carbon ions, the proportion of clustered damage can reach 90%, with the number of lesions in each cluster also rising [Lomax et al., 2013].

One reason for the lethality of such lesions is interference between repair machinery recruited to damage sites in close proximity, which delays or even blocks effective processing of these sites. For example, the repair machinery working on one site can act on another nearby lesion, carrying out repair steps in the wrong order so that the resultant products are not recognised by downstream components, while SSBs and abasic sites reciprocally inhibit their repair, and simultaneous processing of abasic sites causes complex DSBs that are challenging to repair [Blaisdell et al., 2001; Lomax et al., 2002; Dianov et al., 2001]. The slower the repair process, the

more likely it is that DNA damage will be present when the cell enters S phase, causing mutation through base mispairing during DNA replication, or further DSBs through stalling a replication fork [reviewed by Eccles et al., 2011]. While mutations may be beneficial to the cell, persistence of DSBs into G2 and mitosis trigger the G2/M checkpoint and mitotic catastrophe respectively, both of which result in cell death to enact the phenotypic effect of IR.

Given the fundamental role of DNA damage in the cellular impact of IR, it is unsurprising that the factors influencing the efficiency of its repair also influence radiosensitivity. The efficacy of this repair relies on 3 main pathways: base excision repair (BER) for oxidised or removed bases and into which SSB repair feeds; non-homologous end joining (NHEJ) (Figure 1), and homologous recombination (HR) (Figure 2). The latter two pathways repair DSBs but differ in their mechanisms and timings. NHEJ is active throughout the cell cycle and is initiated by Ku70/Ku80 heterodimers binding to the DNA ends almost as soon as they form, likely due to the high abundance of these proteins in the cell [Vogt and He, 2023]. As well as facilitating recruitment of downstream factors, Ku dimers help to produce compatible DNA ends by removing abasic sites [Roberts et al., 2010]. DNA-PKcs then binds to the DNA and Ku dimer, completing the DNA-PK complex and bridging the gap in the DNA by interacting with its counterpart on the opposite side of the break. LIG4 and XRCC4 are also recruited to the Ku dimers [McElhinny et al., 2000] and, together with XLF, form a second bridge across the break. DNA-PK phosphorylates itself, causing its dissociation to expose the DNA ends for repair, and at the same time, the whole DNA-protein complex switches from a long-range to a short-range synapse, pulling the DNA ends close enough together for ligation. If DNA ends are not compatible (e.g. single-strand overhangs), additional processing machinery is recruited at this stage, but the presence of LIG4 as soon as the ends are released from DNA-PKcs means that compatible ends are joined before further processing can occur, reducing the risk of deletions or other mutations through end processing.

During G1, there are two variants of NHEJ, one of which progresses slowly, incorporating DNA resection and with a higher risk of genetic rearrangements, while the other is more rapid with a

lower risk and no resection. The factors that determine variant selection are unknown, but may be linked to chromatin accessibility and the chemical complexity of the DNA damage [Biehs et al., 2017]. Although the slower pathway incorporates a resection step and can therefore be considered a microhomology-mediated end joining (MMEJ) mechanism, it is distinct from the alternative NHEJ (alt-NHEJ) pathway often considered synonymous with MMEJ. Removing or inhibiting alt-NHEJ proteins such as DNA ligase 1 and PARP respectively did not affect the slow, Artemis-dependent translocations observed in G1 unless Ku80 was also removed, consistent with previous data that alt-NHEJ is only active once canonical NHEJ (c-NHEJ) components are lost. The slow pathway, including the resection steps subsequently characterised, was consequently attributed to c-NHEJ.

In G2 and S phase, the slow NHEJ variant is replaced with HR, which, unlike NHEJ, is confined to these phases. The balance between the two repair pathways shifts, with HR use peaking around halfway through S phase [Biehs et al., 2017; Karanam et al., 2012]. This peak is not, however, enough to exceed NHEJ-mediated repair, which accounts for ~80% of X-ray-induced DSB repair during G2 [Shibata et al., 2014; Mao et al., 2009; Kim et al., 2005]. The focus of HR may instead be repair of more persistent lesions, including those whose repair is delayed by the complexity of the surrounding damage. Proteins involved in this pathway were found to bind to damaged DNA for longer than those involved in NHEJ, suggesting they may act as an alternative mechanism when NHEJ fails [Kim et al., 2005]. While NHEJ joins blunt ends or short homologous overhangs, HR uses the sister chromatid as a template to resynthesise this sections that may be lost during end processing, hence its restriction to G2 and S phase after the genome has been replicated. It is initiated by the MRN complex, containing Mre11, Rad50 and Nbs1, but this cannot bind until Ku dimers have been displaced [Sun et al., 2019b; Lee et al., 2016]. It is thought that cell cycle stage-specific phosphorylation of Ku proteins reduces their affinity for DNA and allows the MRN complex to displace them, redirecting DNA repair towards homologous recombination [Lee et al., 2016]. In combination with CtIP, the MRN complex begins DNA

resection and nucleases such as Bloom syndrome protein (BLM), DNA replication ATP-dependent helicase/nuclease 2 (DNA2) and Exonuclease 1 (EXO1) complete this step [Zhao et al., 2020]. RPA coats the single-strand DNA generated by resection until RAD52 and BRCA2 facilitate its replacement by RAD51 [Holloman, 2011; Lok and Powell, 2012]. RAD51 ATPase activity then stretches the bound DNA to promote identification of an homologous region as a repair template [Baumann and West, 1998].

The next step in HR is synapsis. HOP2 and MND1 bind to the RAD51-DNA filament to help stabilise it, and also to double-stranded DNA to facilitate its capture by the filament [San Filippo et al., 2008]. Successful capture produces a D loop, with the invading strand displacing part of another DNA duplex. RAD54 is required for DNA polymerase to access the invading 3' end, and only polymerases capable of displacing the other strand of the duplex are suitable for the elongation step [McVey et al., 2016; Li and Heyer, 2009]. RAD52 then facilitates capture of the second end of the DSB [Nimonkar et al., 2009]. At this point, the HR pathway branches into 4 variants [Li and Heyer, 2008; McVey et al., 2016]. In DSB repair, both parts of the duplex are used as repair templates, and both overhanging ends are extended, while in synthesis-dependent strand annealing, the invading strand is extended using the captured template until the other overhang can be used instead. The remaining gaps are then filled using the overhangs themselves as templates. Alternatively, if there is sufficient homology in the resected single-stranded filaments, the overhangs can be used as templates for each other. This typically happens in repetitive regions of the genome and deletes one repeat. Lastly, if the break only has one end, such as those induced by replication stress, break-induced replication ensues to copy the remainder of the chromosome.

Following repair, the four strands of the template and repaired DNA duplexes are connected to each other through hydrogen bonding to form Holliday junctions that are subsequently disentangled by dissolution or resolution in the final step of HR. In dissolution, BLM, RMI1 and RMI2 push two adjacent junctions together and topoisomerase IIIα decatenates the resultant

structure to keep the template helix intact (non-crossover). In resolution, however, the strands are cut, allowing genetic material to be exchanged between the duplexes. [Ho and West, 2022; Matos and West, 2014]

Overactivation of these pathways improves survival after IR, as demonstrated by higher levels of Ku70/Ku80 DNA binding and DNA-PKcs activity in radio-resistant B-chronic lymphocyte leukaemia cells, indicative of elevated NHEJ, and restoration of DSB-induced apoptosis following treatment with a DNA-PK inhibitor [Deriano et al., 2005]. In the opposite direction, loss of NBS1 in Nijmegen breakage syndrome impairs HR, among other pathways, contributing to the increased sensitivity to IR seen in patients with this condition [Tauchi et al., 2002].

Alongside efficacy, the second component to efficiency is speed. Cell cycle progression with damaged DNA will result in cell death, so delaying this progress allows more time for effective repair. p53 is one of the most commonly mutated proteins in cancer, and contributes to loss of the G1 checkpoint so that cancer cells often rely heavily on the G2/M checkpoint to prevent mitotic catastrophe. This is borne out by the increased radiosensitivity caused by inhibition of WEE1 and CHK1, both of which contribute to stalling the cell at this checkpoint [Li et al., 2023a; Melia et al., 2025]. At the same time, p53 mutations draw attention to another delay tactic – inhibition of apoptosis so that prolonged DNA damage signalling cannot trigger this cell death mechanism. Radioresistant prostate cancer cells, for example, were sensitised to IR by inhibition of BCL-2, an anti-apoptotic protein commonly overexpressed in this cancer type. Alternatively, tumour cells can use senescence as a way to avoid cell cycle progression and subsequent cell death. On the surface, this seems like a good therapeutic outcome – the tumour cells might survive but they will no longer divide. However, in the context of cancer, senescence is not permanent and is instead associated with upregulation of stem cell markers and recurrence [Milanovic et al., 2018], presenting it as merely another way for altering radiosensitivity.

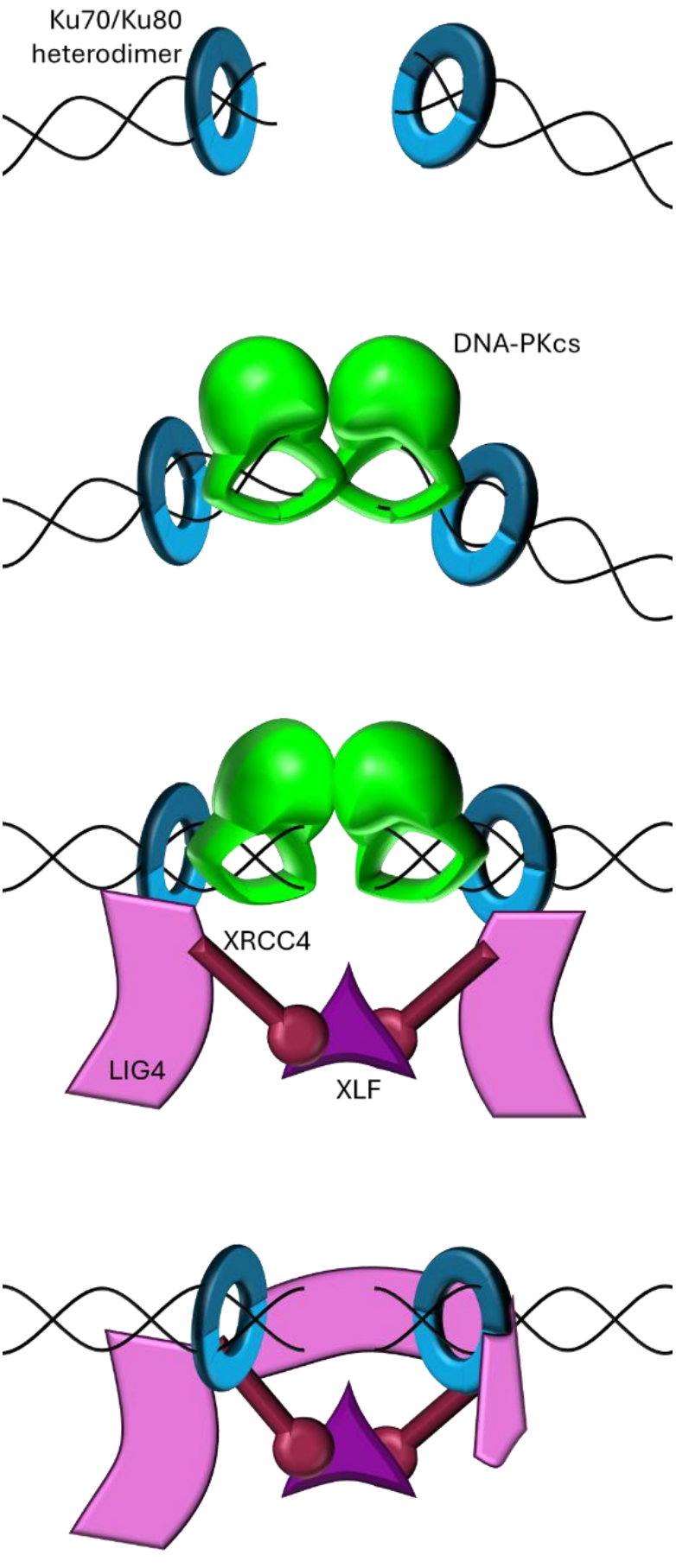

Ku70/Ku80
heterodimer
DNA-PKcs
XRCC4
LIG4
XLF

Figure 1: Non-homologous end joining pathway
Ku heterodimers form almost immediately on the exposed ends of the DSB. DNA-PKcs forms a homodimer bridging the Ku dimers, and a second bridge forms from LIG4, XRCC4 and XLF. DNA-PKcs phosphorylation induces DNA-PK dissociation plus conformational change to bring the exposed ends into close proximity. If the ends are not compatible, editing happens at this stage; otherwise, the ends are ligated to complete the repair.

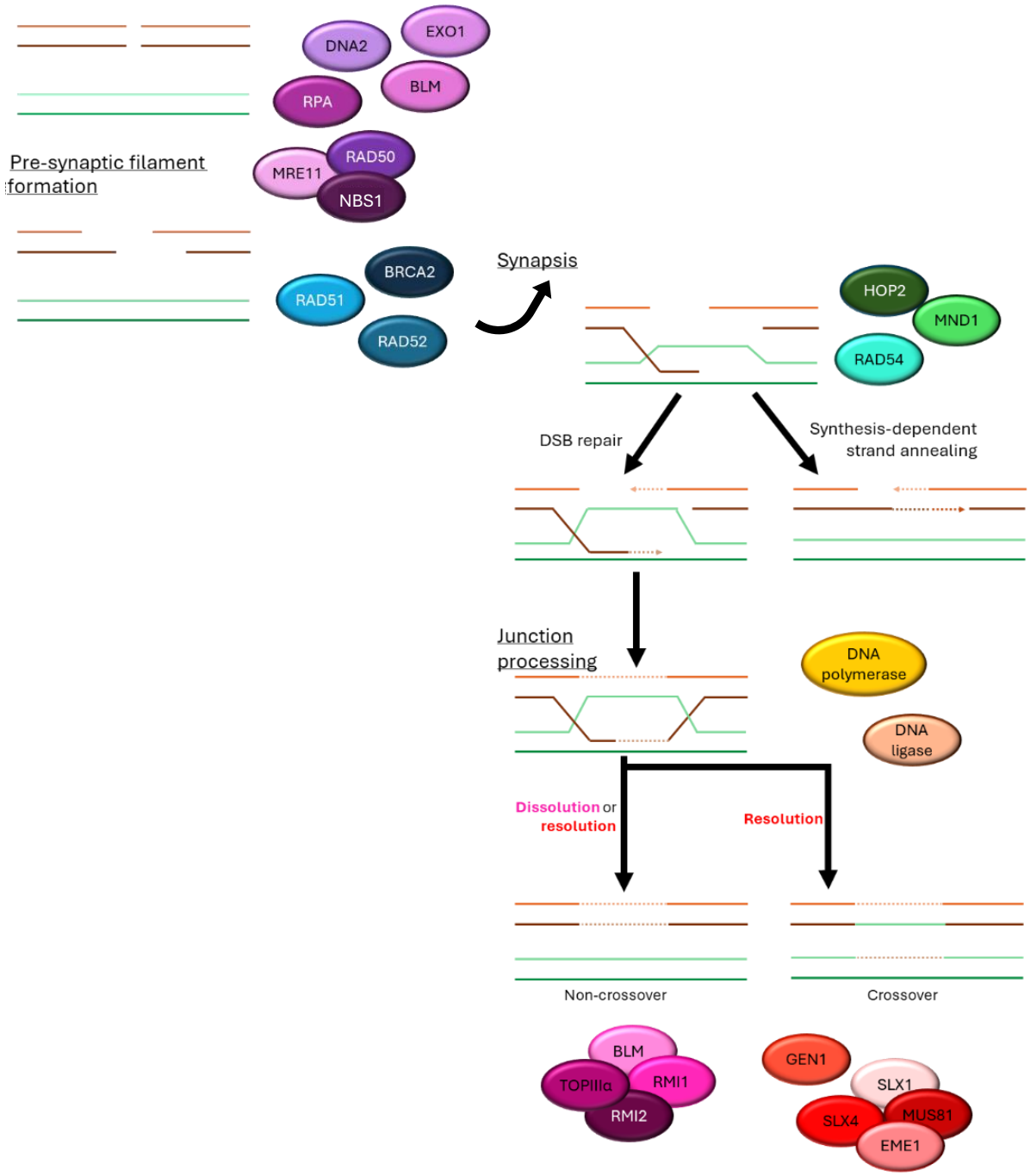


Figure 2: Homologous recombination pathway
Exposed ends are resected initially by the MRN complex and then more extensively by EXO1, BLM and DNA2. RPA protects the exposed ends until it is replaced with RAD51 by BRCA2 and RAD52.

HOP2 and MND1 facilitate capture of an homologous template, and RAD54 captures the opposite end of the DSB in some cases. Repair then proceeds in one of 4 ways. DSB repair uses each strand of the intact duplex as a template for one of the broken strands, while synthesis-dependent strand annealing (SDSA) repairs one strand based on the template, then uses the repair as the template for the other strand. Break-induced repair and use of the opposing overhang (in repetitive regions where overhangs can act as a template) are not shown.

The final step is junction processing to separate the two DNA duplexes. Without second end capture, as in SDSA, the invading strand can simply be detached from the template duplex. It both ends of the DSB were held in the repair complex, the strands must be cut to separate the duplexes. In dissolution, two strands are cut simultaneously, allowing exchange of genetic material between duplexes to form a cross-over product.

1.2.2 - Re-assortment

Radiosensitivity has been shown to vary across the cell cycle, with cells being most vulnerable in mitosis and most resistant in S phase [Biade et al., 1997]. This is one reason for fractionated radiotherapy – a series of smaller doses increases the likelihood of each cell being in mitosis when irradiated at least once in the treatment protocol. IR-induced DNA damage activates cell cycle checkpoints, effectively synchronising the population. The ability to avoid this synchronisation has been demonstrated in head and neck squamous cell carcinoma cell lines. HPV-positive lines showed greater levels of G2 arrest and remained in this state for longer than HPV-negative lines, which were relatively radioresistant [Arenz et al., 2014]. Similar results were seen when comparing HPV-positive and -negative cervical cancer cells, with the added detail that the virus-mediated radioresistance is achieved through upregulation of miRNA-21 that downregulates LATS1 to push cells into S phase [Liu et al., 2015].

1.2.3 - Repopulation

Another way in which the cell cycle impacts tumour radiosensitivity is through its speed. Faster-growing cells will be able to repopulate the affected area between doses, making it less likely that all tumour cells will be eradicated by the end of treatment. Interruption of radiotherapy protocols correlated negatively with treatment outcome in a breast cancer study [Bese et al., 2005], while longer intervals between doses increases the dose required to control tumour progression [Maciejewski and Majewski, 1991; reviewed by Kim and Tannock, 2005]. Combined analysis of proliferation and radioresistance gene sets in colorectal cancer identified more than 200 genes upregulated in both, including 4 with strong prognostic value [Song et al., 2023]. Repopulation is also associated with increased radioresistance through other mechanisms, since the new population is derived from cells that survived the initial therapy and are therefore likely to be better able to withstand the cytotoxic effects of IR [Bao et al., 2006; Woodward et al., 2007].

1.2.4 - Reoxygenation

When tumour vascularisation fails to match tumour growth, areas of the tumour distal to blood vessels become hypoxic due to inadequate oxygen supply by diffusion. Since normal oxygen levels vary between tissues, the exact partial pressure of oxygen (pO_2) deemed to be hypoxic is context-dependent, but in the brain, for example, pO_2 is mostly reported as being 0.1-10% and 4-15% for tumour and normal tissue respectively [Albert et al., 2014; Muz et al., 2015]. 1% oxygen is typically used for *in vitro* hypoxia studies in glioblastoma cells [Musah-Eroje & Watson, 2019; Evans et al., 2004; Beppu et al., 2002; Chédeville & Madureira, 2021]. The main signalling effect of low oxygen levels is impairment of prolyl- and asparaginyl-hydroxylases. They are prevented from hydroxylating HIFα, which is therefore protected from the proteasomal degradation normally triggered by its modification. Stabilised HIFα then upregulates expression of genes for processes such as angiogenesis, metabolic changes, and metastasis, explaining the correlation of hypoxia with worse prognosis [Bakleh and Al Haj Zen, 2025 – references experiments with 0-5% oxygen for 2-72 h; Infantino et al., 2021 – hypoxia not defined; Ponente et al., 2017 – constitutively active HIF1α used to mimic hypoxia response]. Marallano et al. demonstrated that transcriptional changes could be detected in glioblastoma cells after 16 h in hypoxic conditions (1% oxygen) [2024].

Hypoxia has also been linked to poor response to radiotherapy, through both its downstream genetic changes and simply the reduction in pO_2 that defines the term. Levels of IR-induced DNA damage are significantly higher when oxygen is present, and this 'oxygen enhancement effect' is explained by the 'oxygen fixation hypothesis' [Horan et al., 1999 – 21% (normoxic) or <0.005% (hypoxic); Grimes and Partridge, 2015 – modelled DNA ionisation at 0-100 mmHg pO_2]. IR generates free radicals, either in DNA directly or from surrounding water molecules that then generate the DNA radical, but in either case, the DNA damage is easily reversed chemically [Held, 1988 – anoxic, normoxic, or with 100% O_2 or N_2 bubbled through sample during irradiation]. This changes, however, if oxygen is present. The hydroxyl radicals generated from water are oxidised

to form peroxyl radicals, and this additional oxygen is transferred to the DNA damage site, hindering repair. Alongside its chemical effect, hypoxia contributes to radioresistance by altering other cellular pathways, including cell cycle progression and apoptosis. For example, Menegakis et al. showed that RPE-1 cells remain radioresistant upon reoxygenation despite DSB induction returning to normoxia levels (typically considered 21% oxygen), and that radiosensitivity could be restored by HPV E7-mediated inhibition of hypoxia-induced quiescence [Menegakis et al., 2021 – hypoxia defined as 1% oxygen for 72 h, and oxygen levels returned to normoxia or 0.1% oxygen before IR treatment]. In prostate cancer cell lines, the radioprotective effect of post-IR hypoxia (0.5% oxygen for 24 h after IR) was attributed to cell cycle arrest at the G_2/M checkpoint as well as impaired apoptosis and senescence [Hennessey et al., 2013]. At the patient level, a higher pre-surgery tumour:blood oxygen ratio[2] in glioblastoma patients correlated with faster progression and lower survival times, although no mechanistic detail was proposed [Spence et al., 2008].

1.2.5 - Intrinsic mechanisms and cellular stress

1.2.5.1 - Reactive oxygen species (ROS)

The indirect damage described above constitutes the majority of IR-induced DNA lesions are caused by ROS produced by water radiolysis [Sage and Shikazono, 2017]. In water radiolysis, water is split to produce free radicals, which then transfer an electron to the DNA helix. Far more ROS are produced during normal cellular homeostasis, primarily through electrons leaking from the mitochondrial electron transport chain [Leach et al., 2001; Richardson and Harper, 2016], but they are more diffuse so do not cause the clusters of DNA damage that make IR so toxic. However, this category of ROS does contribute to sensitivity to IR-induced damage, as demonstrated by increased ROS levels in more radiosensitive cells. Comparison of 2 pancreatic

[2] >90% of brain and muscle samples produced a ratio of <1.2, so values above this were considered hypoxic, and splitting patients based on the median ratio for the group found a significant survival advantage in those below the median value.

cancer cell lines showed that IR-induced DNA damage and apoptosis levels were higher in the one with higher ROS concentrations and lower levels of glutathione, an antioxidant. The more resistant cell line also showed greater levels of basal expression and IR-responsive induction of NRF2, a transcription factor that targets antioxidation genes [Jayakumar et al., 2014]. In glioma patients treated with radio- and chemotherapy, greater expression of copper/zinc superoxide dismutase, an enzyme involved in removing superoxide radicals, correlated with shorter time to progression, while an *in vitro* study confirmed that SOD inhibition sensitises glioblastoma cells to both temozolomide and radiotherapy as separate treatments, as well as in combination [Yoshii et al., 1999; Hsueh et al., 2025]. ROS levels have also been implicated in the increased radioresistance of cancer stem cells (CSCs) compared with bulk tumour cells, with the stem cells showing reduced ROS concentrations and correspondingly lower levels of IR-induced DNA damage. Diehn et al. used a mouse model of breast cancer to demonstrate that antioxidant treatment could confer CSC levels of radioprotection on non-tumorigenic cells, while CSCs were sensitised to IR by glutathione depletion [Diehn et al., 2009].

As well as their contribution to DNA damage, ROS facilitate other responses to IR, falling under the umbrella of oxidative stress. It is thought that elevated ROS production in tumours puts them closer to the threshold at which the cells can no longer withstand the corresponding stress signals and therefore the added burden of IR responses is more likely to cause apoptosis in tumour cells than surrounding healthy tissue. ROS stimulate p53 signalling to upregulate pro-apoptotic gene expression [Macip et al., 2003], and increase mitochondrial membrane permeability, which results in release of cytochrome *c* into the cytoplasm where it triggers formation of the apoptosome complex [reviewed by Tajeddine, 2016]. This exacerbates the DNA damage-mediated radiosensitive phenotype associated with high ROS levels.

1.2.5.2 - Metabolism

The Warburg effect is a well-established hallmark of cancer and it refers to the metabolic shift towards aerobic glycolysis and away from the oxidative phases of glucose metabolism. A key marker of this shift is an increase in glucose consumption, facilitated by increased expression of transporter GLUT1, which has also been found to correlate with increased radioresistance [Kunkel et al., 2007; Zhao et al., 2016; Shimura et al., 2014]. More broadly, Lin et al. found that the expression of 200 glycolysis-associated genes could predict response to radiotherapy in breast cancer patients, with a low glycolytic signature correlating with greater survival benefit to IR [Lin et al., 2025]. Several mechanisms have been suggested for the radioprotective effect of increased glycolytic activity. When Bhatt et al. increased radioresistance by treating cells with mitochondrial respiratory modifiers that upregulated glycolysis, they observed a simultaneous increase in NHEJ and HR activity in cells, suggesting that glycolytic activity may facilitate cell survival by improving DNA repair capacity [Bhat et al., 2015]. Alternatively, aerobic glycolysis may increase redox capacity by converting pyruvate into lactate instead of passing it into the tricarboxylic acid (TCA) cycle as acetyl-CoA. The TCA cycle and subsequent oxidative phosphorylation pathway generate ROS, whereas lactate production oxidises NADH to NAD+, which prevents NADH entering the ROS-generating electron transport chain and regenerates NAD+ whose reductive properties protect against ROS [Lin et al., 2022]. Expression of lactate dehydrogenase A, which favours lactate production in the reversible pyruvate-lactate reaction, is often upregulated in cancer cells [Jiang et al., 2015; Huang et al., 2016; Juan et al., 2016], and its inhibition causes increased oxidative stress and impairs tumour progression [Le et al., 2010; Xie et al., 2014].

1.2.5.3 - Endoplasmic reticulum stress

Endoplasmic reticulum (ER) stress is caused by the accumulation of misfolded proteins. The ER-associated degradation (ERAD) pathway facilitates translocation of the problematic proteins

from the ER to the cytosol for proteasomal degradation, but when this fails to keep unfolded proteins low, ER stress mechanisms inhibit protein synthesis and alter gene expression to compensate. Like the oxidative stress pathways triggered by ROS accumulation, ER stress can also cause apoptosis, and in the context of IR, these additional cell death signals reduce the probability of cell survival. In an oesophageal cancer cell line, tunicamycin treatment to induce cell death increased the number of apoptotic cells after IR, as well as those stalled at the G2/M checkpoint [Pang et al., 2013], while 2-deoxy-D-glucose was used to the same effect in glioblastoma stem cells, producing a dose-dependent reduction in viability and expression of apoptotic markers following IR [Shah et al., 2019]. Additionally, inhibition of eIF4A, an RNA helicase that forms part of the eukaryotic translation initiation factor F complex, has been shown to increase radiosensitivity, at least partly through a reduction in γH2Ax foci removal after IR, indicative of DNA repair pathway impairment [Lehman et al., 2022]. As this study demonstrates, any IR response pathways dependent on protein synthesis will be impaired by ER stress-induced inhibition of this process, highlighting another connection between ER stress and radiosensitivity.

1.2.6 - Reactivation of the immune response

Just as it has both an oncogenic and tumour-suppressive function, so too can the immune system facilitate both survival and eradication of an irradiated tumour. IR upregulates expression of major histocompatibility complex class I (MHC-I) genes, which are responsible for presentation of endogenous antigens to stimulate CD8+ cytotoxic T cells, thereby making the tumour more visible to the immune system. It also increases protein degradation, increasing the likelihood that a neo-antigen (specific to the tumour and not healthy tissue, and therefore recognised by the immune system as foreign) will be produced [Reits et al., 2006]. Tumour properties that augment this process are associated with a stronger anti-tumour immune response following IR and consequently a more complete response to radiotherapy. A murine melanoma model compared tumours generated from cells with high or low MHC-I expression

and found that, in order to achieve the same magnitude of response, tumours with low MHC-I levels needed an IR dose 4 times higher than that used for tumours with high MHC-I expression [Constanzo et al., 2025].

The equivalent of antigen presentation in the innate immune system is detection of damage- or pathogen-associated molecular patterns (DAMPs or PAMPs), the former of which is highly relevant to IR-induced responses. Cytosolic DNA is an indicator of cellular damage, such as micronucleus formation due to genomic instability such as that caused by tumour development or IR [Mackenzie et al., 2018]. When the micronuclear membrane breaks down, cGAS detects the presence of DNA in the cytosol and, along with STING, initiates a signalling pathway that upregulates interferon genes for further immune signalling [Pan et al., 2023]. However, higher radiation doses also activate expression of TREX1, a DNA endonuclease that degrades cytosolic DNA to prevent cGAS/STING signalling [Vanpouille-Box et al., 2017]. This impairs the IR-induced immune response, as demonstrated by the inefficacy of immune checkpoint inhibitors once TREX1 is upregulated, but *TREX1* knockdown was sufficient to restore both IR-induced tumour regression and immune checkpoint inhibitor response, highlighting the influence of this gene on radiosensitivity. [Vanpouille-Box et al., 2017].

Another role of cytokines such as interferons is immune cell recruitment, which can both promote and hinder an anti-tumour response. In lung adenocarcinoma, RRM2 inhibits cGAS/STING signalling to downregulate chemokines CCL5 and CXCL10, both of which increase CD8+ T cell numbers in the tumour and the spleen, offering a potential explanation for the poorer prognosis associated with greater RRM2 expression [Jiang et al., 2021; Mowat et al., 2021]. By contrast, elevated TGF-β expression in prostate cancer is associated with radioresistance by increasing tumour levels of regulatory T cells (Tregs) with immunosuppressive function [Wu et al., 2014]. TGF-β signalling promotes radioresistance in tumour cells grown *in vitro*, but the additional significance of its paracrine effect was confirmed in a mouse model by the observation

that depletion of Tregs with antibodies against their CD25 marker significantly impaired tumour regrowth after irradiation. The importance of tumour-derived cytokines in determining radiosensitivity is neatly underscored by HPV+ and HPV- HNSCC, which are known to be relatively sensitive and resistant to IR respectively [Chen et al., 2019]. Both types recruit macrophages after treatment with IR, but in HPV+ HNSCC, IL-6 secretion is high compared to HPV- HNSCC, and this pushes macrophage polarisation towards the classical M1 type. In HPV- HNSCC, on the other hand, the majority of macrophages are alternatively activated and of the M2 type. Since the main function of M1 macrophages is cytotoxicity, while M2 macrophages are associated with angiogenesis, tissue repair and stromal remodelling, all of which promote tumour progression, this difference in polarisation likely explains or at least contributes to the difference in radiosensitivity [Lendeckel et al., 2022].

As the details of the 6 Rs of Radiobiology demonstrate, there are many factors that influence tumour radiosensitivity so identifying new players in this intricate network, and therapeutic mechanisms with which to target them, poses an overwhelming array of starting points. One way to narrow this down to a more practical range is to select a single protein family or pathway that will allow broad exploration with a common approach. E3 ubiquitin ligases are one such family - with over 600 members implicated in virtually every cellular process, they are likely to cover every aspect of radiosensitivity, and they are also the focus of increasing attention for new treatments. Growing libraries of ligands for both E3s and proteins to which their enzymatic activity could be usefully directed offer a common strategy for manipulating any member of this family to combat tumour radioresistance.

1.3 - E3 ligases

1.3.1 - Definition

E3 ubiquitin ligases are the enzymes responsible for the third and final stage of ubiquitylation, the process of covalently attaching the small protein ubiquitin to the target protein substrate. Prior to E3 involvement, an E1 enzyme activates ubiquitin, then transfers it to an E2 enzyme that presents it to an E3 in the correct orientation for conjugation to an E3-bound substrate. The human genome encodes 2 E1s [Jin et al., 2007], ~30 E2s [Stewart et al., 2016], and hundreds of E3s [Li et al., 2008], such that the specificity of the pathway increases at each step, with the E3 ultimately determining the target protein [Iconomou & Saunders, 2016]. There are three families of E3s – HECT (homologous to the E6AP carboxyl terminus), RING (really interesting new gene) and RBR (RING between RING) - whose members are characterised by different structural and catalytic properties.

1.3.2 - RING E3s

With almost 600 members in the human genome, the RING family is the largest group of E3 ligases [Li et al., 2008]. Structurally, the group is characterised by the presence of a RING domain, a cysteine-rich region that ligates two Zn^{2+} ions with a consensus C3HC4 motif [Barlow et al., 1994; Freemont et al., 1991; Lovering et al., 1993; Saurin et al., 1996], and its conserved mechanistic feature is the direct transfer of ubiquitin from an E2 to a lysine residue in the target substrate [Budhidarmo et al., 2012]. This E3 family can be subdivided into monomeric, dimeric and multimeric E3s of increasing complexity [Metzger et al., 2014]. Monomeric RING E3s contain domains for substrate selection and E2 interaction in the same polypeptide chain, and the same is often true for dimeric RING E3s, although in some heterodimers, only one E3 interacts with the cognate E2 and the other promotes ubiquitin transfer. For example, BMI1 interaction with RING1b increases ubiquitylation of H2A, but mutagenic analysis of the expected E2 binding site indicates that only the E2-RING1b interaction is required for catalysis and that the stimulatory

effect of BMI1 is likely structural [Buchwald et al., 2006]. Multimeric RING E3s are the most complex, containing a minimum of four components – a RING domain, a scaffold protein, an adaptor and a substrate receptor. The most numerous type of multimeric RING E3s is the cullin-RING ligases (CRLs), which use a cullin protein as their scaffold and account for around half of all RING E3s [Sarikas et al., 2011]. The value of the complexity afforded by this modular system is frequently exemplified by APC/C, which contains at least a dozen subunits, including cullin-like scaffold APC2 and different substrate receptors at different points in the cell cycle to carry out multiple functions [Pines et al., 2011]. As might be expected from such a large family, this multiplicity of function is reflected across RING E3s, which are involved in processes from DNA repair to growth factor signalling [Hu et al., 2021; Inoue and Imamura, 2008].

1.3.3 – U-box E3s

First discovered in yeast, U-box E3s share a conserved carboxyl-terminal domain with high sequence and structural similarity to the RING domain [Koegl et al., 1999; Aravind & Koonin, 2000]. The key exception is loss of the cysteine and histidine residues that give RING domains their metal chelation function, which is also lost in U-box domains [Aravind & Koonin, 2000]. Although members of this family of E3s were originally labelled as E4s on the basis that they elongated chains established by other E3s, they have since been shown to initiate ubiquitylation independently, although the mechanism for this is unclear [Hatakeyama et al., 2001]. The U-box is essential for ubiquitylation activity, likely by facilitating the direct E2-to-substrate transfer also used by RING E3s [Hatakeyama et al., 2001; Benirschke et al., 2011; Pruneda et al., 2012]. Research to date implicates this activity in cellular stress responses [Bhuripanyo et al., 2018; Jiang et al., 2001].

1.3.4 - HECT E3s

As the name suggests, HECT E3s share a catalytic carboxyl-terminal domain (CTD) with E6AP [Huibregtse et al., 1995; Scheffner et al., 1993], while their amino-terminal domains (NTDs) are

more variable and mediate substrate selection. Of the 28 HECT E3s identified in humans, 9 belong to the NEDD4 family with a C2 domain upstream of 2-4 WW domains, while another 6 form the HERC family with at least one regulator of chromosome condensation 1 (RCC1)-like domains (RLDs) near their amino terminus. The remaining 13 have more distinct NTDs and are classified simply as 'other HECTs' [Wang et al., 2020; Rotin & Kumar, 2009]. The range of substrates targeted by the different HECT E3s involves the family in many processes, from apoptosis [Qiao et al., 2020], to differentiation [Xiao et al., 2014], to metabolism [Moroishi et al., 2014], but the use of a two-step catalytic mechanism is common to all HECT E3s. A detailed mechanism has yet to be determined, but the formation of a thioester link between ubiquitin and a conserved cysteine in the CTD is consistent [Scheffner et al., 1995; Kamadurai et al., 2013] and distinguishes HECT E3s from those in the RING family, which facilitate direct ubiquitin transfer from the E2 to the substrate.

1.3.5 - RBR E3s

RBR E3s form a middle ground between the HECT and RING families, sharing the RING domain of the latter but the catalytic mechanism of the former. Their characteristic structure of two RING domains separated by C6HC-type cysteine-rich domain (in-between RING (IBR) or double RING finger-linked (DRIL) domain) [Morett & Bork, 1999; Van Der Reijden et al., 1999] led to their classification as a subfamily of RING E3s until two members were shown to retain auto-ubiquitylation activity when bound to mutated E2s that failed to support RING E3 function [Wenzel et al., 2011]. An RBR E3-ubiquitin conjugate was isolated and the bond shown to be a thioester, in contrast to the isopeptide linkage formed when ubiquitin binds to a substrate lysine residue. A conserved cysteine residue was identified in the second RING domain, with no impact on structural stability or the affinity of the RING finger for its zinc ligand, but whose mutation abrogated ubiquitin transfer activity. This confirmed the catalytic similarities between RBR and HECT E3s and establishing RBR E3s as a family distinct from the RING group. There are 15 RBR E3s in the human genome and their functions include endosomal transport [Hassink et al., 2012],

mitophagy [Narendra et al., 2008; Villa et al., 2017] and cell cycle progression [Ng et al., 2003], with implications for the development of cancers and neurodegenerative diseases in particular [Marín et al., 2004].

1.3.5 - Function

The basic function of an E3 ligase is evident from the definition of this class of enzyme – to catalyse the covalent attachment of activated ubiquitin to a specific substrate. The detail surrounding this simple outline, however, is far more complex. Firstly, the substrate is typically modified at a lysine residue, using the amino group in the side chain to form a peptide bond with the carboxyl-terminal glycine of ubiquitin. However, modification of cysteine, serine and threonine residues, and the amino-terminal methionine has also been documented [reviewed by McDowell & Philpott, 2016]. A second layer of complexity is added by the ability of ubiquitin itself to be ubiquitylated, giving rise to chains of varying lengths. Ubiquitin contains 7 lysine residues, which, along with its amino-terminal methionine, can each be ubiquitylated to produce a different linkage type. Different types result in different downstream processes, and each type can trigger multiple responses [reviewed in Akutsu et al., 2016]. Combinations of linkage types extend chain types further into linear and branched chains [reviewed in Haakonsen and Rape, 2019], resulting in a highly complex 'ubiquitin code' with a broad range of functions (Figure 3 and Table 2).

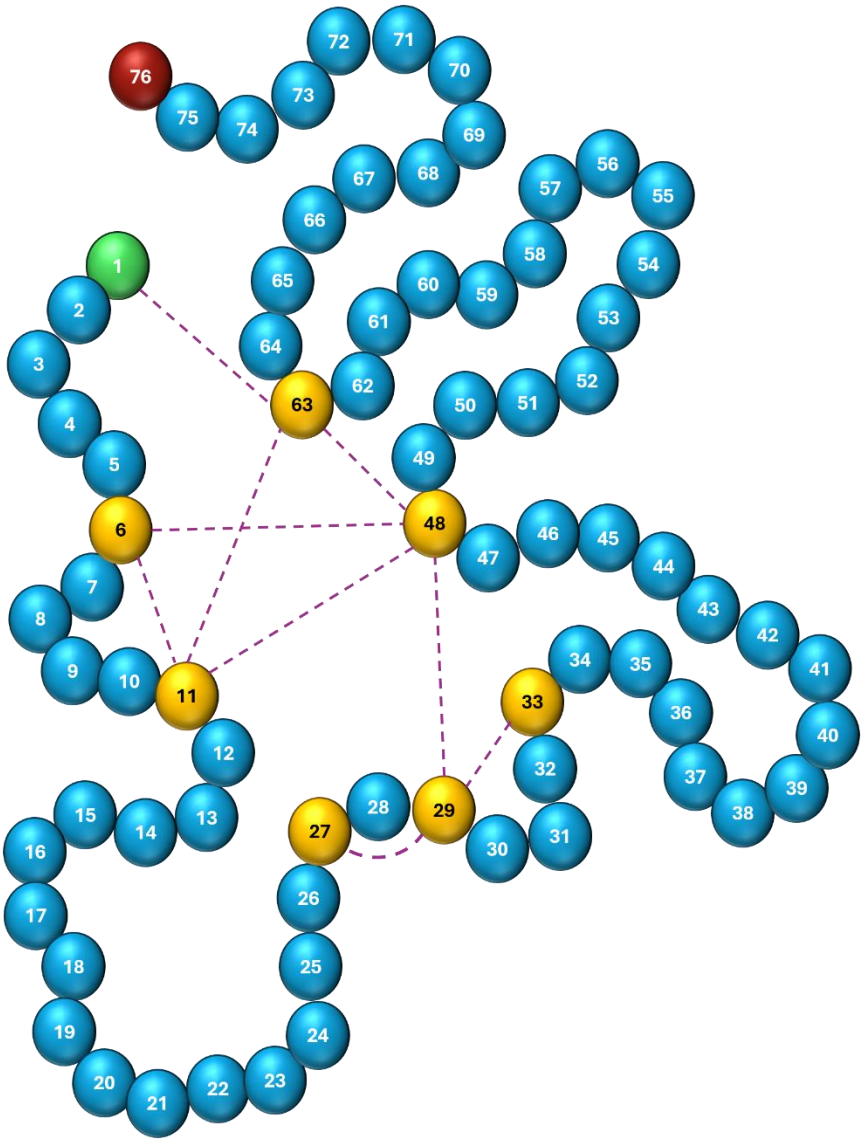


Figure 3: Ubiquitylation linkage types
Each circle represents a residue in ubiquitin. Yellow circles are lysine residues to which other ubiquitin proteins can be added, green is methionine which can be modified in a similar manner, and red is the carboxyl-terminal glycine used to attach to other proteins. Dotted lines indicate linkage types that have been identified in the same chain of ubiquitin moieties.

Monoubiquitylation and multi-monoubiquitylation		DNA repair	Mishra et al., 2024; Sareen et al., 2012
		Protein localisation	Shen et al., 2024; Seki et al., 2013
		Transcription regulation	Kim et al., 2024; Chen et al., 2020
		Signalling	Haglund et al., 2003 ; Ray et al., 2014; La Rosa et al., 2011
		Endocytosis	Haglund et al., 2003
Polyubiquitylation (single linkage type – linear chain)	M1	Signalling (NF-κB)	Zhang et al., 2017; Fischer et al., 2025
		Immune system (TLR and IFN signalling; lymphocyte homeostasis)	Zhang et al., 2017
		Signalling (NF-κB)	Zhang et al., 2017; Fischer et al., 2025
	K6	Mitophagy	Durcan & Fon, 2014
		Cell death inhibition	Seo et al., 2018
		Immune system (PRR)	Zhang et al., 2017
		Signalling (JNK, MAPKKK, iκB)	Zhang et al., 2017
	K11	Proteasomal degradation • Cell cycle regulation • ERAD	Budhavarapu et al., 2012 Locke et al., 2014
		Signalling (e.g. NF-κB, Hedgehog)	Dynek et al., 2010; Zhang et al., 2013
		Translocation	Zhou et al., 2025
	K27	Cell proliferation	Shearer et al., 2022
		Immune system (anti-fungal)	Cao et al., 2015
		Mitochondria	Birsa et al., 2014
		Mitophagy	Wu et al., 2024
		Signalling (TGF-β, Hippo)	Tu et al., 2022; Xu et al., 2023
		Signalling – immune system	Zhou and Zhang, 2021
		Cell proliferation	Shearer et al., 2022
	K29	Apoptosis (ER stress)	Wang et al., 2013
		Unfolded protein response	Zhang et al., 2025a
		Signalling (Wnt/β-catenin; Hippo)	Fei et al., 2023; Xu et al., 2023b
		Immune system	Gao et al., 2021
		Migration	Weinberg et al., 2024
	K33	Immune system – signalling (TCR, IFN)	Huang et al., 2010
		Immune system (inflammasome)	Liu et al., 2024a
		Protein trafficking	Yuan et al., 2014
	K48	Proteasomal degradation • Metabolism • Differentiation • Signalling (immune system – TLR)	Ghosh et al., 2016 Wang et al., 2024 Zhang et al., 2023
		Lysosomal degradation	Zhang et al., 2013; Kim et al., 2015
		Transcription regulation	Flick et al., 2004
		ESCRT I complex	Zhang et al., 2017
	K63	DNA replication and repair	Liu et al., 2018; Haahr et al., 2018
		Protein synthesis in oxidative stress	Simões et al., 2022
		Autophagy	Xu et al., 2016
		Protein-protein interactions	De Melo et al., 2014
		Signalling	Lawrence and Kornbluth, 2016
		NF-κB pathway	Chen et al., 2006
		Splicing	Song et al., 2010
		Immune system (anti-viral)	Zhang et al., 2017
		Synapse activity	Zhang et al., 2017
		Vesicle transport	Zhang et al., 2017
		Lysosomal degradation	Zhang et al., 2013

Polyubiquitylation (multiple linkage types – branched chain)	M1-K63	Signalling (IKK)	Emmerich et al., 2013
	K6-K11		French et al., 2021
	K6-K48		French et al., 2021
	K11-K48	Proteasomal degradation – mitosis	Yau et al., 2017
	K11-K63	Endocytosis (MHC molecules)	Boname et al., 2010
	K27-K29		French et al., 2021
	K29-K33		French et al., 2021
	K29-K48	Proteasomal degradation	Liu et al., 2017
	K48-K63	NF-κB signalling	Ohtake et al., 2016

Table 2: Examples of different ubiquitylation patterns and their downstream functions

1.3.6 - Roles in radiosensitivity and therapeutic potential

Mirroring their involvement in practically every cellular process, E3s are heavily involved in cancer cells, from their transformation to their response to treatment. One study estimated that 10% of driver mutations affected components of the ubiquitin-proteasome system, by interfering with substrate recognition or E3 activity directly [Martínez-Jiménez et al., 2020], while dozens of E3s have been implicated in the efficacy of radiotherapy [reviewed by Zhang et al., 2023b]. For example, in irradiated colorectal cancer, NPRL2 translocates to the nucleus where it inhibits E3s HERC2 and RNF8 and thereby prevents degradation of DNA repair proteins. AMPK inhibitors blocked the signalling cascade that causes NPRL2 translocation, resulting in decreased DNA repair and increased radiosensitivity [Wang et al., 2025]. In glioblastoma, E3 ligase Cullin2 (Cul2) is frequently downregulated, correlating with radioresistance through increased VEGF-A, HIF-1α, EGFR and cyclin B1 levels [Zheng et al., 2021]. This suggests a link to the role of hypoxia and reoxygenation in radiosensitivity, while another radiosensitivity mechanism is highlighted in glioblastoma cells by the observation that RNF138 causes degradation of rpS3 to block IR-induced apoptosis. In the absence of RNF138, rpS3 interacts with ER stress-associated DDIT3 (DNA damage-inducible transcript 3) after IR, promoting its activity as a stimulatory transcription factor for pro-apoptotic genes [Kim et al., 2018].

Despite the apparent wealth of opportunity to influence radiosensitivity through E3-targeting drugs, very few such compounds have reached the clinic. Inhibition of MDM2, the E3 that targets p53 for degradation, by nutlin-3 has been shown to increase radiation-induced apoptosis in oesophageal squamous cancer with wildtype p53 [He et al., 2018], and nutlin-3 has been supplemented by an array of alternative MDM2 inhibitors, but none have yet completed clinical trials [Schöffski et al., 2023; Sekiguchi et al., 2023]. In pancreatic cancer cells, curcumin downregulates SKP2, a key component in the SCF E3 ligase complex that contributes to cell cycle regulation. Curcumin treatment inhibits growth and promotes apoptosis, and increases radiosensitivity in both pancreatic cancer and glioblastoma cell lines, but results from clinical

trials have been underwhelming [Su et al., 2016; Schwarz et al., 2020; Kim et al., 2022]. It causes little toxicity, and shows biological activity at a genetic level, but this does not seem to translate to improved clinical outcomes [Dhillon et al., 2008; Gunther et al., 2022].

While treatments that target E3s have yet to yield substantial clinical results, treatments that *use* E3s may hold the key to a system of rational drug design that could manipulate any mechanism in any cancer. There is increasing interest in PROTACs (proteolysis-targeting chimeras) – small molecules consisting of a section that binds to an E3, one that binds to a protein of interest, and a linker region between the two. The protein of interest then becomes a 'neo-substrate' of that E3, which ubiquitylates it to cause its proteasomal degradation. To date, research has focused on only 4 of the ~600 human E3s (VHL, Cereblon, cIAP1 and MDM2), leaving plenty of untapped potential [Sun et al., 2019a]. Current PROTACs are also limited to causing neo-substrate degradation, confining their use to oncogenes, but use of other E3s that favour non-degradative ubiquitylation may allow neo-substrates stabilisation to counteract downregulation of tumour suppressor genes [Bhole et al., 2024]. Additionally, a recently discovered PROTAC for HECT E3 ligase HERC4 demonstrates the intrinsic reduction in degradative ubiquitylation of natural substrates. AK59 induces STING degradation by connecting STING to HERC4, and in so doing, it reduces degradation of SMO, which has been identified as an HERC4 substrate [Mutlu et al., 2023]. This supports a doubly effective model in which overexpressed E3s could be diverted to overexpressed neo-substrates, preventing the excessive degradation of their normal targets that would induce pro-tumour processes.

It is evident that, as a group, E3s provide valuable access to mechanisms that influence radiosensitivity, but it is also clear that current knowledge is adequate only to hint at the potential this enzyme family holds, and that further investigation of the connection between E3 activity and radiosensitivity is required.

1.3.7 - Identification of HERC4 as potential radiosensitiser

Given the likelihood of uncharacterised E3 involvement in radiosensitivity, an E3-restricted CRISPR screen was conducted to identify the strongest candidates [Dr Hongbin Yang, unpublished data]. From a panel of 7 glioblastoma cell lines, DBTRG cells were selected for an enrichment screen due to their relatively high radiosensitivity giving the most scope for detecting improved survival following CRISPR-mediated knockdown [Yang et al., 2024]. Stable Cas9 expression was introduced using a lentiviral system, and Edit-R lentiviral sgRNA constructs were packaged and used to transduce the Cas9+ cells. Following puromycin-mediated selection, successfully transduced cells were irradiated with 6 Gy (a dose previously found almost to eliminate growth in DBTRG colony formation assays and therefore with the greatest sensitivity towards sgRNA-induced survival advantages) and allowed to recover. 22 days after irradiation, cells were harvested and their genomic DNA extracted for sequencing of the incorporated sgRNA constructs. Relative enrichment or depletion of these constructs was then used to calculate a Z-score for each gene in the sgRNA library. Those with a strongly positive Z-score (≥2) were labelled as radiosensitisers, since DBTRG post-IR survival increased when these genes were removed, while those with a strongly negative Z-score (≤-2) were considered radioprotective for the opposite reason. Among the identified radiosensitisers, HERC4 was the strongest hit (Figure 1A). One gene, *PRPF19*, had a higher Z-score, but it was found to be an essential gene in DBTRG and was therefore discarded as having only an indirect effect on IR survival. DBTRG cells all but stopped proliferating in the absence of PRPF19, preventing them from entering mitosis when cells are most susceptible to the deleterious effects of radiation [Terasima and Tolmach, 1961]. Upon further testing with siHERC4, no proliferation defect was found for HERC4, indicating that it may increase radiosensitivity through more direct mechanisms (Figure 1C). Although the radioprotective effect of HERC4 loss could not be replicated at 6 Gy, siRNA-mediated knockdown did increase cell survival up to 4 Gy in colony formation assays, confirming that HERC4 is a viable candidate for a radiosensitiser, likely with a dose-dependent role (Figure 1B).

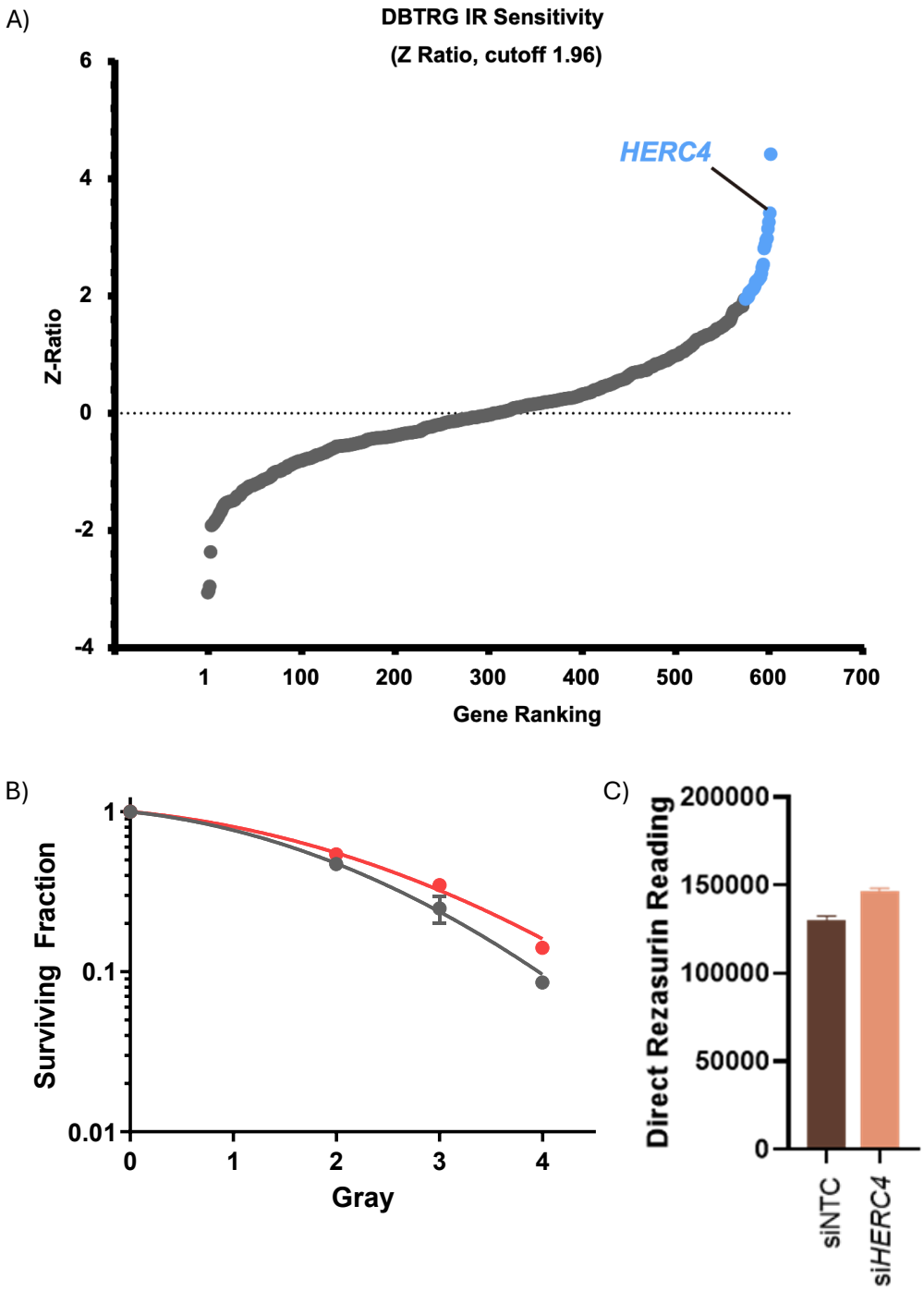


Figure 4: Initial identification of HERC4 as a potential radiosensitiser
Data collected, analysed and graphed by Dr Hongbin Yang.

A) A CRISPR screen was conducted in DBTRG cells using an sgRNA library targeting E3 ubiquitin ligases. Except for one protein, HERC4 gave the most positive Z-score (indicative of better survival when the protein was knocked out than in wildtype cells). The protein with a more positive Z-score was identified as an essential gene, meaning that the protective effect seen when it was knocked out was likely due to minimal cell growth under control conditions, an effect previously shown to be radioprotective, rather than to a direct impact on radiosensitivity.

siRNA-mediated HERC4 knockdown also showed improved survival up to 4 Gy in a colony formation assay (B), and resazurin measurements of non-irradiated cells indicated minimal difference in cell viability following knockdown (C).

1.3.8 - HERC4 – current knowledge

1.3.8.1 - Discovery

HERC4 was first identified in a set of novel cDNA clones from adult and foetal brain tissue [Nagase et al., 2000]. An homology search in various databases revealed 41% identity with E6AP and 56% identity with HECT-domain containing proteins. It was then confirmed as a member of the HERC family 5 years later by Hochrainer et al. through its homology with HERC6 [Hochrainer et al., 2005]. They suggested that it was the evolutionary progenitor of the HERC family, based on its presence in nematodes whereas other HERC genes are only detected in insect species that evolved later. This hypothesis was confirmed at least for small HERCs the detection of HERC4 in sea lampreys, which are descended from jawless fish that evolved ~595 million years ago. By comparison, the next oldest gene, HERC3, appeared a mere ~476 million years ago, based on its modern-day appearance in elephant sharks that are thought to be the most slowly evolving jawed vertebrate [Paparisto et al., 2018].

1.3.8.2 - Structure

Adding weight to the placement of HERC4 as the founding member of the HERC family, the predicted structure of HERC4 shows many quintessential features of this group and the wider HECT family, including, at its amino- and carboxyl-termini respectively, a β-propeller fold typical of the RLD, and a bilobal HECT domain with a flexible linker between the amino- and carboxyl-lobes (N- and C-lobe) [Verdecia et al., 2003; Paparisto et al., 2018; Fleming et al., 2025] (Figure 4). The β-propeller contains the classic 7 “blades”, although each is formed from a β-sheet of only 3 strands compared to the expected 4 [Stevens & Paoli, 2007] (Figure 2B-C). The HECT domain contains the required catalytic cysteine residue, phenylalanine 4 residues from the carboxyl-terminus whose conservation in this position is important for E3 activity, plus an amino-terminal helix predicted to be important for protein stability, solubility and enzymatic function [Fleming et al., 2025; Koldenhof et al., 2024; Salvat et al., 2004; Kamadurai et al., 2013; Kane et

al., 2022] (Figure 2D-E). It also contains the flexible carboxyl-terminal tail observed in other HECT E3s, in a position from which it is feasible for it to lie between the N-lobe of the HECT domain and ubiquitin during catalysis, as shown for HECT E3 HUWE1 [Maspero et al., 2013; Nair et al., 2021].

1.3.8.3 - Interactors

Substrate specificity is typically attributed to the N-terminal domain, since this is more variable between E3s. This model is supported by the two putative substrates whose interaction with HERC4 has been characterised in more detail, with both SAV1 and SMO binding the RLD domain of HERC4 [Aerne et al., 2015; Jiang et al., 2019]. It should be noted, however, that SMO also interacts with the isolated HECT domain, and interaction of another substrate, LATS1, was abrogated when both of its suggested ubiquitylation sites were mutated, indicating that substrate recruitment, if not specificity, can be driven by the catalytic domain alone [Jiang et al., 2019; Xu et al., 2019].

These 3 proteins are the best-evidenced HERC4 substrates, since SAV1 and SMO are the only ones identified by multiple papers, while LATS1 strengthens the proposed involvement of HERC4 in the Hippo pathway [Aerne et al., 2015; Huang et al., 2021; Zhang et al., 2025b; Sun et al., 2019; Zhu et al., 2019; Jiang et al., 2019; Mutlu et al., 2019]. However, a handful of other interactors and substrates have been reported, including c-MAF and MafA, which are the only substrates with characterised linkage types [Zhang et al., 2016; Zhang et al., 2023a]. The majority of HERC4 substrates are degraded following ubiquitylation, including c-MAF, which is modified with the typically degradative K48 linkage, but MafA appears to be stabilised by K63-linked ubiquitylation, albeit that the modification simultaneously inhibits its activity [Zhang et al., 2016; Zhang et al., 2023a]. This gives the smallest of hints that HERC4 may be capable of multiple linkage types, but the full extent of its capabilities has yet to be determined.

A final point illustrated by putative HERC4 interactors is the potential role of oligomerisation in regulating HERC4 activity. Homodimerisation in other HECT E3s such as HUWE1 and SMURF1

has been shown to be both inhibitory, while heterodimerisation of HERC2 and E6AP facilitates HERC2-mediated activation of E6AP, independently of HERC2 ubiquitylation activity [Sander et al., 2017; Wan et al., 2011; Kühnle et al., 2011]. The observation that HERC4 interacts with HERC6 in co-immunoprecipitation experiments, and co-localises with HERC3 in the cell, indicates that HERC4 activity may be influenced by similar mechanisms [Hochrainer et al., 2008].

1.3.8.4 - Expression

Alongside characterisation of its structure and interactome, HERC4 studies have also explored its relative expression in different tissues, confirming the ubiquitous expression that is increased in the brain, especially foetal brain, a pattern identified for the original cDNA clone [Nagase et al., 2000; Hochrainer et al., 2005]. At an mRNA level, its expression was found to vary in different parts of the primate brain, but this variation was lost at a protein level, which remained consistent [Qin et al., 2024]. In mice, by contrast, protein-level expression was dependent on region, and even in the regions with highest HERC4 expression, it remain noticeably less abundant than other HERC proteins [Pérez-Villegas et al., 2022]. Hochrainer et al. also reported higher HERC4 expression in testes than in other tissues, including the brain in one study, contrary to the findings of the original study but in line with subsequent investigations into its function [Nagase et al., 2000; Hochrainer et al., 2005; Rodriguez and Stewart, 2007]. Based on TCGA data, glioblastoma cells show a marked reduction in HERC4 expression at both the mRNA and the protein level [UALCAN, TCGA] (Figure 5). Kidney chromophobe carcinoma also shows downregulation of HERC4 mRNA (no protein data), while cholangiocarcinoma, oesophageal carcinoma and liver hepatocellular carcinoma are among those with a noticeable upregulation [UALCAN, TCGA].

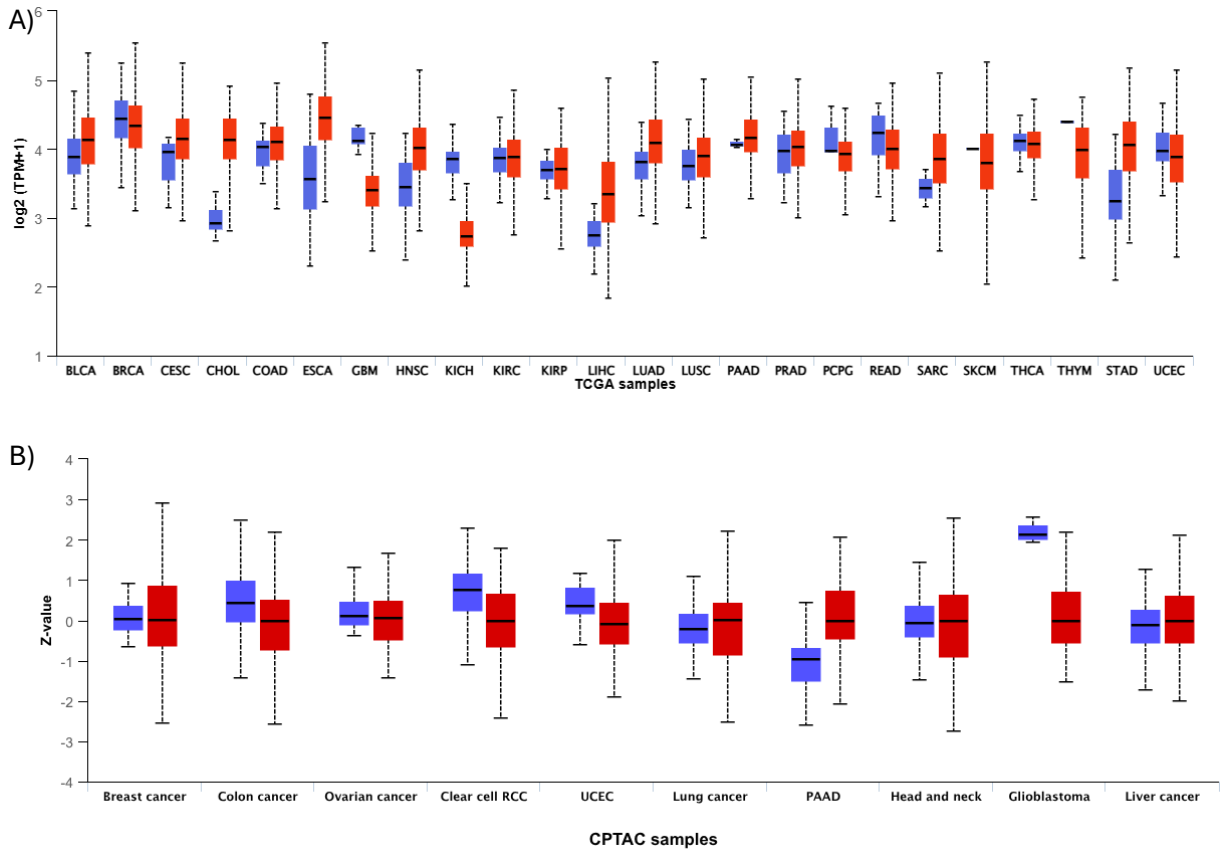


Figure 5: HERC4 mRNA (A) and protein (B) expression levels across cancer types
Normal tissue Tumour tissue
Graphs generated from TCGA data using UALCAN (June 2026).

BLCA = bladder urothelial carcinoma; BRCA = breast invasive carcinoma; CESC = cervical squamous cell carcinoma and endocervical adenocarcinoma; CHOL = cholangiocarcinoma; ESCA = oesophageal carcinoma; GBM = glioblastoma; HNSC = head and neck squamous cell carcinoma; KICH = kidney chromophobe carcinoma; KIRC = kidney renal clear cell carcinoma; KIRP = kidney renal papillary cell carcinoma; LIHC = liver hepatocellular carcinoma; LUAD = lung adenocarcinoma; LUSC = lung squamous cell carcinoma; PAAD = pancreatic adenocarcinoma; PRAD = prostate adenocarcinoma; PCPG = pheochromocytoma and paraganglioma; READ = rectum adenocarcinoma; SARC = sarcoma; SKCM = skin cutaneous melanoma; THCA = thyroid carcinoma; THYM = thymoma; STAD = stomach carcinoma; UCEC = uterine corpus endometrial carcinoma; RCC = renal cell carcinoma

1.3.8.5 - Function

Male fertility

One of the most researched areas of function for HERC4 is in male fertility, consistent with its elevated expression in the testis compared to most other tissue types [Hochrainer et al., 2005; Rodriguez and Stewart, 2007]. Herc4 expression was found to increase during spermatogenesis in mice, and homozygous loss-of-function mutations did not affect viability, growth or behaviour, nor do they affect female fertility. However, offspring numbers in litters produced from male mice with the mutations were found to be more variable and on the whole smaller than those produced from wildtype controls. Deeper investigation showed normal testis size and morphology, and no change in spermatozoon number, but a decrease in spermatozoon motility that was attributed to a 3-fold increase in the number of angulated tails. The point at which these tails bent encased a cytoplasmic droplet, which often contained deformed vacuoles and mitochondria. Ubiquitylation had been previously implicated in spermatozoon development, particularly through UBE2B activity, which tentatively suggests that HERC4 may use this E2, given the lack of alternative proposals in the literature [Rodriguez and Stewart, 2007]. A decrease in Herc4 expression in mouse testis was reported following *Trichinella spiralis* infection, and was also found to correlate with the decrease in spermatozoon number and increase in their defects following *Neospora caninum* infection of male mice [Li et al., 2023b; Li et al., 2021]. Motility was impaired, and mitochondrial defects were also reported, along with abnormal structures in spermatogenic cells [Li et al., 2021]. In Rhesus macaques, Herc4 expression was substantially increased by chronic delta-9-tetrahydrocannabinol use, which also impairs male fertility, although in this study, spermatozoon motility and morphology was comparable with the controls [Hedges et al., 2023].

Immune responses

Changes in HERC4 expression during response to viral infections in fish, usually resulting in its upregulation in brain and head-kidney [López-Vázquez et al., 2023; He et al., 2017; Eslamloo et

al., 2018]. This was not universally reported, with one study showing no change in HERC4 expression in the brain following infection [Valero et al., 2024a], and another showing downregulation of HERC4 in the brain of fish carrying high nodavirus levels [Rise et al., 2010], but the majority of studies show elevated HERC4 levels during anti-viral responses. Paparisto et al. reported that HERC4 inhibits viral production, albeit to a lesser extent than HERC5, suggesting it could replace the immune system function of HERC5 or -6 in species that lack these proteins [Paparisto et al. 2018]. However, a subsequent paper showed little efficacy for HERC4 against Ebola replication, so this activity, if present, may not be specific to certain viruses [Paparisto et al., 2021]. Other studies implicate small RNAs in the role of HERC4 in immune responses. At 48 h post infection, Eslamloo et al. detected a drop in levels of a microRNA predicted to target HERC4, while their previous study showed an increase in HERC4 expression at the same time point [Eslamloo et al., 2016; Eslamloo et al., 2018]. Another group identified an HERC4-derived circular RNA among those upregulated by grass carp reovirus exposure [He et al., 2017]. However, studies outside fish are limited to the observation that HERC4 expression correlates with human responses to immune checkpoint inhibitors, and to the expression of genes associated with antigen presentation [Liu et al., 2024b]. In light of this, along with the evidence from *in silico* analysis that Herc4 transcripts from fish may in fact be Herc7, a member of the HERC family with anti-viral activity but identified only in fish, the connection between HERC4 and the immune system should be viewed sceptically, but warrants further investigation [Valero et al., 2024b].

1.3.8.6 - Disease

Other putative functions for HERC4, besides roles in male fertility and the immune system, have largely been illuminated by its implication in non-infectious diseases such as diabetes, neurological disease and various types of cancer. In diabetes patients, hyperglycaemia increases levels of advanced glycation end products (AGEs), which in turn promote expression of osteoblast markers in smooth muscle cells, resulting in atherosclerotic calcification. Loss of

nuclear factor 90 (NF90), an RNA-binding protein involved in innate anti-viral immune responses, blocks this process. The primary mechanism identified is loss of NF90-mediated stabilisation of *FBXW7* mRNA, leading to increased abundance of the encoded E3 ligase that ubiquitylates AGE receptor 1 (AGER1) and causes its degradation to prevent its activity in reducing AGE levels. However, several other E3s showed increased and reduced mRNA expression following AGE exposure and NF90 knockdown respectively, including HERC4, suggesting that HERC4 may also be involved in processing these metabolic byproducts [Xie et al., 2024]. On the other hand, a separate study showed only a small and negative change in HERC4 expression following AGE treatment of pancreatic ductal epithelial cells, so this role may be misleading or at best cell type-specific [Senavirathna et al., 2024].

In cancer studies, HERC4 has shown conflicting results, with higher expression sometimes correlating with worse prognosis, sometimes better. Several pathways remain consistent, however, namely proliferation, migration and apoptosis, aligning with the proposal of SMO and SAV1 as HERC4 substrates since these pathways rely on genes regulated by SMO and SAV1 signalling cascades [Xu et al., 2019; Zhu et al., 2024; Sun et al., 2019; Zheng et al., 2017]. Notably in the context of this project, it is thought to oppose the acquisition of temozolomide resistance in glioblastoma by relieving ferroptosis inhibition [Miao et al., 2024]. A more detailed review of the links between HERC4 and cancer is provided in Chapter 2.1.

It is clear from this literature review that characterisation of the cellular roles of HERC4 is still in its infancy, giving few leads as to how it might influence radiosensitivity but also offering no evidence to conflict with the hypothesis of HERC4 as a radiosensitiser. Multiple studies confirm its function as an E3 ligase, while others confirm its relevance in the brain through expression patterns or disease implications, including glioblastoma specifically. HERC4 is consequently an exciting candidate for increasing sensitivity to radiotherapy in glioblastoma patients.

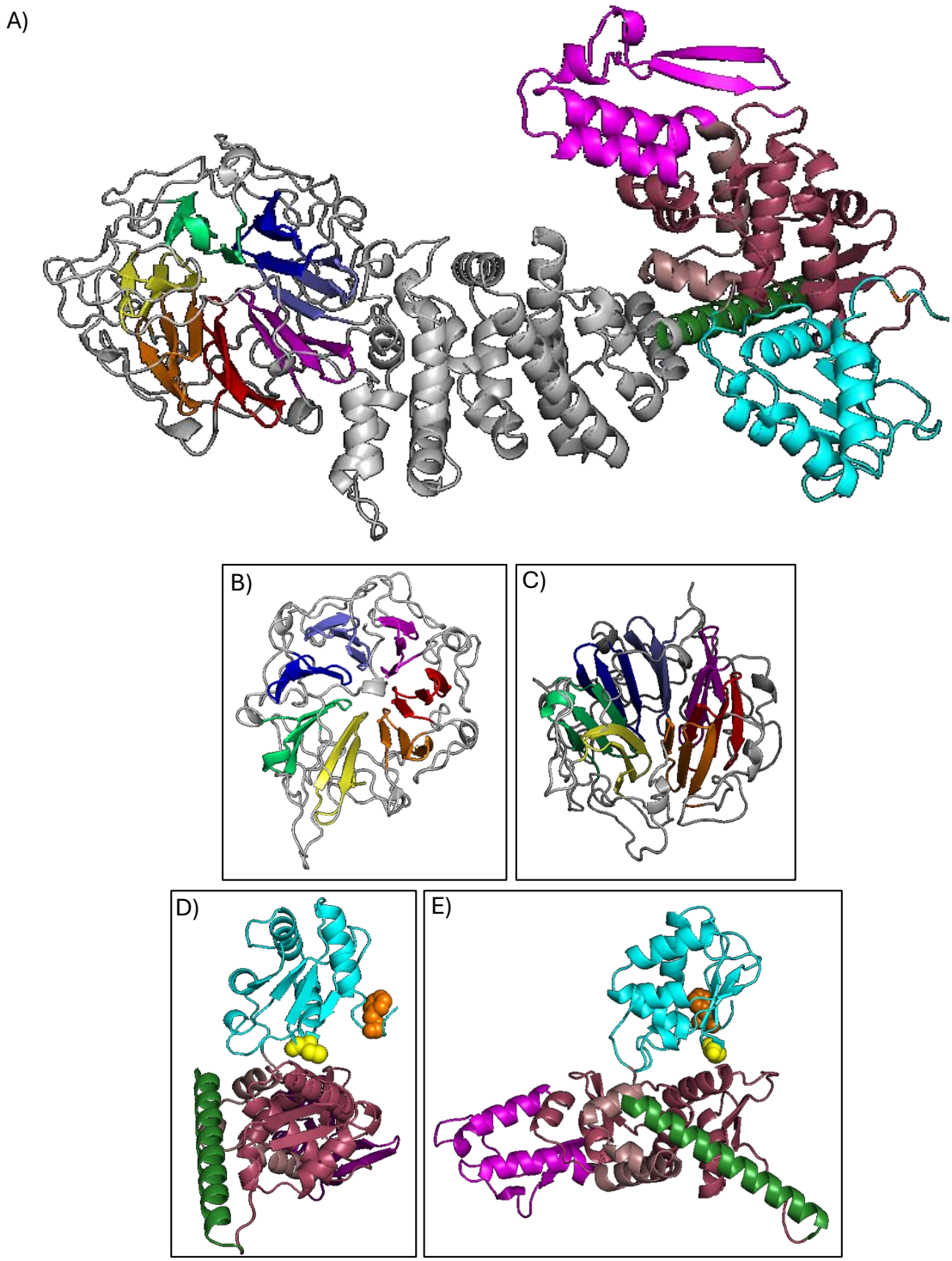


Figure 6: HERC4 structure as predicted by AlphaFold

The predicted structure (A) contains the expected β-barrel at the amino-terminus of the protein, with the typical 7 blades but with only 3 strands in each compared to the more standard 4 (B-C). The catalytic HECT domain is at the carboxyl-terminus of the protein (D-E), with a distinctive α-helix (green) at the amino-terminus of this region, in line with the observation of similar, stabilising helices in other HECT E3s. The HECT domain is also visibly divided into 2 lobes, with the carboxyl one shown in cyan and the amino one in 2 shades of pink to mark the small (bright) and large (dark) lobes. The orange residue is the phenylalanine conserved at 4 residues from the carboxyl-terminus, and the yellow residue is the catalytic cysteine.

Structures formatted in PyMOL [The PyMOL Molecular Graphics System, Version 3.0 Schrödinger, LLC]

1.4 – Objectives

The hypothesis on which this project is based is that HERC4 is a radiosensitiser and that without it, cell populations will show better survival after treatment with IR. An initial CRISPR screen conducted by Dr Hongbin Yang identified HERC4 as the strongest candidate for this phenotype from an E3-focused sgRNA library, and published data indicates a role for HERC4 in proliferation and apoptosis via substrates such as SMO and SAV1, offering a potential explanation for the screen result. There is, however, no data directly linking HERC4 to radiosensitivity, and limited evidence to support putative HERC4 functions, which are often broad and lacking mechanistic detail. The overaching aim of this project was therefore to test the hypothesis and in so doing, to expand and strengthen the available dataset on the cellular role of HERC4. In order to achieve this, the following objectives were set:

1. **Generate stable knockout clones** to provide a clean background for studying the effects of HERC4 loss. Clones with complete knockout should be selected to avoid dose-dependent effects and to ensure consistent absence of HERC4 expression.
2. **Test cell survival after IR.** The results of the initial screen could be explained by HERC4 loss improving tolerance of otherwise lethal doses so that more cells survive irradiation. Colony formation assays are considered the gold standard for assessing radiosensitivity.
3. **Test cell proliferation after IR.** If HERC4 loss does not affect the proportion of cells surviving a given radiation dose, it may accelerate the recovery of those that do survive (improved tolerance of sub-lethal doses). Repopulation is one of the 6 Rs of radiobiology and can be assessed through comparison of proliferation rates with and without IR.
4. **Identify the process(es) through which HERC4 influences radiosensitivity.** Survival and recovery can be influenced by various factors, such as changes in DNA repair systems either to improve speed and efficacy or in cell cycle distribution after to increase the proportion of cells in relatively radioresistant phases. The aim of this step is to highlight

the area of cell activity altered by HERC4 loss, with a focus on areas influencing radiosensitivity if this phenotype is confirmed.

5. **Identify a potential mechanism** for the cellular role of HERC4 through proteomic analysis. If a cellular function is found for HERC4, it can be characterised more extensively by identifying other proteins involved and how their abundance is influenced by HERC4. If a cellular function cannot be confirmed in the context of radiosensitivity, exploring the proteins affected by HERC4 loss offers a broader approach to highlight more promising areas for investigation.

1.5 - References

Aerne, B.L.; Gailite, I.; Sims, D. and Tapon, N. (2015) Hippo Stabilises Its Adaptor Salvador by Antagonising the HECT Ubiquitin Ligase Herc4 *PLOS One* 10(6):e0131113

Akutsu, M.; Dikic, I. and Bremm, A. (2016) Ubiquitin Chain Diversity at a Glance *Journal of Cell Science* 129(5):875-880

Albert, I.; Hefti, M. and Luginbuehl, V. (2014) Physiological oxygen concentration alters glioma cell malignancy and responsiveness to photodynamic therapy *in vitro Neurological Research* 36(11):1001-1010

Aravind, L. and Koonin, E.V. (2000) The U box is a modified RING finger – a common domain in ubiquitination *Current Biology* 10(4):R132-R134

Arenz, A.; Ziemann, F.; Mayer, C.; Wittig, A.; Dreffke, K.; Preising, S.; Wagner, S.; Klussmann, J.P.; Engenhart-Cabillic, R. and Wittekindt, C. (2014) Increased Radiosensitivity of HPV-Positive Head and Neck Cancer Cell Lines Due to Cell Cycle Dysregulation and Induction of Apoptosis *Strahlentherapie und Onkologie* 190:839-846

Bakleh, M.Z. and Al Haj Zen, A. (2025) The Distinct Role of HIF-1α and HIF-2α in Hypoxia and Angiogenesis *Cells* 14(9):673

Balana, C.; Vaz, M.A.; Sepúlveda, J.M.; Mesia, C.; Del Barco, S.; Pineda, E.; Muñoz-Langa, J.; Estival, A.; de Las Peñas, R.; Fuster, J.; Gironés, R.; Navarro, L.M.; Gil-Gil, M.; Alonso, M.; Herrero, A.; Peralta, S.; Olier, C.; Perez-Segura, P.; Covela, M.; Martinez-García, M.; Berrocal, A.; Gallego, O.; Luque, R.; Perez-Martín, F.J.; Esteve, A.; Munne, N.; Domenech, M.; Villa, S.; Sanz, C. and Carrato, C. (2020) A Phase II Randomized, Multicenter, Open-Label Trial of Continuing Adjuvant Temozolomide Beyond 6 Cycles in Patients with Glioblastoma (GEINO 14-01) *Neuro-Oncology* 22(12):1851-1861

Bao, S.; Wu, Q.; McLendon, R.E.; Hao, Y.; Shi, Q.; Hjelmeland, A.B.; Dewhirst, M.W.; Bigner, D.D. and Rich, J.N. (2006) Glioma Stem Cells Promote Radioresistance by Preferential Activation of the DNA Damage Response *Nature* 44(7120):756-760

Barlow, P.N.; Luisi, B.; Milner, A.; Elliott, M. and Everett, R. (1994) Structure of the C3HC4 Domain by 1H-nuclear Magnetic Resonance Spectroscopy.: A New Structural Class of Zinc-finger *Journal of Molecular Biology* 237(2):201-211

Baumann, P. and West, S.C. (1998) Role of the human RAD51 protein in homologous recombination and double-stranded-break repair *Trends in Biochemical Sciences* 23(7):247-251

Benirschke, R.C.; Thompson, J.R.; Nominé, Y.; Wasielewski, E.; Juranić, N.; Macura, S.; Hatakeyama, S.; Nakayama, K.; Botuyan, M.V. and Mer, G. (2011) Molecular Basis for the Association of Human E4B U box Ubiquitin Ligase with E2 Conjugating Enzymes UbcH5c and Ubc4 *Structure* 18(8):955-965

Beppu, T.; Kamada, K.; Yoshida, Y.; Arai, H.; Ogasawara, K. and Ogawa, A. (2002) Change of Oxygen Pressure in Glioblastoma Tissue under Various Conditions *Journal of Neuro-Oncology* 58:47-52

Bese, N.S.; Sut, P.A. and Ober, A. (2005) The Effect of Treatment Interruptions in the Postoperative Irradiation of Breast Cancer *Oncology* 69(3):214-223

Bhat, A.N.; Chauhan, A.; Khanna, S.; Rai, Y.; Singh, S.; Soni, R.; Kalra, N. and Dwarakanath, B.S. (2015) Transient Elevation of Glycolysis Confers Radioresistance by Facilitating DNA Repair in Cells *BMC Cancer* 15:335

Bhole, R.P.; Labhade, S. and Gurav, S.S. (2024) Conquering PROTAC Molecular Design and Drugability *Bioanalysis* 17(7):455-470

Bhuripanyo, K.; Wang, Y.; Liu, X.; Zhou, L.; Liu, R.; Duong, D.; Zhao, B.; Bi, Y.; Zhou, H.; Chen, G.; Seyfried, N.T.; Chazin, W.J.; Kiyokawa, H. and Yin, J. (2018) Identifying the substrate proteins of U-box E3s E4B and CHIP by orthogonal ubiquitin transfer *Science Advances* 4(1)

Biade, S.; Stobbe, C.C. and Chapman, J.D. (1997) The Intrinsic Radiosensitivity of Some Human Tumor Cells Throughout Their Cell Cycles *Radiation Research* 147(4):416-421

Biehs, R.; Steinlage, M.; Barton, O.; Juhász, S.; Künzel, J.; Spies, J.; Shibata, A.; Jeggo, P.A. and Löbrich, M. (2017) DNA Double-Strand Break Resection Occurs during Non-homologous End Joining in G1 but Is Distinct from Resection during Homologous Recombination *Molecular Cell* 65(4):671-684

Birsa, N.; Norkett, R.; Wauer, T.; Mevissen, T.E.T.; Wu, H.C.; Foltynie, T.; Bhatia, K.; Hirst, W.D.; Komander, D.; Plun-Favreau, H. and Kittler, J.T. (2014) Lysine 27 Ubiquitination of the Mitochondrial Transport Protein Miro is Dependent on Serine 65 of the Parkin Ubiquitin Ligase *Journal of Biological Chemistry* 289(21):14569-14582

Blaisdell, J.O.; Harrison, L. and Wallace, S.S. (2001) Base Excision Repair Processing of Radiation-Induced Clustered DNA Lesions *Radiation Protection Dosimetry* 97(1):25-31

Boname, J.M.; Thomas, M.; Stagg, H.R.; Xu, P.; Peng, J. and Lehner, P.J. (2010) Efficient Internalization of MHC I Requires Lysine-11 and Lysine-63 Mixed Linkage Polyubiquitin Chains *Traffic* 11(2):210-220

Boustani, J.; Grapin, M.; Laurent, P.A.; Apetoh, L. and Mirjolet, C. (2019) The 6th R of Radiobiology: Reactivation of Anti-Tumor Immune Response *Cancers* 11(6):860

Brown, P.D.; Chung, C.; Liu, D.D.; McAvoy, S.; Grosshans, D.; Al Feghali, K.; Mahajan, A.; Li, J.; McGovern, S.L.; McAleer, M.F.; Ghia, A.J.; Sulman, E.P.; Penas-Prado, M.; de Groot, J.F.; Heimberger, A.B.; Wang, J.; Armstrong, T.S.; Gilbert, M.R.; Guha-Thakurta, N. and Wefel, J.S. (2021) A Prospective Phase II Randomized Trial of Proton Radiotherapy vs Intensity-Modulated Radiotherapy for Patients with Newly Diagnosed Glioblastoma *Neuro-Oncology* 23(8):1337-1347

Brown, F.N.; Ottaviani, D.; Tazare, J.; Gregson, J.; Kitchen, N.; Brandner, S.; Fersht, N. and Mulholland, P. (2022) Survival Outcomes and Prognostic Factors in Glioblastoma *Cancers (Basel)* 14(13):3161

Buchwald, G.; van der Stoop, P.; Weichenrieder, O.; Perrakis, A.; van Lohuizen, M. and Sixma, T.K. (2006) Structure and E3-Ligase Activity of the Ring-Ring Complex of Polycomb Proteins Bmi1 and Ring1b *The European Molecular Biology Organization Journal* 25:2465-2474

Budhavarapu, V.; White, E.; Mahanic, C.; Chen, L.; Lin, F.T. and Lin, W.C. (2012) Regulation of E2F1 by APC/CCdh1 via K11 Linkage-Specific Ubiquitin Chain Formation *Cell Cycle* 11(10):2030-2038

Budhidarmo, R.; Nakatani, Y. and Day, C.L (2012) RINGs Hold the Key to Ubiquitin Transfer *Trends in Biochemical Sciences* 37(2):58-65

Cao, Z.; Conway, K.L.; Heath, R.J.; Rush, J.S.; Leshchiner, E.S.; Ramirez-Ortiz, Z.G.; Nedelsky, N.B.; Huang, H.; Ng, A.; Gardet, A.; Cheng, S.C.; Shamji A.F.; Rioux, J.D.; Wijmenga, C.; Netea, M.G.; Means, T.K.; Daly, M.J. and Xavier, R.J. (2015) Ubiquitin Ligase TRIM62 Regulates CARD9-Mediated Anti-fungal Immunity and Intestinal Inflammation *Immunity* 43(4):715-726

Chandrashekar, D.S.; Karthikeyan, S.K.; Korla, P.K.; Patel, H.; Shovon, A.R.; Athar, M.; Netto, G.J.; Qin, Z.S.; Kumar, S.; Manne, U.; Creighton, C.J. and Varambally, S. (2022) UALCAN: An Update to the Integrated Cancer Data Analysis Platform *Neoplasia* 25:18-27

Chédeville, A.L. and Madureira, P.A. (2021) The Role of Hypoxia in Glioblastoma Radiotherapy Resistance *Cancers* 13(3):542

Chen, F.; Bhatia, D.; Chang, Q. and Castranova, V. (2006) Finding NEMO by K63-Linked Polyubiquitin Chain *Cell Death & Differentiation* 13:1835-1836

Chen, J.; Li, Y.; Yu, T.S.; McKay, R.M.; Burns, D.K.; Kernie, S.G. and Parada, L.F. (2012) A Restricted Cell Population Propagates Glioblastoma Growth After Chemotherapy *Nature* 448:522-526

Chen, X.; Fu, E.; Lou, H.; Mao, X.; Yan, B.; Tong, F.; Sun, J. and Wei, L. (2019) IL-6 Induced M1 Type Macrophage Polarization Increases Radiosensitivity in HPV-Positive Head and Neck Cancer *Cancer Letters* 456:69-79

Chen, L.L.; Smith, M.D.; Lv, L.; Nakagawa, T.; Li, Z.; Sun, S.C.; Brown, N.G.; Xiong, Y. and Xu, Y.P. (2020) USP15 Suppresses Tumor Immunity via Deubiquitylation and Inactivation of TET2 *Scientific Advances* 6(38):eabc9730

Coderre, J.A. and Morris, G.M. (1999) The radiation biology of boron neutron capture therapy *Radiation Research* 151(1):1-18

Constanzo, J.; Parach, A.; David, T.; Karam, J.; Bruchertseifer, F.; Morgenstern, A.; Jarlier, M.; Bardiès, M.; Deshayes, E.; Gudin-de-Vallerin, A.; Boissière-Michot, F.; Lopez-Crapez, E. and Pouget, J.P. (2025) MHC-I-Driven Antitumor Immunity Counterbalances Low Absorbed Doses of Radiopharmaceutical Therapy *Journal of Nuclear Medicine* 66(5):785-792

Courville, C.B. (1936) Multiple Primary Tumors of the Brain: Review of the Literature and Report of Twenty-one Cases *The American Journal of Cancer* 26(4):703-731

Daley, J.M.; Gaines, W.A.; Kwon, Y.H. and Sung, P. (2014) Regulation of DNA Pairing in Homologous Recombination *Cold Spring Harbor Perspectives in Biology* 6(11):a017954

De Melo, J.; Lin, X.; He, L.; Wei, F.; Major, P. and Tang, D. (2014) SIPL1-Facilitated PTEN Ubiquitination Contributes to its Association with PTEN *Cellular Signalling* 26(12):2749-2756

de Mendonça, M.L.; Coletti, R.; Gonçalves, C.S.; Martins, E.P.; Costa, B.M.; Vinga, S. and Lopes, M.B. (2025) Updating TCGA Glioma Classification Through Integration of Molecular Data Following the Latest WHO Guidelines *Scientific Data* 12:935

Deriano, L.; Guipaud, O.; Merle-Béral, H.; Binet, J.L.; Ricoul, M.; Potocki-Veronese, G.; Favaudon, V.; Maciorowski, Z.; Muller, C.; Salles, B.; Sabatier, L. and Delic, J. (2005) Human Chronic Lymphocytic Leukemia B Cells Can Escape DNA Damage-Induced Apoptosis Through the Nonhomologous End-Joining DNA Repair Pathway *Blood* 105(12):4776-4783

Dhillon, N.; Aggarwal, B.B.; Newman, R.A.; Wolff, R.A.; Kunnumakkara, A.B.; Abbruzzese, J.L.; Ng, C.S.; Badmaev, V. and Kurzrock, R. (2008) Phase II Trial of Curcumin in Patients with Advanced Pancreatic Cancer *Clinical Cancer Research* 14(14):4491-4499

Dianov, G.L.; O'Neill, P. and Goodhead, D.T. (2001) Securing Genome Stability By Orchestrating DNA Repair: Removal of Radiation-Induced Clustered Lesions in DNA *BioEssays* 23(8):745-749

Diehn, M.; Cho, R.W.; Lobo, N.A.; Kalisky, T.; Dorie, M.J.; Kulp, A.N.; Qian, D.; Lam, J.S.; Ailles, L.E.; Wong, M.; Joshua, B.; Kaplan, M.J.; Wapnir, I.; Dirbas, F.M.; Somlo, G.; Garberoglio, C.; Paz, B.; Shen, J.; Lau, S.K.; Quake, S.R.; Brown, J.M.; Weissman, I.L. and Clarke, M.F. (2009) Association of Reactive Oxygen Species Levels and Radioresistance in Cancer Stem Cells *Nature* 485:780-783

Dundar, B.; Alsawas, M.; Masaadeh, A.; Conway, K.; Snow, A.N.; Sompallae, R.R.; Bossler, A.D.; Ma, D. and Neto, O.L.A. (2024) Molecular Characterization and Survival Analysis of a Cohort of Glioblastoma, IDH-Wildtype *Pathology - Research and Practice* 257:155272

Durcan, T.M. and Fon, E.A. (2015) USP8 and PARK2/Parkin-Mediated Mitophagy *Autophagy* 11(2):428-429

Dynek, J.N; Goncharov, T.; Dueber, E.C.; Fedorova, A.V.; Izrael-Tomasevic, A.; Phu, L.; Helgason, E.; Fairbrother, W.J.; Deshayes, K.; Kirkpatrick, D.S. and Vucic, D. (2010) c-IAP1 and UbcH5 Promote K11-Linked Polyubiquitination of RIP1 in TNF Signalling *The European Molecular Biology Organization Journal* 29(24):4198-4209

Eccles, L.J.; O'Neill, P.; Lomax, M.E. (2011) Delayed Repair of Radiation Induced Clustered DNA Damage: Friend or Foe *Mutation Research - Fundamental and Molecular Mechanisms of Mutagenesis* 711(1-2):134-141

Eslamloo, K.; Xue, X.; Booman, M.; Smith, N.C. and Rise, M.L. (2016) Transcriptome Profiling of the Antiviral Immune Response in Atlantic Cod Macrophages *Developmental & Comparative Immunology* 63:187-205

Eslamloo, K.; Inkpen, S.M.; Rise, M.L. and Andreassen, R. (2018) Discovery of microRNAs Associated with the Antiviral Immune Response of Atlantic Cod Macrophages *Molecular Immunology* 93:152-161

Evans, S.M.; Judy, K.D.; Dunphy, I.; Jenkins, W.T.; Hwang, W.T.; Nelson, P.T.; Lustig, R.A.; Jenkins, K.; Magarelli, D.P.; Hahn, S.A.; Collins, R.A.; Grady, M.S. and Koch, C.J. (2004) Hypoxia is Important in the Biology and Aggression of Human Brain Tumours *Clinical Cancer Research* 10(24):8177-8184

Fabbro-Peray, P.; Zouaoui, S.; Darlix, A.; Fabbro, M.; Pallud, J.; Rigau, V.; Mathiew-Daude, H.; Bessaoud, F.; Bauchet, F.; Riondel, A.; Sorbets, E.; Charissoux, M.; Amelot, A.; Mandonnet, E.; Figarella-Branger, D.; Duffau, H.; Tretarre, B.; Taillandier, L. and Bauchet L. (2018) Association of Patterns of Care, Prognostic Factors, and Use of Radiotherapy-Temozolomide Therapy with Survival in Patients with Newly Diagnosed Glioblastoma: a French National Population-Based Study *Journal of Neuro-oncology* 142(1) 91-101

Farr, L.E.; Sweet, W.H.; Robertson, J.S.; Foster, C.G.; Locksley, H.B.; Sutherland, D.L.; Mendelsohn, M.L. and Stickley, E.E. (1954) Neutron capture therapy with boron in the treatment of glioblastoma multiforme *American journal of roentgenology, radium therapy, and nuclear medicine* 71(2):279-293

Fedele, M.; Cerchia, L.; Pegoraro, S.; Sgarra, R. and Manfioletti, G. (2019) Proneural-Mesenchymal Transition: Phenotypic Plasticity to Acquire Multitherapy Resistance in Glioblastoma International Journal of Molecular Sciences 20(11):2746

Fei, C.; Li, Z.; Li, C.; Chen, Y.; Chen, Z.; He, X.; Mao, L.; Wang, X.; Zeng, R. and Li, L. (2013) Smurf1-Mediated Lys29-Linked Nonproteolytic Polyubiquitination of Axin Negatively Regulates Wnt/β-Catenin Signaling *Molecular and Cellular Biology* 33(20):4095-4105

Fischer, T.D.; Bunker, E.N.; Zhu, P.P.; Le Guerroué, F.; Hadjian, M.; Dominguez-Martin, E.; Scavone, F.; Cohen, R.; Yao, T.; Wang, Y.; Werner, A. and Youle, R.J. (2025) STING Induces HOIP-Mediated Synthesis of M1 Ubiquitin Chains to Stimulate NF-κB Signaling *The European Molecular Biology Organization Journal* 44:141-165

Fleming, J.; Magana, P.; Nair, S.; Tsenkov, M.; Bertoni, D.; Pidruchna, I.; Afonso, M.Q.L.; Midlik, A.; Paramval, U.; Žídek, A.; Laydon, A.; Kovalevskiy, O.; Pan, J.; Cheng, J.; Avsec, Ž.; Bycroft, C.; Wong, L.H.; Last, M.; Mirdita, M.; Steinegger, M.; Kohli, P.; Váradi, M. and Velankar, S. (2025) AlphaFold Protein Structure Database and 3D-Beacons: New Data and Capabilities *Journal of Molecular Biology* 437(15):168967

Flick, K.; Ouni, I.; Wohlschlegel, J.A.; Capati, C.; McDonald, W.H.; Yates 3rd, J.R. and Kaiser, P. (2004) Proteolysis-Independent Regulation of the Transcription Factor Met4 by a Single Lys48-Linked Ubiquitin Chain *Nature Cell Biology* 6:634-641

Freemont, P.S.; Hanson, I.M. and Trowsdale, J. (1991) A Novel Cysteine-Rich Sequence Motif *Cell* 64(3):483-484

French, M.E.; Koehler, C.F. and Hunter, T. (2021) Emerging Functions of Branched Ubiquitin Chains *Cell Discovery* 7:6

Friedmann-Morvinski, D.; Bushong, E.A.; Ke, E.; Soda, Y.; Marumoto, T.; Singer, O.; Ellisman, M.H. and Verma, I.M. (2012) Dedifferentiation of Neurons and Astrocytes by Oncogenes Can Induce Gliomas in Mice *Science* 338(6110):1080-1084

Ghosh, M.; Niyogi, S.; Bhattacharyya, M.; Adak, M.; Nayak, D.K.; Chakrabarti, S. and Chakrabarti, P. (2016) Ubiquitin Ligase COP1 Controls Hepatic Fat Metabolism by Targeting ATGL for Degradation *Diabetes* 65(12):3561-3572

Goetz, J.D.M.; Motycka, T.A.; Han, M.; Jasin, M. and Tomkinson, A.E. (2005) Reduced Repair of DNA Double-Strand Breaks by Homologous Recombination in a DNA Ligase I-Deficient Human Cell Line *DNA Repair* 4(6):649-654

Goodwin, J.T.; Farr, L.E.; Sweet, W.H. and Robertson, J.S. (1955) Pathological study of eight patients with glioblastoma multiforme treated by neutron-capture therapy using boron 10 *Cancer* 8(3):601-615

Graf, R.; Hildebrandt, B.; Tilly, W.; Sreenivasa, G.; Ullrich, R.; Maier-Hauff, K.; Felix, R. and Wust, P. (2005) Dose-Escalated Conformal Radiotherapy of Glioblastomas - Results of a Retrospective Comparison Applying Radiation Doses of 60 and 70 Gy *Onkologie* 28(6-7):325-330

Graus, F.; Bruna, J.; Pardo, J.; Escudero, D.; Vilas, D.; Barceló I.; Brell, M.; Pascual, C.; Crespo, J.A.; Erro, E.; García-Romero, J.C.; Estela, J.; Martino, J.; García-Castaño, A.; Lema, E.M.M.; Gelabert, M.; Fuentes, R.; Pérez, P.; Manzano, A.; Aguas, J.; Belenguer, A.; Simón, A.; Henríquez, I.; Murcia, M.; Vivanco, R.; Rojas-Marcos, I.; Muñoz-Carmona, D.; Navas, I.; de Andrés, P.; Mas, G.; Gil, M. and Verger, E. (2013) Patterns of Care and Outcome for Patients with Glioblastoma Diagnosed During 2008-2010 in Spain *Neuro-Oncology* 15(6):797-805

Grimes, D.R. and Partridge, M. (2015) A Mechanistic Investigation of the Oxygen Fixation Hypothesis and Oxygen Enhancement Ratio *Biomedical Physical Engineering Express* 1:045209

Gunther, J.R.; Chadha, A.S.; Guha, S.; Raju, G.S.; Maru, D.M.; Munsell, M.F.; Jiang, Y.; Yang, P.; Felix, E.; Clemons, M.; Mathew, G.G.; Singh, P.K.; Skibber, J.M.; Rodriguez-Bigas, M.A.; Chang, G.J.; Eng, C.; Delclos, M.E.; Crane, C.H.; Das, P. and Krishnan, S. (2022) A Phase II Randomized Double Blinded Trial Evaluating the Efficacy of Curcumin with Pre-Operative Chemoradiation for Rectal Cancer *Journal of Gastrointestingal Oncology* 13(6):2938-2950

Haahr, P.; Borgermann, N.; Guo, X.; Typas, D.; Achuthankutty, D.; Hoffmann, S.; Shearer, R.; Sixma, T.K. and Mailand, N. (2018) ZUFSP Deubiquitylates K63-Linked Polyubiquitin Chains to Promote Genome Stability *Molecular Cell* 70(1):165-174

Haakonsen, D.L. and Rape, M. (2019) Branching Out: Improved Signaling by Heterotypic Ubiquitin Chains *Trends in Cell Biology* 29(9):704-716

Haglund, K.; Sigismund, S.; Polo, S.; Szymkiewicz, I.; Di Fiore, P.P. and Dikic, I. (2003) Multiple Monoubiquitination of RTKs is Sufficient for Their Endocytosis and Degradation *Nature Cell Biology* 5:461-466

Hao, H.; Wang, W.; Yang, M.; Peng, B.; Bai, S.; Gu, W.; Zhang, W.; Xing, G. and Li, J. (2026) Evaluating the Boron Neutron Capture Therapeutic Threshold of Boron-Containing Carbon Dots in Diverse Tumor Cell Lines *Disease & Research*

Hassink, G.; Slotman, J.; Oorschot, V.; Van Der Reijden, B.A.; Monteferrario, D.; Noordermeer, S.M.; Van Kerkhof, P.; Klumperman, J. and Strous, G.J. (2012) Identification of the Ubiquitin Ligase Triad1 as a Regulator of Endosomal Transport *Biology Open* 1(6):607-614

Hatakeyama, S.; Yada, M.; Matsumoto, M.; Ishida, N. and Nakayama, K.I. (2001) U Box Proteins as a New Family of Ubiquitin-Protein Ligases *Journal of Biological Chemistry* 276(35):33111-33120

He, L.; Zhang, A.; Xiong, L.; Li, Y.; Huang, R.; Liao, L.; Zhu, Z. and Wang, Y. (2017) Deep Circular RNA Sequencing Provides Insights into the Mechanism Underlying Grass Carp Reovirus Infection *International Journal of Molecular Sciences* 18(9):1977

He, T.; Guo, J.; Song, H.; Zhu, H.; Di, X.; Min, H.; Wang, Y.; Chen, G.; Dai, W.; Ma, J.; Sun, X. and Ma, J. (2018) Nutlin-3, an Antagonist of MDM2, Enhances the Radiosensitivity of Esophageal Squamous Cancer with Wild-Type p53 Pathology *Oncology Research* 24(1):75-81

Hedges, J.C.; Hanna, C.B.; Shorey-Kendrick, L.E.; Boniface, E.R.; Bash, J.C.; Rice-Stitt, T.L.; Burch, F.C.; D'Mello, R.; Morgan, T.K.M.; Lima, A.C.; Terrobia, J.J.D.; Graham, J.A.; Mishler, E.C.; Jensen, J.V.; Hagen, O.L.; Urian, J.W.; Spindel, E.R.; Easley, C.A.; Murphy, S.K. and Lo, J.O. (2023) Cessation of Chronic Delta-9-Tetrahydrocannabinol Use Partially Reverses Impacts on Male Fertility and the Sperm Epigenome in Rhesus Macaques *Fertility and Sterility* 120(1):163-174

Held, K.D. (1988) Models for Thiol Protection of DNA in Cells *Pharmacology & Therapeutics* 39(1-3):123-131

Hennessey, D.; Martin. L.M.; Atzberger, A.; Lynch, T.H.; Hollywood, D. and Marignol, L. (2013) Exposure to Hypoxia Following Increases Radioresistance in Prostate Cancer Cells *Urologic Oncology: Seminars and Original Investigations* 31(7):1106-1116

Ho, H.N. and West, S.C. (2022) Generation of Double Holliday Junction DNAs and Their Dissolution/Resolution Within a Chromatin Context *Proceedings of the National Academy of Sciences* 119(18):e2123420119

Hochrainer, K.; Mayer, H.; Baranyi, U.; Binder, B.R.; Lipp, J. and Kroismayr, R. (2005) The Human HERC Family of Ubiquitin Ligases: Novel Members, Genomic Organization, Expression Profiling, and Evolutionary Aspects *Genomics* 85(2):153-164

Hochrainer, K.; Kroismayr, R.; Baranyi, U.; Binder, B.R. and Lipp, J. (2008) Highly Homologous HERC Proteins Localize to Endosomes and Exhibit Specific Interactions with hPLIC and Nm23B *Cellular and Molecular Life Sciences* 65:2105-2117

Holloman, W.K. (2011) Unraveling the mechanism of BRCA2 in homologous recombination *Nature Structural and Molecular Biology* 18:748-754

Horan, A.D.; Giandomenico, A.R. and Koch, C.J. (1999) Effect of Oxygen on Radiation-Induced DNA Damage in Isolated Nuclei *Radiation Research* 152(2):144-153

Hsueh, W.T.; Chang, K.Y.; Chuang, J.Y.; Liu, M.S.; Chung, P.H.; Chu, J.M. and Chien, C.H. (2025) SOD2-mediated TMZ-resistant Glioblastoma Cells Exhibit Cross-resistance to Irradiation *Anticancer Research* 45(9):3711-3718

Hu, Q.; Botuyan, M.V.; Zhao, D.; Cui, G.; Mer, E. and Mer, G. (2021) Mechanisms of BRCA1-BARD1 Nucleosome Recognition and Ubiquitylation *Nature* 596:438-443

Huang, H.; Jeon, M.S.; Liao, L.; Yang, C.; Elly, C.; Yates 3rd, J.R. and Liu, Y.C. (2010) K33-Linked Polyubiquitination of T Cell Receptor-ζ Regulates Proteolysis-Independent T Cell Signaling *Immunity* 33(1):60-70

Huang, X.; Li, X.; Xie, X.; Ye, F.; Chen, B.; Song, C.; Tang, H. and Xie, X. (2016) High Expressions of LDHA and AMPK as Prognostic Biomarkers for Breast Cancer *The Breast* 30:39-46

Huang, F.; Tang, X.; Sun, T.; Wang, G.; Ru, Q. and Zheng, Y. (2021) SAV1, Regulated by HERC4, Inhibits the Proliferation, Migration, and Invasion of Hepatocellular Carcinoma *Translational Cancer Research* 10(1):349-360

Hughes, J.R. and Parsons, J.L. (2020) FLASH Radiotherapy: Current Knowledge and Future Insights Using Proton-Beam Therapy *International Journal of Molecular Sciences* 21(18):6492

Huibregtse, J.M.; Scheffner, M.; Beaudenon, S. and Howley, P.M. (1995) A Family of Proteins Structurally and Functionally Related to the E6-AP Ubiquitin-Protein Ligase *Proceedings of the National Academy of Sciences* 92(7):2563-2567

Ichimura, K.; Pearson, D.M.; Kocialkowski, S.; Baecklund, L.M.; Chan, R.; Jones, D.T.W.; Collins, V.P. (2009) IDH1 mutations are present in the majority of common adult gliomas but rare in primary glioblastomas *Neuro-Oncology* 11(4):341-347

Iconomou, M. and Saunders, D.N. (2016) Systematic Approaches to Identify E3 Ligase Substrates *Biochemical Journal* 473(22):4083-4101

Infantino, V.; Santarsiero, A.; Convertini, P.; Todisco, S. and Iacobazzi, V. (2021) Cancer Cell Metabolism in Hypoxia: Role of HIF-1 as Key Regulator and Therapeutic Target *International Journal of Molecular Science* 22(11):5703

Inoue, Y. and Imamura, T. (2008) Regulation of TGF-β Family Signaling by E3 Ubiquitin Ligases *Cancer Science* 99(11):2107-2112

Jafri, N.F.; Clarke, J.L.; Weinberg, V.; Barani, I.J. and Cha, S. (2013) Relationship of Glioblastoma Multiforme to the Subventricular Zone is Associated with Survival *Neuro-Oncology* 15(1):91-96

Jayakumar, S.; Kunwar, A.; Sandur, S.K.; Pandey, B.N. and Chaubey, R.C. (2014) Differential Response of DU145 and PC3 Prostate Cancer Cells to Ionizing Radiation: Role of Reactive Oxygen Species, GSH and Nrf2 in Radiosensitivity *Biochimica et Biophysica Acta - General Subjects* 1840(1):485-494

Jiang, J.; Ballinger, C.A.; Wu, Y.; Dai, Q.; Cyr, D.M.; Höhfeld, J. and Patterson, C. (2001) CHIP Is a U-box-dependent E3 Ubiquitin Ligase Identification of HSC70 as a Target for Ubiquitylation *Journal of Biological Chemistry* 276(46):42938-42944

Jiang, W.; Zhou, F.; Li, N.; Li, Q. and Wang, L. (2015) FOXM1-LDHA Signaling Promoted Gastric Cancer Glycolytic Phenotype and Progression *International Journal of Clinical and Experimental Pathology* 8(6):6756-6763

Jiang, W.; Yao, X.; Shan, Z.; Li, W.; Gao, Y. and Zhang, Q. (2019) E3 Ligase Herc4 Regulates Hedgehog Signalling Through Promoting Smoothened Degradation *Journal of Molecular Cell Biology* 11(9):791-803

Jiang, X.; Li, Y.; Zhang, N.; Gao, Y.; Han, L.; Li, S.; Li, J.; Liu, X.; Gong, Y. and Xie, C. (2021) RRM2 Silencing Suppresses Malignant Phenotype and Enhances Radiosensitivity via Activating cGAS/STING Signaling Pathway in Lung Adenocarcinoma *Cell & Bioscience* 11(74)

Jin, J.; Li, X.; Gygi, S.P. and Harper, J.W. (2007) Dual E1 Activation Systems for Ubiquitin Differentially Regulate E2 Enzyme Charging *Nature* 447:1135-1138

Jumper, J.; Evans, R.; Pritzel, A.; Green, T.; Figurnov, M.; Ronneberger, O.; Tunyasuvunakool, K.; Bates, R.; Žídek, A.; Potapenko, A.; Bridgland, A.; Meyer, C.; Kohl, S.A.A.; Ballard, A.J.; Cowie, A.; Romera-Paredes, B.; Nikolov, S.; Jain, R.; Adler, J.; Back, T.; Petersen, S.; Reiman, D.; Clancy, E.; Zielinski, M.; Steinegger, M.; Pacholska, M.; Berghammer, T.; Bodenstein, S.; Silver, D.; Vinyals, O.; Senior, A.W.; Kavukcuoglu, K.; Kohli, P. and Hassabis, D. (2021) Highly Accurate Protein Structure Prediction with AlphaFold *Nature* 596:583-589

Kamadurai, H.B.; Qiu, Y.; Deng, A.; Harrison, J.S.; MacDonald, C.; Actis, M.; Rodrigues, P.; Miller, D.J.; Souphron, J.; Lewis, S.M.; Kurinov, I.; Fujii, N.; Hammel, M.; Piper, R.; Kuhlman, B. and Schulman, B.A. (2013) Mechanism of Ubiquitin Ligation and Lysine Prioritization by a HECT E3 *eLife* 2:e00828

Kane, E.I.; Beasley, S.A.; Schafer, J.M.; Bohl, J.E.; Lee, Y.S.; Rich, K.J.; Bosia, E.F. and Spratt, D.E. (2022) Redefining the Catalytic HECT Domain Boundaries for the HECT E3 Ubiquitin Ligase Family *Bioscience Reports* 42(10):BSR20221036

Karanam, K.; Kafri, R.; Loewer, A. and Lahav, G. (2012) Quantitative Live Cell Imaging Reveals a Gradual Shift Between DNA Repair Mechanisms and a Maximal Use of HR in Mid-S Phase *Molecular Cell* 47(2):320-329

Kawabata, S.; Miyatake, S.I.; Nonoguchi, N.; Hiramatsu, R.; Iida, K.; Miyata, S.; Yokoyama, K.; Doi, A.; Kuroda, Y.; Kuroiwa, T.; Michiue, H.; Kumada, H.; Kirihata, M.; Imahori, Y.; Maruhashi, A.; Sakurai, Y.; Suzuki, M.; Masunaga, S.I. and Ono, K. (2009) Survival benefit from boron neutron capture therapy for the newly diagnosed glioblastoma patients *Applied Radiation and Isotopes* 67(7-8):S15-S18

Kim, J.J. and Tannock, I.A. (2005) Repopulation of Cancer Cells During Therapy: an Important Cause of Treatment Failure *Nature Reviews Cancer* 5:516-525

Kim, J.S.; Krasieva, T.B.; Kurumizaka, H.; Chen, D.J.; Taylor, A.M.R. and Yokomori, K. (2005) Independent and Sequential Recruitment of NHEJ and HR Factors to DNA Damage Sites in Mammalian Cells *Journal of Cell Biology* 170(3):341-347

Kim, H.; Vick, P.; Hedtke, J.; Ploper, D. and De Robertis, E.M. (2015) Wnt Signaling Translocates Lys48-Linked Polyubiquitinated Proteins to the Lysosomal Pathway *Cell Reports* 11(8):1151-1159

Kim, W.; Youn, H.S.; Lee, S.; Kim, E.G.; Kim, D.; Lee, J.S.; Lee, J.M. and Youn, B.H. (2018) RNF138-Mediated Ubiquitination of rpS3 is Required for Resistance of Glioblastoma Cells to Radiation-Induced Apoptosis *Experimental & Molecular Medicine* 50:e434

Kim, J.Y.; Jung, C.W.; Lee, W.S.; Kim, H.J.; Jeong, H.J.; Park, M.J.; Jang, W.I. and Kim, E.H. (2022) Interaction of Curcumin with Glioblastoma Cells via High and Low Linear Energy Radiation Therapy Inducing Radiosensitization Effects *Journal of Radiation Research* 63(3):342-353

Kim, D.H.; Kim, S.L.; Sing, V. and Ramakrishna, S. (2024) Usp7 Regulates Glial Lineage Cell-Specific Transcription Factors by Modulating Histone H2B Monoubiquitination *International Journal of Stem Cells* 17(4):427-436

Koegl, M.; Hoppe, T.; Schlenker, S.; Ulrich, H.D.; Mayer, T.U. and Jentsch, S. (1999) A Novel Ubiquitination Factor, E4, Is Involved in Multiubiquitin Chain Assembly *Cell* 96(5):635-644

Koldenhof, P.; Bemelmans, M.P.; Ghosh, B.; Damm-Ganamet, K.L.; van Vlijmen, H.W.T. and Pande, V. (2024) Application of AlphaFold Models in Evaluating Ligandable Cysteines Across E3 Ligases *Proteins: Structure, Function, and Bioinformatics* 92(7):819-829

Krejci, L.; Altmannova, V.; Spirek, M. and Zhao, X. (2012) Homologous Recombination and Its Regulation *Nucleic Acids Research* 40(13):5795-5818

Krishnamoorthy, K. and Prasa, M. (2026) Glioblastoma treatment with Boron Neutron Capture Therapy (BNCT): a revolutionary approach *Holistic Integrative Oncology* 5(2)

Kühnle, S.; Kogel, U.; Glockzin, S.; Marquardt, A.; Ciechanover, A.; Matentzoglu, K. and Scheffner, M. (2011) Physical and Functional Interaction of the HECT Ubiquitin-protein Ligases E6AP and HERC2 *Journal of Biological Chemistry* 286(22):19410-19416

Kunkel, M.; Moergel, M.; Stockinger, M.; Jeong, J.H.; Fritz, G.e; Lehr, H.A. and Whiteside T.L. (2007) Overexpression of GLUT-1 is Associated With Resistance to Radiotherapy and Adverse Prognosis in Squamous Cell Carcinoma of the Oral Cavity Oral Oncology 43(8):796-803

La Rosa, P.; Pesiri, V.; Marino, M. and Acconcia, F. (2011) 17β-Estradiol-Induced Cell Proliferation Requires Estrogen Receptor (ER) α Monoubiquitination *Cellular Signalling* 23(7):1128-1135

Lawrence, D.W. and Kornbluth, J. (2016) E3 Ubiquitin Ligase NKLAM Ubiquitinates STAT1 and Positively Regulates STAT1-Mediated Transcriptional Activity *Cellular Signalling* 28(12):1833-1841

Le, A.; Cooper, C.R.; Gouw, A.M.; Dinavahi, R.; Maitra, A.; Deck, L.M.; Royer, R.E.; Jagt, D.L.V.; Semenza, G.L. and Dang, C.V. (2010) Inhibition of Lactate Dehydrogenase A Induces Oxidative Stress and Inhibits Tumor Progression *Proceedings of the National Academy of Sciences USA* 107(5):2037-2042

Leach, J.K.; Van Tuyle, G.; Lin, P.S.; Schmidt-Ullrich, R. and Mikkelsen, R.B. (2001) Ionizing Radiation-induced, Mitochondria-dependent Generation of Reactive Oxygen/Nitrogen *Biochemistry and Biophysics* 61(10):3894-3901

Lee, K.J.; Saha, J.; Sun, J.; Fattah, K.R.; Wang, S.C.; Jakob, B.; Chi, L.; Wang, S.Y.; Taucher-Scholz, G.; Davis, A.J. and Chen, D.J. (2016) Phosphorylation of Ku dictates DNA double-strand break (DSB) repair choice in S phase *Nucleic Acids Research* 44(4):1732-1745

Lee, J.H.; Lee, J.E.; Kahng, J.Y.; Kim, S.H.; Park, J.S.; Yoon, S.J.; Um, J.Y.; Kim, W.K.; Lee, J.K.; Park, J.; Kim, E.H.; Lee, J.H.; Lee, J.H.; Chung, W.S.; Ju, Y.S.; Park, S.H.; Chang, J.H.; Kang, S.G. and Lee, J.H. (2018) Human Glioblastoma Arises from Subventricular Zone Cells with Low-Level Driver Mutations *Nature* 560(7717):243-247

Lehman, S.L.; Wechsler, T.; Schwartz, K.; Brown, L.E.; Porco Jr, J.A.; Devine, W.G.; Pelletier, J.; Shankavaram, U.T.; Camphausen, K. and Tofilon, P.J. (2023) Inhibition of the Translation Initiation Factor eIF4A Enhances Tumor Cell Radiosensitivity *Molecular Cancer Therapeutics* 21(9):1406-1414

Lendeckel, U.; Venz, S. and Wolke, C. (2022) Macrophages: Shapes and Function *Textbook Journal of Chemistry* 8(2):12

Li, W.; Bengtson, M.H.; Ulbrich, A.; Matsuda, A.; Reddy, V.A.; Orth, A.; Chanda, S.K.; Batalov, S. and Joazeiro, C.A.P. (2008) Genome-Wide and Functional Annotation of Human E3 Ubiquitin Ligases Identifies MULAN, a Mitochondrial E3 that Regulates the Organelle's Dynamics and Signaling *Public Library Of Science One* 1:e1487

Li, X. and Heyer, W.D. (2008) Homologous Recombination in DNA Repair and DNA Damage Tolerance *Cell Research* 18:99-113

Li, X. and Heyer, W.D. (2009) RAD54 controls access to the invading 3'-OH end after RAD51-mediated DNA strand invasion in homologous recombination in *Saccharomyces cerevisiae Nucleic Acids Research* 37(2):638-646

Li, J.; Zhu, S.; Tong, J.; Hao, H.; Yang, J.; Liu, Z. and Wang, Y. (2016) Suppression of Lactate Dehydrogenase A Compromises Tumor Progression by Downregulation of the Warburg Effect in Glioblastoma *NeuroReport* 27(2):110-115

Li, H.; Yang, B.Y.; Liu, M.M.; Zhao, S.W.; Xie, S.Z.; Wang, H.; Zhang, S.; Xuan, X.N. and Jia, L.J. (2021) Reproductive Injury in Male BALB/c Mice Infected with *Neospora caninum*. *Parasites & Vectors* 14:158

Li, C.; Liao, J.; Wang, X.; Chen, F.X.; Guo, X. and Chen, X. (2023 a) Combined Aurora Kinase A and CHK1 Inhibition Enhances Radiosensitivity of Triple-Negative Breast Cancer Through Induction of Apoptosis and Mitotic Catastrophe Associated With Excessive DNA Damage Internation *Journal of Radiation Oncology*Biology*Physics* 5(1):1241-1254

Li, G.; Zhang, T.; Hu, B.; Han, S.; Xiang, C.; Yuan, G. and He, H. (2023 b) Infection of Trichinella spiralis Affects the Reproductive Capacity of ICR/CD-1 Male Mice by Reducing the Urine Pheromone Contents and Sperm Quality *International Journal of Molecular Science* 24(6):5731

Lin, Y.; Wang, Y. and Li, P.F. (2022) Mutual Regulation of Lactate Dehydrogenase and Redox Robustness *Frontiers in Physiology* 13(2022)

Lin, X.; Hu, S.; Huang, L.; Xu, T. and Lai, J. (2025) Glycolysis-Related Radiosensitivity Signature for Predicting Radiotherapy Response in Breast Cancer *Frontiers in Immunology* 16(2025)

Liu, C.; Sage, J.C.; Miller, M.R.; Verhaak, R.G.W.; Hippenmeyer, S.; Vogel, H.; Foreman, O.; Bronson, R.T.; Nishiyama, A.; Luo, L. and Zong, H. (2011) Mosaic Analysis with Double Markers Reveals Tumor Cell of Origin in Glioma *Cell* 146(2):209-221

Liu, S.; Song, L.; Zhang, L.; Zeng, S. and Gao, F. (2015) miR-21 Modulates Resistance of HR-HPV Positive Cervical Cancer Cells to Radiation Through Targeting LATS1 *Biochemical and Biophysical Research Communications* 459(4):679-685

Liu, C.; Liu, W.; Ye, Y. and Li, W. (2017) Ufd2p Synthesizes Branched Ubiquitin Chains to Promote the Degradation of Substrates Modified with Atypical Chains *Nature Communication* 8:14274

Liu, P.; Gan, W.; Su, S.; Hauenstein, A.V.; Fu, T.M.; Brasher, B.; Schwerdtfeger, C.; Liang, A.C.; Xu, M. and Wei, W. (2018) K63-Linked Polyubiquitin Chains Bind to DNA to Facilitate DNA Damage Repair *Science Signaling* 11(533):eaar8133

Liu, C.; Fan, C.; Liu, J.; Zhang, S.; Tang, H.; Liu, Y.; Zhang, S.; Wu, Q.; Zhang, J.; Qi, Z. and Shen, Y. (2024a) YOD1 Protects Against MRSA Sepsis-Induced DIC Through Lys33-Linked Deubiquitination of NLRP3 *Cell Death & Disease* 15:360

Liu, M.; Zhao, Z.; Wang, C.; Sang, S.; Cui, Y.; Lv, C.; Yang, X.; Zhang, N.; Xiong, K.; Chen, B.; Dong, Q.; Liu, K. and Gu, Y. (2024b) Harnessing Genetic Interactions for Prediction of Immune Checkpoint Inhibitors Response Signature in Cancer Cells *Cancer Letters* 594:216991

Locke, M.; Toth, J.I. and Petroski, M.D. (2014) Lys11- and Lys48-Linked Ubiquitin Chains Interact with p97 During Endoplasmic-Reticulum-Associated Degradation *Biochemical Journal* 459(1):205-216

Lok, B.H. and Powell, S.N. (2012) Molecular Pathways: Understanding the Role of Rad52 in Homologous Recombination for Therapeutic Advancement *Clinical Cancer Research* 18(23):6400-6406

Lomax, M.E.; Gulston, M.K. and O'Neill, P.O. (2002) Chemical Aspects of Clustered DNA Damage Induction by Ionising Radiation *Radiation Protection Dosimetry* 99(1-4):63-68

Lomax, M.E.; Folkes, L.K. and O'Neill, P. (2013) Biological Consequences of Radiation-induced DNA Damage: Relevance to Radiotherapy *Clinical Oncology* 25(10):578-585

Loparo, J.L. (2023) Holding It Together: DNA End Synapsis During Non-Homologous End Joining *DNA Repair (Amsterdam)* 130:103553

López-Vázquez, C.; Souto, S.; Olveira, J.G.; Riaza, A.; González, Ó.; Brea, C.; Labella, A.M.; Castro, D. and Bandín, I. (2023) Nervous Necrosis Virus (NNV) Booster Vaccination Increases Senegalese Sole Survival and Enhances Immunoprotection *Animals* 13(1):51

Louis, D.N.; Perry, A.; Wesseling, P.; Brat, D.J.; Cree, I.A.; Figarella-Branger, D.; Hawkins, C.; Ng, H.K.; Pfister, S.M.; Reifenberger, G.; Soffietti, R.; von Deimling, A.; Ellison, D.W (2021) The 2021 WHO Classification of Tumors of the Central Nervous System: a Summary *Neuro-Oncology* 23(8):1231-1251

Lovering, R.; Hanson, I.M.; Borden, K.L.; Martin, S.; O'Reilly, N.J.; Rahman, D.; Pappin, D.J.; Trowsdale, J. and Freemont, P.S. (1993) Identification and Preliminary Characterization of a Protein Motif Related to Zinc Finger *Proceedings of the National Academy of Sciences* 90(6):2112-2116

Maciejewski, B. and Majewski, S. (1991) Dose Fractionation and Tumour Repopulation in Radiotherapy for Bladder Cancer *Radiation Oncology* 21(3):163-170

Macip, S.; Igarashi, M.; Berggren, P.; Yu, J.; Lee, S.W. and Aaronson, S.A. (2003) Influence of Induced Reactive Oxygen Species in p53-Mediated Cell Fate Decisions *Cell Growth and Development* 23(23):8576-8585

Mackenzie, K.J.; Carroll, P.; Martin, C.A.; Murina, O.; Fluteau, A.; Simpson, D.; Olova, N.; Sutcliffe, H.; Rainger, J.; Robertson, A.; Osborn, R.; Wheeler, A.; Nowotny, M.; Gilbert, N.; Chandra, T.; Reijns, M.A.M. and Jackson, A.P. (2018) cGAS Surveillance of Micronuclei Links Genome Instability to Innate Immunity *Nature* 548(7668):461-465

Mao, Z.; Bozzella, M.; Seluanov, A. and Gorbunova, V. (2009) DNA Repair by Nonhomologous End Joining and Homologous Recombination During Cell Cycle in Human Cells *Cell Cycle* 7(18):2902-2906

Marallano, V.J.; Ughetta, M.E.; Tejero, R.; Nanda, S.; Ramalingam, R.; Stalbow, L.; Sattiraju, A.; Huang, Y.; Ramakrishnan, A.; Shen, L.; Wojcinski, A.; Kesari, S.; Zou, H.; Tsankov, A.M. and Friedel, R.H. (2024) Hypoxia drives shared and distinct transcriptomic changes in two invasive glioma stem cell lines *Scientific Reports* 14:7246

Marín, I.; Lucas, I.; Gradilla, A.C. and Ferrús, A. (2003) Parkin and Relatives: the RBR Family of Ubiquitin Ligases *Phsyiological Genomics* 17(3):253-263

Martínez-Jiménez, F.; Muiños, F.; López-Arribillaga, E.; Lopez-Bigas, N. and Gonzalez-Perez, A. (2019) Systematic Analysis of Alterations in the Ubiquitin Proteolysis System Reveals its Contribution to Driver Mutations in Cancer *Nature Cancer* 1:122-135

Maspero, E.; Valentini, E.; Mari, S.; Cecatiello, V.; Soffientini, P.; Pasqualato, S. and Polo, S. (2013) Structure of a Ubiquitin-Loaded HECT Ligase Reveals the Molecular Basis for Catalytic Priming *Nature Structural & Molecular Biology* 20:696-701

Matos, J. and West, S.C. (2014) Holliday Junction Resolution: Regulation in Space and Time *DNA Repair* 19:176-181

McCutcheon, I.E. and Preul, M.C. (2021) Historical Perspective on Surgery and Survival with Glioblastoma: How Far Have We Come? *World Neurosurgery* 149:148-168

McDowell, G.S. and Philpott, A. (2016) Chapter Two- New Insights Into the Role of Ubiquitylation of Proteins *International Review of Cell and Molecular Biology* 325:35-88

McVey, M.; Khodaverdian, V.Y.; Meyer, D.; Cerqueira, P.G. and Heyer, W.D. (2016) Eukaryotic DNA Polymerases in Homologous Recombination *Annual Review of Genetics* 50:393-421

Melia, E.; Fisch, A.S.; Tinhofer, I. and Parsons, J.L. (2025) Targeting Chk1 and Wee1 Kinases Enhances Radiosensitivity of 2D and 3D Head and Neck Cancer Models to X-rays and Low/High-LET Protons *Cell Death & Disease* 16(128)

Menegakis, A.; Klompmaker, R.; Vennin, C.; Arbusà, A.; Damen, M.; van den Broek, B.; Zips, D.; van Rheenen, J.; Krenning, L. and Medema, R.H. (2021) Resistance of Hypoxic Cells to Ionizing Radiation is Mediated in Part via Hypoxia-Induced Quiescence *Cells* 10(3):610

Metzger, M.B.; Pruneda, J.N.; Klevit, R.E. and Weissman, A.M. (2014) RING-Type E3 Ligases: Master Manipulators of E2 Ubiquitin-Conjugating Enzymes and Ubiquitination *Biochimica et Biophysica Acta - Molecular Cell Research* 1843(1):47-60

Miao, Z.; Xu, L.; Gu, W.; Ren, Y.; Li, R.; Zhang, S.; Chen, C.; Wang, H.; Ji, J. and Chen, J. (2024) A Targetable PRR11-DHODH Axis Drives Ferroptosis- and Temozolomide-Resistance in Glioblastoma *Redox Biology* 73:103220

Milanovic, M.; Fan, D.N.Y.; Belenki, D.; Däbritz, J.H.M.; Zhao, Z.; Yu, Y.; Dörr, J.R.; Dimitrova, L.; Lenze, D.; Barbosa, I.A.M.; Mendoza-Parra, M.A.; Kanashova, T.; Metzner, M.; Pardon, K.; Reimann, M.; Trumpp, A.; Dörken, B.; Zuber, J.; Gronemeyer, H.; Hummel, M.; Dittmar, G.; Lee, S. and Schmitt, C.A. (2018) Senescence-Associated Reprogramming Promotes Cancer Stemness *Nature* 553(7686):96-100

Mishra, S.; Krawic, C.; Luczak, M.W. and Zhitkovich, A. (2024) Monoubiquitinated H2B, a Main Chromatin Target of Formaldehyde, Is Important for S-Phase Checkpoint Signaling and Genome Stability *Molecular Carcinogenesis* 63(12):2414-2424

Mitchel, R.B. (1883) Two Cases of Brain-Tumour *Edinburgh Medical Journal* 29(5):430-437

Morett, E. and Bork, P. (1999) A Novel Transactivation Domain in Parkin *Trends in Biochemical Sciences* 24(6):229-231

Moroishi, T.; Yamauchi, T.; Nishiyama, M. and Nakayama, K.I. (2014) HERC2 Targets the Iron Regulator FBXL5 for Degradation and Modulates Iron Metabolism *Protein Synthesis and Degradation* 289(23):16430-16441

Mowat, C.; Mosley, S.R.; Namdar, Schiller, D. and Baker, K. (2021) Anti-Tumor Immunity in Mismatch Repair-Deficient Colorectal Cancers Requires Type I IFN-Driven CCL5 and CXCL10 *Journal of Experimental Medicine* 218(9):e20210108

Musah-Eroje, A. and Watson, S. (2019) Adaptive Changes of Glioblastoma Cells Following Exposure to Hypoxic (1% Oxygen) Tumour Microenvironment *Internation Journal of Molecular Sciences* 20(9):2091

Mutlu, M.; Schmidt, I.; Morrison, A.I.; Goretzki, B.; Freuler, F.; Begue, D.; Simic, O.; Pythoud, N.; Ahrne, E.; Kapps, S.; Roest, S.; Bonenfant, D.; Jeanpierre, D.; Tran, T.T.T.; Maher, R.; An, S.; Rietsch, A.; Nigsch, F.; Hofmann, A.; Reece-Hoyes, J.; Parker, C.N. and Guerini, D. (2024) Small Molecule Induced STING Degradation Facilitated by the HECT Ligase HERC4 *Nature Communications* 15:4584

Muz, B.; de la Puente, P.; Azab, F. and Azab, A.K. (2015) The Role of Hypoxia in Cancer Progression, Angiogenesis, Metastasis, and Resistance to Therapy *Hypoxia (Auckland)* 3:83-92

Nagase, T.; Kikuno, R.; Ishikawa, K.; Hirosawa, M. and Ohara, O. (2000) Prediction of the Coding Sequences of Unidentified Human Genes. XVI. The Complete Sequences of 150 New cDNA Clones from Brain Which Code for Large Proteins *in Vitro*. *DNA Research* 7(1):65-73

Nair, R.M.; Seenivasan, A.; Liu, B.; Chen, D.; Lowe, E.D. and Lorenz, S. (2021) Reconstitution and Structural Analysis of a HECT Ligase-Ubiquitin Complex via an Activity-Based Probe *American Chemical Society Chemical Biology* 16(9):1615-1621

Narendra, D.; Tanaka, A.; Suen, D.F. and Youle, R.J. (2008) Parkin is Recruited Selectively to Impaired Mitochondria and Promotes Their Autophagy *Journal of Cell Biology* 183(5):795-803

Narita, Y. (2015) Bevacizumab for Glioblastoma *Therapeutics and Clinical Risk Management* 11:1759-1765

Neftel, C.; Laffy, J.; Filbin, M.G.; Hara, T.; Shore, M.E.; Rahme, G.J.; Richman, A.R.; Silverbush, D.; Shaw, M.L.; Hebert, C.M.; Dewitt, J.; Gritsch, S.; Perez, E.M.; Castro, L.N.G.; Lan, X.; Druck, N.; Rodman, C.; Dionne, D.; Kaplan, A.; Bertalan, M.S.; Small, J.; Pelton, K.; Becker, S.; Bonal, D.; Nguyen, Q.D.; Servis, R.L.; Fung, J.M.; Mylvaganam, R.; Mayr, L.; Gojo, J.; Haberler, C.; Geyeregger, R.; Czech, T.; Slavc, I.; Nahed, B.V.; Curry, W.T.; Carter, B.S.; Wakimoto, H.; Brastianos, P.K.; Batchelor, T.T.; Stemmer-Rachamimov, A.; Martinez-Lage, M; Frosch, M.P.; Stamenkovic, I.; Riggi, N.; Rheinbay, E.; Monje, M.; Rozenblatt-Rosen, O.; Cahill, D.P.; Patel,

A.P.; Hunter, T.; Verma, I.M.; Ligon, K.L.; Louis, D.N.; Regev, A.; Bernstein, B.E.; Tirosh, I and Suvà, M.L. (2019) An Integrative Model of Cellular States, Plasticity and Genetics for Glioblastoma *Cell* 178(4):835-849

Ng, C.C.; Arakawa, H.; Fukuda, S.; Kondoh, H. and Nakamura, Y. (2003) p53RFP, a p53-Inducible RING-Finger Protein, Regulates the Stability of p21WAF1 *Oncogenomics* 22:4449-4458

Nimonkar, A.V.; Sica, R.A. and Kowalczykowski, S.C. (2009) Rad52 promotes second-end DNA capture in double-stranded break repair to form complement-stabilized joint molecules *Proceedings of the National Academy of Sciences* 106(9):3077-3082

Nobusawa, S.; Watanabe, T.; Kleihues, P. and Ohgaki, H. (2009) IDH1 Mutations as Molecular Signature and Predictive Factor of Secondary Glioblastomas *Clinical Cancer Research* 15(19):6002-6007

Ohtake, F.; Saeki, Y.; Ishido, S.; Kanno, J. and Tanaka, K. (2016) The K48-K63 Branched Ubiquitin Chain Regulates NF-κB Signaling *Molecular Cell* 64(2):251-266

O'Neill, P. (2001) Radiation-induced damage in DNA *Studies in Physical and Theoretical Chemistry* 87:585-622

Pan, J.; Fei, C.J.; Hu, Y.; Wu, X.Y.; Nie, L. and Chen, J. (2023) Current Understanding of the cGAS-STING Signaling Pathway: Structure, Regulatory Mechanisms, and Related Diseases *Zoological Research* 44(1):183-218

Pang, X.L.; He, G.; Liu, Y.B.; Wang, Y. and Zhang, B. (2013) Endoplasmic Reticulum Stress Sensitizes Human Esophageal Cancer Cell to Radiation World *Journal of Gastroenterology* 19(11):1736-1748

Paparisto, E.; Woods, M.W.; Coleman, M.D.; Moghadasi, S.A.; Kochar, D.S.; Tom, S.K.; Kohio, H.P.; Gibson, R.M.; Rohringer, T.J.; Hunt, N.R.; Di Gravio, E.J.; Zhang, J.Y.; Tian, M.; Gao, Y.; Arts, E.J. and Barr, S.D. (2018) Evolution-Guided Structural and Functional Analyses of the HERC Family Reveal an Ancient Marine Origin and Determinants of Antiviral Activity *Journal of Virology* 92(13):1128

Paparisto, E.; Hunt, N.R.; Labach, D.S.; Coleman, M.D.; Di Gravio, E.J.; Dodge, M.J.; Friesen, N.J.; Côté, M.; Müller, A.; Hoenen, T. and Barr, S.D. (2021) Interferon-Induced HERC5 Inhibits Ebola Virus Particle Production and Is Antagonized by Ebola Glycoprotein *Cells* 10(9):2399

Parsons, D.W.; Jones, S.; Zhang, X.; Lin, J.C.H.; Leary, R.J.; Angenendt, P.; Mankoo, P.; Carter, H.; Siu, I.M.; Gallia, G. L.; Olivi, A.; McLendon, R.; Rasheed, B. A.; Keir, S.; Nikolskaya, T.; Nikolsky, Y.; Busam, D. A.; Tekleab, H.; Diaz, L. A. Jr; Hartigan, J.; Smith, D.R.; Strausberg, R.L.; Marie, S.K.N.; Shinjo, S.M.O.; Yan, H.; Riggins, G.J.; Bigner, D.D.; Karchin, R.; Papadopoulos, N.; Parmigiani, G.; Vogelstein, B.; Velculescu, V.E. and Kinzler, K. W. (2008) An Integrated Genomic Analysis of Human Glioblastoma Multiforme *Science (New York, N.Y.)* 321(5897):1807–1812

Pellettieri, L.; H-Stenstam, B.; Rezaei, A.; Giusti, V. and Sköld, K. (2008) An investigation of boron neutron capture therapy for recurrent glioblastoma multiforme *Acta Neurologica Scandinavica* 117:191-197

Pérez-Villegas, E.M.; Ruiz, R.; Bachiller, S.; Ventura, F.; Armengol, J.A. and Rosa, J.L. (2022) The HERC Proteins and the Nervous System *Seminars in Cell & Developmental Biology* 132:5-15

Pines, J. (2011) Cubism and the Cell Cycle: the Many Faces of the APC/C *Nature Reviews Molecular Cell Biology* 12:427-438

Ponente, M.; Campanini, L.; Cuttano, R.; Piunti, A.; Delledonne, A.G.; Coltella, N.; Valsecchi, R.; Villa, A.; Cavallaro, U.; Pattini, L.; Doglioni, C. and Bernardi, R. (2017) PML Promotes Metastasis of Triple-Negative Breast Cancer Through Transcriptional Regulation of HIF-1A Target Genes *Journal of Clinical Investigation Insight* 2(4):e87380

Price, M.; Ballard, C.A.P.; Benedetti, J.R.; Kruchko, C.; Barnholtz-Sloan, J.S. and Ostrom, Q.T. (2025) CBTRUS Statistical Report: Primary Brain and Other Central Nervous System Tumors Diagnosed in the United States in 2018-2022 *Neuro-Oncology* 27(S4):iv1-iv66

Pruneda, J.N.; Littlefield, P.J.; Soss, S.E.; Nordquist, K.A.; Chazin, W.J.; Brzovic, P.S. and Klevit, R.E. (2012) Structure of an E3:E2~Ub Complex Reveals an Allosteric Mechanism Shared among RING/U-box Ligases 47(6):933-942

Qiao, X.; Liu, Y.; Prada, M.L.; Mohan, A.K.; Gupta, A.; Jaiswal, A.; Sharma, M.; Merisaari, J.; Haikala, H.M.; Talvinen, K.; Yetukuri, L.; Pylvänäinen, J.W.; Klefström, J.; Kronqvist, P.; Meinander, A.; Aittokallio, T.; Hietakangas, V.; Eilers, M. and Westermarck, J. (2020) UBR5 is Coamplified with MYC in Breast Tumors and Encodes an Ubiquitin Ligase That Limits MYC-Dependent Apoptosis *Cancer Research* 80(7):1414-1427

Qin, Y.; Chen, L.; Zhu, W.; Song, J.; Lin, J.; Li, Y.; Zhang, J.; Song, X.; Xing, T.; Guo, T.; Duan, X.; Zhang, Y.; Ruan, E.; Wang, Q.; Li, B.; Yang, W.; Yin, P.; Yan, X.X.; Li, S.; Li, X.J. and Yang, S. TRIM37 is a Primate-Specific E3 Ligase for Huntingtin and Accounts for the Striatal Degeneration in Huntington's Disease *Science Advances* 10(20):eadl2036

Ray, S.; Zhao, Y.; Jamaluddin, M.; Edeh, C.B.; Lee, C. and Brasier, A.R. (2014) Inducible STAT3 NH2 Terminal Monoubiquitination Promotes BRD4 Complex Formation to Regulate Apoptosis *Cellular Signalling* 26(7):1445-1455

Reits, E.A.; Hodge, J.W.; Herberts, C.A.; Groothuis, T.A.; Chakraborty, M.; Wansley, E.K.; Camphausen, K.; Luiten, R.M.; de Ru, A.H.; Neijssen, J.; Griekspoor, A.; Mesman, E.; Verreck, F.A.; Spits, H.; Schlom, J.; van Veelen, P. and Neefjes, J.J. (2006) Radiation Modulates the Peptide Repertoire, Enhances MHC Class I Expression, and Induces Successful Antitumor Immunotherapy *Journal of Experimental Medicine* 203(5):1259-1271

Richardson, R.B. and Harper, M.E. (2016) Mitochondrial Stress Controls the Radiosensitivity of the Oxygen Effect: Implications for Radiotherapy *Oncotarget* 7(16):1469-21483

Rise, M.L.; Hall, J.R.; Rise, M.; Hori, T.S.; Browne, M.J.; Gamperl, A.K.; Hubert, S.; Kimball, J.; Bowman, S. and Johnson, S.C. (2010) Impact of Asymptomatic Nodavirus Carrier State and Intraperitoneal Viral Mimic Injection on Brain Transcript Expression in Atlantic Cod (Gadus Morhua) *Physiological Genomics* 42(2):266-280

Roberts, S.A.; Strande, N.; Burkhalter, M.D.; Strom, G.; Havener, J.M.; Hasty, P. and Ramsden, D.A. (2010) Ku is a 5'dRP/AP Lyase That Excises Nucleotide Damage Near Broken Ends *Nature* 464(7292):1214-1217

Roder, C.; Bisdas, S.; Ebner, F.H.; Honegger, J.; Naegele, T.; Ernemann, U. and Tatagiba, M. (2014) Maximizing the Extent of Resection and Survival Benefit of Patients in Glioblastoma Surgery: High-Field iMRI Versus Conventional and 5-ALA-Assisted Surgery *European Journal of Surgical Oncology* 40(3):297-304

Rodriguez, C.I. and Stewart, C.L. (2007) Disruption of the Ubiquitin Ligase HERC4 Causes Defects in Spermatozoon Maturation and Impaired Fertility *Developmental Biology* 312(2):501-508

Rotin, D. and Kumar, S. (2009) Physiological Functions of the HECT Family of Ubiquitin Ligases *Nature Reviews Molecular Cell Biology* 10:398-409

Rudawska, A., Szczygieł, A., Węgierek-Ciura, K., Mierzejewska, J., Kozień, D., Żeliszewska, P., Chaszczewska-Markowska, M.; Rusiniak, P.; Wątor,K.; Pędzich, Z.; Pajtasz-Piasecka, E.; Szermer-Olearnik, B. (2026). Bone Marrow-Derived Macrophages Loaded with Boron Carbide Nanoparticles Targeting the Glioblastoma Microenvironment for Boron Neutron Capture Therapy. *International Journal of Nanomedicine*, *21*:604151

Sage, E. and Shikazono, N. (2017) Radiation-Induced Clustered DNA Lesions: Repair and Mutagenesis *Free Radical Biology and Medicine* 107:125-135

Salvat, C.; Wang, G.; Dasture, A.; Lyon, N. and Huibregtse, J.M. (2004) The -4 Phenylalanine Is Required for Substrate Ubiquitination Catalyzed by HECT Ubiquitin Ligases *Protein Synthesis, Post-Translation Modification, and Degradation* 279(18):18935-18943

San Filippo, J.; Sung, P. and Klein, H. (2008) Mechanism of Eukaryotic Homologous Recombination *Annual Review of Biochemistry* 77:229-257

Sander, B.; Xu, W.; Eilers, M.; Popov, N. and Lorenz, S. (2017) A Conformational Switch Regulates the Ubiquitin Ligase HUWE1 *eLife* 6:e21036

Sareen, A.; Chaudhury, I.; Adams, N. and Sobeck, A. (2012) Fanconi Anemia Proteins FANCD2 and FANCI Exhibit Different DNA Damage Responses During S-Phase *Nucleic Acids Research* 40(17):8425-8439

Sarikas, A.; Hartmann, T. and Pan, Z.Q. (2011) The Cullin Protein Family *Genome Biology* 12:220

Saurin, A.J.; Borden, K.L.B.; Boddy, M.N. and Freemont, P.S. (1996) Does This Have a Familiar RING? *Trends in Biochemical Sciences* 21(6):208-214

Scheffner, M.; Huibregtse, J.M.; Vierstra, R.D. and Howley, P.M (1993) The HPV-16 E6 and E6-AP Complex Functions as a Ubiquitin-Protein Ligase in the Ubiquitination of p53 *Cell* 75(3):495-505

Scherer, H.J. (1940) A Critical Review: The Pathology of Cerebral Gliomas *Journal of Neurology and Psychiatry* 3(2):147-177

Schöffski, P.; Lahmar, M.; Lucarelli, A. and Maki, R.G. (2022) Brightline-1: Phase II/III Trial of the MDM2-p53 Antagonist BI 907828 Versus Doxorubicin in Patients with Advanced DDLPS *Future Oncology* 19(9):621-629

Schwarz, K.; Dobiasch, S.; Nguyen, L.; Schilling, D. and Combs, S.E. (2020) Modification of Radiosensitivity by Curcumin in Human Pancreatic Cancer Cell Lines *Scientific Reports* 10:3815

Segerman, A.; Niklasson, M.; Haglund, C.; Bergström, T.; Jarvius, M.; Xie, Y.; Westermark, A.; Sönmez, D.; Hermansson, A.; Kastemar, M.; Naimaie-Ali, Z.; Nyberg, F.; Berglund, M.; Sundström, M.; Hesselager, G.; Uhrbom, L.; Gustafsson, M.; Larsson, R.; Fryknäs, M.; Segerman, B. and Westermark B. (2016) Clonal Variation in Drug and Radiation Response among Glioma-Initiating Cells Is Linked to Proneural-Mesenchymal Transition *Cell Reports* 17(11):2994-3009

Seki, T.; Gong, L.; Williams, A.J.; Sakai, N.; Todi, S.V. and Paulson, H.L. JosD1, a Membrane-Targeted Deubiquitinating Enzyme, is Activated by Ubiquitination and Regulates Membrane Dynamics, Cell Motility, and Endocytosis *Journal of Biological Chemistry* 288(24):17145-17155

Sekiguchi, N.; Kasahara, S.; Miyamoto, T.; Kiguchi, T.; Ohno, H.; Takagi, T.; Tachibana, M.; Sumi, H.; Kakurai, Y.; Yamashita, T. Usuki, K. (2023) Phase I Dose-Escalation Study of Milademetan in Patients with Relapsed or Refractory Acute Myeloid Leukemia *International Journal of Hematology* 117:68-77

Senavirathna, L.; Hasapes, C.; Chen, R. and Pan, S. (2024) Accumulation of Intracellular Protein Advanced Glycation End Products Alters Cellular Homeostasis for Protein Clearance in Pancreatic Ductal Epithelial Cells *Biochemistry* 63(14):1723-1729

Seo, J.; Lee, E.W.; Shin, J.; Seong, D.; Nam, Y.W.; Jeong, M.; Lee, S.H.; Lee, C. and Song, J. (2018) K6 Linked Polyubiquitylation of FADD by CHIP Prevents Death Inducing Signaling Complex Formation Suppressing Cell Death *Oncogene* 37(2018): 4994-5006

Shah, S.S.; Rodriguez, G.A.; Musick, A.; Walters, W.M.; de Cordoba, N.; Barbarite, E.; Marlow, M.M.; Marples, B.; Prince, J.S.; Komotar, R.J.; Vanni, S. and Graham, R.M. (2019) Targeting Glioblastoma Stem Cells with 2-Deoxy-D-Glucose (2-DG) Potentiates Radiation-Induced Unfolded Protein Response (UPR) *Cancers* 11(2):159

Shearer, R.F.; Typas, D.; Coscia, F.; Schovsbo, S.; Kruse, T.; Mund, A. and Mailand, N. (2022) K27-Linked Ubiquitylation Promotes p97 Substrate Processing and is Essential for Cell Profileration *The European Molecular Biology Organization Journal* 41:EMBJ2021110145

Shen, Y.; Wang, J.; Liang, J.; Chen, Y.; Wu, X.; Ren, Z.; Zhou, J.; Feng, L. and Shen, Y. (2024) E3 Ubiquitin Ligase Ring Finger Protein 2 Alleviates Cerebral Ischemia-Reperfusion Injury by Stabilizing Mesencephalic Astrocyte-Derived Neurotrophic Factor Through Monoubiquitination *CNS Neuroscience and Therapeutics* 30(11):e70136

Shibata, A.; Moiani, D.; Arvai, A.S.; Perry, J.; Harding, S.M.; Genois, M.M.; Maity, R.; van Rossum-Fikkert, S.; Kertokalio, A.; Romoli, F.; Ismail, A.; Ismalaj, E.; Petricci, E.; Neale, M.J.; Bristow, R.G.; Masson, J.Y.; Wyman,

C.; Jeggo, P.A. and Tainer, J.A. (2014) DNA Double-Strand Break Repair Pathway Choice Is Directed by Distinct MRE11 Nuclease Activities *Molecular Cell* 53(1):7-18

Shimura, T.; Noma, N.; Sano, Y.; Ochiai, Y.; Oikawa, T.; Fukumoto, M. and Kunugita, N. (2014) AKT-Mediated Enhanced Aerobic Glycolysis Causes Acquired Radioresistance by Human Tumor Cells *Radiobiology* 112(2):302-307

Simões, V.; Cizubu, B.K.; Harley, L.; Zhou, Y.; Pajak, J.; Snyder, N.A.; Bouvette, J.; Borgnia, M.J.; Arya, G.; Bartesaghi, A. and Silva, G.M. (2022) Redox-Sensitive E2 Rad6 Controls Cellular Response to Oxidative Stress via K63-Linked Ubiquitination of Ribosomes *Cell Reports* 39(8):110860

Song, E.J.; Werner, S.L.; Neubauer, J.; Stegmeier, F.; Aspden, J.; Rio, D.; Harper, J.W.; Elledge, S.J.; Kirschner, M.W. and Rape, M. (2010) The Prp19 Complex and the Usp4Sart3 Deubiquitinating Enzyme Control Reversible Ubiquitination at the Spliceosome *Genes & Development* 24:1434-1447

Song, Y.; Deng, Z.; Sun, H.; Zhao, Y.; Zhao, R.; Cheng, J. and Huang, Q. Predicting Tumor Repopulation Through the Gene Panel Derived from Radiation Resistant Colorectal Cancer Cells *Journal of Translation Medicine* 21:390

Sottoriva, A.; Spiteri, I.; Piccirillo, S.G.M.; Touloumis, A.; Collins, V.P.; Marioni, J.C.; Curtis, C.; Watts, C. and Tavaré, S. (2013) Intratumor Heterogeneity in Human Glioblastoma Reflects Cancer Evolutionary Dynamics *Proceedings of the National Academy of Sciences* 110(1):4009-4014

Spence, A.M.; Muzi, M.; Swanson, K.R.; O'Sullivan, F.; Rockhill, J.K.; Rajendran, J.G.; Adamsen, T.C.H.; Link, J.M.; Swanson, P.E.; Yagle, K.J.; Rostomily, R.C.; Silbergeld, D.L. and Krohn, K.A. (2008) Regional Hypoxia in Glioblastoma Multiforme Quantified with [18F]Fluoromisonidazole Positron Emission Tomography before Radiotherapy: Correlation with Time to Progression and Survival *Clinical Cancer Research* 14(9):2623-2630

Stevens, T.J. and Paoli, M. (2007) RCC1-Like Repeat Proteins: A Pangenomic, Structurally Diverse New Superfamily of β-propeller Domains *Proteins: Structure, Function, and Bioinformatics* 70(2):378-387

Stewart, M.D.; Ritterhoff, T.; Klevit, R.E. and Brzovic, P.S. (2016) E2 Enzymes: More Than Just Middle Men *Cell Research* 26:423-440

Stinson, B.M. and Loparo, J.J. (2022) Repair of DNA Double-Strand Breaks by the Non-Homologous End Joining Pathway *Annual Review of Biochemistry* 90:137-164

Stupp, R.; Mason, W.P.; van den Bent, M.J.; Weller, M.; Fisher, B.; Taphoorn, M.J.B.; Belanger, K.; Brandes, A.A.; Marosi, C.; Bogdahn, U.; Curschmann, J.; Janzer, R.C.; Ludwin, S.K.; Gorlia, T.; Allgeier, A.; Lacombe, D.; Cairncross, J.G.; Eisenhauer, E.; Mirimanoff, R.O.; European Organisation for Research and Treatment of Cancer Brain Tumor and Radiotherapy Groups; National Cancer Institute of Canada Clinical Trials Group (2005) *National England Journal of Medicine* 352(10):987-996

Stupp, R.; Hegi, M.E.; Mason, W.P.; van den Bent, M.J.; Taphoorn, M.J.B.; Janzer, R.C.; Ludwin, S.K.; Allgeier, A.; Fisher, B.; Belanger, K.; Hau, P.; Brandes, A.A.; Gijtenbeek, J.; Marosi, C.; Vecht, C.J.; Mokhtari, K.; Wesseling, P.; Villa, S.; Eisenhauer, E.; Gorlia, T.; Weller, M.; Lacombe, D.; Cairncross, G.; Mirimanoff, R.O.; European Organisation for Research and Treatment of Cancer Brain Tumour and Radiation Oncology Groups, and National Cancer Institute of Canada Clinical Trials Group (2009) Effects of Radiotherapy with Concomitant and Adjuvant Temozolomide Versus Radiotherapy Alone on Survival in Glioblastoma in a Randomised Phase III Study: 5-year Analysis of the EORTC-NCIC Trial *The Lancet Oncology* 10(5):459-466

Stupp, R.; Taillibert, S.; Kanner, A.A.; Kesari, S.; Steinberg, D.M.; Toms, S.A.; Taylor, L.P.; Lieberman, F.; Silvani, A.; Fink, K.L.; Barnett, G.H.; Zhu, J.J.; Henson, J.W.; Engelhard, H.H.; Chen, T.C.; Tran, D.D.; Sroubek, J.; Tran, N.D.; Hottinger, A.F.; Landolfi, J.; Desai, R.; Caroli, M.; Kew, Y.; Honnorat, J.; Idbaih, A.; Kirson, E.D.; Weinberg, U.; Palti, Y.; Hegi, M.E. and Ram, Z. (2015) Maintenance Therapy with Tumor-Treating Fields Plus Temozolomide vs Temozolomide Alone for Glioblastoma: A Randomized Clinical Trial *The Journal of the American Medical Association* 314(23):2535-2543

Su, J.; Zhou, X.; Wang, L.; Yin, X. Wang, Z. (2016) Curcumin Inhibits Cell Growth and Invasion and Induces Apoptosis Through Down-Regulation of Skp2 in Pancreatic Cancer Cells *American Journal of Cancer Research* 6(9):1949-1962

Sun, X.; Gao, H.; Yang, Y.; He, M.; Wu, Y.; Song, Y.; Tong, Y. and Rao, Y. (2019) PROTACs: Great Opportunities for Academia and Industry *Signal Transduction and Targeted Therapy* 4:64

Sun, X.; Sun, B.; Cui, M. and Zhou, Z. (2019a) HERC4 Exerts an Anti-Tumor Role Through Destabilizing the Oncoprotein Smo *Biochemical and Biophysical Research Communications* 513(4):1013-1018

Sun, Y.; McCorvie, T.J.; Yates, L.A. and Zhang, X. (2019b) Structural basis of homologous recombination *Cellular and Molecular Life Sciences* 77(1):3-18

Tajeddine, N. (2016) How Do Reactive Oxygen Species and Caclium Trigger Mitochondrial Membrane Permeabilisation? *Biochimica et Biophysica Acta - General Subjects* 1860(6):1079-1088

Tauchi, H.; Matsuura, S.; Kobayashi, J.; Sakamoto, S. and Komatsu, K. (2002) Nijmegen Breakage Syndrome, NBS1, and Molecular Links to Factors for Genome Stability *Oncogene* 21(58):8967-80

Terasima, T. and Tolmach, L.J. (1961) Changes in X-ray Sensitivity of HeLa Cells during the Division Cycle *Nature* 190:1210-1211

The Cancer Genome Atlas Research Network (2008) Comprehensive Genomic Characterization Defines Human Glioblastoma Genes and Core Pathways *Nature* 455:1061-1068

Tooth, H.H. (1912) Some observations on the growth and survival-period of intracranial tumours, based on the records of 500 cases, with special reference to the pathology of the gliomata *Brain* 35(2):61-108.

Tu, Y.; Xu, L.; Xu, J.; Bao, Z.; Tian, W.; Ye, Y.; Sun, G.; Miao, Z.; Chao, H.; You, Y.; Liu, N. and Ji, J. (2022) Loss of Deubiquitylase USP2 Triggers Development of Glioblastoma via TGF-β Signaling *Oncogene* 41:2597-2608

Valero, Y.; Souto, S.; Olveira, J.G.; López-Vázquez, C.; Dopazo, C.P. and Bandín, I. (2024 a) Water-in-Oil Adjuvant Challenges in Fish Vaccination: An Experimental Inactivated Adjuvanted Vaccine Against Betanodavirus Infection in Senagalese Sole *Journal of Fish Diseases* 47(7):e13945

Valero, Y.; Chaves-Pozo, E. and Cuesta, A. (2024 b) Fish HERC7: Phylogeny, Characterization, and Potential Implications for Antiviral Immunity in European Sea Bass International *Journal of Molecular Sciences* 25(14):7751

Van Der Reijden, B.A.; Erpelinck-Verschueren, C.A.J.; Löwenberg, B. and Jansen, J.H. (2008) TRIADs: A New Class of Proteins with a Novel Cysteine-Rich Signature Protein *Science* 8(7):1557-1561

Vanpouille-Box, C.; Alard, A.; Aryankalayil, M.J.; Sarfraz, Y.; Diamond, J.M.; Schneider, R.J.; Inghirami, G.; Coleman, C.N.; Formenti, S.C. and Demaria, S. (2017) DNA Exonuclease Trex1 Regulates Radiotherapy-Induced Tumour Immunogenicity *Nature Communications* 8(2017):15618

Verdecia, M.A.; Joazeiro, C.A.P.; Wells, N.J.; Ferrer, J.L.; Bowman, M.E.; Hunter, T. and Noel, J.P. (2003) Conformational Flexibility Underlies Ubiquitin Ligation Mediated by the WWP1 HECT Domain E3 Ligase *Molecular Cel*l 11(1):249-259

Verhaak, R.G.W.; Hoadley, K.A.; Purdom, E.; Wang, V.; Qi, Y.; Wilkerson, M.D.; Miller, C.R.; Ding, L.; Golub, T.; Mesirov, J.P.; Alexe, G.; Lawrence, M.; O'Kelly, M.; Tamayo, P.; Weir, B.A.; Gabrie, S.; Winckler, W.; Gupta, S.; Jakkula, L.; Feiler, H.S.; Hodgson, J.G.; James, C.D.; Sarkaria, J.N.; Brennan, C.; Kahn, A.; Spellman, P.T.; Wilson, R.K.; Speed, T.P.; Gray, J.W.; Meyerson, M.; Getz, G.; Perou, C.M.; Hayes, D.N. and The Cancer Genome Atlas Research Network (2010) An Integrated Genomic Analysis Identifies Clinically Relevant Subtypes of Glioblastoma Characterized by Abnormalities in PDGFRA, IDH1, EGFR and NF1 *Cancer Cell* 17(1):98

Villa, E.; Proïcs, E.; Rubio-Patiño, C.; Obba, S.; Zunino, B.; Bossowski, J.P.; Rozier, R.M.; Chiche, J.; Mondragón, L.; Riley, J.S.; Marchetti, S.; Verhoeyen, E.; Tait, S.W.G. and Ricci, J.E. (2017) Parkin-Independent Mitophagy Controls Chemotherapeutic Response in Cancer Cells *Cell Reports* 20(12):2846-2859

Villanueva-Meyer, J.E.; Han, S.J.; Cha, S. and Butowski, N.A. (2017) Early Tumor Growth Between Initial Resection and Radiotherapy of Glioblastoma: Incidence and Impact on Clinical Outcomes *Journal of Neuro-Oncology* 134:213-219

Virchow, R. (1867) Die krankhaften Geschwuelste: dreissig Vorlesungen gehalten waehrend des Wintersemesters 1862-1863 an der Universitaet zu Berlin, Volume 4, University of Lausanne

Vogt, A. and He, Y. (2023) Structure and Mechanism in Non-Homologous End Joining *DNA Repair (Amsterdam)* 130:103547

Walker, M.D.; Strike, T.A. and Sheline, G.E. (1979) An Analysis of Dose-Effect Relationship in the Radiotherapy of Malignant Gliomas *International Journal of Radiation Oncology*Biology*Physics* 5(10):1725-1731

Wan,L.; Zou, W.; Gao, D.; Inuzuka, H.; Fukushima, H.; Berg, A.H.; Drapp, R.; Shaik, S; Hu, D.; Lester, C.; Eguren, M.; Malumbres, M.; Glimcher, L.H. and Wei, W. (2011) Cdh1 Regulates Osteoblast Function through an APC/C-Independent Modulation of Smurf1 *Molecular Cell* 44(5):721-733

Wang, P.; Wu, Y.; Li, Y.; Zheng, J. and Tang, J. (2013) A Novel RING Finger E3 Ligase RNF186 Regulate ER Stress-Mediated Apoptosis Through Interaction with BNip1 Cellular Signalling 25(11):2320-2333

Wang, Q.; Hu, B.; Hu, X.; Kim, H.; Squatrito, M.; Scarpace, L.; deCarvalho, A.C.; Lyu, S.; Li, P.; Li, Y.; Barthel, F.; Cho, H.J.; Lin, Y.H.; Satani, N.; Martinez-Ledesma, E.; Zheng, S.; Chang, E.; Sauvé, C.E.G.; Olar, A.; Lan, Z.D.; Finocchiaro, G.; Phillips, J.J.; Berger, M.S.; Gabrusiewicz, K.R.; Wang, G.; Eskilsson, E.; Hu, J.; Mikkelsen, T.; DePinho, R.A.; Muller, F.; Heimberger, A.B.; Sulman, E.P.; Nam, D.H. and Verhaak, R.G.W. (2017) Tumor Evolution of Glioma-Intrinsic Gene Expression Subtypes Associates with Immunological Changes in the Microenvironment *Cancer Cell* 32(1):42-56 E6

Wang, Y.; Argiles-Castillo, D.; Kane, E.I.; Zhou, A. and Spratt, D.E. (2020) HECT E3 Ubiquitin Ligases - Emerging Insights Into Their Biological Roles and Disease Relevance *Journal of Cell Science* 133(7):jcs228072

Wang, S.; Zhang, Z.; Miao, L. and Li, Y. (2022) Boron Neutron Capture Therapy: Current Status and Challenges *Frontiers in Oncology* 12

Wang, L.; Cheng, H.; Wang, X.; Zhu, F.; Tian, N.; Xu, Z.; Yin, H.; Liang, M.; Yang, X.; Liu, X.; Shan, H.; Fu, R.; Cao, B.; Li, D.; Xiao, L.; Lu, L.; Dai, S.M.; Wang, Q.; Lv, L.; Zou, H. and Li, B. (2024) Deubiquitination of Aryl Hydrocarbon Receptor by USP21 Negatively Regulates T Helper 17 Cell Differentiation *Journal of Leukocyte Biology* 117(1):qiae148

Wang, X.; Zhao, Y.; Yang, X.; Liu, T.; Zhou, W.; Niu, S.; Jin, M.; Chen, Y.; Liu, R.; Bao, Y. and Yue, X. (2025) Radiation-Induced Nuclear Translocation of NPRL2 Hijacks E3 Ubiquitin Ligases to Enhance DNA Repair via the AMPK/WDR24 Axis, Contributing to CRC Radioresistance *Acta Pharmaceutica Sinica B* 16(1):252-269

Wang, W.; Zhang, E.; Shan, J.; Zhang, M.; Cai, R.; Li, R.; Pang, L.; Li, B. and Zang, D. (2026) State-of-the-art boron clusters for boron neutron-capture therapy *Theranostics* 16(1):417-464

Weinberg, J.; Whitcomb, E.; Bohm, A.; Chekkilla, U.K. and Taylor, A. (2024) The E3 Ligase SMURF1 Stabilizes p27 via UbcH7 Catalyzed K29-Linked Ubiquitin Chains to Promote Cell Migration SMURF1-UbcH7 K29 Ubiquitination of p27 and Cell Migration *Journal of Biological Chemistry* 300(3):105693

Wenzel, D.M.; Lissounov, A.; Brzovic, P.S. and Klevit, R.E. (2011) UBCH7 Reactivity Profile Reveals Parkin and HHARI to be RING/HECT Hybrids *Nature* 474:105-108

Woodward, W.A.; Chen, M.S.; Behbod, F.; Alfaro, M.P.; Buchholz, T.A. and Rosen, J.A. (2007) WNT/Beta-Catenin Mediates Radiation Resistance of Mouse Mammary Progenitor Cells *Proceedings of the National Academy of Sciences in the USA* 104(2):618-623

Wu, Q.; Wang, Z.; Chen, S.; She, X.; Zhu, S.; Li, P.; Liu, L.; Zhao, C.; Li, K.; Liu, A.; Huang, C.; Chen, Y.; Hu, F.; Wang, G. and Hu, J. (2024) USP26 Promotes Colorectal Cancer Tumorigenesis by Restraining PRKN-Mediated Mitophagy *Oncogene* 43:1581-1593

Wu, C.T.; Hsieh, C.C.; Yen, T.C.; Chen, W.C. and Chen, M.F. (2015) TGF-β1 Mediates the Radiation Response of Prostate Cancer *Journal of Molecular Medicine* 93:73-82

Xiao, N.; Eto, D.; Elly, C.; Peng, G.; Crotty, S. and Liu, Y.C. (2014) The E3 Ubiquitin Ligase Itch is Required for the Differentiation of Follicular Helper T Cells *Nature Immunology* 15:657-666

Xie, H.; Hanai, J.I.; Ren, J.G.; Kats, L.; Burgess, K.; Bhargava, P.; Signoretti, S.; Billiard, J.; Duffy, K.J.; Grant, A.; Wang, X.; Lorkiewicz, P.K.; Schatzman, S.; Bousamra 2nd, M.; Lane, A.N.; Higashi, R.M.; Fan, T.W.M.; Pandolfi, P.P.; Sukhatme, V.P. and Seth, P. (2014) Targeting Lactate Dehydrogenase --a inhibits Tumorigenesis and Tumor Progression in Mouse Models of Lung Cancer and Impacts Tumor-Initiating Cells *Cell Metabolism* 19(5):795-809

Xie, F.; Liu, B.; Qiao, W.; He, J.Z.; Cheng, J.; Wang, Z.Y.; Hou, Y.M.; Zhang, X.; Xu, B.H.; Zhang, Y.; Chen, Y.G. and Zhang, M.X. (2024) Smooth Muscle NF90 Deficiency Ameliorates Diabetic Atherosclerotic Calcification in Male Mice via FBXW7-AGER1-AGEs Axis *Nature Communications* 15:4985

Xu, D.; Shan, B.; Sun, H.; Xiao, J.; Zhu, K.; Xie, X.; Li, X.; Liang, W.; Lu, X.; Qian, L. and Yuan, J. (2016) USP14 Regulates Autophagy by Suppressing K63 Ubiquitination of Beclin 1 *Genes and Development* 30:1718-1730

Xu, Y.; Ji, K.; Wu, M.; Hao, B.; Yao, K. and Xu, Y. (2019) A miRNA-HERC4 Pathway Promotes Breast Tumorigenesis by Inactivating Tumor Suppressor LATS1 *Protein & Cell* 10(8):595-605

Xu, S.; Frakulli, R. and Lin, Y. (2023) Comparison of the Effectiveness of Radiotherapy with 3D-CRT, IMRT, VMAT and PT for Newly Diagnosed Glioblastoma: A Bayesian Network Meta-Analysis *Cancers* 15(23):5698

Xu, Y.; Qu, M.; He, Y.; He, Q.; Shen, T.; Luo, J.; Tan, D.; Bao, H.; Xu, C.; Ji, X.; Hu, X.; Barkat, M.Q.; Zeng, L.H. and Wu, X. (2023) Smurf1 Polyubiquitinates on K285/K282 of the Kinases Mst1/2 to Attenuate Their Tumor-Suppressor Functions *Journal of Biological Chemistry* 299(12):105395

Yan, H; Parsons, D.W.; Jin, G.; McLendon, R.; Rasheed, B.A.; Yuan, W.; Kos, I.; Batinic-Haberle, I.; Jones, S.; Riggins, G.J.; Friedman, H.; Friedman, A.; Reardon, D.; Herndon, J.; Kinzler, K.W.; Velculescu, V.E.; Vogelstein, B. and Bigner, D.D. (2009) IDH1 and IDH2 Mutations in Gliomas *The New England Journal of Medicine* 360(8):765-773

Yang, H.; Fouad, S.; Smith, P.; Bae, E.Y.; Ji, Y.; Lan, X.; Van Ess, A.; Buffa, F.M.; Fischer, R.; Vendrell, I.; Kessler, B.M. and D'Angiolella, V. (2024) Cyclin F-EXO1 Axis Controls Cell Cycle-Dependent Execution of Double-Strand Break Repair *Science Advances* 10(32):eado0636

Yau, R.G.; Doerner, K.; Castellanos, E.R.; Haakonsen, D.L.; Werner, A.; Wang, N.; Yang, X.W.; Martinez-Martin, N.; Matsumoto, M.L.; Dixit, V.M. and Rape, M. (2017) Assembly and Function of Heterotypic Ubiquitin Chains in Cell-Cycle and Protein Quality Control *Cell* 171(4):918-933.e20

Yoshii, Y.; Saito, A.; Zhao, D.W. and Nose, T. (1999) Copper/Zinc Superoxide Dismutase, Nuclear DNA Content, and Progression in Human Gliomas *Journal of Neuro-Oncology* 42:103-108

Yuan, W.C.; Lee, Y.R.; Lin, S.Y.; Chang, L.Y.; Tan, Y.P.; Hung, C.C.; Kuo, J.C.; Liu, C.H.; Lin, M.Y.; Xu, M.; Chen, Z.J. and Chen, R.H. (2014) K33-Linked Polyubiquitination of Coronin 7 by Cul3-KLHL20 Ubiquitin E3 Ligase Regulates Protein Trafficking *Molecular Cell* 54(4):586-600

Zhang, Z.; Lv, X.; Yin, W.C.; Zhang, X.; Feng, J.; Wu, W.; Hui, C.C.; Zhang, L. and Zhao, Y. (2013) Ter94 ATPase Complex Targets K11-Linked Ubiquitinated Ci to Proteasomes for Partial Degradation *Development Cell* 25(6):636-644

Zhang, L.; Xu, M.; Scotti, E.; Chen, Z.J. and Tontonoz, P. (2013) Both K63 and K48 Ubiquitin Linkages Signal Lysosomal Degradation of the LDL Receptor *Journal of Lipid Research* 54(5):1410-1420

Zhang, Z.; Tong, J.; Tang, X.; Juan, J.; Cao, B.; Hurren, R.; Chen, G.; Taylor, P.; Xu, X.; Shi, C.X.; Du, J.; Hou, J.; Wang, G.; Wu, D.; Stewart, A.K.; Schimmer, A.D.; Moran, M.F. and Mao, X. (2016) The Ubiquitin Ligase HERC4 Mediates c-Maf Ubiquitination and Delays the Growth of Multiple Myeloma Xenografts in Nude Mice *Blood* 127(13):1676-1686

Zhang, X.; Smits, A.H.; van Tilburg, G.B.A.; Jansen, P.W.T.C.; Makowski, M.M.; Ovaa, H. and Vermeulen, M. (2017) An Interaction Landscape of Ubiquitin Signaling *Molecular Cell* 65(5):941-955

Zhang, Z.; Li, M.; Lin, P.; Ren, Y.; He, Y.; Wang, S.; Xu, Y.; Cao, B.; Wang, G.; Moran, M.F. and Mao, X. (2023a) The Ubiquitin Ligase HERC4 Suppresses MafA Transcriptional Activity Triggered by GSK3β in Myeloma by Atypical K63-Linked Polyubiquitination *Journal of Biological Chemistry* 299(5):104675

Zhang, M.; Shao, Y. and Gu, W. (2023b) The Mechanism of Ubiquitination or Deubiquitination Modifications in Regulating Solid Tumor Radiosensitivity *Biomedicines* 11(12):3240

Zhang, Q.; Teng, X.; Dai, Y.; Wu, Y.; Hou, H. and Li, J. (2025a) K29-Linked Ubiquitination of Transcription Regulators Controls Cell Proliferation in the Unfolded Protein Response *Advanced Science* 12(42):e09817

Zhang, W.; Zhang, X.; Chen, K. and Wang, Y. (2025b) The Epidermal Growth Factor Receptor Regulates YAP Signalling and Promotes Diabetic Retinal Fibrosis by Modulating the Degradation SAV1 *Journal of Translation Medicine* 23:1319

Zhang, S.; Wei, Y.; Gu, W.; Li, S.; Liu, T.; Shuai, L.; Tang, Y.; Jiang, Y.; Zhou, X.; Wei, Y.; Wang, G.; Gu, L.; Li, Y.; Tang, F. and Zuo, D. (2025c) Uptakes of boronophenylalanine in the *in vitro* and *in situ* glioblastoma and the potential efficacy of boron neutron capture therapy *IBRO Neuroscience Reports* 19:192-197

Zhao, F.; Ming, J.; Zhou, Y. and Fan, L. (2016) Inhibition of Glut1 by WZB117 Sensitizes Radioresistant Breast Cancer Cells to Irradiation *Cancer Chemotherapy and Pharmacology* 77:963-972

Zhao, F.; Kim, W.; Kloeber, J.A. and Lou, Z. (2020) DNA end resection and its role in DNA replication and DSB repair choice in mammalian cells *Experimental and Molecular Medicine* 52:1705-1714

Zheng, Y.; Li, J.; Pan, C.; Zhou, G.; Zhuge, L.; Jin, L. and Fang, P. (2017) HERC4 Is Overexpressed in Hepatocellular Carcinoma and Contributes to the Proliferation and Migration of Hepatocellular Carcinoma Cells *DNA and Cell Biology* 36(6):490-500

Zheng, S.; Wu, Y. and Li, Z. (2021) Integrating Cullin2-RING E3 Ligase as a Potential Biomarker for Glioblastoma Multiforme Prognosis and Radiosensitivity Profiling *Radiotherapy and Oncology* 154:36-44

Zhou, Q. and Zhang, J. (2022) K27-Linked Noncanonic Ubquitination in Immune Regulation *Journal of Leukocyte Biology* 111(1):223-235

Zhou, S.; Li, Y.; Wang, C.; Zhao, Y. and Zheng, X. (2025) K11- and K29-Ubiquitination-Mediated Nuclear Translocation of Glycolytic Enzyme Aldolase A Promotes Pancreatic Cancer Progression by NF-κB Activation *Cell Death & Differentation* 2025

Zhu, Q.; Yang, X. and Lv, Y. (2024) HERC4 Modulates Ovarian Cancer Cell Proliferation by Regulating SMO-Elicited Hedgehog Signalling *Biochimica et Biophysica Acta - General Subjects* 1868(4):130557

2 - Phenotypic changes after HERC4 loss

2.1 – Introduction

HERC4 is the evolutionary founding member of the HERC family of E3 ligases, named for the HECT and RCC1-like domains in each protein [Hochrainer et al., 2005; Paparisto et al., 2018]. It can be traced as far back as nematodes and, along with HERC3, is the most conserved HERC protein between species. Despite its long evolutionary history, its present-day function is unclear. There is a reasonable quantity of evidence linking it to spermatozoon development primarily in mice [Rodriguez and Stewart, 2007; Li et al., 2021; Hedges et al., 2023; Li et al., 2023a], and to the immune system mainly in fish [e.g. Rise et al., 2010; Liu et al., 2024b; Valero et al., 2024], but its role in humans remains ambiguous. When testing its relevance to anti-viral responses, Paparisto et al. found that HERC4 can impair virus production but that this function is dominated by HERC5. This led to the proposal that HERC4 is important to the immune system in species that lack HERC5 but is otherwise redundant in this capacity, and it is plausible that this is true for all HERC4 functions. However, changes in HERC4 expression have been linked to phenotypes in various diseases (see below for references), suggesting that its significance and role may not be completely usurped by its evolutionary successors.

The evidence implicating HERC4 in disease is currently thin and spread across a range of conditions, from Parkinsons to cataracts. In the study that first identified HERC4, its transcripts were found to be most abundant in brain tissue, particularly adult compared to foetal brain [Nagase et al., 2000]. Although it now seems that HERC4 is fairly ubiquitously expressed in human tissues [Human Protein Atlas], the brain remains the only tissue with multiple disease links to it [Asif et al., 2024; Goralski et al., 2024]. HERC4 was the fourth most upregulated protein in 5 individuals with a ZFTRAF1-linked neurodevelopmental disorder, despite no change in HERC4 mRNA levels compared to controls. Mass spectrometry data identified HERC4 as a

putative ZFTRAF1 interactor, and since ZFTRAF1 is also mutated in paediatric low-grade gliomas [Chen et al., 2021], this creates scope for another link between HERC4 and neurological disease.

Choquet et al. also found a developmental connection for HERC4, this time in mouse eye fibre cells [2024]. In mouse embryos, HERC4 levels were substantially higher in this cell type compared to epithelial cells, but they fell by around 60% after birth, remaining around 3-fold higher than epithelial levels, which remained roughly consistent. Alongside this, HERC4 was among the genes they linked to the risk of cataract development, with a 1.38-fold reduction in a model based on overexpression of Foxe3, a gene whose downregulation is linked to cataract formation [Wada et al., 2011].

At the other end of the age spectrum, the second published connection between HERC4 and neuropathologies is that it is downregulated at the transcriptome level in neurons displaying Lewy pathology. This phenotype is characterised by α-synuclein aggregates and is associated with Parkinson's disease [Goralski et al., 2024]. Interestingly, given the context of HERC4 in the IR CRISPR screen underpinning this project, this reduction in HERC4 expression is juxtaposed with the upregulation of base excision and mismatch repair genes. It also appears to be human-specific, since HERC3 was downregulated in mice instead. The connection is reinforced by the inclusion of a HERC4-derived circular RNA (circRNA), hsa_circ_0007113, in a dataset linked to senescence and aging, and whose enriched pathways include Parkinson's disease [Li et al., 2023b]. Hsa_circ_0007113 inhibits p21 and p53 expression, putatively by acting as a sponge for a microRNA (miRNA) involved in regulating this pathway. Therefore, as expression of the circRNA decreases with age, it causes an increase in p53 pathway activity, which is associated with cell senescence [reviewed by Rufini et al., 2013].

The same circRNA was identified by He et al. as a mediator of cell invasion in colorectal cancer [2021]. Hsa_circ_0007113 levels are elevated in the tumour, with greater upregulation associated with increased metastasis and shorter survival. This is once again achieved through

its function as a miRNA sponge, this time for a miRNA that downregulates a Notch pathway inhibitor. In cellular and mouse models, siRNAs against hsa_circ_0007113 reduced cell proliferation, survival, migration and invasion, without impacting HERC4 mRNA levels. This was consistent with the lack of difference in HERC4 mRNA expression between tumour and healthy tissues, and the insignificant effect of HERC4 levels on overall survival. It is interesting to consider that the *HERC4* gene may have functions beyond those of its protein product.

While He et al. only found differences in HERC4 circRNA, other studies have shown oncogenic connections at the protein level. According to Kaplan-Meier plots produced by UALCAN from TCGA data, 6 of the 32 cancer types studied showed a significant ($p<0.05$) correlation between high or low HERC4 expression and survival times [Chandrashekar et al., 2022; database accessed September 2025]. In all 6 types, high HERC4 expression was associated with worse prognosis, a trend supported by approximately half of the limited literature on the subject. Increased HERC4 expression was detected in papillary thyroid cancer compared to paired non-tumour tissue [Iacobas & Iacobas, 2024], and found to correlate with severity in lung cancer [Zeng et al., 2015], but neither study identified a mechanism behind the correlation. The same correlation was found in breast cancer, with HERC4 knockdown reducing cell proliferation, migration and invasion, and increasing apoptosis in cellular assays. It also produced significantly smaller tumours in xenograft models compared to normal HERC4 levels [Zhou et al., 2013; Xu et al., 2019]. 2 miRNAs that target HERC4 were found to be significantly lower in breast cancer samples compared to tumour-adjacent normal tissue, 1 of which was also associated with longer survival for higher expression, and LATS1 was identified as a relevant HERC4 substrate in this effect. This produced a model in which miRNA downregulation increases HERC4 abundance and consequently LATS1 ubiquitylation, resulting in its degradation. Loss of LATS1 relieves inhibition of oncogenic proteins YAP and TAZ, which then activate the Hippo signalling pathway, promoting cell proliferation and explaining the clinical correlations observed. Changes in exon composition described in another studied added therapeutic context to the

connection between HERC4 and breast cancer [Wang et al., 2020]. Once again, HERC4 was found to be upregulated in tumour samples, and while there was a noticeable difference in HERC4 levels between stable disease and partial response groups following neoadjuvant chemotherapy and modified radical mastectomy, this difference was only statistically significant for expression of exon 23. An exon skip event was among the 14 most common alternative splicing events linked to survival, and exon loss was significantly higher in the partial response group compared to patients showing stable disease.

HERC4 was also linked to treatment response in melanoma, with higher expression in patients in whom treatment was effective [Liu et al., 2024a]. Its expression was also found to correlate with that of antigen-presentation genes reinforced by data from lung adenocarcinoma patients, and it showed synthetic lethality with CD274 in several cancer types including breast and oesophageal cancer, further implicating HERC4 in the immune system. Additional therapeutic relevance was identified by Olivieri et al. in their screen for genes involved in DNA damage response, with many of the drugs tested being common chemotherapy compounds [2020]. Network analysis found 27 hits linked to HERC4, with a minimum correlation of 0.55, and pathway enrichment analysis highlighted several DNA repair pathways (Figure 1) [analysis tool built by Ge et al., 2020], suggesting that HERC4 may be involved in sensitivity to such treatments. The other dominant area of cell function highlighted by this analysis was the cell cycle. Since many cancer therapies rely on differing proliferation rates to distinguish between healthy and cancerous cells, it is interesting to consider that HERC4 may further contribute to treatment sensitivity by influencing the speed or timing of cell cycle progression.

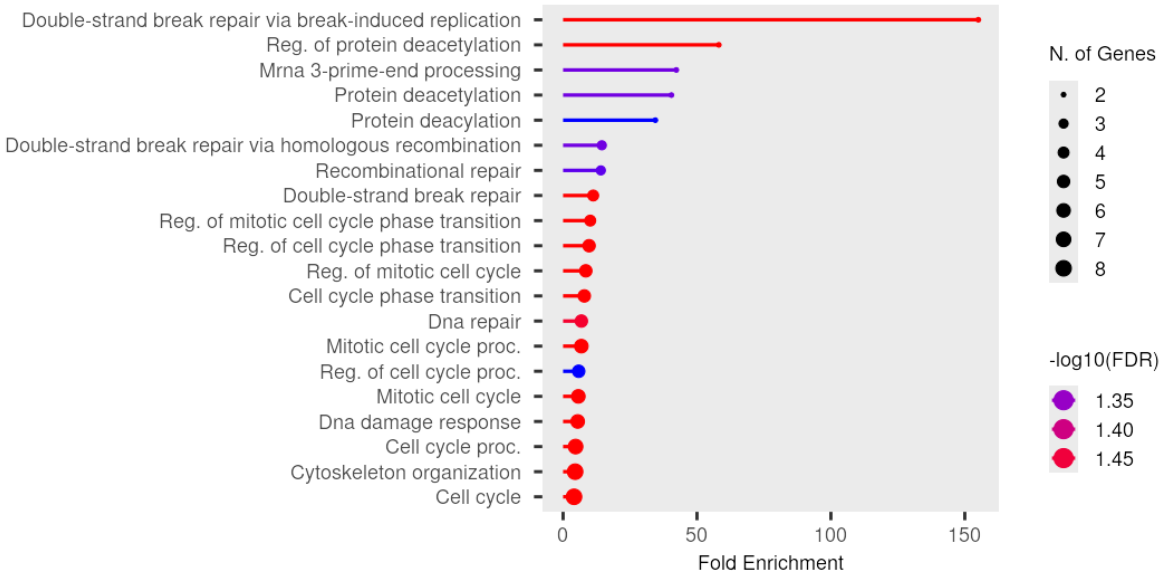


Figure 1: DNA repair and cell cycle pathways are enriched in proteins associated with HERC4 in DNA damage responses

In a screen for genes influencing DNA damage sensitivity, Olivieri et al. identified 27 genes with a connection to HERC4 [2020]. Pathway enrichment analysis of these genes mainly identified pathways in DNA damage and the cell cycle, suggesting that HERC4 may influence these processes to alter cell viability after treatment with DNA-damaging agents. Analysis run and figure produced using the online tool built by Ge et al. (https://bioinformatics.sdstate.edu/go/) [2020].

Although there is currently limited evidence for, or independent validation of, many of the disease phenotypes proposed for HERC4, these papers do highlight the breadth of putative roles that the *HERC4* gene could play in cells, at both the RNA and protein level. The phenotypes for which there is most experimental evidence are proliferation, metastasis and survival, all of which change in favour of tumour growth when HERC4 protein levels increase in hepatocellular carcinoma, and breast and cervical cancer [Huang et al., 2021; Zheng et al., 2017; Xu et al., 2019; Wei et al., 2016]. In contrast, ovarian cancer, NSCLC and multiple myeloma show increased growth when HERC4 levels drop, suggesting that HERC4 regulates substrates with opposing roles in the cell [Sun et al., 2019; Zhu et al., 2024; Zhang et al., 2016]. This therefore raises the question of how HERC4 might influence glioblastoma development, since little data is currently available on this topic. According to glioblastoma data from The Cancer Genome Atlas (TCGA) analysed on the Human Protein Atlas website, there is no significant difference in overall survival between individuals with high and low levels of HERC4 [The TCGA Research Network, 2008; Uhlén et al., 2015]. Several other datasets also found no difference in HERC4 expression between glioblastoma and healthy tissue, or between primary and recurrent tumours [Lemée et al., 2018; Tatari et al., 2022]. However, in the Human Protein Atlas validation set, a striking and statistically significant increase in survival is seen in patients with high HERC4 expression [Uhlén et al., 2015]. There is a clear downregulation of HERC4 expression in glioblastoma, but this appears to be largely attributable to copy number losses caused by the deletion of chromosome 10 that is characteristic of the disease [Horiguchi et al., 1999; Louis et al., 2021]. The only published connection between HERC4 and glioblastoma describes HERC4 as a downstream effector of PRR11, a protein upregulated in recurrent tumours that promotes resistance to ferroptosis and temozolomide [Miao et al., 2024]. Although this suggests that HERC4 could hold a key to unlocking therapeutic progress in a disease for which treatment has stagnated for decades (reviewed by Angom et al., 2023), there is no published follow-up to this study. Given the lack of published work on this protein and its gene, especially in the context of human cancer,

its identification as a potential radioprotector alongside hints at various roles in tumorigenesis and treatment sensitivity, makes it an attractive target for further research. Its putative connections to DNA repair and proliferation pathways support an influence on radiosensitivity and warrant further exploration of the phenotypes generated by manipulating HERC4 expression in glioblastoma.

2.2 – Methods

2.2.1 – Tissue culture

DBTRG and LN229 cells were taken from lab stocks and short tandem repeat analysis was not conducted. They were grown in DMEM with 10% FBS and no antibiotics (D10-) unless otherwise indicated, and they were incubated at 37°C, 5% CO_2. Cells were detached using TrypLE and counted on a Countess machine using trypan blue.

Cells were checked for mycoplasma contamination approximately every 2 years by Dr Irene Sechi.

2.2.2 – CRISPR knockouts

2.2.2.1 – CRISPR

sgRNA sequences were designed by and ordered from Synthego (sequences in Appendix 1), and transfected into DBTRG and LN229 cells according to manufacturer's instructions. As part of this protocol, Cas9 protein was also transfected into the cells to avoid complications of sustained Cas9 expression. Transfected cells were then manually split into 96-well plates at a dilution likely to put only one cell in each well (≤1 cell per 200 µl). Once the media in a well started to change colour, cells were transferred to a larger plate and expanded until they were confluent in a 6-well plate. Samples were taken for western blot validation and the remaining cells were expanded back to confluency and frozen at -80°C in FBS with 10% DMSO.

No selection agent was used and cells were analysed once ~10 clones reached confluency in a 6-well plate. Based on western blot data, the cleanest knockout clones were selected, and the first 3 suitable clones were chosen, numbered left to right on the western blot.

2.2.2.2 – PCR validation

Genomic DNA was extracted using a Qiagen DNeasy Blood and Tissue kit according to manufacturer's instructions, then the HERC4 region around the CRISPR cut sites was amplified using primer sequences recommended by Synthego (Appendix 2) and Q5 DNA polymerase (reaction parameters in Appendix 3). Products were run on a 1% agarose gel containing 0.5% ethidium bromide and extracted using a QIAquick Gel Extraction kit. PCR and gel extraction steps were repeated to obtain sufficient product, which was then sequenced by Sanger sequencing through Source Bioscience, using the primers recommended by Synthego.

2.2.2.3 – Western blot validation

For antibody validation, knockdown of HERC4 by siRNA transfection was performed according to manufacturer's instructions.

Cell pellets were lysed in RIPA buffer with protease inhibitors and quantified by BCA or modified Lowry assay. Lysates were diluted to match the lowest concentration and denatured in Laemmli buffer at 95°C, then run on a NuPAGE™ Bis-Tris 4-12% gel in MOPS buffer. Proteins were transferred to activated PVDF and protein concentration normalisation was checked using Ponceau S dye. After the dye was washed off, the membranes were blocked in 5% milk diluted PBS with 0.1% Tween for at least 30 minutes at room temperature or overnight at 4°C. Membranes were washed in distilled water or PBS with 0.1% Tween then incubated at 4°C overnight in 1:1000 HERC4 primary antibody (13691-1-AP, polyclonal) in 3% BSA (bovine serum albumin) with <1% sodium azide. The wash step was repeated before membranes were incubated in rabbit secondary antibody in milk (dilutions in Appendix 4) for at least 1 h at room temperature. Following at least 3 washes in distilled water or PBS with 0.1% Tween, membranes were developed in SuperSignal™ West Pico PLUS Chemiluminescent Substrate on an iBright machine.

2.2.3 – Morphology imaging

Cells were seeded into 96-well plates in D10-, excluding at least the outer ring of wells, which were instead filled with media or PBS to protect cells in more central wells from evaporation. The sequence of cells in each row was also varied to minimise the effect of positional variance across the plate. Cells were incubated for 48 h before being imaged at 10X magnification on an IncuCyte S3, and images (5 per well) were analysed using the cell-by-cell protocol in the IncuCyte image analysis software (parameters in Appendix 5). 4 seeding densities were plated – 1000, 2000, 4000 and 8000 cells/well – but only the middle two were used in the final analysis. 8000 cells/well resulted in high cell densities at 48 h, potentially altering cell morphology, while at the very low densities reached from 1000 cells/well meant that background debris constituted a high percentage of the detected cell count.

Area and eccentricity values were exported for each detected cell, and graphed using R (Appendix 6). Statistical significance was determined by one-way ANOVA for each parameter in GraphPad Prism.

2.2.4 – Resazurin assay

Cells were seeded into 96-well plates as described in 2.2.3, with the same seeding densities (the same plates were used for both experiments). Cells were incubated for 48 hours to ensure full attachment and normal growth, before being imaged and analysed as for 2.2.3. Resazurin solution was then added to a final concentration of 10 µg/ml and the cells incubated for a further 3 h before the fluorescence of each well was measured using a CLARIOstar Plus plate reader (parameters in Appendix 7). Blank-corrected fluorescence measurements were normalised to cell count and confluency in Microsoft Excel, then the results were graphed in R (Appendix 6) and statistical significance assessed by one-way ANOVA and Dunnett's test in GraphPad Prism.

2.2.5 – Proliferation assays

Cells seeded into 96-well plates as described in 2.2.3, with 750 and 1000 cells/well for LN229 and DBTRG cells respectively. Plates were incubated overnight, then transferred to an IncuCyte S3 where they continued to be incubated with images taken at 4X magnification every 6-8 h. The whole-well imaging protocol was used to ensure confluency measurements would not be skewed if cells did not settle evenly across the well.

For radiation experiments, all plates were removed from the incubator ~24 h after imaging started, and kept at room temperature during the irradiation process. The relevant plates were treated with 4 and 10 Gy using a caesium source before plates were returned to the IncuCyte and imaging continued for at least 1 week.

For drug treatments, ~24 h after imaging started, media was removed from each well and replaced with D10- containing the appropriate concentration of the target compound. Media for untreated controls contained PBS for bleomycin and Zeocin plates, and DMSO for camptothecin and Olaparib plates, and the volume of each solution matched the volume used for the highest drug concentration. Plates were returned to the IncuCyte for another ~24 h before the media was removed again and replaced with fresh D10-, and imaging continued for at least 5 days.

Variation in initial seeding densities prevented accurate visual comparison of proliferation curves (Appendix 8), and normalisation of confluency measurements to initial values for each well exacerbated this issue. Additionally, normalising treated proliferation curves to their untreated counterpart in the same experiment biased the results towards slower growing populations at higher treatment doses that might exceed the sensitivity of the assay. Doses that virtually stop cell proliferation would produce similar percentage confluency measurements, meaning that fold change calculations depend disproportionately on the confluency and therefore proliferation rate of the untreated controls. While not immune to this effect, direct comparison of proliferation rates means that the treated value approaches 0 as the assay reaches its

sensitivity limit, pushing the fold change towards infinity and minimising the differences between cell types. Comparing proliferation rates consequently offers the most intuitive graphical representation of the data as well as the lowest risk of significant false positives.

Proliferation rates were measured as the gradient of $\log_2$(percentage confluency) for each well, with averages obtained from these rates, not the gradient of the average proliferation curve. Where rates were normalised to wildtype or untreated controls, mean values for each condition were used, and standard error of the mean was used to combine errors from each of these values. All calculations were done in R and Excel, graphs were plotted in R, and statistical comparisons made by one-way ANOVA with Dunnett's test in GraphPad Prism.

2.2.6 – Cell cycle analysis

2.2.6.1 – Flow cytometry

Cells were seeded into 6-well plates in D10- (80,000 and 100,000 cells/well for LN229 and DBTRG cells respectively) and incubated for 2 days. EdU was added to a final concentration of 10 μM and cells were incubated in the dark at 37°C for 30 minutes. Cells were detached in TrypLE and collected alongside the EdU media. They were washed once in 0.1% BSA in PBS, then fixed in 4% PFA for 15 minutes at room temperature. After another wash, they were permeabilised in 1% BSA, 0.5% Triton in PBS for 1 h at room temperature or overnight at 4°C. EdU was labelled with Alexa fluor 647 azide by incubation in a click reaction mixture (Appendix 9) for 1 h at room temperature. The reaction was quenched in 1% BSA in PBS for 5 minutes at room temperature, then cells were washed in 0.1% BSA in PBS and resuspended in 5 μg/ml DAPI before being analysed on an Attune NxT. The proportion of cells in each cell cycle phase was determined using floreada.io, and graphs of the resultant data were produced in R (Appendix 6). Statistical significance was assessed by two-way ANOVA in GraphPad Prism.

2.2.6.2 – Western blot

Cells were seeded into 6-cm plates (160,000 cells/well and 200,000 cells/well for LN229 and DBTRG cells respectively) and incubated for 2 days before being harvested by scraping and frozen as dry pellets at -80°C until lysis. Pellets were lysed in RIPA buffer and lysates were boiled in Laemmli buffer at 95°C before being run on NuPage Bis-Tris 4-12% gels in MOPS buffer, with each sample split across 4-5 wells. Western blotting was completed as described in 2.2.2.3. The full length of the membrane was stained and developed for each cyclin, then stained and developed again for HERC4 and/or α-tubulin (dilutions in Appendix 4).

2.2.7 – Colony formation assay

Cells were diluted in D10- and used to seed CellBind 6-well plates. Plating efficiencies varied substantially between experiments, with values consistently higher for the knockout lines compared to wildtype cells in the same experiment (Appendix 14). Plates were shaken gently to encourage even distribution of cells across the well, then incubated overnight. All plates were kept at room temperature while each one was treated with the appropriate dose from a caesium source, before being incubated until colonies in the untreated plate were visible by eye (~2 weeks). Media was removed from all plates and wells were gently washed with PBS prior to staining with 0.3% crystal violet in 50% methanol and 10% ethanol. Plates were incubated in the crystal violet solution for approximately 30 minutes, rocking gently, before the solution was removed and the plates rinsed gently in water. Once dry, colonies were imaged on a GelCount machine and counted manually. Colonies were identified based on size, density and proximity to other larger or denser colonies (since smaller, adjacent colonies could have detached from the main colony rather than growing independently). For example, Figure 10B contains 2, 1 and 4 colonies in parts i, ii and iii respectively, In part iii, the uppermost colonies were deemed to have grown independently based on their similar size and density, whereas the patch attached to the bottom of the third colony from the left was much lighter and therefore considered to have

grown from the denser colony. Plating efficiencies and surviving fractions were calculated using the CFAssay library in R (Appendix 6) [Braselmann et al., 2015], which was then used to fit the data to a linear quadratic model, plot the results, and check for statistically significant differences between wildtype cells and the clones using a one-way ANOVA for each comparison.

2.2.8 – DNA Damage Western Blots

~6 x 10^5 cells were seeded in ~7 ml DMEM + 10% FBS + 1% Pen-Strep (D10+) in 10-cm plates and incubated overnight. Irradiated plates were then treated with 10 Gy from a caesium source, and for camptothecin treatment, camptothecin was added to a final concentration of 1 µg/ml. The equivalent dilution of DMSO was added to the DMSO control plates. Cells were harvested by scraping at the time points indicated, and frozen at -80°C until lysis. Samples were prepared and blots run and analysed as per 2.2.2.3, except with nitrocellulose membranes in place of PVDF. The membranes were cut into fragments for γH2Ax, GAPDH or α-tubulin, HERC4 and pATM (dilutions in Appendix 4).

2.3 – Results

2.3.1 – Cell Lines

2.3.1.1 – Selection of complementary glioblastoma cell lines

DBTRG cells were selected as the first cell line in order to validate the results of the initial CRISPR screen. A second cell line with contrasting features was then sought to facilitate identification of factors underpinning any phenotypes that might be identified, and LN229 cells were chosen for this. Both cell lines were derived from female patients of around 60 years of age and meet the four molecular criteria for glioblastoma (Figure 2 and Tables 1-2): wildtype IDH, mutations in the *TERT* promoter, *EGFR* amplification, and Chromosome 7 duplication with Chromosome 10 deletion [Gabler et al., 2019; Patil et al., 2015 ; Schnöller et al., 2023 ; Kruse et al., 1992]. The cell lines have different morphologies and express two contrasting mutations – DBTRG cells have wildtype *TP53* and a *BRAF* V600E gain-of-function mutation, whereas LN229 cells have a loss-of-function P98L mutation in *TP53* but wildtype BRAF [Nicolaides et al., 2011; Tsai et al., 2021]. Although BRAF mutations are rare in glioblastoma [Di Nunno et al., 2023], making LN229 the more representative model in this regard, *TP53* frequently contains gain-of-function mutations [Zhang et al., 2018], making the loss of active p53 unusual. p53 activity was therefore checked by western blot of PUMA, which is upregulated by active p53 [Cregan et al., 2004] (Figure 2ii). PUMA showed increasing abundance in DBTRG cells after treatment with 10 Gy, but it was not detected at all in LN229, despite clear p53 expression. This confirmed the loss of p53 function reported for LN229. However unusual this loss may be, p53 activity is known to correlate with radiosensitivity (reviewed by Okazaki, 2022), so this difference provides an interesting point of contrast nonetheless. Another difference relevant to treatment sensitivity is MGMT promoter methylation – the modification is present in LN229 but absent in DBTRG cells [Nie et al., 2018; Schnöller et al., 2023], suggesting they may show different responses to DNA-alkylating drugs such temozolomide [Hegi et al., 2005]. Lastly, DBTRG cells contain 2 copies of Chromosome 10, containing HERC4, whereas LN229 cells contain 3 copies [Kruse et al., 1992; Weber et al., 2023; Schnöller et al., 2023].

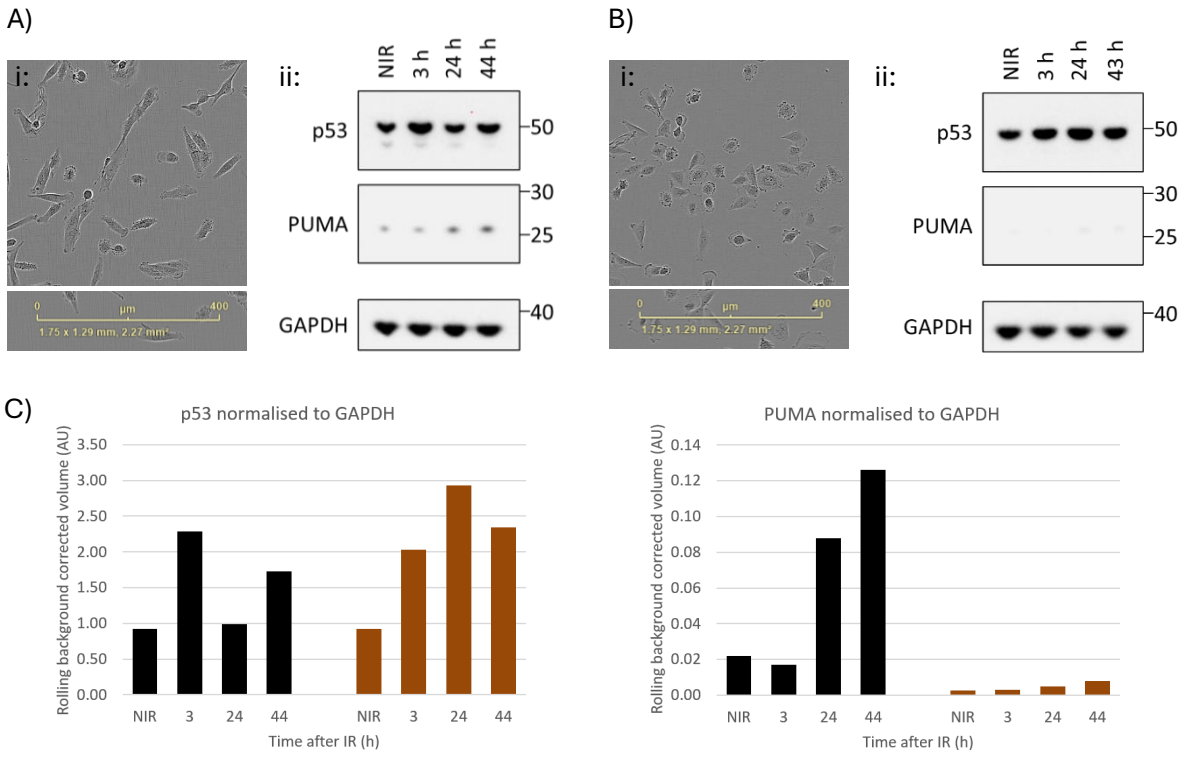


Figure 2: Morphology and cytogenetic properties of A) DBTRG and B) LN229 cells

i. Phase images taken on IncuCyte S3 at 10X magnification

ii. p53 response after 10 Gy – DBTRG cells show upregulation of PUMA, a downstream target of p53, while LN229 do not, consistent with the cell lines expressing wildtype and non-functional p53 respectively. (N=1)

C) Quantification of western blots (1 blot quantified) DBTRG LN229

	DBTRG	LN229
Patient	59-year old Caucasian female	60-year old Caucasian female
Morphology	Fibroblast	Epithelial
Chromosome number	87 (2 copies of Chr 10)	86 (3 copies of Chr 10)
p53 status	p53 WT [3]	$p53^{P98L}$ (loss of function) [3]
MGMT promoter methylation	- [1]	+ [1-2]

Table 1: Key cell line features

Both cell lines were derived from female patients of similar ages but they have different morphologies. Both are near-tetraploid, but DBTRG cells have 2 copies of chromosome 10, containing HERC4, while LN229 cells have 3 copies. As shown in ii, DBTRG cells have functional p53 while LN229 have a loss-of-function mutation in this gene, and differing methylation patterns on the promoter of the MGMT gene suggest differing sensitivities to temozolomide, a key chemotherapy drug in high-grade glioma treatments.

[1] Nie et al., 2018
[2] Schnöller et al., 2023
[3] Tsai et al., 2021

Gene	Change	DBTRG	Astrocytoma	Oligodendrocytoma	Glioblastoma	References	LN229	Astrocytoma	Oligodendrocytoma	Glioblastoma	References
IDH1/2	Mutation	×					×				
ATRX	Deletion, mutation	×					×				
TP53	Mutation (loss-of-function)	×					✓				
CDKN2A/B	Deletion	✓					✓				
1p/19q	Co-deletion	×					×				
pTERT	Mutation	✓				[1]	✓				[2]
CIC	Mutation	×					×				
FUBP1	Mutation	×					×				
NOTCH1	Mutation	×					×				
EGFR	Amplification	✓				[4]	✓				[3]
Chr7/10	Gain/loss	✓				[4]	×				[3]

Table 2: Cell line classification by WHO criteria 2021

Genetic changes are marked green or red for each tumour type to indicate if the status of this change in DBTRG or LN229 cells matches the expected status for the corresponding tumour type. For example, IDH mutations are expected in astrocytoma and oligodendrocytoma cases, but not in glioblastoma, so their absence in DBTRG cells is marked as red for the first 2 tumour types (no match) but green for glioblastoma (cells match tumour). Both DBTRG and LN229 cells have all 4 glioblastoma characteristics, as well as several properties of other types of brain tumour.

[1] Gabler et al., 2019
[2] Patil et al., 2015
[3] Schnöller et al., 2023
[4] Kruse et al., 1992

2.3.1.2 – Generation of HERC4 knockout clones

3 sgRNA sequences were designed against the first coding exon based on the canonical HERC4 isoform (204) (Figure 3C), 1 from the reverse and 2 from the coding strands respectively (Figure 2B), to reduce the probability of accurate repair and facilitate deletions that would be discernible by gel electrophoresis of PCR products. DBTRG and LN229 cells were transfected with the RNA guides and Cas9 protein, and the resultant populations were split into single cells in a 96-well plate. 8 and 11 of these clones were checked for each cell line respectively (Appendix 10), and 3 potential knockouts from each cell line were selected for further validation by PCR and sequencing (Figure 3D and E).

PCR validation – LN229

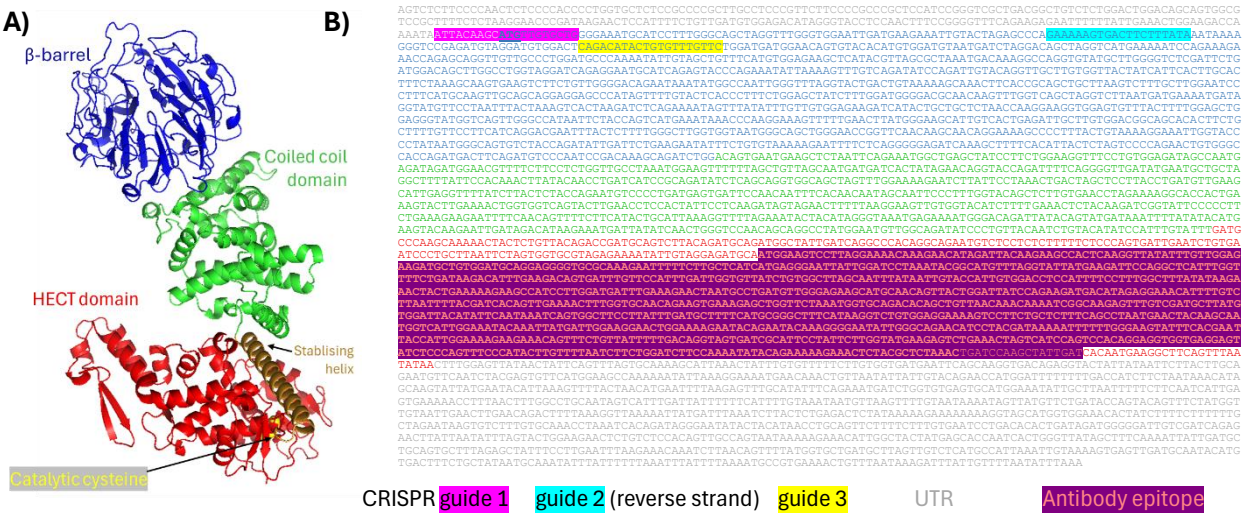
In LN229 Clone 1, all copies of *HERC4* contained deletions of the same length, giving only one size of PCR product. This contained a 137-bp deletion that puts the rest of the gene out of the correct reading frame. Clone 2 produced the same sequence, and Clone 3 had a similar 136-bp deletion, also causing a frameshift in the rest of the gene. Both clones had second copies of HERC4 with smaller indels that nonetheless had the same downstream effect. Clone 2 produced a third band in the initial PCR, but this was not detected in subsequent gels using products of concurrent reactions (Appendix 11). Clone 3 was more complex, containing two other bands, one with a 205-bp deletion, the other with a 172-bp insertion and an 11-bp deletion. The fourth band either suggests that the clonal population is instead a mixture of 2 or more cell lines, therefore giving the possibility of more than 3 forms of HERC4, or reflects the mixed origin of the parental cell line, for which several karyotypes have been identified [Schnöller et al., 2023; Weber et al., 2023]. All 3 reported karyotypes in these papers show 3 copies of Chromosome 10, however, suggesting that there were multiple cells at the point of cloning.

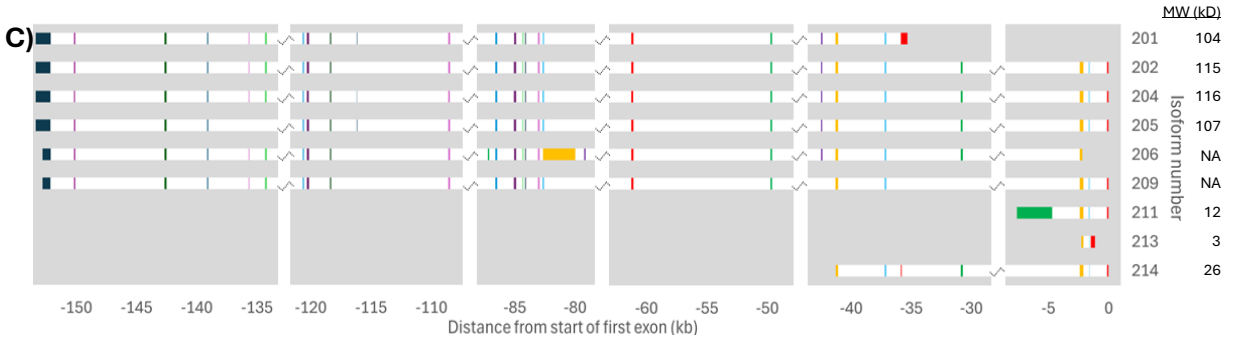
PCR validation – DBTRG

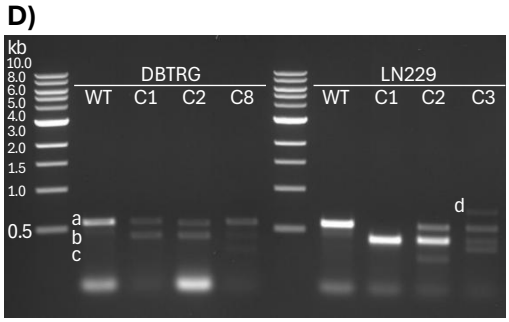
DBTRG Clones 1 and 2 both gave 2 PCR products – 1 of approximately wildtype size, the other with a 137-bp deletion. For Clone 1, the larger product contained a 166-bp deletion but also a 167-bp insertion, causing a net frameshift of 1 base, while the larger product in Clone 2 contained a 14-bp deletion. Clone 8 contained two products with 137- and 247-bp deletions respectively, but was also found still to contain the wildtype sequence as the dominant band. However, when checked again by western blot (Figure 3G), the clone again produced no band at the appropriate molecular weight, suggesting that the PCR band may be a contaminant from a neighbouring wildtype sample during a gel extraction step.

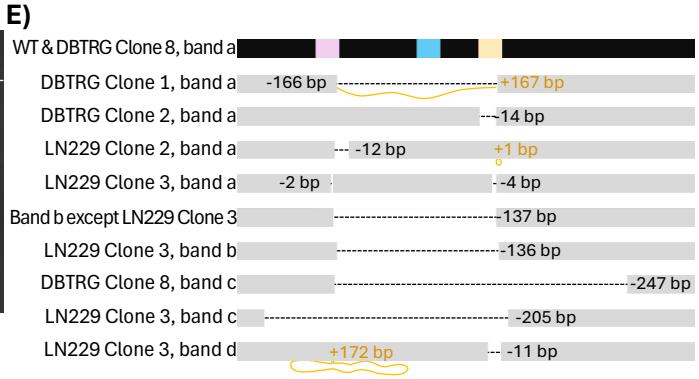
Western blot validation

A HERC4 antibody was validated on samples in which HERC4 had been knocked down by siRNA (Figure 3F). Wildtype DBTRG cells produced 2 bands – 1 at the appropriate molecular weight for HERC4 isoforms 202 and 204, and the other, lower band for isoform 201 (~118 and 104 kD respectively). Since Isoform 201 has an alternative start codon in an exon downstream of the CRISPR guide RNAs (Figure 3C), and the antibody recognises an epitope in the HECT domain that is common to all 3 isoforms (Figure 3A-C), it was plausible that this second band represented residual HERC4. However, the knockdown cells did not produce a significantly fainter band at this molecular weight, whereas the higher band was substantially fainter than the counterpart from wildtype cells. This confirmed that only the higher band at 118 kD was specific for HERC4. Additional bands were visible in subsequent western blots (e.g. Figure 2G-H), but none of these were at molecular weights corresponding to other predicted HERC4 isoforms (Figure 3C), so they were also deemed non-specific. The selected clones were then checked again by western blot to confirm that the genetic alterations resulted in the absence of HERC4 protein (Figure 3G-H).


A)
β-barrel
Coiled coil domain
HECT domain
Stablising helix
Catalytic cysteine
B)
CRISPR guide 1
guide 2 (reverse strand)
guide 3
UTR
Antibody epitope


C)
MW (kD)
201 104
202 115
204 116
205 107
206 NA
209 NA
211 12
213 3
214 26
Isoform number
-150 -145 -140 -135 -120 -115 -110 -85 -80 -60 -55 -50 -40 -35 -30 -5 0
Distance from start of first exon (kb)


D)
kb
10.0
8.0
6.0
5.0
4.0
3.0
2.0
1.5
1.0
0.5
DBTRG
WT C1 C2 C8
LN229
WT C1 C2 C3
a
b
c
d


E)
WT & DBTRG Clone 8, band a
DBTRG Clone 1, band a
-166 bp
+167 bp
DBTRG Clone 2, band a
-14 bp
LN229 Clone 2, band a
-12 bp
+1 bp
LN229 Clone 3, band a
-2 bp
-4 bp
Band b except LN229 Clone 3
-137 bp
LN229 Clone 3, band b
-136 bp
DBTRG Clone 8, band c
-247 bp
LN229 Clone 3, band c
-205 bp
LN229 Clone 3, band d
+172 bp
-11 bp

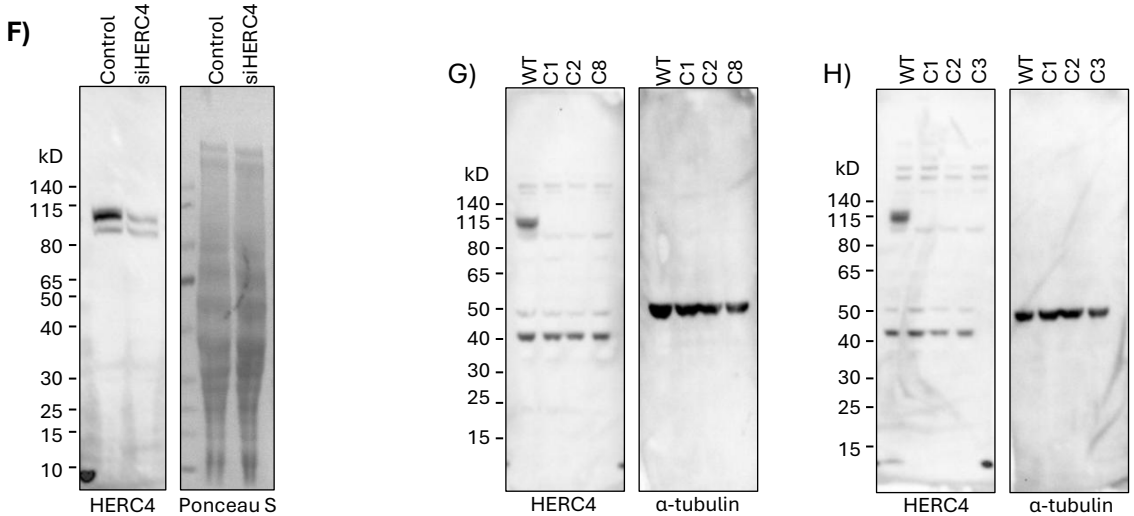

F)
Control
siHERC4
Control
siHERC4
kD
140
115
80
65
50
40
30
25
15
10
HERC4
Ponceau S
G)
WT C1 C2 C8
WT C1 C2 C8
kD
140
115
80
65
50
40
30
25
15
HERC4
α-tubulin
H)
WT C1 C2 C3
WT C1 C2 C3
kD
140
115
80
65
50
40
30
25
15
HERC4
α-tubulin

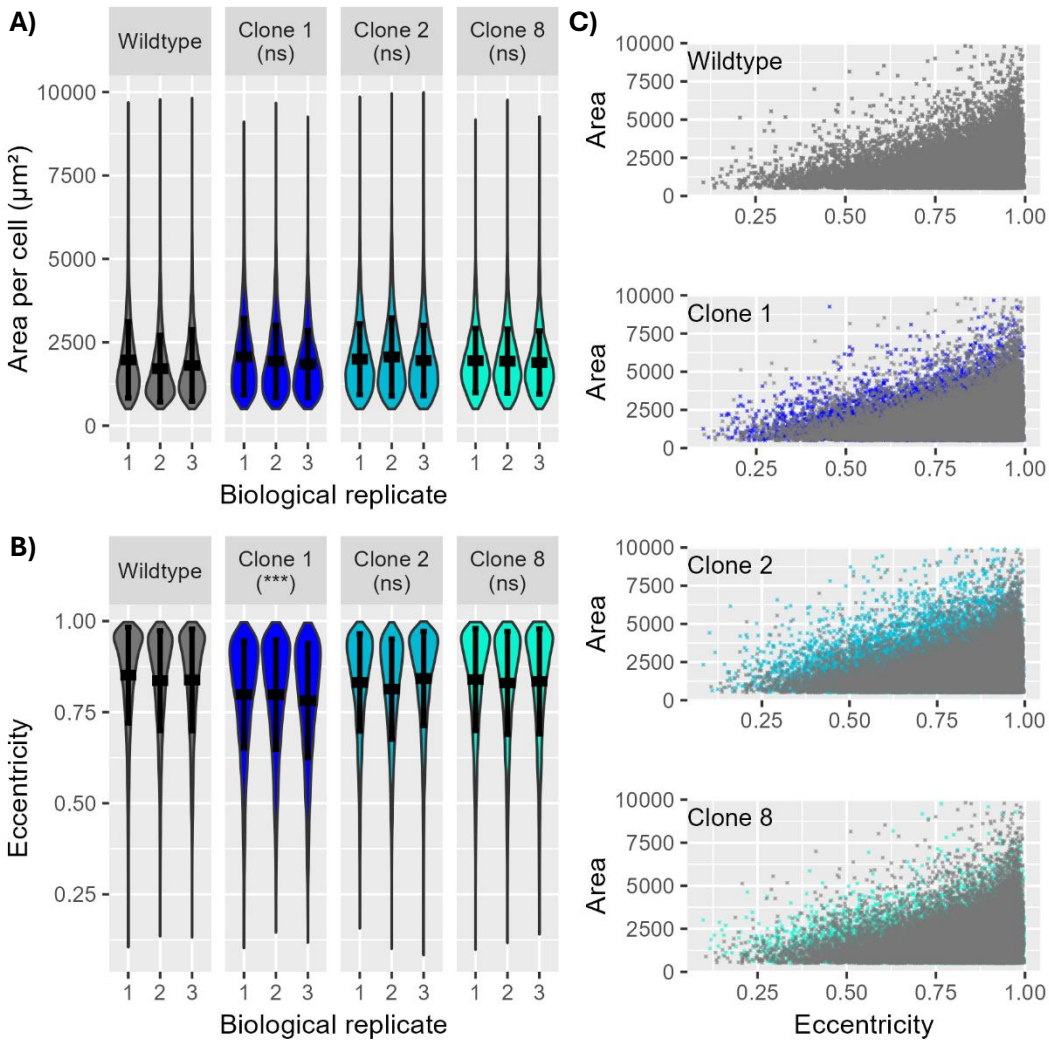
Figure 3: HERC4 knockout clone generation

A) Protein structure of HERC4 predicted by AlphaFold and formatted in PyMOL [The PyMOL Molecular Graphics System, Version 3.0 Schrödinger, LLC]. Downloaded from the AlphaFold database on 02/06/2024; average pLDDT = 0.9162. B) HERC4 coding sequence (canonical isoform 202) with CRISPR guides and antibody epitope highlighted. Text colours correspond to protein structure in A. C) Gene structure of protein-coding isoforms [Ensembl, August 2025]. Exons are shown in colour and introns are shown in white. Negative numbers reflect the position of HERC4 on the negative strand of Chromosome 10, with the start of the gene on the righthand side of the diagram. Predicted molecular weights are shown to the right, with "NA" indicating isoforms subject to nonsense-mediated decay [Ensembl, August 2025]. D and E) Size and sequence of HERC4 PCR products from selected clones. (N=1, n=1) F) HERC4 antibody validation by siRNA knockdown. (N=1, n=1) G and H) HERC4 protein levels in wildtype cells and selected knockout clones in DBTRG and LN229 respectively. ◀HERC4 (118 kD) (N>3, n≥1)

2.3.2 – HERC4 Knockout Clone Characterisation

2.3.2.1 – HERC4 loss has no consistent effect on cell morphology

Cells were imaged by phase microscopy at 10X magnification then analysed for their area and eccentricity (Figures 4-5). All 3 DBTRG clones were consistent with the wildtype line, except for Clone 1 being more circular. This was consistent with it attaching to tissue culture surfaces less readily than the wildtype or other clones. LN229 clones showed more deviation from the wildtype population, with both Clone 1 and 2 being less circular, and Clone 2 also being larger. It is possible that HERC4 loss caused the change in eccentricity, since it occurred in 2 out of 3 LN229 clones; however, the change was not consistent across all 3 LN229 clones, nor the DBTRG clones, indicating more substantial evidence is required to establish a connection between HERC4 levels and cell morphology, should one exist.


A)
Wildtype
Clone 1 (ns)
Clone 2 (ns)
Clone 8 (ns)
Area per cell (µm²)
10000
7500
5000
2500
0
1 2 3
Biological replicate
B)
Wildtype
Clone 1 (***)
Clone 2 (ns)
Clone 8 (ns)
Eccentricity
1.00
0.75
0.50
0.25
Biological replicate
C)
Wildtype
Clone 1
Clone 2
Clone 8
Area
0.25 0.50 0.75 1.00
Eccentricity

D)

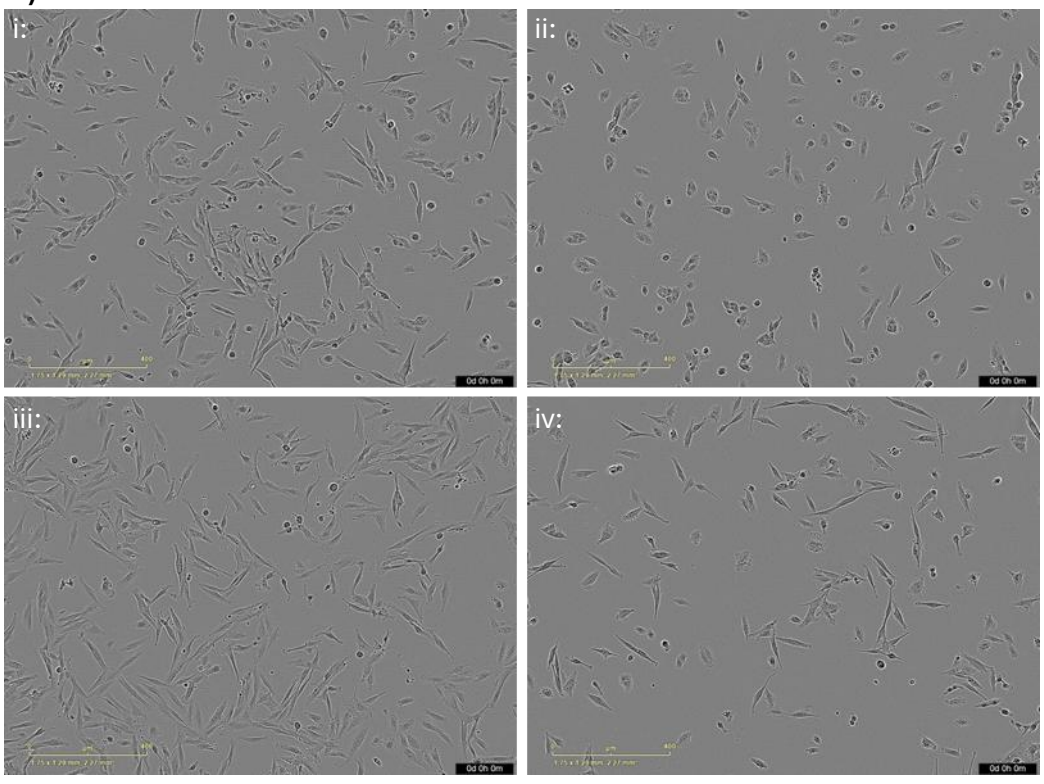
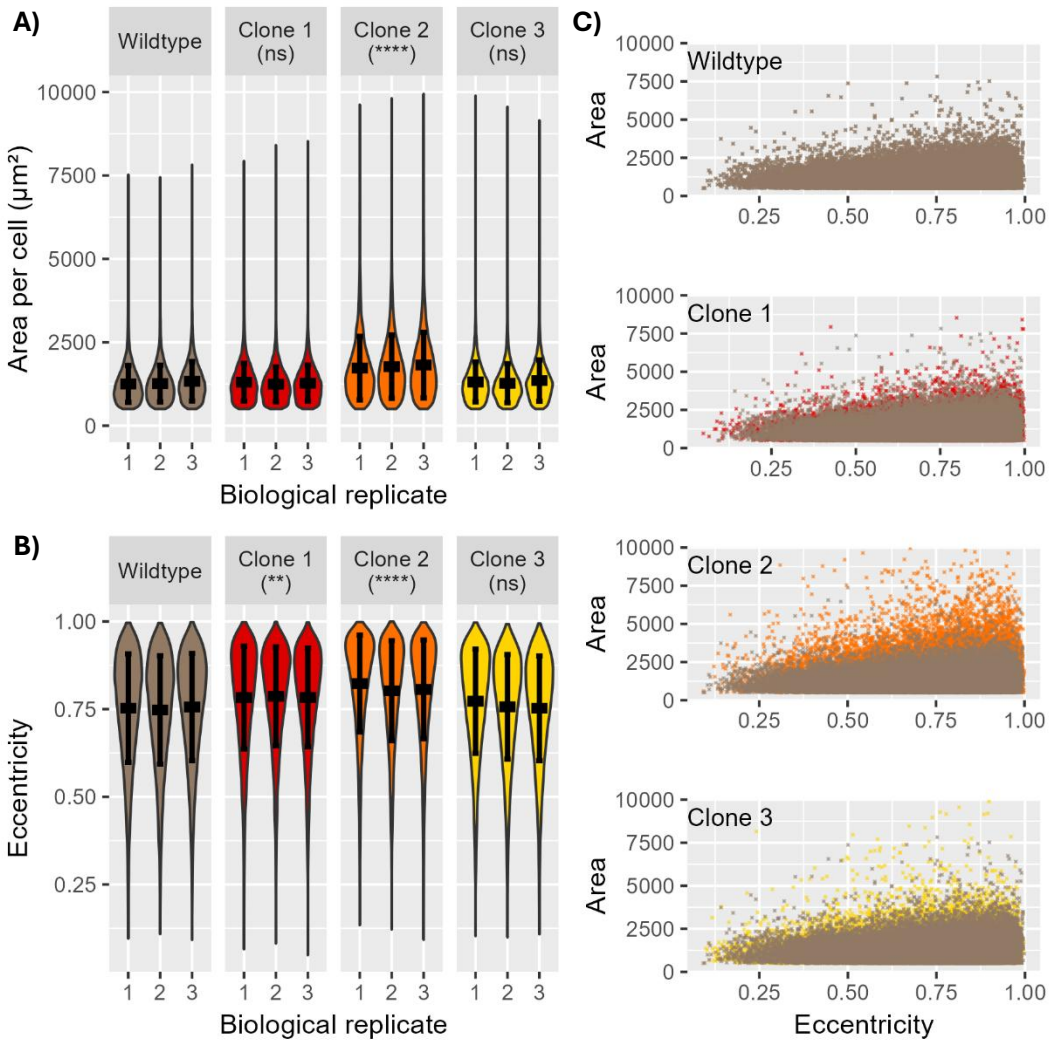

i:
ii:
iii:
iv:

Figure 4: HERC4 loss does not significantly alter DBTRG cell morphology

Cells were seeded at 4 densities 48 h prior to imaging on an IncuCyte S3 at 10X magnification (D). The images were then analysed using the cell-by-cell setting on IncuCyte software to detect individual cells and measure their area (A) and eccentricity (0 = perfect circle) (B and C). Values measured at the highest seeding density were excluded due to difficulty resolving the cells (Figure 6). The highest and lowest remaining values for each cell type were excluded prior to analysis, and statistical significance for comparing each clone to wildtype cells was determined in GraphPad Prism by one-way ANOVA with Dunnett's test. The only comparison to reach significance was Clone 1 for eccentricity, suggesting that this is a clonal effect and that HERC4 loss does not significantly alter cell morphology in DBTRG cells.

N=3; n = 10 DBTRG: Wildtype (i) Clone 1 (ii) Clone 2 (iii) Clone 8 (iv)

ns = non-significant; p<0.05 = *; p<0.01 = **; p<0.001 = ***; p<0.0001 = ****


A)
Wildtype
Clone 1 (ns)
Clone 2 (****)
Clone 3 (ns)
Area per cell (µm²)
10000
7500
5000
2500
0
1 2 3
Biological replicate
B)
Wildtype
Clone 1 (**)
Clone 2 (****)
Clone 3 (ns)
Eccentricity
1.00
0.75
0.50
0.25
1 2 3
Biological replicate
C)
Wildtype
Clone 1
Clone 2
Clone 3
Area
10000
7500
5000
2500
0
0.25
0.50
0.75
1.00
Eccentricity

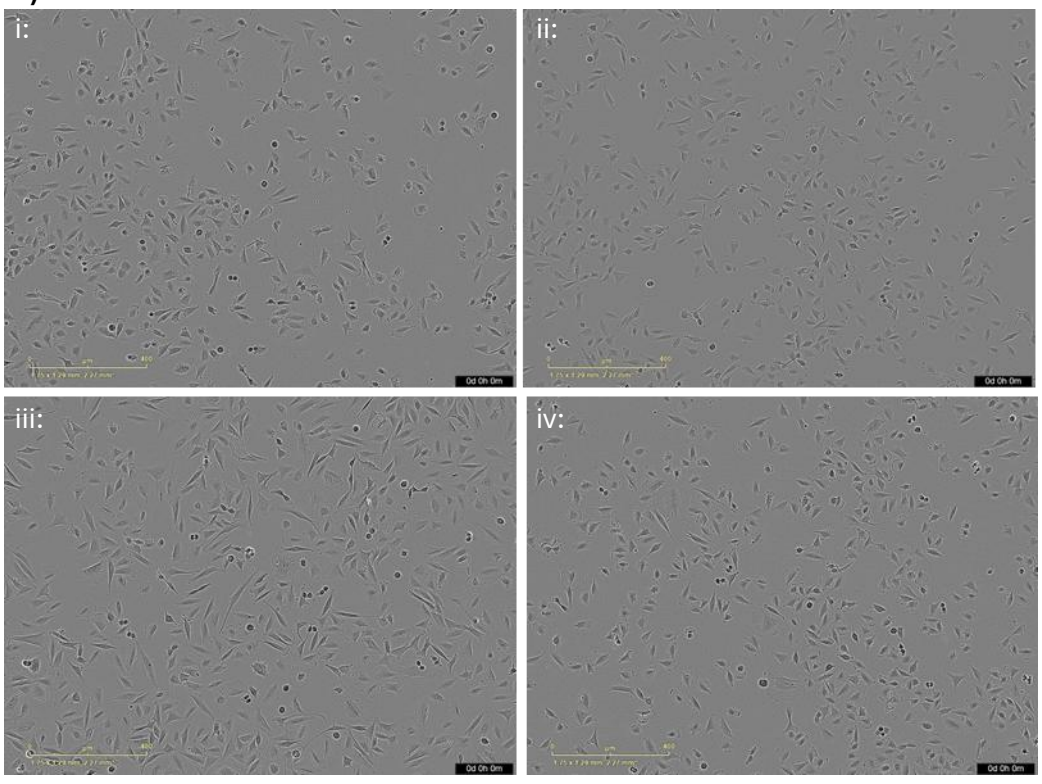

D)
i:
ii:
iii:
iv:

Figure 5: HERC4 loss may alter LN229 cell morphology

Cells were seeded at 4 densities 48 h prior to imaging on an IncuCyte S3 at 10X magnification (D). The images were then analysed using the cell-by-cell setting on IncuCyte software to detect individual cells and measure their area (A) and eccentricity (0 = perfect circle) (B and C). The highest and lowest 3 values for each cell type were excluded prior to analysis, and statistical significance for comparing each clone to wildtype cells was determined in GraphPad Prism by one-way ANOVA with Dunnett's test. Clones 1 and 2 were significantly less round than wildtype cells, and Clone 2 cells were also significantly larger, suggesting that HERC4 loss may have influenced cell morphology. The data does not rule out that the clones could simply be different from the wildtype population average, independent of HERC4 expression.

N=3; n = 10 LN229: Wildtype (i) Clone 1 (ii) Clone 2 (iii) Clone 3 (iv)

ns = non-significant; p<0.05 = *; p<0.01 = **; p<0.001 = ***; p<0.0001 = ****

2.3.2.2 – HERC4 loss may slow cell proliferation

Cells were again imaged by phase microscopy, this time at 4X magnification to image the whole well and at multiple time points. Percentage confluency was then determined and log_2-transformed so that the gradient could be taken as the proliferation rate (Appendix 8) and the reciprocal of this rate as the doubling time (Table 3). 2 DBTRG and 2 LN229 clones had a slower mean proliferation rate than their wildtype counterparts, but the difference was only statistically significant for one of each pair (Figure 6) . This rose to both DBTRG clones if the rates from each biological replicate were normalised to that of the equivalent wildtype result. The normalisation step may reduce the variation introduced by environmental factors influencing proliferation rates, such as fluctuations in temperature or CO_2 concentrations. However, the resultant values should be interpreted cautiously as it is unclear if the influence of such factors would be also affected by HERC4 levels. The raw rate values are therefore more likely to give an accurate comparison point, suggesting that if the loss of HERC4 slows cell proliferation, it does so only slightly.

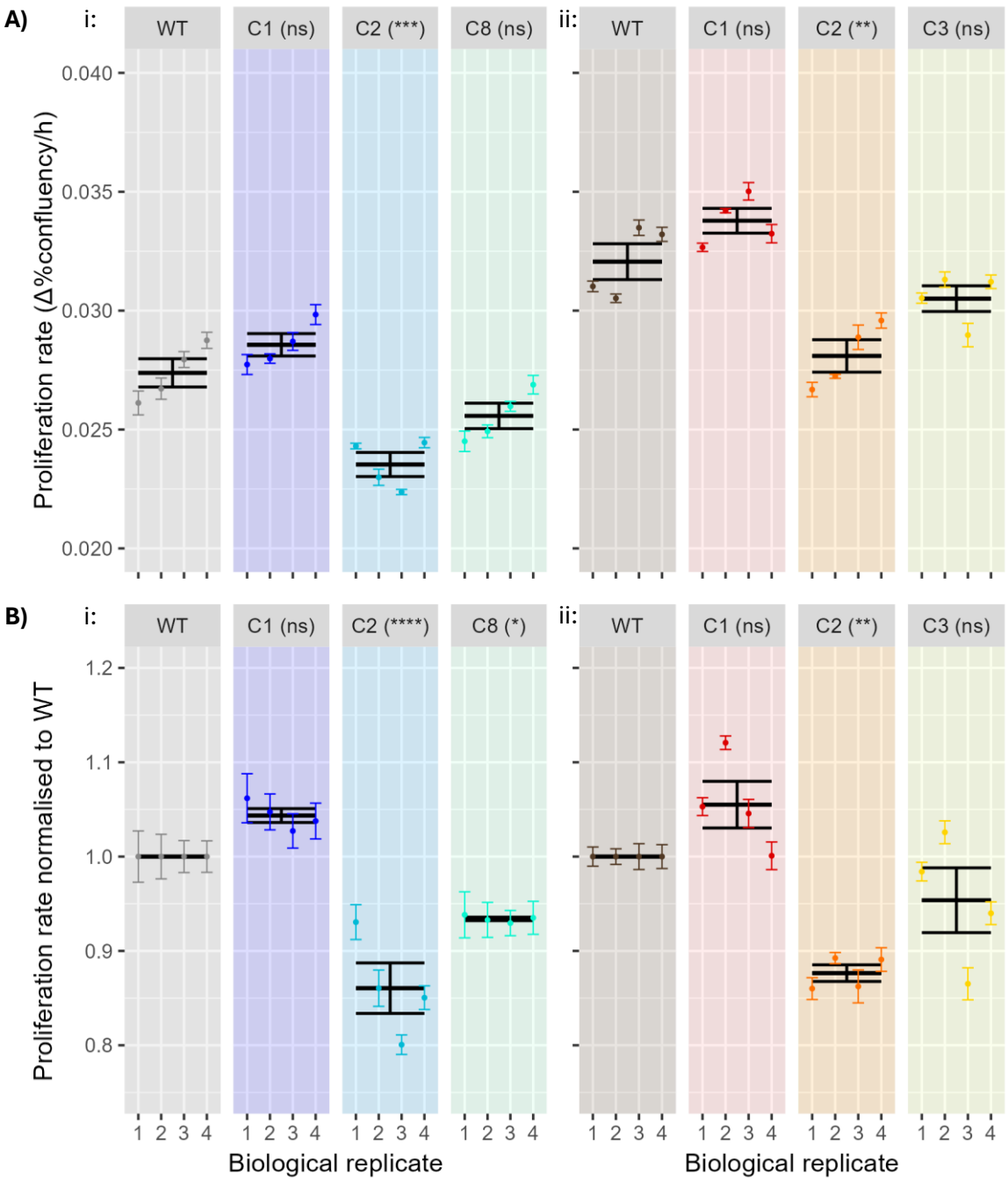


Figure 6: HERC4 loss may slow proliferation in DBTRG (i) and LN229 cells (ii)

Cells were imaged every 6-8 h at 4X magnification using an Incucyte S3 and percentage confluency was measured using IncuCyte analysis software. The proliferation rate for each well was calculated as the gradient of linear regression lines on log_2-transformed graphs between 48 h and ~50% confluency, then the mean rate for each cell line was normalised to the mean wildtype rate within a biological replicate. Each clone was compared to its wildtype control by one-way ANOVA with Dunnett's multiple comparisons test in Graphpad Prism.

N=4; n = 5, 4, 5, 4 for biological replicates 1-4 respectively

● mean (technical replicates) — mean (biological replicates) I SEM

ns = non-significant; p<0.05 = *; p<0.01 = **; p<0.001 = ***; p<0.0001 = ****

DBTRG: Wildtype Clone 1 Clone 2 Clone 8 LN229: Wildtype Clone 1 Clone 2 Clone 3

Cell line	Lower limit (h)	Mean doubling time (h)	Upper limit (h)
Wildtype	39.22	**36.52**	34.16
HERC4 KO Clone 1	36.95	**35.01**	33.26
HERC4 KO Clone 2	45.63	**42.50**	39.78
HERC4 KO Clone 8	41.90	**39.10**	36.66
Wildtype	33.71	**31.19**	29.02
HERC4 KO Clone 1	31.13	**29.60**	28.22
HERC4 KO Clone 2	38.57	**35.59**	33.04
HERC4 KO Clone 3	34.74	**32.78**	31.04

Table 3: Doubling times for DBTRG and LN229 cells with and without HERC4
Proliferation rates were calculated as described for Figure 4. Confidence limits were calculated based on the mean rate of biological replicates, and doubling times were then calculated as the reciprocal of the mean and upper and lower limits.
N=4; n = 5, 4, 5, 4 for biological replicates 1-4 respectively
DBTRG: Wildtype Clone 1 Clone 2 Clone 8 LN229: Wildtype Clone 1 Clone 2 Clone 3

2.3.2.3 – HERC4 loss has no significant effect on aerobic metabolic rate

It was hypothesised that the putative reduction in proliferation rate following HERC4 loss could be indicative of a more global reduction in cell activity. Cell metabolism was therefore estimated by the extent of resazurin reduction in ~3 h, normalised to cell number or percentage confluency (Appendix 10). Higher seeding densities were excluded from DBTRG analysis because the low contrast of the cells prevented accurate detection of cell boundaries (Figure 7). DBTRG clones showed substantially more variation than the LN229 clones, but showed no statistically significant difference from their wildtype control and no trend that would not be more likely attributed to clonal differences (Figure 8). The only notable difference among the LN229 populations was that Clone 2 reduced noticeably more resazurin per cell than the other cell types, but this difference did not reach statistical significance and disappeared when fluorescence was normalised to confluency rather than cell count. Given that Clone 2 cells are larger than the other LN229 populations used (2.3.3), it is likely that the discrepancy in activity per cell is due to a proportional increase in mitochondria with cell size, rather than increased activity in the electron transport chain. It should also be noted that while resazurin reduction reflects mitochondrial activity, it does not give a direct readout of glycolysis, upregulation of which is common in and favourable to glioblastoma. It is therefore plausible that cellular metabolism is in fact increased, but disproportionately through glycolysis and other pathways that glioblastoma cells are already reprogrammed to prioritise.

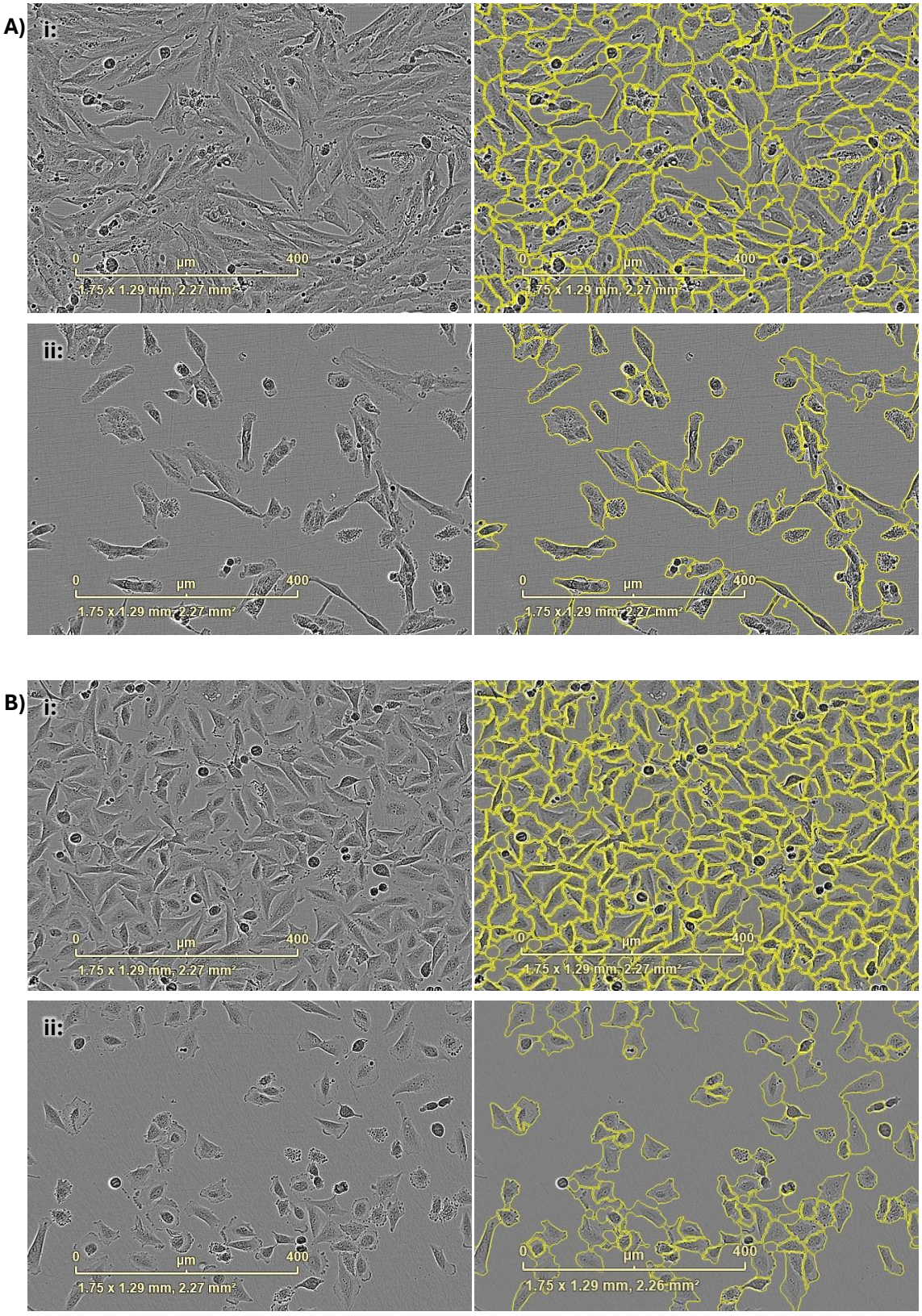


Figure 7: Analysis software could not identify DBTRG cell boundaries at high confluency
The contrast between DBTRG cells (A) is insufficient for IncuCyte software to identify cell boundaries accurately at high confluency. LN229 cells (B), on the other hand, showed higher contrast and could be distinguished at high densities as well as at lower ones. (i: 8000 cells/well; ii: 4000 cells/well)

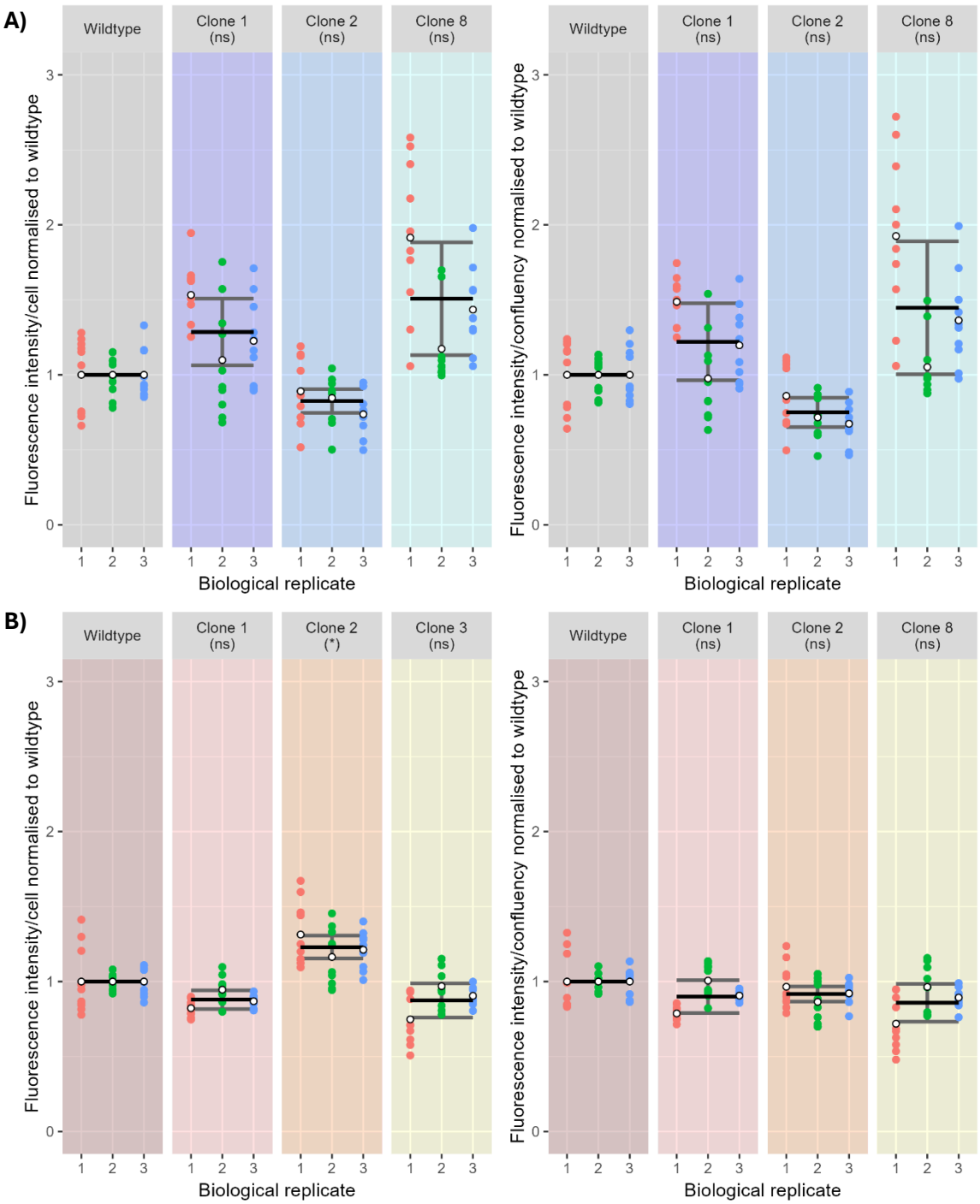


Figure 8: HERC4 knockout has no significant effect on metabolic rate in A) DBTRG and B) LN229 cells
For each biological replicate, 2 96-well plates were seeded at 4 different cell densities and incubated at 37°C, 5% CO_2 for ~2 days. Plates were imaged on an IncuCyte S3 at 10X magnification, then 10 µl/ml resazurin added for a further 3-h incubation at 37°C. Fluorescence was measured on a CLARIOstar Plus plate reader, and percentage confluency and cell counts were calculated using the cell-by-cell function of the IncuCyte analysis software. Data from all 4 seeding densities were combined for each cell line, and the highest 3 and lowest 3 values excluded from the mean. Statistical significance was calculated using biological replicate means by one-way ANOVA with Dunnett's test in GraphPad Prism.
N=3; n = 4 per seeding density Biological replicate 1, 2, 3 ○Technical replicate mean
—Biological replicate mean ⌶Biological replicate standard deviation
ns = non-significant; p<0.05 = *; p<0.01 = **; p<0.001 = ***; p<0.0001 = ****

2.3.2.4 – HERC4 loss does not significantly affect population distribution through the cell cycle

Since any differences in proliferation rate following HERC4 loss cannot be attributed to a general decrease in cell activity, it was next hypothesised that cells may be delayed in a specific phase of the cell cycle. Cell cycle pathways were among those enriched in the network of genes associated with HERC4 in the DNA damage response dataset from Olivieri et al. [2020], and longer time in S phase, for example, might allow longer for effective DNA repair, facilitating the improved survival after IR seen in the initial CRISPR screen. Cells were stained with EdU and DAPI, and analysed by flow cytometry to identify the percentage of cells in each cell cycle phase (Figure 9). LN229 clones tended to have a lower proportion of cells in non-standard phases such as sub-G1, compared to their wildtype equivalent, but this trend did not reach statistical significance and there was no consistent complementary change in other phases. In DBTRG cells, there were no noticeable differences between wildtype and knockout populations, and this was supported by western blot analysis of key cyclins for each stage of the cell cycle (Figure 10 and Appendix 15). One experiment showed higher cyclin D1 levels in wildtype DBTRG cells compared to the clones (0.72 vs 0.20, 0.14 and 0.07 for clones 1, 2 and 8 respectively, after normalisation to α-tubulin – Appendix 15), and the inverse pattern in LN229 cells (0.12 vs 0.18, 0.25 and 0.30 for clones 1-3 after normalisation to α-tubulin – Appendix 15), but this was not reproducible. Once normalised to the loading control, LN229 cells showed a 20-30% reduction in cyclin B expression in repeat 1 (Appendix 15), but no equivalent change consistently compensated for changes in cyclin D levels across all 3 DBTRG clones. It is therefore unlikely that HERC4 loss significantly alters cell cycle progression under normal conditions.

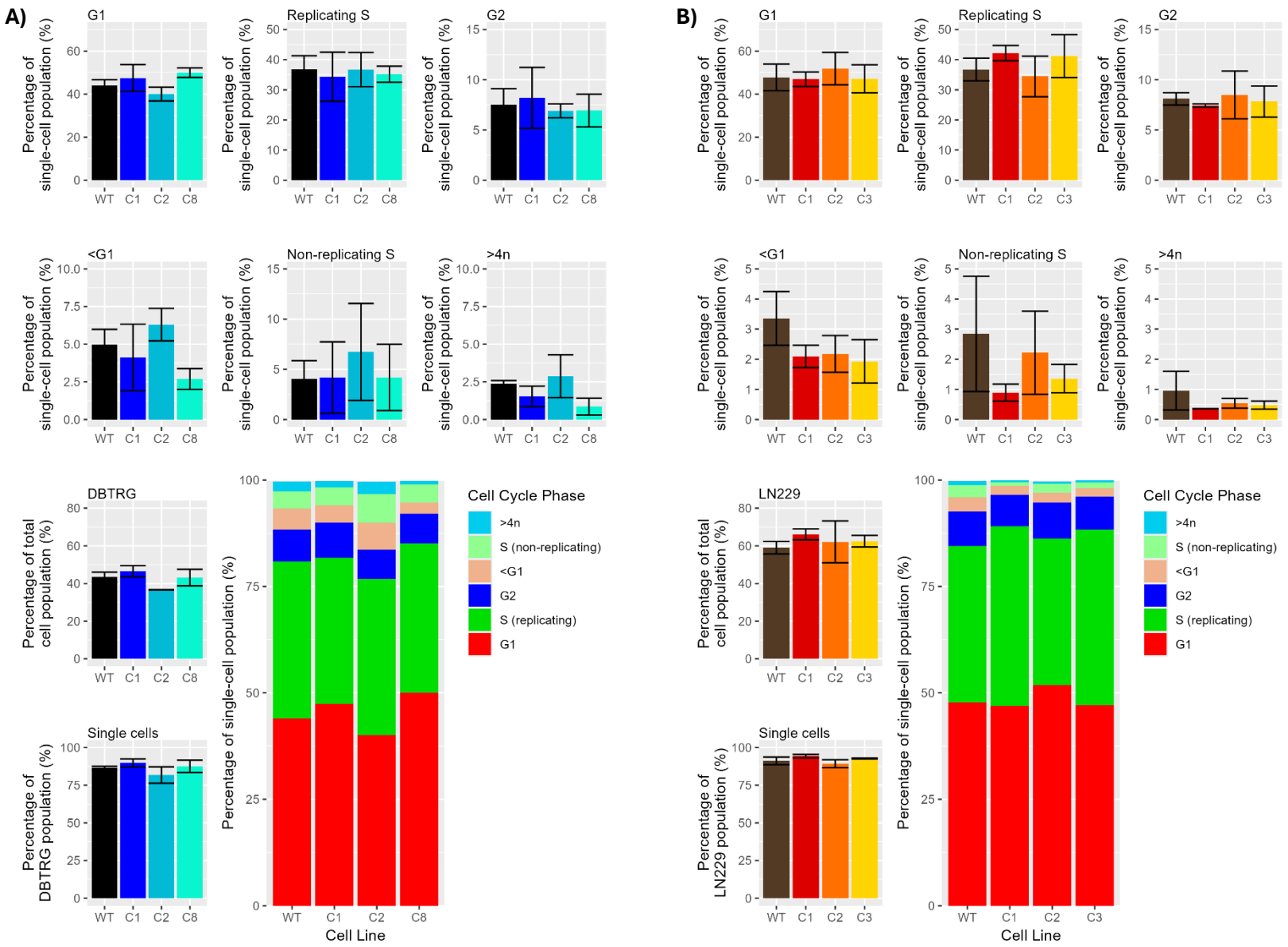

A)
B)
G1
Replicating S
G2
<G1
Non-replicating S
>4n
DBTRG
LN229
Single cells
Percentage of single-cell population (%)
Percentage of total cell population (%)
Percentage of DBTRG population (%)
Percentage of LN229 population (%)
WT C1 C2 C8
WT C1 C2 C3
Cell Cycle Phase
>4n
S (non-replicating)
<G1
G2
S (replicating)
G1
Cell Line

Figure 9: HERC4 knockout has no significant effect on the distribution of A) DBTRG or B) LN229 cells through the cell cycle

Cells were stained with 10 μM EdU for 30 minutes at 37°C prior to collection by trypsinisation. Cells were then permeabilised and Alexa fluor 647 attached to retained EdU by a click reaction. After staining with DAPI, cells were sorted on an Attune NxT Flow Cytometer and the results analysed in Floreada.io. Mean and standard deviation values across biological repeats are shown. LN229 knockouts tended towards smaller percentage populations in non-standard cell cycle phases (<G1, >4n and non-replicating S phase), but this trend did not reach statistical significance for any phase. There were no other differences from wildtype cells that were consistent between knockout lines.

Statistical significance was calculated using biological replicate means by two-way ANOVA with Dunnett's test in GraphPad Prism. The only statistically significant comparison was selection of LN229 cells for Clone 2 vs wildtype ($p<0.05$), and the overall variation between knockouts and their corresponding wildtype line was insignificant.

N=3; n = 3

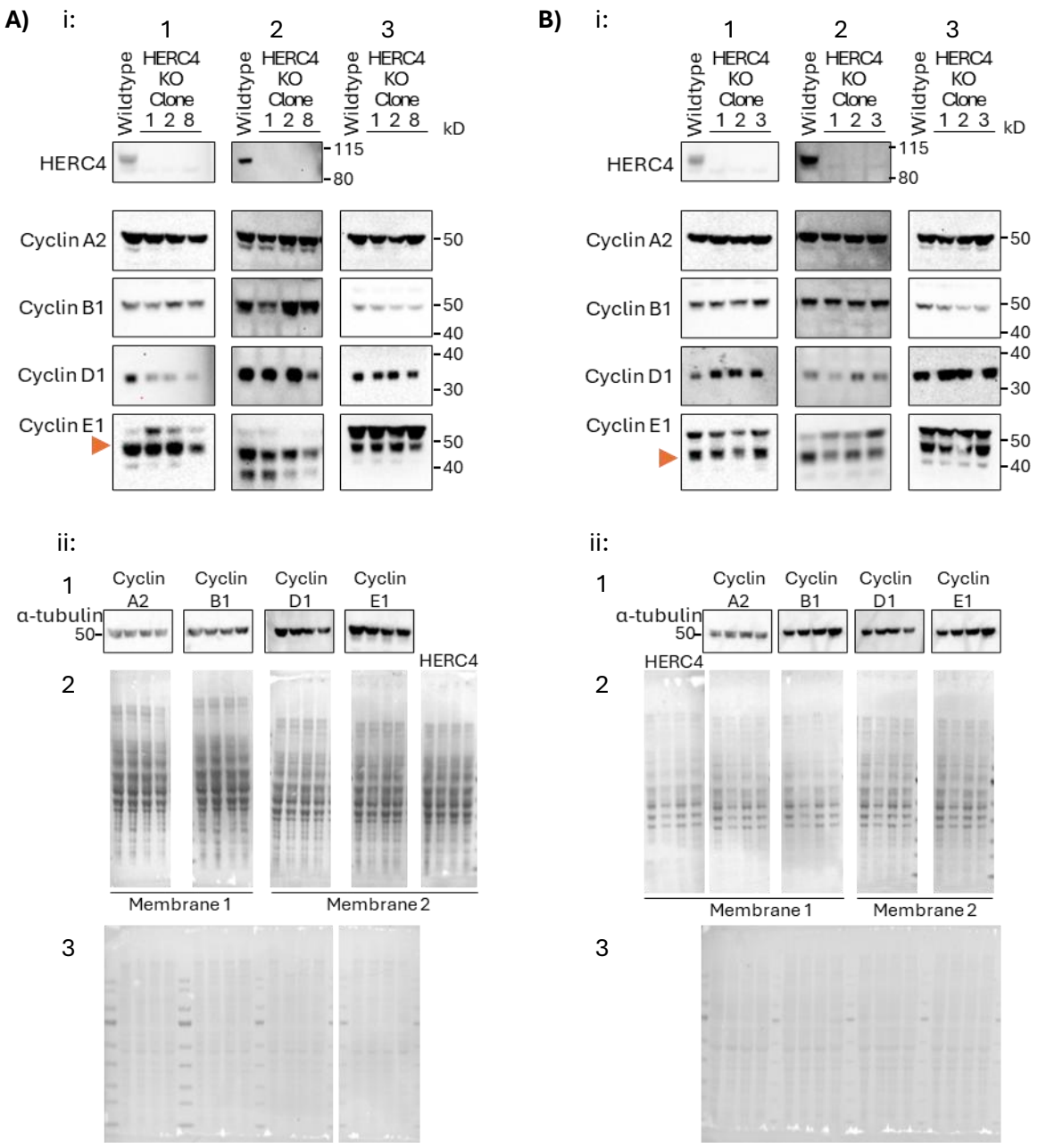


Figure 10: HERC4 knockout has no significant effect on cyclin expression in A) DBTRG and B) LN229 cells
i: Untreated knockout cells showed no reproducible differences in cyclin expression compared to their wildtype counterpart. Consistent with the flow cytometry data in Figure 7, this suggests that there is no change in cell cycle progression or regulation following HERC4 loss. ii: Normalisation data for blots in part i by staining with α-tubulin antibody (1) or Ponceau S dye (2,3). For replicate 1, HERC4 staining was done on the same membrane as Cyclin D1, so a separate normalisation blot is not shown. Western blot quantification shown in Appendix 15.
N=3; n = 1 ▶Cyclin E (48 kD)

2.3.3 – Effect of HERC4 on DNA Damage Response

2.3.3.1 – Colony formation assays may not be suitable for assessing survival in DBTRG cells

The minimal discernible differences between HERC4 knockouts and their wildtype equivalents indicated that they would provide a simple model for validating the protective effect of HERC4 loss seen in the IR CRISPR screen. Colony formation assays are the gold standard protocol for assessing survival after DNA damage, but proved challenging with DBTRG cells. Clones 1 and 2 produced opposite average trends to each other (Figure 11A), but also failed to give consistent results relative to the wildtype control (Figure 11C). This may in part be attributable to the tendency of DBTRG cells to form irregularly shaped colonies, produce high background at the higher seeding densities needed for colony growth at higher IR doses, and clump together upon seeding (Figure 11Bi-iii). Irregular colony shapes prevent accurate distinction of colonies with multiple protrusions from protrusions formed by multiple colonies, and also prevented effective automated analysis, which would have minimised variation in counting and colony identification. Colonies were instead counted manually based on size, density and proximity to other larger or denser colonies, since smaller colonies may have spread from adjacent colonies rather than growing from a separate cell. More adherent plates were tried to encourage tighter colonies, but this proved ineffective, and the issue was compounded by the tendency of the cells to clump together, blurring colonies into each other. Different plating protocols were tried to improve this, but again with limited success. Lastly, the high background made it difficult to identify the small colonies produced at high IR doses, limiting the effective dose range of the assay. No consistent effect of HERC4 was observed, but in light of these limitations, it is likely that any effect would have been obscured, so no confident conclusions can be drawn from this dataset.

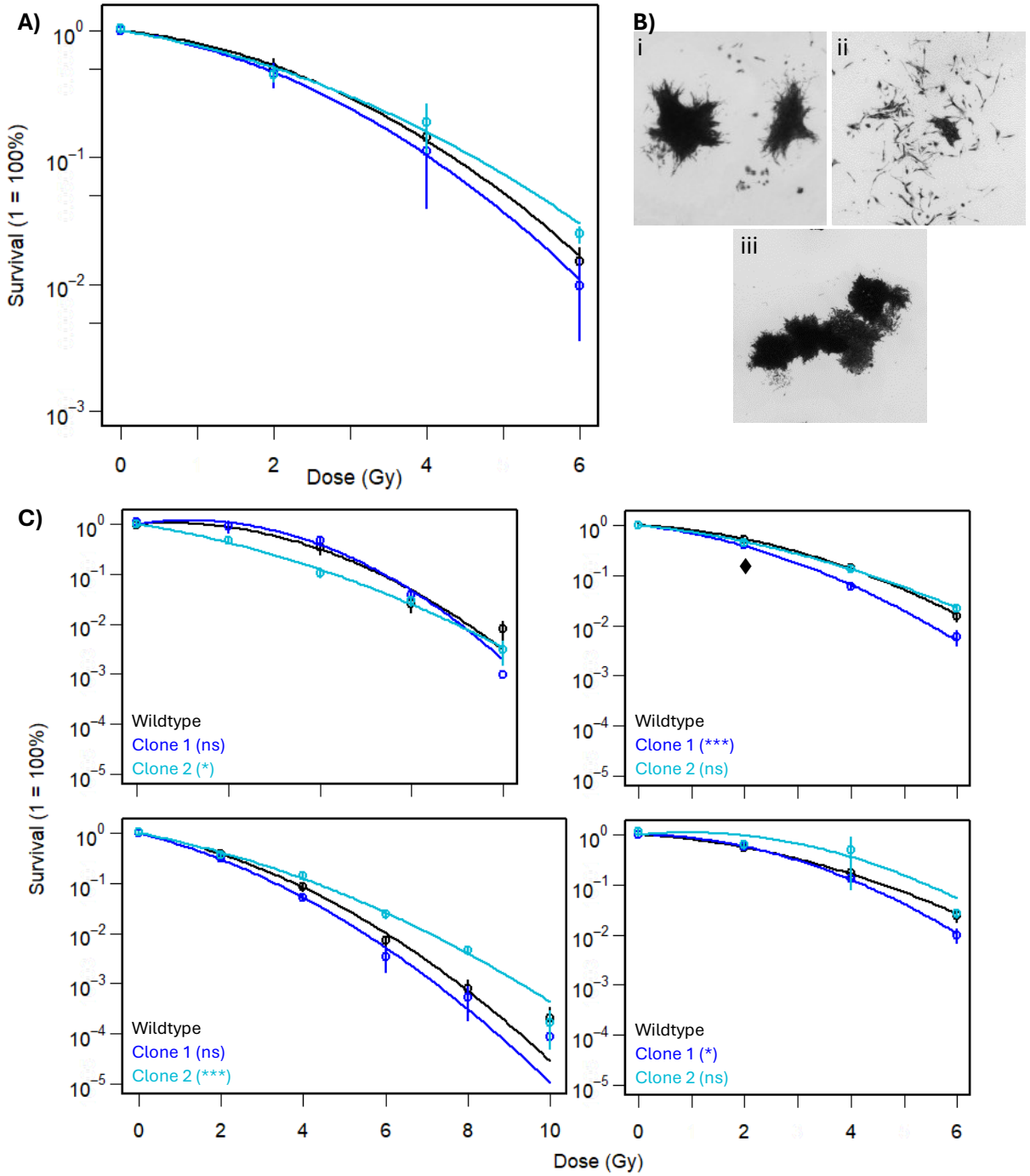


Figure 11: HERC4 loss has no detectable effect on DBTRG cell survival after IR (A) but colony formation assays may not be suitable for this cell type (B,C)

Cells were seeded into 6-well plates and irradiated ~1 day later. They were then incubated at 37°C, 5% CO_2 for ~2 weeks until colonies were visible under the microscope. Colonies were fixed and stained in crystal violet and methanol solution, imaged on a GelCount machine and counted manually. Plating efficiencies and surviving fractions were calculated and linear quadratic models fitted using CFAssay in R. The same package was used to calculate statistical significance by two-way ANOVA. A) Biological replicates showed no significant difference in cell survival after IR between wildtype and HERC4 knockout cells. B) However, issues with irregular colony shapes (i), high cell background (ii) and the tendency of cells to clump together upon seeding (iii) may limit the accuracy of colony counting, likely contributing to the high variation between biological replicates (C).

N=4; n = 3-4 (♦KO lines n=2) ○ mean | standard deviation

ns = non-significant; p<0.05 = *; p<0.01 = **; p<0.001 = ***

2.3.3.2 – HERC4 loss does not affect cell proliferation after IR

As for the proliferation assay in Figure 6, cells were imaged every 6-8 h and percentage confluency used to monitor proliferation. Cells were irradiated ~24 h after imaging started, with 4 or 10 Gy to test for dose-dependent phenotypes. Proliferation rates were calculated from $\log_2$-transformed percentage confluency values, and those for treated cells were normalised to the non-irradiated control for the same cell type (Figure 12). Despite the strong protective phenotype observed in the initial CRISPR screen, none of the clones showed a smaller change in proliferation after IR than their wildtype control. LN229 clones showed very similar changes to the wildtype population, and two of the DBTRG clones showed a greater fold reduction in proliferation rates, with the difference reaching statistical significance for Clone 8. The lack of comparable differences in other knockouts suggests, however, that this is not due to loss of HERC4.

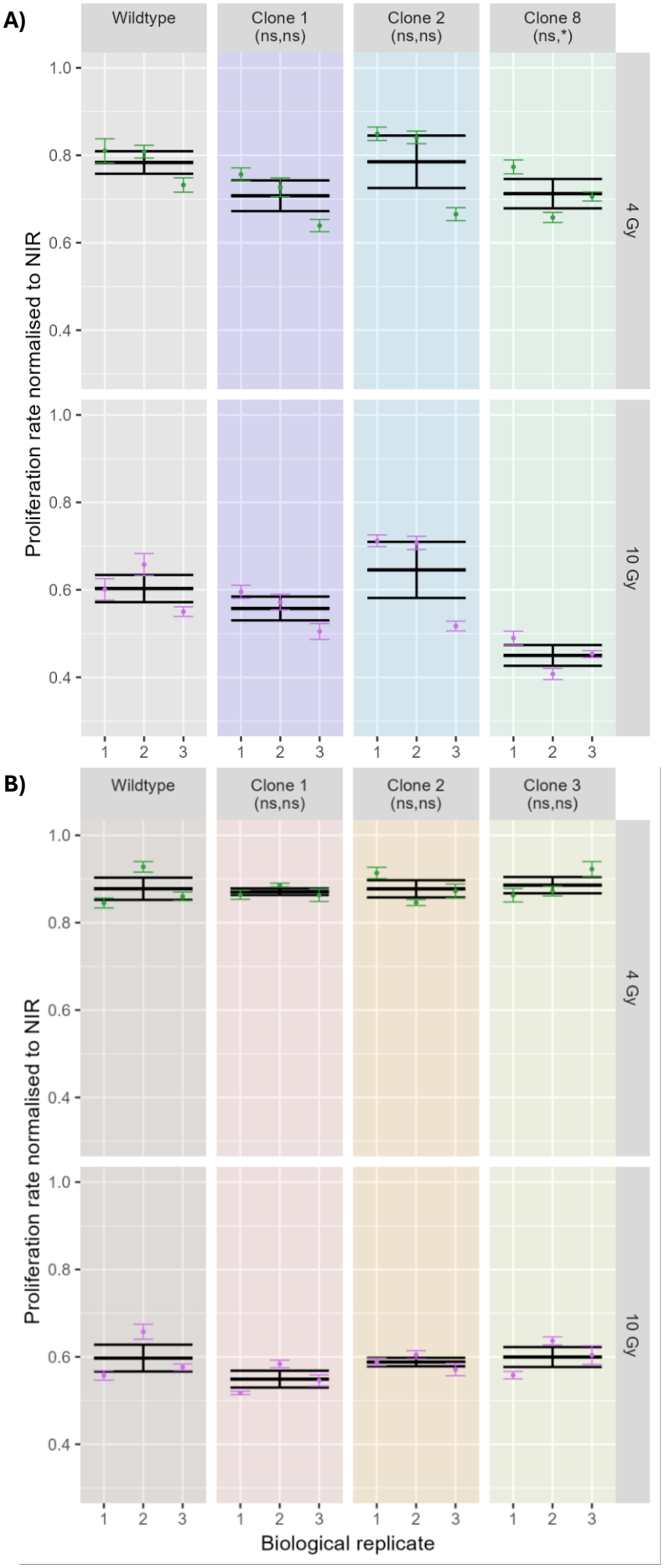

A)
Wildtype
Clone 1 (ns,ns)
Clone 2 (ns,ns)
Clone 8 (ns,*)
4 Gy
10 Gy
Proliferation rate normalised to NIR
1.0
0.8
0.6
0.4
1
2
3
B)
Wildtype
Clone 1 (ns,ns)
Clone 2 (ns,ns)
Clone 3 (ns,ns)
4 Gy
10 Gy
Proliferation rate normalised to NIR
Biological replicate

Figure 12: HERC4 loss has no significant effect on proliferation rate after IR in A) DBTRG and B) LN229 cells
Cells were imaged every 6-8 h at 4X magnification using an Incucyte S3 and percentage confluency was measured using IncuCyte analysis software. Cells were irradiated ~24 h after imaging started, and the proliferation rate of each well was calculated as the gradient of linear regression lines on log_2-transformed graphs of percentage confluency between 48 h and ~50% confluency. For each cell line, the mean rate at each dose was normalised to the NIR control of the same cell type. Each clone was compared to its wildtype control by two-way ANOVA with Dunnett's test in Graphpad Prism but only DBTRG Clone 8 showed a statistically significant difference in proliferation rate compared to the control, and only at 10 Gy. Since there is no clear biological or statistical trend among the other cell lines and conditions, this is likely a false positive.
N=3; n = 5, 4, 5 for biological replicates 1-3 respectively
ns = non-significant; p<0.05 = *; p<0.01 = **; p<0.001 = ***; p<0.0001 = ****
4 Gy 10 Gy ● mean (technical replicates) — mean (biological replicates) I SEM
DBTRG: Wildtype Clone 1 Clone 2 Clone 8 LN229: Wildtype Clone 1 Clone 2 Clone 3

2.3.3.3 – HERC4 loss may influence DNA damage signalling pathways

DBTRG cells after IR

DBTRG wildtype cells and Clones 2 and 8 were irradiated with 10 Gy and harvested at various timepoints over 2 days. γH2Ax and pATM were used as markers of DNA double-strand break signalling and repair (Figure 13). pATM levels were fairly comparable between the clones and the wildtype population, but phosphorylation of its downstream target H2Ax was more pronounced in the clones. Bands at higher molecular weights consistent with ubiquitylation and acetylation of γH2Ax were also more intense in the clones compared to the wildtype, suggesting that the increase in H2Ax phosphorylation translates into increased pathway activity. 3 h after irradiation, for example, clones 2 and 8 had modified γH2Ax levels of 0.44 and 0.64 respectively, compared to 0.14 in wildtype cells (all values normalised to signal intensity of GAPDH loading controls). This was supported by levels of unmodified γH2Ax of 1.37, 1.70 and 0.48 for Clone 2, Clone 8 and wildtype cells respectively at the 3-h time point. Higher levels of γH2Ax in the clones persisted until 44 h after irradiation (between 2- and 6-fold higher for Clone 8, and 4- and 10-fold for Clone 2) , but it is unclear if this reflects sustained signalling or simply that there was no change in degradation rate and therefore more time was needed to remove the additional protein. A further limitation is that samples were not stained for unmodified ATM and H2Ax levels, so it is not possible to distinguish between increased phosphorylation and increased abundance with proportional phosphorylation.

LN229 cells after camptothecin treatment

Although its lethality stems predominantly from the DSBs it induces, IR is a crude method of DNA damage that introduces a wide range of lesions, so camptothecin was selected as an alternative DNA damaging agent to induce DSBs more selectively, thereby providing a simpler model. These replication-induced DSBs have a specific chemical structure, further constraining the model. In contrast to irradiated DBTRG cells, LN229 cells treated with camptothecin showed greater and lower levels of pATM and γH2Ax respectively when HERC4 was removed compared to the wildtype control (Figure 14). For pATM, this difference was also visible in untreated samples (2-4 times higher for clones 1 and 2 compared to wildtype, and up to 6.7 times higher for clone 3, with all

values normalised to GAPDH loading controls), although there was still a further increase in pATM band intensity after exposure to camptothecin, reaching a maximum of a ~5- or ~8-fold difference depending on the clone. This peak was reached 2 h after camptothecin treatment, and the clones showed the same substantial decrease as the wildtype cells 24 h after treatment, although pATM levels remained higher in the clones than the wildtype population. For γH2Ax, the biggest difference in quantified and normalised signal was observed 24 h after camptothecin treatment, at the point at which the drug was removed from the cells. In wildtype cells, γH2Ax levels increased over 10-fold to ~1.5 AU, while for the clones, the fold-change was equal or greater, but the low starting point meant that normalised levels reached a maximum of 0.25, 0. 15 and 0.55 for clones 1-3 respectively. Only the lowest molecular-weight band could be detected for γH2Ax, however, and further experiments with higher protein concentrations or longer membrane exposures are required to check downstream γH2Ax modifications. An additional difference to the DBTRG dataset was the delayed appearance of γH2Ax relative to pATM. γH2Ax was not detected until 24 h after camptothecin treatment, by which point pATM levels had started to decline.

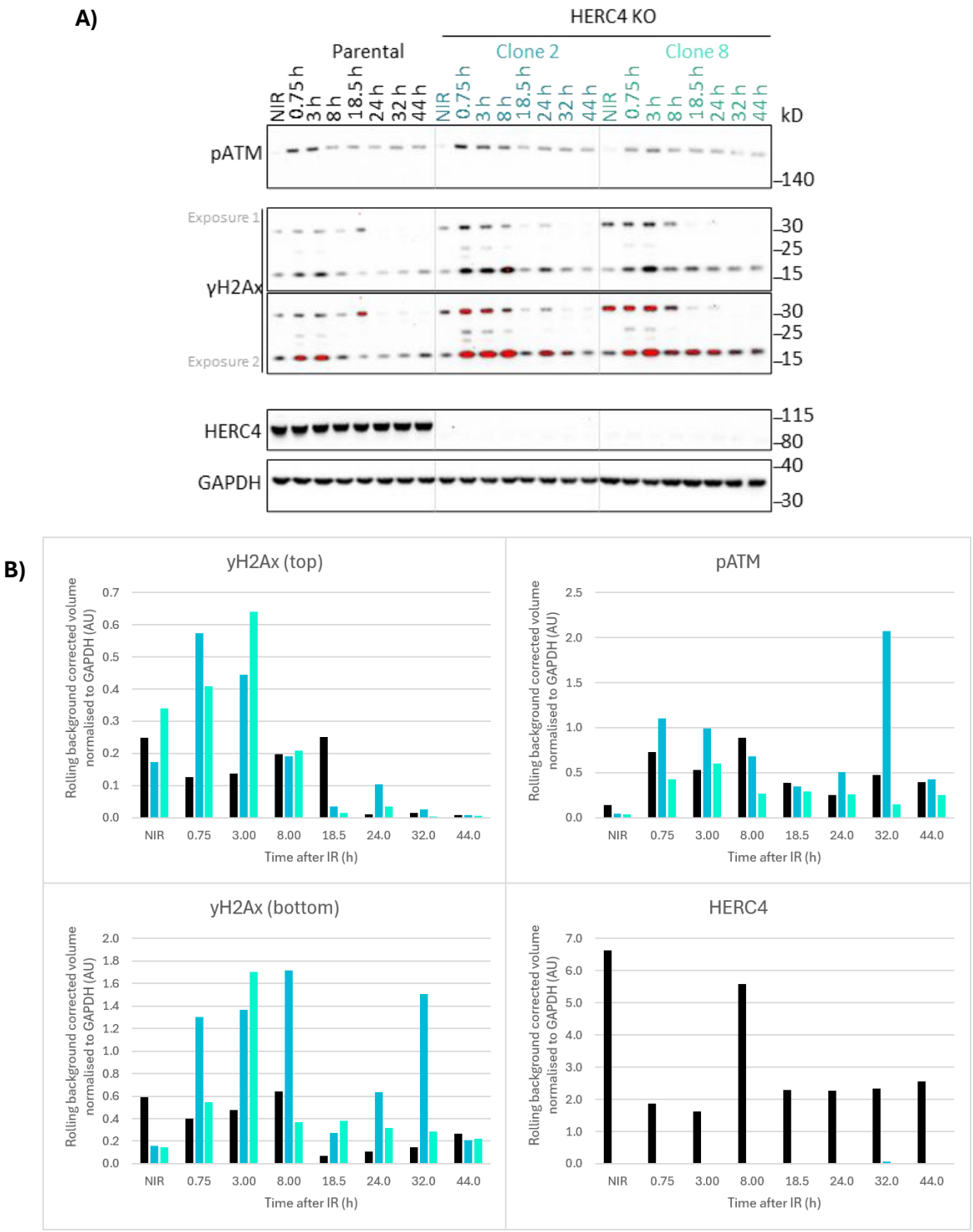


Figure 13: HERC4 loss may alter cellular responses to DNA damage by IR

A) DBTRG cells were treated with 10 Gy and their DNA damage response monitored by western blot for phosphoATM (pATM) and γH2Ax. HERC4 knockout showed increased γH2Ax expression and ubiquitylation compared to the wildtype control, while pATM levels were roughly comparable. Red patches indicate areas of overexpression.

B) Quantification of western blot

N=1; n=1

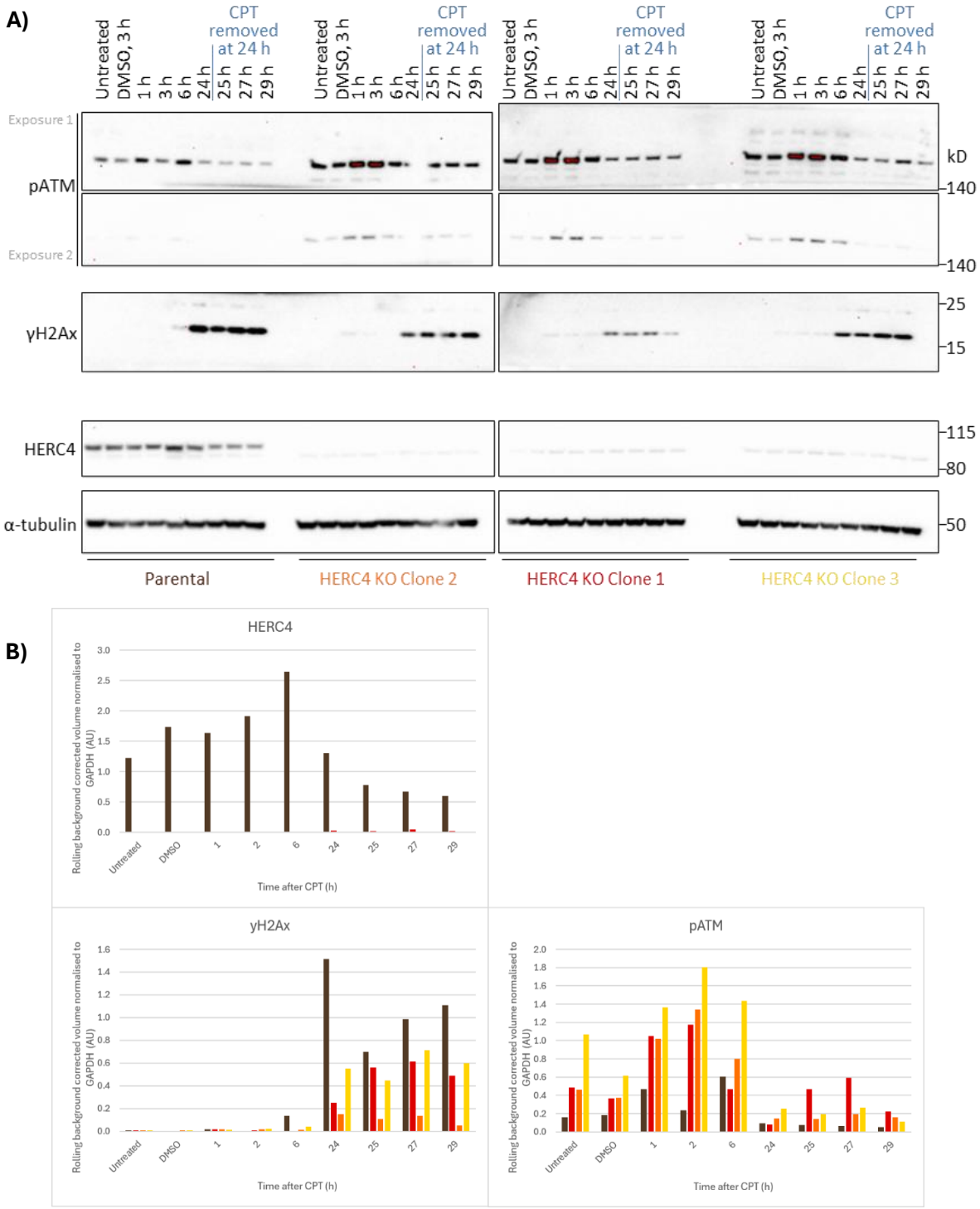


Figure 14: HERC4 loss may alter cellular responses to DNA damage by chemical agents
A) LN229 cells were treated with 1 µM camptothecin (CPT) and their DNA damage response before and after CPT removal monitored by western blot for pATM and γH2Ax. HERC4 knockouts showed increased pATM but lower γH2Ax levels compared to the wildtype control. Staining was insufficient to see ubiquitylated γH2Ax. This change in marker levels contradicted the trend seen in irradiated DBTRG cells despite both CPT and IR being reported to affect cells predominantly through DSBs. The pATM difference may be at least partially attributable to higher levels in the untreated controls, but no equivalent explanation was observed for γH2Ax.
Red patches indicate areas of overexposure.
B) Quantification of western blot
N=1; n=1

2.3.3.4 – HERC4 loss does not improve cell proliferation after chemically-induced DNA damage

In light of the signalling pathway differences observed in 2.3.3.3, other DNA damage mechanisms were tested for the influence of HERC4 loss (Figures 16-17, Appendix 11). Camptothecin and Olaparib[3] were used to induce DSBs, and like IR, neither treatment distinguished consistently between HERC4 knockouts and the wildtype population. Both compounds induce a simple DNA damage profile dominated by one-ended, replication-induced DSBs, caused by stalling either Topoisomerase I or PARP (poly-ADP-ribose polymerase) to prevent ligation or repair of the SSB to which they are bound [Liu et al., 2000; Menear et al., 2008; El-Sehrawy et al., 2025]. Collision of a replication fork with this stalled structure produces a DSB (Figure 15A-B) that relies on HR, not NHEJ, for repair [Ensminger and Löbrich, 2020]. Bleomycin and Zeocin (a bleomycin analogue) were used as more direct radiomimetics, inducing a broader range of damage (abasic sites and strand breaks – Figure 15C) to more closely reflect the spectrum if not proportions (~10% of damage sites affect both strands) of lesion types caused by IR [Povirk, 1996]. As for IR, DSBs are believed to be the biggest contributor to bleomycin, and by extension Zeocin, cytotoxicity. While Zeocin showed a slight trend towards a greater fold reduction in proliferation following HERC4 loss at higher doses, this was not a strong phenotype, nor was it supported by the effects of bleomycin. It is unlikely that HERC4 significantly affects cell proliferation after treatment with any of these drugs in isolation.

[3] LN229 cells are HR-proficient and therefore should be sensitive to Olaparib [Berte et al., 2016]

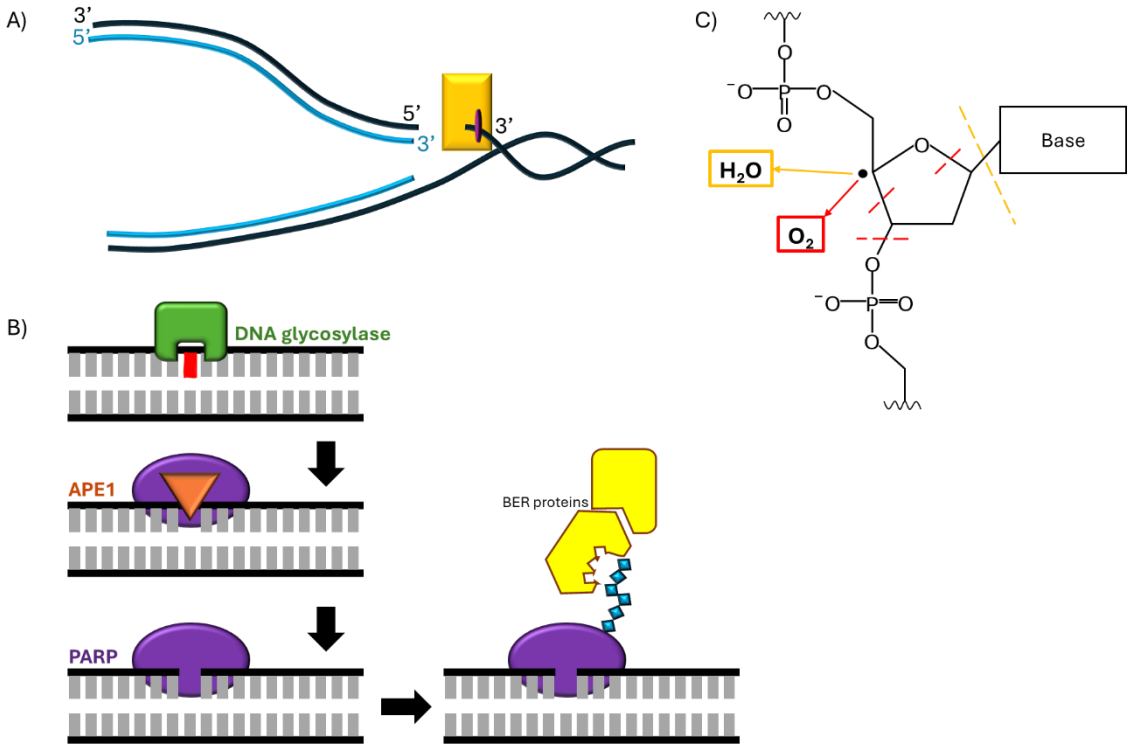


Figure 15: Mechanism of action of DNA-damaging drugs
A) Camptothecin intercalates the DNA in the active site of topoisomerase I, altering the position of the surrounding nucleotides [Jiang et al., 2018; Staker et al., 2002]. This prevents topoisomerase from re-ligating the nick it introduces to relieve DNA supercoiling for DNA replication. Camptothecin also interacts with topoisomerase itself, preventing its dissociation. When a replication fork encounters this SSB and ternary complex on the template strand, it produces cytotoxic DSBs. Outside of S phase, RNA polymerase may cause the same effect during transcription, but replication-dependent damage is the primary mechanism of action for camptothecin [Liu et al., 2000].

B) Olaparib is a competitive PARP inhibitor – it does not prevent PARP recruitment to SSBs, such as those generated by the combined action of DNA glycosylase and APE1 in base excision repair, but it does prevent PARylation and PARP dissociation [reviewed by El-Sehrawy et al., 2025]. Like the ternary complex formed by Camptothecin with DNA and topoisomerase, this then disrupts recruitment of downstream repair proteins so that the SSB persists until replication, when collision when a replication fork converts it to a single-ended DSB.

C) Bleomycin and Zeocin convert the 4' carbon of ribose moieties to a free radical [Povirk, 1996]. If this reacts with water, the ribose-base bond is cleaved, producing an abasic site. If the radical instead reacts with oxygen, an aldehyde product containing the base is released and the DNA backbone broken [Zheng et al., 2022]. ~10% of bleomycin-induced damage is double-stranded, resulting in a profile that mimics IR-induced damage in its variety but not necessarily proportions [Povirk, 1996].

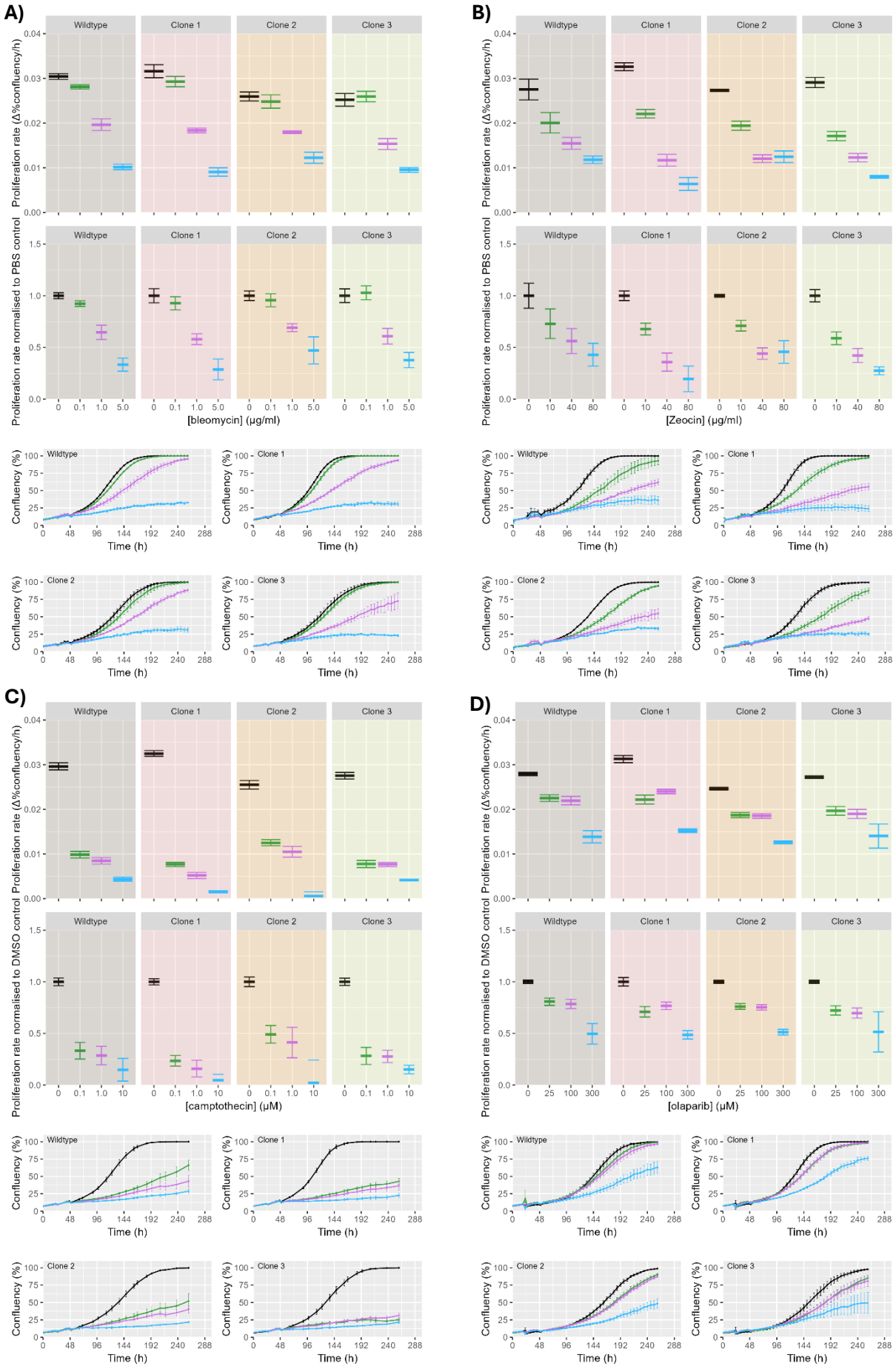

A)
B)
C)
D)
Wildtype
Clone 1
Clone 2
Clone 3
Proliferation rate (Δ%confluency/h)
Proliferation rate normalised to PBS control
[bleomycin] (μg/ml)
[Zeocin] (μg/ml)
Proliferation rate normalised to DMSO control
[camptothecin] (μM)
[olaparib] (μM)
Confluency (%)
Time (h)

Figure 16: Selected drug concentrations result in a range of proliferation rates
Cells were seeded into 96-well plates and imaging started 1 day later. 2 days after seeding, cells were treated with A) bleomycin, B) Zeocin, C) Olaparib or D) camptothecin. Compounds were removed the following day and replaced with fresh media. Proliferation rates were calculated as the gradient of the log_2-transformed confluency graph for each well, then the mean rate for each cell line in each condition was normalised to the PBS or DMSO control for that cell line.
N=1; n=4 for mock-treated control and doses A and B; 3 for dose C
Mock-treated control Dose A Dose B Dose C — mean (technical replicates) I SEM
LN229: Wildtype Clone 1 Clone 2 Clone 3

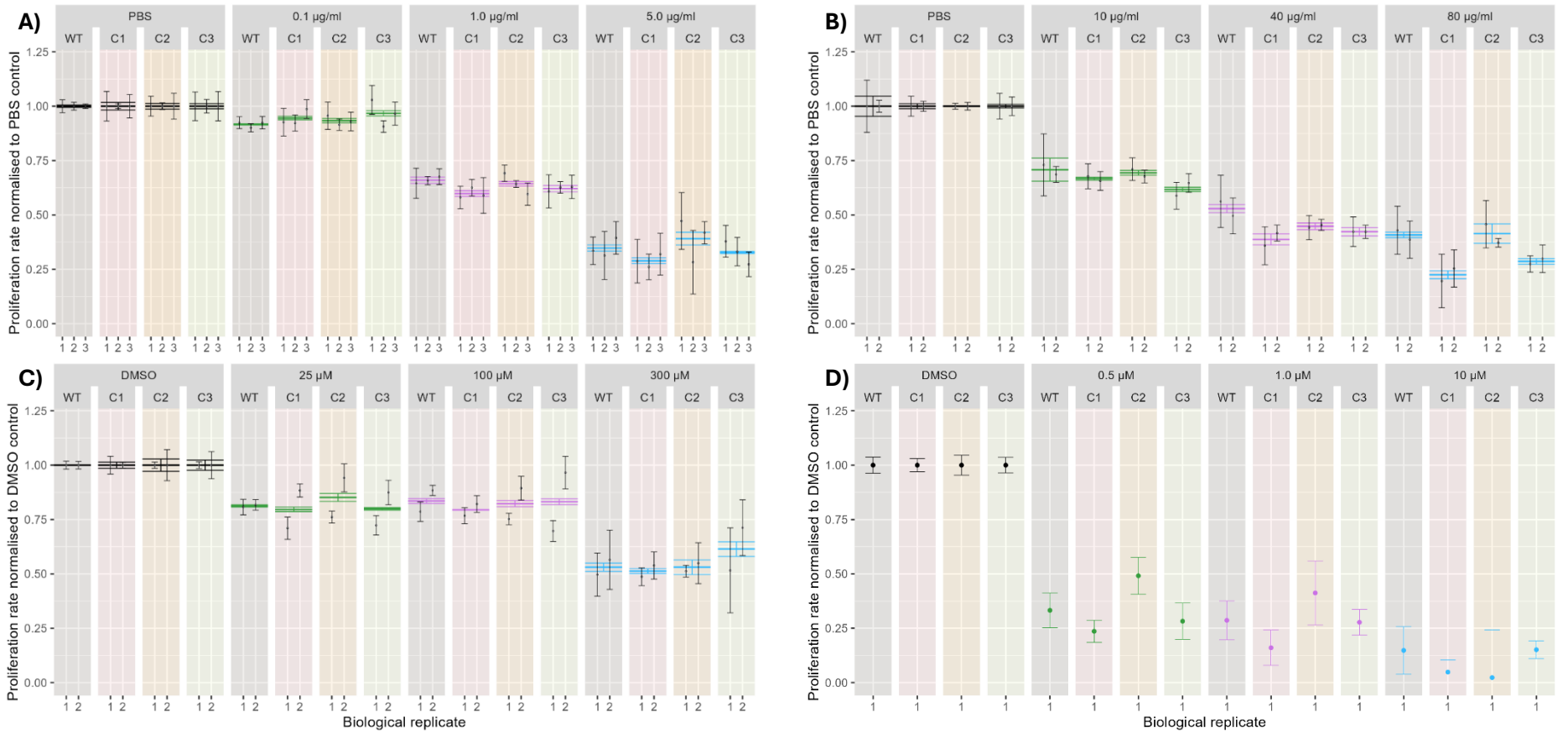


Figure 17: HERC4 loss has no significant effect on LN229 proliferation after different types of DNA damage

Cells were grown and treated with A) bleomycin, B) Zeocin, C) Olaparib or D) camptothecin as described in Figure 12. Proliferation rates were calculated as the gradient of the $\log_2$-transformed confluency graph for each well, then the mean rate for each cell line in each condition was normalised to the PBS or DMSO control for that cell line. HERC4 knockouts appear slightly more sensitive to higher doses of Zeocin compared to the wildtype control, but it is unlikely that this difference would reach statistical significance with further repeats and no other trends were observed.

N=1-3; n= n=4 for mock-treated control and doses A and B; 3 for dose C (for each biological replicate)

Mock-treated control Dose A Dose B Dose C ● mean (technical replicates) — mean (biological replicates) I SEM

LN229: Wildtype Clone 1 Clone 2 Clone 3

2.4 – Discussion

HERC4 knockout clones were readily obtained in both DBTRG and LN229 cells, suggesting that the gene is not essential in unchallenged cells. Knockout and wildtype cells were visually very similar, with cell eccentricity being the most frequently statistically significant difference. DBTRG Clone 1 was more spherical than its wildtype counterpart, perhaps due to its poorer adherence to tissue culture surfaces compared to the other DBTRG cells. In contrast, LN229 Clones 1 and 2 were less circular than the wildtype cell line. LN229 Clone 2 cells were also larger, which may indicate stronger adherence, allowing less circular shapes and spreading the cell across a larger area. This might suggest that HERC4 loss facilitates cell attachment, therefore reducing the likelihood of cell migration, in line with trends seen in several cancer types including breast and cervical cancers [Huang et al., 2021; Wei et al., 2016; Xu et al., 2019; Zheng et al., 2017]. However, this requires significant extrapolation of the limited data, and it is undermined by the contrasting phenotype in DBTRG Clone 1 and the increased mitochondrial metabolic activity per cell observed for Clone 2. This increase was lost when activity was normalised to total confluency, suggesting that activity scaled with size and that the increase in area is therefore the result of increased volume (and consequently mitochondria), not the same volume spread more thinly. A more conservative conclusion would be that the small morphological differences are simply due to clonal variation and that further experiments are needed to test migratory and invasive tendencies.

The next parameter to be assessed in the knockout clones was proliferation rate. Opposing correlations between HERC4 levels and tumour growth have been reported in different cancer types, with ovarian cancer, NSCLC and multiple myeloma showing an inverse relationship while hepatocellular carcinoma, and breast and cervical cancer show a direct correlation [Zhu et al., 2024; Sun et al., 2019; Zhang et al., 2016; Huang et al., 2021; Wei et al., 2016; Xu et al., 2019], but no data has been reported for the effect of HERC4 on glioblastoma proliferation. Slower

proliferation is known to be radioprotective, so it was hypothesised that this could be the mechanism behind the initial result from the screen, should it be validated. While the data shown here does not indisputably link HERC4 loss with slower proliferation, it does display a trend in this direction. 2 out 3 clones in each cell line have a lower mean proliferation rate than their wildtype counterparts, although only 1 of each pair reached statistical significance. This is, however, incongruous with the depletion of HERC4 in glioblastoma through characteristic Chromosome 10 deletions [Cho et al., 2025]. If HERC4 truly has a deleterious effect on proliferation, gene amplification events or transcriptional upregulation might be expected to prevent HERC4 expression dropping with chromosome abundance. It could therefore be speculated that the mild phenotype observed here is dose-dependent and only seen through complete loss of HERC4 expression. Since 1 clone in each cell type showed faster proliferation than the wildtype control, it is also very plausible that differing proliferation rates are once again due to clonal variation. However, it should also be noted that clone selection is likely to have favoured faster-growing cells, perhaps giving more weight to the trend towards slower proliferation than the wildtype population.

To provide additional context that might clarify the results of the proliferation assay, cells were tested for their mitochondrial metabolic rate in case a global reduction in cell activity correlated with the small changes in proliferation rate. As discussed above, LN229 Clone 2 showed an increase in metabolic activity per cell compared to wildtype cells, but this difference was likely due to an increase in cell volume and consequently mitochondria, rather than upregulation of metabolic pathways. Average values for DBTRG Clones 1 and 3 were noticeably higher than for the wildtype population, but the wide range of values within replicates prevented this reaching statistical significance, and the tendency towards lower metabolic activity seen in Clone 2 undermines the trend. However, in contrast to the minimal variance seen between LN229 clones and their wildtype control, the fold change from wildtype rates seen in DBTRG Clones 1 and 3 is notable and may reflect the different metabolic tendencies of the 2 cell lines. Dibutyryl cyclic

AMP (dbcAMP) upregulates mitochondrial biogenesis to drive differentiation of glioblastoma cells into astrocytes, and this effect is more pronounced in DBTRG cells than in LN229 cells [Xing et al., 2017]. Additionally, while glioblastoma favours glycolysis over oxidative phosphorylation, consistent with the Warburg effect so characteristic of cancer cells, LN229 cells are not dependent on glucose for proliferation [Elstrom et al., 2004] and are substantially less sensitive than DBTRG cells to dichloroacetate, a pyruvate dehydrogenase kinase inhibitor that reverses the Warburg effect [Shen et al., 2015]. It is therefore tempting to speculate that HERC4 may interfere with glycolysis, thereby forcing use of oxidative phosphorylation. To fit this to the data shown here, in LN229 cells where this pathway is already significantly active, there is minimal fold change to its activity, but in DBTRG cells that rely more on glycolysis, the impact is far greater. Substantially more data would be required to validate this model, however, not least a comparison of glycolytic and mitochondrial metabolism, the former of which is beyond the scope of the resazurin protocol used here. The most that can be confidently gleaned from this data set is that, following HERC4 loss, there is no change in mitochondrial respiration that would support the trend towards slower proliferation.

An alternative explanation for slower proliferation is that cells are delayed in a specific part of the cell cycle, rather than moving more slowly through the whole process. This was examined by flow cytometry using EdU and DAPI staining and by western blot for a cyclin present at each of the four main cell cycle phases. In LN229, 2 clones had a higher mean proportion of cells in replicating S phase compared to wildtype cells, and all 3 clones had lower mean proportions in non-standard phases. This could reflect more time in replicating S phase and therefore more time to resolve replication stress, reducing the probability of cells stalling in non-replicating S phase or errors being carried into G2 and mitosis where they could cause non-standard chromosome numbers through segregation errors or apoptosis (>4n and sub-G1 populations). This would provide a putative mechanism behind the protective effect of HERC4 loss seen in the IR CRISPR screen, with knockout cells having more opportunity for DNA repair and consequently

more ability to reverse the radiation damage. However, even in LN229 cells, overlapping variance on the mean values undermines this model, and in the DBTRG cell line used for the screen, the trend is faint to non-existent (2 clones have lower means than the wildtype in sub-G1 and >4n, but all 3 have comparable or higher means compared to the wildtype in non- and replicating S phase). An increase in cyclin A levels might also be expected if this model were true, and this was not observed by western blot for either cell line. Based on one repeat, LN229 cells matched this model most closely, with clone 3 showing a 62% increase in signal strength (1.70 compared to 1.05 in wildtype cells, both values normalised to α-tubulin) and clone 1 increasing by a more modest 17%, but clone 2 was 26% lower than the wildtype, and 2 out 3 DBTRG clones showed sub-wildtype cyclin D levels (0.73 and 0.62 for clones 2 and 8 respectively, compared to 0.88 for wildtype cells). Since the flow cytometry differences are only slight, it is possible that western blot is not sufficiently sensitive to detect changes in cyclin levels, or that there is a compensatory decrease in cells in G2 that was not detected by flow cytometry. Probing for CDK1 and -2 levels might produce a more confident conclusion but it seems likely that the results shown here are representative and that there is no change in cell cycle distribution following HERC4 loss.

The data discussed so far indicates limited change in general cell activity when HERC4 is removed, with a possible slight reduction in proliferation rate and increase in mitochondrial metabolism. This presented the knockout clones as a reasonably clean model for validating HERC4 as a radioprotector, as detected in the IR CRISPR screen. Both proliferation rate and metabolic preference alter radiosensitivity - one of the key tenets of radiotherapy is the increased sensitivity of cancer cells over normal tissue due to their faster proliferation, and the Warburg effect has been shown to facilitate DNA repair and redox homeostasis so that cells relying more on glycolysis than oxidative phosphorylation are better placed to resolve the damage caused by radiation (reviewed in Kang et al., 2023). It is therefore important that any differences, however small, in these factors are considered when probing for changes in radiosensitivity, but the lack of substantial contrast between the clones compared to wildtype suggests that the tentative

variation will not obscure the magnitude of change expected from such a strong hit in the CRISPR screen.

DBTRG cells were first tested by colony formation assay to look for differences in survival after IR, and to gauge their sensitivity to a range of doses. The method was ill-suited to this cell line so no confident conclusions could be drawn about the effect of HERC4 on post-IR survival, but the results were sufficient to inform dose selection. 4 Gy was a relatively mild dose at which cell survival was impaired but possible while 10 Gy virtually stopped growth altogether, so they were chosen as a combination intended to cover both repair efficacy and overall damage tolerance. To avoid some of the problems encountered in the colony formation assay, a proliferation assay was used as an alternative measure of radiosensitivity. Cells could be grown at a higher density from the start of the assay, giving much more typical conditions than the isolation needed for successful colony formation, and with a final readout of total confluency, there was no requirement to distinguish between groups of cells, or individual cells as caused problems for the metabolism assay.

Both LN229 and DBTRG cells were included in the proliferation assay and, reassuringly, LN229 cells showed a smaller fold change in proliferation rate from their untreated control compared to DBTRG cells at 4 Gy, but this difference was lost at 10 Gy. This supported the selection of the higher dose as being close to the tolerance limit of both cell lines, but not exceeding it since both lines showed an increase in percentage confluency over time under these conditions, albeit very slowly. This was, however, the most notable difference in the dataset, as most other patterns were inconsistent between clones. It is interesting to note that DBTRG Clone 2 tended to cope better with 10 Gy than wildtype DBTRG cells, as demonstrated by a smaller reduction in proliferation rate compared to untreated conditions, while Clone 8 seemed to be more affected than the wildtype control, being the only clone to reach statistical significance in either condition. Clones 2 and 8 also showed opposing (statistically insignificant) trends in the metabolic assay,

with Clone 2 showing slightly lower and Clone 8 notably higher mitochondrial activity than the wildtype population. A similar comparison can be made between the smaller variance seen for LN229 clones compared to DBTRG clones in both assays, potentially reflecting a role for HERC4 in radiosensitivity by altering cellular preferences for glycolysis or oxidative phosphorylation. LN229 cells show negligible difference in mitochondrial activity after HERC4 loss, and a correspondingly small difference in proliferation after IR, whereas DBTRG Clone 8 may show the greatest increase in mitochondrial activity compared to wildtype, potentially shifting away from upregulated glycolysis and its radioprotective effects to produce its relatively poor proliferation rate after 10 Gy. The inverse would be true of DBTRG Clone 2, and although Clone 1 shows only marginal differences in proliferation after IR, it tends to be worse than the wildtype population, in line with its possible increase in mitochondrial activity. Although the relatively good proliferation rates in LN229 compared to DBTRG cells at 4 Gy might undermine this model, it is likely that comparing between different cell lines introduces variation in far more factors that influence IR sensitivity than simply metabolic biases or proliferation rates. Independent of these possible differences, the dataset crucially does not support the original findings of the IR CRISPR screen, indicating that HERC4 as a radioprotector was a false positive.

If HERC4 loss truly influences IR sensitivity by shifting cellular metabolism towards oxidative phosphorylation and away from glycolysis, there are 2 likely mechanisms for this – reduced capacity for redox homeostasis and for DNA repair. Since a direct influence of HERC4 on DNA repair had also been considered as a possible mechanism behind the CRISPR screen result, this was selected as the primary target. DBTRG cells were irradiated with 10 Gy to achieve a strong damage response, and then pATM and γH2Ax levels were assessed by western blot to monitor response magnitude and duration. Both proteins are phosphorylated in the response to DSBs [Zhao et al., 2017], which is considered the most lethal type of DNA damage caused by ionising radiation. Clone 1 was not used, but both Clones 2 and 8 showed elevated levels of γH2Ax after irradiation compared to the wildtype control (up to 10- and 6-fold higher for clones 2 and 8

respectively), although their untreated levels were ~4 times lower. Compared to wildtype cells, Clone 2 produced similar levels of pATM while Clone 8 showed slightly lower abundance, suggesting that differences in γH2Ax levels are not mediated by a simple increase in pATM availability. Since unmodified H2Ax levels were not assessed, it is plausible that HERC4 knockout caused an increase in total H2A expression, but this might also be expected to raise the level of γH2Ax seen in the untreated control, contrary to the results seen here.

To build on the tentative model of HERC4 altering metabolic preferences, reversal of the Warburg effect through HERC4 knockout could involve reversal of the pyruvate kinase M2 (PKM2) upregulation often seen in glioblastoma [Stanke et al., 2021]. PKM2 silencing has been associated with stronger γH2Ax responses in cervical cancer and NSCLC [Lin et al., 2019; Wang et al., 2015], so if the increase in mitochondrial activity seen in DBTRG Clone 8 compensates for a decrease in glycolysis caused by PKM2 downregulation, this could also drive the increase in γH2Ax. However, this logic implies that the stronger increase in γH2Ax levels in Clone 2 reflects a more substantial reduction in PKM2 expression, which should therefore produce a stronger increase in mitochondrial metabolism, in contradiction with the observed results. It also contrasts strongly with the changes in γH2Ax levels seen in LN229 cells after camptothecin-induced DSBs. Camptothecin was used because although it only acts during S phase compared to IR, which effects damage throughout the cell cycle, it also predominantly causes a singular lesion type, compared to the broad-spectrum damage caused by ionising radiation, allowing cleaner analysis of the subsequent response. It was also the treatment most affected by HERC4 loss in the screen by Olivieri et al., with RPE1 cells showing increased sensitivity after HERC4 mutation [2020]. Although all 3 LN229 clones show increased pATM levels (2-6.7 times higher than wildtype in untreated conditions, and 5-8 times higher after IR), in line with the effect of PKM2 downregulation, they also show substantially lower γH2Ax levels compared to the wildtype control (as much as 20-fold lower in the clone deviating the most from the wildtype population), which does not fit this model. The opposing effects of IR in DBTRG and camptothecin in LN229

could reflect differences between the cell lines, or between the cell cycle phases most influenced by IR and camptothecin. Overall, HERC4 loss seems to alter DNA damage markers but significantly more data is required to identify a mechanism or effect.

In light of the strong change in pATM and γH2Ax levels seen in LN229 cells following camptothecin treatment, other methods of DNA damage were assessed for their effect on proliferation, namely single-strand breaks caused by bleomycin and Zeocin, and DSBs caused by Olaparib-mediated PARP inhibition. Like camptothecin, bleomycin and Olaparib were tested by Olivieri et al., and cells were more sensitive to each treatment after HERC4 mutation [2020]. Camptothecin itself produced no obvious trend in a single biological repeat, although further experiments are needed to confirm this, and Olaparib was no more effective at distinguishing between knockouts and wildtype cells at any of the doses used. Zeocin tended towards causing a greater reduction in the clones than the wildtype control, but this trend was not seen after bleomycin treatment, despite their similar modes of action. If cellular responses to other methods of DNA damage are affected by HERC4 loss, it is unlikely to be to an extent that confers any sensitivity difference on the cells.

2.5 – Conclusions and Future Directions

The phenotypic data shown here suggests that HERC4 loss has at most subtle effects on cellular activity in glioblastoma cells, and that the high confidence of HERC4 as a radiosensitiser in the initial CRISPR screen is potentially misleading. However, slight changes in proliferation and mitochondrial metabolic rate were detected across multiple clones in both cell lines, so it may be that cells are not completely ambivalent to HERC4 loss. It seems likely that, as the evolutionary founder of the HERC family, the function of HERC4, like its gene, has been duplicated, and that other HERC proteins are able to compensate in its absence, or perhaps dominate even when it is present. It would be interesting to explore the proliferation and metabolic rates of additional knockout clones to strengthen or undermine the trends observed here, and to compare the findings with those obtained from cells overexpressing HERC4. Conclusions could be further strengthened through the use of additional protocols, such as synchronising the cells prior to monitoring their progress through the cell cycle via flow cytometry, or a metabolism assay distinguishing between glycolysis and oxidative phosphorylation. It is clear that much more work is required to uncover a phenotypic effect for HERC4 loss, and that starting from a less targeted approach may offer a more streamlined route to determining the function of HERC4 in glioblastoma.

2.7 - References

Angom, R.S.; Nakka, N.M.R. and Bhattacharya, S. (2023) Advances in Glioblastoma Therapy: An Update on Current Approaches *Brain Sciences* 13(11):1536

Asif, M.; Khayyat, A.I.A.; Alawbathani, S.; Abdullah, U.; Sanner, A.; Georgomanolis, T.; Haasters, J.; Becker, K.; Budde, B.; Becker, C.; Thiele, H.; Baig, S.M.; Isidoro-García, M.; Winter, D.; Pogoda, H.M.; Muhammad, S.; Hammerschmidt, M.; Kraft, F.; Kurth, I.; Martin, H.G.; Wagner, M.; Nürnberg, P. and Hussain, M.S. (2024) Biallelic Loss-of-Function Variants of *ZFTRAF1* Cause Neurodevelopmental Disorder with Microcephaly and Hypotonia *Genetics in Medicine* 26(7):101143

Berte, N.; Piée-Staffa, A.; Piecha, N.; Wang, M.; Borgmann, K.; Kaina, B. and Nikolova, T. (2016) Targeting Homologous Recombination by Pharmacological Inhibitors Enhances the Killing Response of Glioblastoma Cells Treated with Alkylating Drugs *Molecular Cancer Therapeutics* 15(11):2665-2678

Braselmann, H.; Michna, A.; Heß, J. and Unger, K. (2015) CFAssay: Statistical Analysis of the Colony Formation Assay *Radiation Oncology* 10:223

Chandrashekar, D.S.; Karthikeyan, S.K.; Korla, P.K.; Patel, H.; Shovon, A.R.; Athar, M.; Netto, G.J.; Qin, Z.S.; Kumar, S.; Manne, U.; Creighton, C.J. and Varambally, S. (2022) UALCAN: An Update to the Integrated Cancer Data Analysis Platform *Neoplasia* 25:18-27

Chen, F.; Zhang, Y. and Creighton, C.J. (2021) Systematic Identification of Non-Coding Somatic Single Nucleotide Variants Associated with Altered Transcription and DNA Methylation in Adult and Pediatric Cancers *Nucleic Acids Research Cancer* 3(1)::zcab001

Cho, M.; Tang, G.; Rogers, C.S.; Dove, M.; Liu, X.; Li, Y. and Wang, X. (2025) OncoDB 2.0: a Comprehensive Platform for Integrated Pan-Cancer Omics Analysis *Nucleic Acids Research* gkaf952

Choquet, H.; Duot, M.; Herrera, V.A.; Shrestha, S.K.; Meyers, T.J.; Hoffmann, T.J.; Sangani, P.K. and Lachke, S.A. (2024) Multi-Tissue Transcriptome-Wide Association Study Identifies Novel Candidate Susceptibility Genes for Cataract *Frontiers in Ophthalmology* 4(2024)

Cregan, S.P.; Arbour, N.A.; MacLaurin, J.G.; Callaghan, S.M.; Fortin, A.; Cheung, E.C.C.; Guberman, D.S.; Park, D.S. and Slack, R.S. (2004) p53 Activation Domain 1 is Essential for PUMA Upregulation and p53-Mediated Neuronal Cell Death *Journal of Neuroscience* 24(44) 10003-10012

Di Nunno, V.; Gatto, L.; Tosoni, A.; Bartolini, S. and Franceschi, E. (2023) Implications of BRAF V600E Mutation in Gliomas: Molecular Considerations, Prognostic Value and Treatment Evolution *Frontiers in Oncology* 12

El-Sehrawy, A.A.M.A.; Mukhilf, M.Y.; Khalaf, A.A.; Uthirapathy, S.; Ballal, S.; Singh, A.; Kavitha, V.; Maharana, L.; Ridha-Salman, H. and Al-Altememe, A.R.H. (2025) Breaking Barriers: Deciphering the Mechanisms of Olaparib Resistance in Prostate Cancer *Seminars in Oncology* 52(4):152375

Elstrom, R.L.; Bauer, D.E.; Buzzai, M.; Karnauskas, R.; Harris, M.H.; Plas, D.R.; Zhuang, H.; Cinalli, R.M.; Alavi, A.; Rudin, C.M. and Thompson, C.B. (2004) Akt Stimulates Aerobic Glycolysis in Cancer Cells *Cell and Tumor Biology* 64(11):3892-3899

Ensminger, M. and Löbrich, M. (2020) One End to Rule Them All: Non-Homologous End-Joining and Homologous Recombination at DNA Double-Strand Breaks *British Journal of Radiology* 93(1115):20191054

Gabler, L.; Lötsch, D.; Kirchhofer, D.; van Schoonhoven, S.; Schmidt, H.M.; Mayr, L.; Pirker, C.; Neumayer, K.; Dinhof, C.; Kastler, L.; Azizi, A.A.; Dorfer, C.; Czech, T.; Haberler, C.; Peyrl, A.; Kumar, R.; Slavc, I.; Spiegl-Kreinecker, S.; Gojo, J. and Berger, W. (2019) *TERT* Expression is Susceptible to BRAF and ETS-Factor Inhibition in *BRAF^{V600E}/TERT* Promoter Double-Mutated Glioma *Acta Neuropathologica Communications* 7:128

Ge, S.X.; Jung, D. and Yao, R. (2020) ShinyGo: a Graphical Gene-Set Enrichment Tool for Animals and Plants *Bioinformatics* 36(8):2628-2629

Goralski, T.M.; Meyerdirk, L.; Breton, L.; Brasseur, L.; Kurgat, K.; DeWeerd, D.; Turner, L.; Becker, K.; Adams, M.; Newhouse, D.J. and Henderson, M.X. (2024) Spatial Transcriptomics Reveals Molecular Dysfunction Associated with Cortical Lewy Pathology *Nature Communications* 15:2642

He, J.; Chu, Z.; Lai, W.; Lan, Q.; Zeng, Y.; Lu, D.; Jin, S.; Xu, H.; Su, P.; Yin, D.; Chu, Z. and Liu, L. (2021) Circular RNA circHERC4 as a Novel Oncogenic Driver to Promote Tumor Metastasis via the miR-556-6p/CTBP2/E-cadherin Axis in Colorectal Cancer *Journal of Hematology and Oncology* 14:194

Hedges, J.C.; Hanna, C.B.; Shorey-Kendrick, L.E.; Boniface, E.R.; Bash, J.C.; Rice-Stitt, T.L.; Burch, F.C.; D'Mello, R.; Morgan, T.K.M.; Lima, A.C.; Terrobia, J.J.D.; Graham, J.A.; Mishler, E.C.; Jensen, J.V.; Hagen, O.L.; Urian, J.W.; Spindel, E.R.; Easley, C.A.; Murphy, S.K. and Lo, J.O. (2023) Cessation of Chronic Delta-9-Tetrahydrocannabinol Use Partially Reverses Impacts on Male Fertility and the Sperm Epigenome in Rhesus Macaques *Fertility and Sterility* 120(1):163-174

Hegi, M.E.; Diserens, A.C.; Gorlia, T.; Hamou, M.F.; de Tribolet, N.; Weller , M.; Kros, J.M.; Hainfellner, J.A.; Mason, W.; Mariani, L.; Bromberg, J.; Hau, P.; Mirimanoff, R.O.; Cairncross, J.G.; Janzer, R.C. and Stupp, R. (2005) *MGMT* Gene Silencing and Benefit from Temozolomide in Glioblastoma *The New England Journal of Medicine* 352(10):997-1003

Hochrainer, K.; Mayer, H.; Baranyi, U.; Binder, B.R.; Lipp, J. and Kroismayr, R. (2005) The Human HERC Family of Ubiquitin Ligases: Novel Members, Genomic Organization, Expression Profiling, and Evolutionary Aspects *Genomics* 85(2):153-164

Horiguchi, H.; Hirose, T.; Sano, T. and Nagahiro, S. (1999) Loss of Chromosome 10 in Glioblastoma: Relation to Proliferation and Angiogensis *Pathology International* 49:681-686

Huang, F.; Tang, X.; Sun, T.; Wang, G.; Ru, Q. and Zheng, Y. (2021) SAV1, Regulated by HERC4, Inhibits the Proliferation, Migration, and Invasion of Hepatocellular Carcinoma *Translational Cancer Research* 10(1):349-360

Iacobas, D.A. and Iacobas, S. (2024) Papillary Thyroid Cancer Remodels the Genetic Information Processing Pathways *Genes* 15(5):621

Jiang, Z.; Zhang, Z.; Cui, G.; Sun, Z.; Song, G.; Liu, Y. and Zhong, G. (2018) DNA Topoisomerase 1 Structure-BASED Design Synthesis, Activity Evaluation and Molecular Simulations Study of New 7-Amide Camptothecin Derivatives Against *Spodoptera frugiperda*. *Frontiers in Chemistry* 6(2018)

Kruse, C.A.; Mitchell, D.H.; Kleinschmidt-DeMasters, B.K.; Franklin, W.A.; Morse, H.G.; Spector, E.B. and Lillehei, K.O. (1992) Characterization of a Continuous Human Glioma Cell Line DBTRG-05MG: Growth Kinetics, Karyotype, Receptor Expression, and Tumor Suppressor Gene Analyses *In Vitro Cellular and Developmental Biology - Animal* 28:609-614

Lemée, J.M.; Clavreul, A.; Aubry, M.; Com, E.; de Tayrac, M.; Mosser, J. and Menei, P. (2018) Integration of Transcriptome and Proteome Profiles in Glioblastoma: Looking for the Missing Link *BMC Molecular Biology* 19:13

Li, G.; Zhang, T.; Hu, B.; Han, S.; Xiang, C.; Yuan, G. and He, H. (2023) Infection of *Trichinella spiralis* Affects the Reproductive Capacity of ICR/CD-1 Male Mice by Reducing the Urine Pheromone Contents and Sperm Quality *International Journal of Molecular Science* 24(6):5731

Li, H.; Yang, B.Y.; Liu, M.M.; Zhao, S.W.; Xie, S.Z.; Wang, H.; Zhang, S.; Xuan, X.N. and Jia, L.J. (2021) Reproductive Injury in Male BALB/c Mice Infected with *Neospora caninum*. *Parasites & Vectors* 14:158

Li, H.; Zhen, Z.; Wei, J.; Fan, X.; Cao, P.; Zhang, Y.; Chen, Y.; Li, Y.; Zhu, Y.; Wang, R. and Ma, X. (2024) Endogenous has-circ_0007113 Binds has-miR-515-5p to Regulate Senescence in Human Embryonic Lung Fibroblasts *Advances in Clinical and Experimental Medicine* 33(9):953-964

Lin, Y.; Zhai, H.; Ouyang, Y.; Lu, Z.; Chu, C.; He, Q. and Cao, X. (2019) Knockdown of PKM2 Enhances Radiosensitivity of Cervical Cancer Cells *Cancer Cell International* 19:129

Liu, L.F.; Desai, S.D.; Li, T.K.; Mao, Y.; Sun, M. and Sim, S.P. (2000) Mechanism of Action of Camptothecin *Annals of the New York Academy of Sciences* 922:1-10

Liu, M.; Zhao, Z.; Wang, C.; Sang, S.; Cui, Y.; Lv, C.; Yang, X.; Zhang, N.; Xiong, K.; Chen, B.; Dong, Q.; Liu, K. and Gu, Y. (2024b) Harnessing Genetic Interactions for Prediction of Immune Checkpoint Inhibitors Response Signature in Cancer Cells Cancer Letters 594:216991

Louis, D.N.; Perry, A.; Wesseling, P.; Brat, D.J.; Cree, I.A.; Figarella-Branger, D.; Hawkins, C.; Ng, H.K.; Pfister, S.M.; Reifenberger, G.; Soffietti, R.; von Deimling, A.; Ellison, D.W (2021) The 2021 WHO Classification of Tumors of the Central Nervous System: a summary *Neuro-Oncology* 23(8) 1231-1251

Menear, K.A.; Adcock, C.; Boulter, R.; Cockcroft, X.L.; Copsey, L.; Cranston, A.; Dillon, K.J.; Drzewiecki, J.; Garman, S.; Gomez, S.; Javaid, H.; Kerrigan, F.; Knights, C.; Lau, A.; Loh Jr., V.M.; Matthews, I.T.W.; Moore, S.; O'Connor, M.J.; Smith, G.C.M. and Martin, N.M.B. (2008) 4-[3-(4-Cyclopropanecarbonylpiperazine-1-carbonyl)-4-fluorobenzyl]-2H-phthalazin-1-one: A Novel Bioavailable Inhibitor of Poly(ADP-ribose) Polymerase-1 *Journal of Medicinal Chemistry* 51(20):6581-6591

Miao, Z.; Xu, L.; Gu, W.; Ren, Y.; Li, R.; Zhang, S.; Chen, C.; Wang, H.; Ji, J. and Chen, J. (2024) A Targetable PRR11-DHODH Axis Drives Ferroptosis- and Temozolomide-Resistance in Glioblastoma *Redox Biology* 73:103220

Nagase, T.; Kikuno, R.; Ishikawa, K.; Hirosawa, M. and Ohara, O. (2000) Prediction of the Coding Sequences of Unidentified Human Genes. XVI. The Complete Sequences of 150 New cDNA Clones from Brain Which Code for Large Proteins in vitro *DNA Research* 7(1):65-73

Nicolaides, T.P.; Li, H.; Solomon, D.A.; Hariono, S.; Hashizume, R.; Barkovich, K.; Baker, S.J.; Paugh, B.S.; Jones, C.; Forshew, T.; Hindley, G.F.; Hodgson, G.; Kim, J.S.; Rowitch, D.H.; Weiss, W.A.; Waldman, T.A. and James, C.D. (2011) Targeted Therapy for $BRAF^{V600E}$ Malignant Astrocytoma *Cancer Therapy: Preclinical* 17(24):7595-7604

Nie, E.; Miao, F.; Jin, X.; Wu, W.; Zhou, X.; Zeng, A.; Yu, T.; Zhi, T.; Shi, Z.; Wang, Y.; Zhang, J.; Liu, N. and You, Y. (2018) Fstl1/DIP2A/MGMT Signaling Pathway Plays Important Roles in Temozolomide Resistance in Glioblastoma *Oncogene* 38:2706-2721

Okazaki, R. (2022) Role of p53 in Regulating Radiation Responses *Life* 12(7):1099

Olivieri, M.; Cho, T.; Álvarez-Quilón, A.; Li, K.; Schellenberg, M.J.; Zimmermann, M.; Hustedt, N.; Rossi, S.E.; Adam, S.; Melo, H.; Heijink, A.M.; Sastre-Moreno, G.; Moatti, N.; Szilard, R.K.; McEwan, A.; Ling, A.K.; Serrano-Benitez, A.; Ubhi, T.; Feng, Su.; Pawling, J.; Delgado-Sainz, I.; Ferguson, M.W.; Dennis, J.W.; Brown, G.W.; Cortés-Ledesma, F.; Williams, R.S.; Martin, A.; Xu, D. and Durocher, D. (2020) A Genetic Map of the Response to DNA Damage in Human Cells *Cell* 182(2):481-496

Paparisto, E.; Woods, M.W.; Coleman, M.D.; Moghadasi, S.A.; Kochar, D.S.; Tom, S.K.; Kohio, H.P.; Gibson, R.M.; Rohringer, T.J.; Hunt, N.R.; Di Gravio, E.J.; Zhang, J.Y.; Tian, M.; Gao, Y.; Arts, E.J. and Barr, S.D. (2018) Evolution-Guided Structural and Functional Analyses of the HERC Family Reveal an Ancient Marine Origin and Determinants of Antiviral Activity *Journal of Virology* 92(13):1128

Patil, V.; Pal, J. and Somasundaram, K. (2015) Elucidating the Cancer-Specific Genetic Alteration Spectrum of Glioblastoma Derived Cell Lines from Whole Exome and RNA Sequencing *Oncotarget* 6(41):43452-43471

Povirk, L.F. (1996) DNA damage and mutagenesis by radiomimetic DNA-cleaving agents: bleomycin, neocarzinostatin and other enediynes *Mutation Research - Fundamental and Molecular Mechanisms of Mutagenesis* 355(1-2):71-89

Rise, M.L.; Hall, J.R.; Rise, M.; Hori, T.S.; Browne, M.J.; Gamperl, A.K.; Hubert, S.; Kimball, J.; Bowman, S. and Johnson, S.C. (2010) Impact of Asymptomatic Nodavirus Carrier State and Intraperitoneal Viral Mimic Injection on Brain Transcript Expression in Atlantic Cod (Gadus Morhua) *Physiological Genomics* 42(2):266-280

Rodriguez, C.I. and Stewart, C.L. (2007) Disruption of the Ubiquitin Ligase *HERC4* Causes Defects in Spermatozoon Maturation and Impaired Fertility *Developmental Biology* 312(2):501-508

Rufini, A.; Tucci, P.; Celardo, I. and Melino, G. (2013) Senescence and Aging: the Critical Roles of p53 *Oncogene* 32:5129-5143

Schnöller, L.E.; Piehlmaier, D.; Weber, P.; Brix, N.; Fleischmann, D.F.; Nieto, A.E.; Selmansberger, >; Heider, T.; Hess, J.; Niyazi, M.; Belka, C.; Lauber, K.; Unger, K. and Orth, M. (2023) Systematic in Vitro Analysis of Therapy Resistance in Glioblastoma Cell Lines by Integration of Clonogenic Survival Data with Multi-Level Molecular Data *Radiation Oncology* 18:51

Shen, H.; Hau, E.; Joshi, S.; Dilda, P.J. and McDonald, K.L. (2015) Sensitization of Glioblastoma Cells to Irradiation by Modulating the Glucose Metabolism *Molecular Cancer Therapeutics* 14(8):1794-1804

Staker, B.L.; Hjerrild, K.; Feese, M.D.; Behnke, C.A.; Burgin Jr., A.B. and Stewart, L. (2002) The Mechanism of Topoisomerase I poisoning by a Camptothecin Analog *Proceedings of the National Academy of Sciences USA* 99(24):15387-15392

Stanke, K.M.; Wilson, C. and Kidambi, S. (2021) High Expression of Glycolytic Genes in Clinical Glioblastoma Patients Correlates With Lower Survival *Frontiers in Molecular Biosciences* 8(2021)

Sun, X.; Sun, B.; Cui, M. and Zhou, Z. (2019) HERC4 Exerts an Anti-Tumor Role Through Destabilizing the Oncoprotein Smo *Biochemical and Biophysical Research Communications* 513(4):1013-1018

Tatari, N.; Khan, S.; Livingstone, J.; Zhai, K.; Mckenna, D.; Ignatchenko, V.; Chokshi, C.; Gwynne, W.D.; Singh, M.; Revill, S.; Mikolajewicz, N.; Zhu, C.; Chan, J.; Hawkins, C.; Lu, J.Q.; Provias, J.P.; Ask, K.; Morrissy, S.; Brown, S.; Weiss, T.; Weller, M.; Han, H.; Greenspoon, J.N.; Moffat, J.; Venugopal, C.; Boutros, P.C.; Singh, S.K. and Kislinger, T. (2022) The Proteomic Landscape of Glioblastoma Recurrence Reveals Novel and Targetable Immunoregulatory Drivers *Acta Neuropathologica* 144:1127-1142

The Cancer Genome Atlas Research Network (2008) Comprehensive Genomic Characterization Defines Human Glioblastoma Genes and Core Pathways *Nature* 455 1061-1068

Tsai, H.C.; Wei, K.C.; Chen, P.Y.; Huang, C.Y.; Chen, K.T.; Lin, Y.J.; Cheng, H.W.; Chen, Y.R. and Wang, H.T. (2021) Valproic Acid Enhanced Temozolomide-Induced Anticancer Activity in Human Glioma Through the p53–PUMA Apoptosis Pathway *Frontiers in Oncology* 11:722754

Uhlén, M.; Fagerberg, L.; Hallström; B.M.; Lindskog, C.; Oksvold, P.; Mardinoglu, A.; Sivertsson, Å.; Kampf, C.; Sjöstedt, E.; Asplund, A.; Olsson, I.; Edlund, K.; Lundberg, E.; Navani, S.; Szigyarto, C.A.K.; Odeberg, J.; Djureinovic, D.; Takanen, J.O.; Hober, S.; Alm, T.; Edqvist, P.H.; Berling, H.; Tegel, H.; Mulder, J.; Rockberg, J.; Nilsson, P.; Schwenk, J.M.; Hamsten, M.; von Feilitzen, K.; Forsberg, M.; Persson, L.; Johansson, F.; Zwahlen, M.; von Heijne, G.; Nielsen, J. and Pontén, F. (2015) Tissue-Based Map of the Human Proteome *Science* 347(6220)

Valero, Y.; Souto, S.; Olveira, J.G.; López-Vázquez, C.; Dopazo, C.P. and Bandín, I. (2024) Water-in-Oil Adjuvant Challenges in Fish Vaccination: An Experimental Inactivated Adjuvanted Vaccine Against Betanodavirus Infection in Senagalese Sole *Journal of Fish Diseases* 47(7):e13945

Wada, K.; Maeda, Y.Y.; Watanabe, K.; Oshio, T.; Ueda, T.; Takahashi, G.; Yokohama, M.; Saito, J.; Seki, Y.; Takahama, S.; Ishii, R.; Shitara, H.; Taya, C.; Yonekawa, H. and Kikkawa, Y. (2011) A Deletion in a *Cis* Element of *Foxe3* Causes Cataracts and Microphthalmia in *rct* mice *Mammalian Genome* 22:693-702

Wang, L.; Wang, Y.; Su, B.; Yu, P.; He, J.; Meng, L.; Xiao, Q.; Sun, J.; Zhou, K.; Xue, Y. and Tan, J. (2020) Transcriptome-wide Analysis and Modelling of Prognostic Alternative Splicing Signatures in Invasive Breast Cancer: a Prospective Clinical Study *Scientific Reports* 10:16504

Wang, P.; Sun, C.; Zhu, T. and Xu. Y. (2015) Structural Insight into Mechanisms for Dynamic Regulation of PKM2 *Protein and Cell* 6(4):275-287

Weber, C.A.M.; Krönke, N.; Volk, V.; Auber, B.; Förster, A.; Trost, D.; Geffers, R.; Esmaeilzadeh, M.; Lalk, M.; Nabavi, A.; Samii, A.; Krauss, J.K.; Feuerhake, F.; Hartmann, C.; Wiese, B.; Brand, F. and Weber, R.G. (2023) Rare Germline Variants in *POLE* and *POLD1* Encoding the Catalytic Subunits of DNA Polymerases ε and δ in Glioma Families *Acta Neuropathologica Communications* 11:184

Wei, M.; Zhang, Y.L.; Chen, L.; Cai, C.X. and Wang, H.D. (2016) RNA Interference of HERC4 Inhibits Proliferation, Apoptosis and Migration of Cervical Cancer Hela Cells *Journal of Southern Medical University* 37(2):232-237

Xing, F.; Luan, Y.; Cai, J.; Wu, S.; Mai, J.; Gu, J.; Zhang, H.; Li, K.; Lin, Y.; Xiao, X.; Liang, J.; Li, Y.; Chen, W.; Tan, Y.; Sheng, L.; Lu, B.; Lu, W.; Gao, M.; Qiu, P.; Su, X.; Yin, W.; Hu, J.; Chen, Z.; Sai, K.; Wang, J.; Chen, F.; Chen, Y.; Zhu, S.; Liu, D.; Cheng, S.; Xie, Z.; Zhu, W. and Yan, G. (2017) The Anti-Warburg Effect Elicited by the cAMP-PGC1α Pathway Drives Differentiation of Glioblastoma Cells into Astrocytes *Cell Reports* 18(2):468-481

Xu, Y.; Ji, K.; Wu, M.; Hao, B.; Yao, K. and Xu, Y. (2019) A miRNA-HERC4 Pathway Promotes Breast Tumorigenesis by Inactivating Tumor Suppressor LATS1 *Protein & Cell* 10(8):595-605

Zeng, W.L.; Chen, Y.W.; Zhou, H.; Zhou, J.Y.; Wei, M. and Shi, R. (2015) Expression of HERC4 in Lung Cancer and its Correlation with Clinicopathological Parameters *Asian Pacific Journal of Cancer Prevention* 16(2):513-517

Zerbino, D.R.; Achuthan, P.; Akanni, W.; Amode, M.R.; Barrell, D.; Bhai, J.; Billis, K.; Cummins, C.; Gall, A.; Girón, C.G.; Gil, L.; Gordon, L.; Haggerty, L.; Haskell, E.; Hourlier, T.; Izuogu, O.G.; Janacek, S.H.; Juettemann, T.; To, J.K.; Laird, M.R.; Lavidas, I.; Liu, Z.; Loveland, J.E.; MAurel, T.; McLaren, W.; Moore, B.; Mudge, J.; Murphy, D.N.; Newman, V.; Nuhn, M.; Ogeh, D.; Ong, C.K.; Parker, A.; Patricio, M.; Riat, H.S.; Schuilenburg, H.; Sheppard, D.; Sparrow, H.; Taylor, K.; Thormann, A.; Vullo, A.; Walts, B.; Zadissa, A.; Frankish, A.; Hunt, S.E.; Kostadmia, M.; Langridge, N.; Martin, F.J.; Muffato, M.; Perry, E.; Ruffier, M.; Staines, D.M.; Trevanion, S.J.; Aken, B.L.; Cunningham, F.; Yates, A. and Flicek, P. (2017) Ensembl 2018 *Nucleic Acids Research* 46(D1):D754-D761

Zhang, Y.; Dube, C.; Gibert, M.; Cruickshanks, N.; Wang, B.; Coughlan, M.; Yang, Y.; Setiady, I.; Deveau, C.; Saoud, K.; Grello, C.; Oxford, M.; Yuan, F. and Abounader, R. (2018) The p53 Pathway in Glioblastoma *Cancers* 10(9):297

Zhang, Z.; Tong, J.; Tang, X.; Juan, J.; Cao, B.; Hurren, R.; Chen, G.; Taylor, P.; Xu, X.; Shi, C.X.; Du, J.; Hou, J.; Wang, G.; Wu, D.; Stewart, A.K.; Schimmer, A.D.; Moran, M.F. and Mao, X. (2016) The Ubiquitin Ligase HERC4 Mediates c-Maf Ubiquitination and Delays the Growth of Multiple Myeloma Xenografts in Nude Mice *Blood* 127(13):1676-1686

Zhao, H.; Halicka, H.D.; Garcia, J.; Li, J. and Darzynkiewicz, Z. (2017) ATM Activation and H2AX Phosphorylation Induced by Genotoxic Agents Assessed by Flow- and Laser Scanning Cytometry In: Kozlov, S. (eds) ATM Kinase. Methods in Molecular Biology, vol 1599. Humana Press, New York, NY.

Zheng, D.Q.; Wang, Y.T.; Zhu, Y.X.; Sheng, H.; Li, K.J.; Sui, Y. and Zhang, K. (2022) Uncovering Bleomycin-Induced Genomic Alterations and Underlying Mechanisms in the Yeast *Saccharomyces cerevisiae*. *Applied and Environmental Microbiology* 88(2):e01703-21

Zheng, Y.; Li, J.; Pan, C.; Zhou, G.; Zhuge, L.; Jin, L. and Fang, P. (2017) HERC4 Is Overexpressed in Hepatocellular Carcinoma and Contributes to the Proliferation and Migration of Hepatocellular Carcinoma Cells *DNA and Cell Biology* 36(6):490-500

Zhou, H.; Shi, R.; Wei, M.; Zheng, W.L.; Zhou, J.Y. and Ma, W.L. (2013) The Expression and Clinical Significance of HERC4 in Breast Cancer *Cancer Cell International* 13:113

Zhu, Q.; Yang, X. and Lv, Y. (2024) HERC4 Modulates Ovarian Cancer Cell Proliferation by Regulating SMO-Elicited Hedgehog Signaling *Biochimica et Biophysica Acta - General Subjects* 1868(4):130557

2.8 - Appendices

Appendix 1 – sequences for HERC4 knockout guide RNAs

sgRNA 1	CAGACAUACUGUGUUUGUUC
sgRNA 2	UAUAAAGAAGUCACUUUUUC
sgRNA 3	AUUACAAGCAUGUUGUGCUG

Appendix 2 - PCR primer sequences for HERC4 CRISPR amplicon

Primer	**Sequence**
Forward	CCACAACATAAAGTACTTAGAACCA
Reverse	AGCAATTATTGTAGCCTAGCACT
Sequencing	AGCAATTATTGTAGCCTAGCACTTGAAAG

Appendix 3 – PCR parameters

Template DNA	10 ng
Forward primer	0.125 µl at 100 nM
Reverse primer	0.125 µl at 100 nM
Q5 PCR master mix	12.5 µl
Water	To 25 µl total reaction volume

Stage	**Temperature (°C)**	**Duration (seconds)**	**Cycles**
Initial denaturation	95.0	60	1
Denaturation	95.0	15	30
Annealing	58.8	15	
Elongation	72.0	60	
Final elongation	72.0	120	1

Appendix 4 – antibodies

Target protein	Dilution	Catalogue number
HERC4	1:1000	13691-1-AP
pATM	1:1000	5883S
γH2Ax	1:1000	NB100-2280
Cyclin A2	1:1000	sc-751
Cyclin B1	1:1000	4138T
Cyclin D1	1:500	sc-246
Cyclin E	1:1000	ab3927
GAPDH	1:5000	MA5-15738
α-tubulin	1:5000	sc-23948
Rabbit IgG	1:10,000 1:10,000	sc-2027 31460
Mouse IgG	1:10,000 1:5,000	sc-2025 31430

Appendix 5 – IncuCyte parameters

Proliferation

Whole-well imaging, 4X magnification

Segmentation adjustment		0.8
Hole fill (μm^2)		0.0
Adjust size (pixels)		0
Area	Minimum	1000.0
	Maximum	NA
Eccentricity	Minimum	NA
	Maximum	NA
Processing Keep-out (pixels)		50

Morphology and resazurin

Cell-by-cell imaging, 5 images per well, 10X magnification

DBTRG

Cell Boundary	
Segmentation adjustment	1.1
Hole fill (μm^2)	0.0
Adjust size (pixels)	0

Seed	
Cell detection sensitivity	1.4
Cell contrast	1
Cell morphology	5

Cell-by-cell		
Area	Minimum	500.00
	Maximum	NA
Eccentricity	Minimum	NA
	Maximum	NA

LN229

Cell Boundary	
Segmentation adjustment	1.3
Hole fill (μm^2)	0.0
Adjust size (pixels)	0

Seed	
Cell detection sensitivity	1
Cell contrast	2
Cell morphology	3

Cell-by-cell		
Area	Minimum	500.00
	Maximum	NA
Eccentricity	Minimum	NA
	Maximum	NA

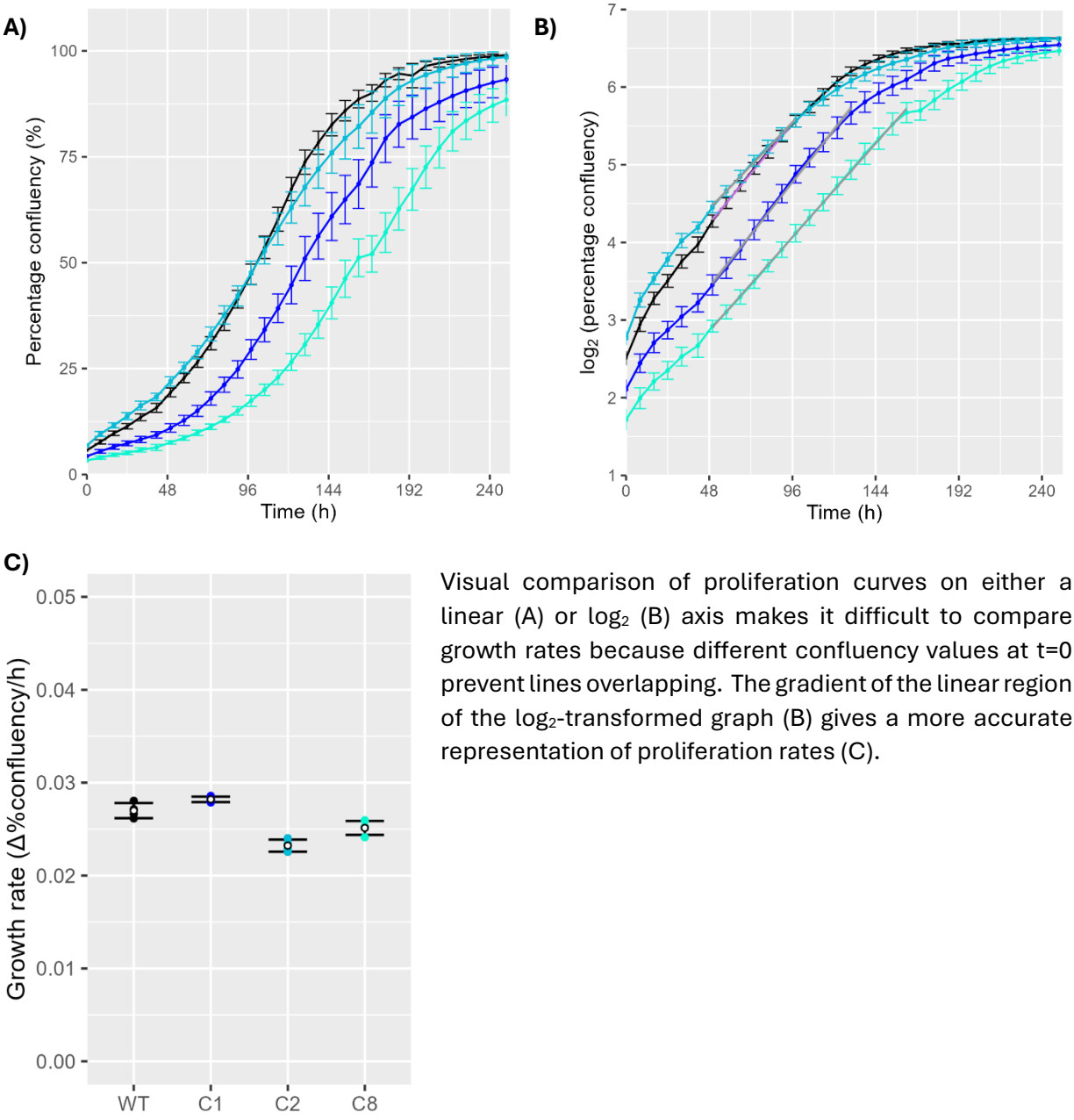
Appendix 6 – R scripts

Ferris_HERC4_Rscripts

Appendix 7 – CLARIOstar parameters

Basic settings	
Measurement type:	Fluorescence (FI)
Microplate name:	GREINER 96 F-BOTTOM
Endpoint settings	
No. of flashes per well:	20
Optic settings	
Presetname:	<user defined settings>
Excitation:	544-15
Dichroic filter:	573.8
Emission:	590-10
Gain obtained by:	enhanced dynamic range
Focal height obtained by:	previous focal height (manually entered)
Focal height [mm]:	5.8
Well used for focus adjustment:	-
General settings	
Bottom optic used	
Extended IR PMT used	
Spoon type:	-
Injection needle holder type:	-
Settling time [s]:	0.5
Reading direction:	bidirectional, horizontal left to right, top to bottom
Target temperature [°C]:	25
Target concentration O2 [%]:	set off
Target concentration CO2 [%]:	NA

Appendix 8 – proliferation curve calculations

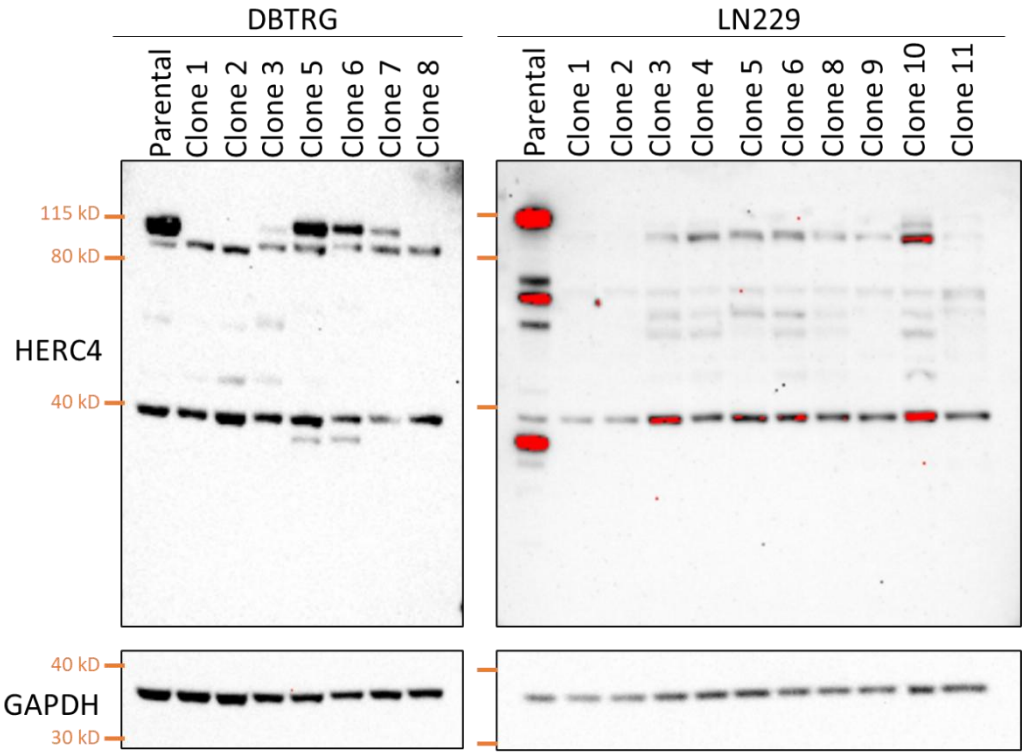


Visual comparison of proliferation curves on either a linear (A) or $\log_2$ (B) axis makes it difficult to compare growth rates because different confluency values at t=0 prevent lines overlapping. The gradient of the linear region of the $\log_2$-transformed graph (B) gives a more accurate representation of proliferation rates (C).

Appendix 9 – click reaction reagents

Reagent	Volume	Concentration
Tris-HCl (pH 7.5)	100 µl	1 M
Sodium ascorbate	100 µl	1 M
$CuSO_4$	20 µl	Commercial stock
Alexa fluor 647 azide	2 µl	1 mM
ddH_2O	778 µl	-

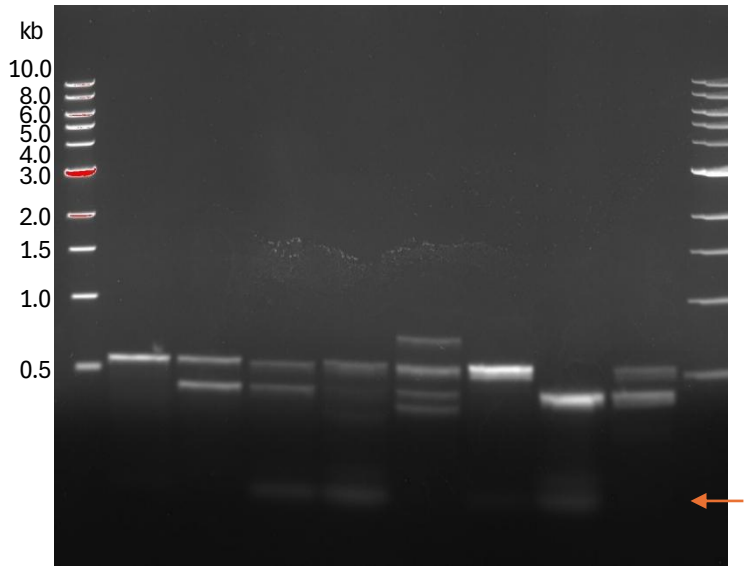
Appendix 10 – western blot validation of HERC4 knockout clones



Red = overexposed

Appendix 11 – PCR validation of HERC4 knockout clones

Left to right: DBTRG wildtype, HERC4 KO Clone 1, Clone 2, Clone 8; LN229 HERC4 KO Clone 3, wildtype, Clone 1, Clone 2

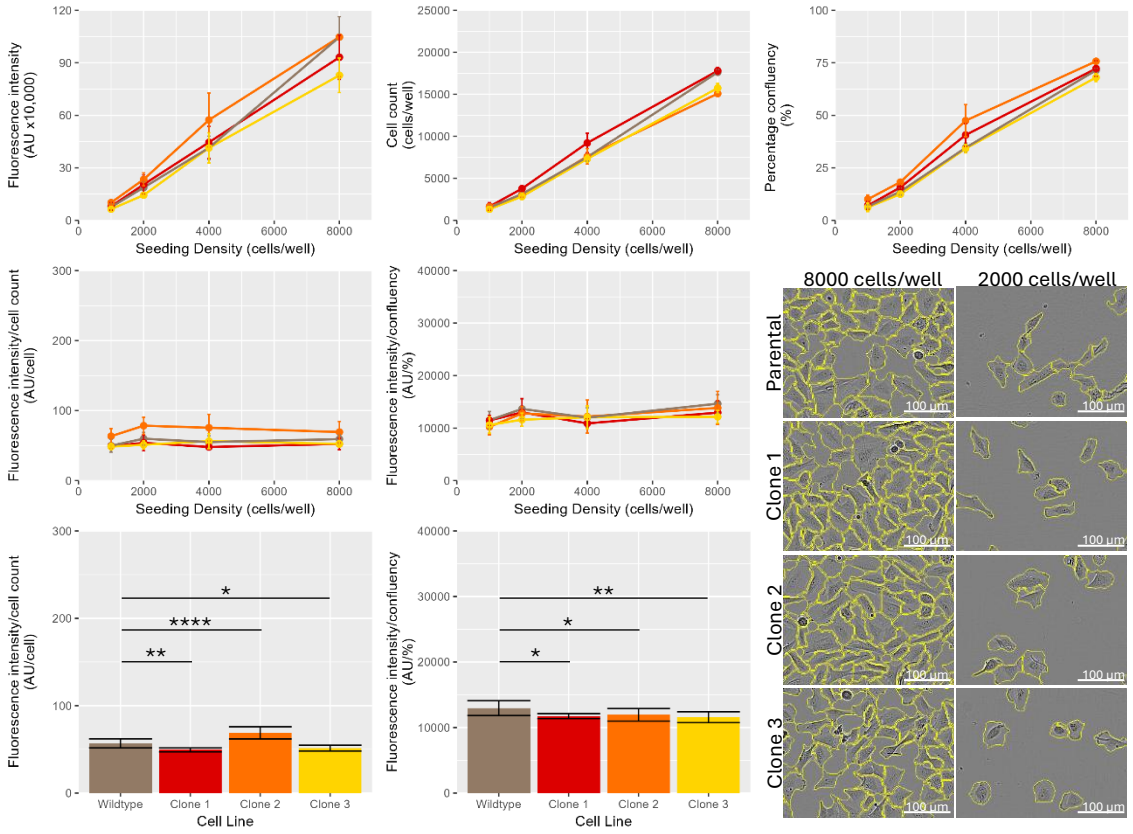


Red = overexposed

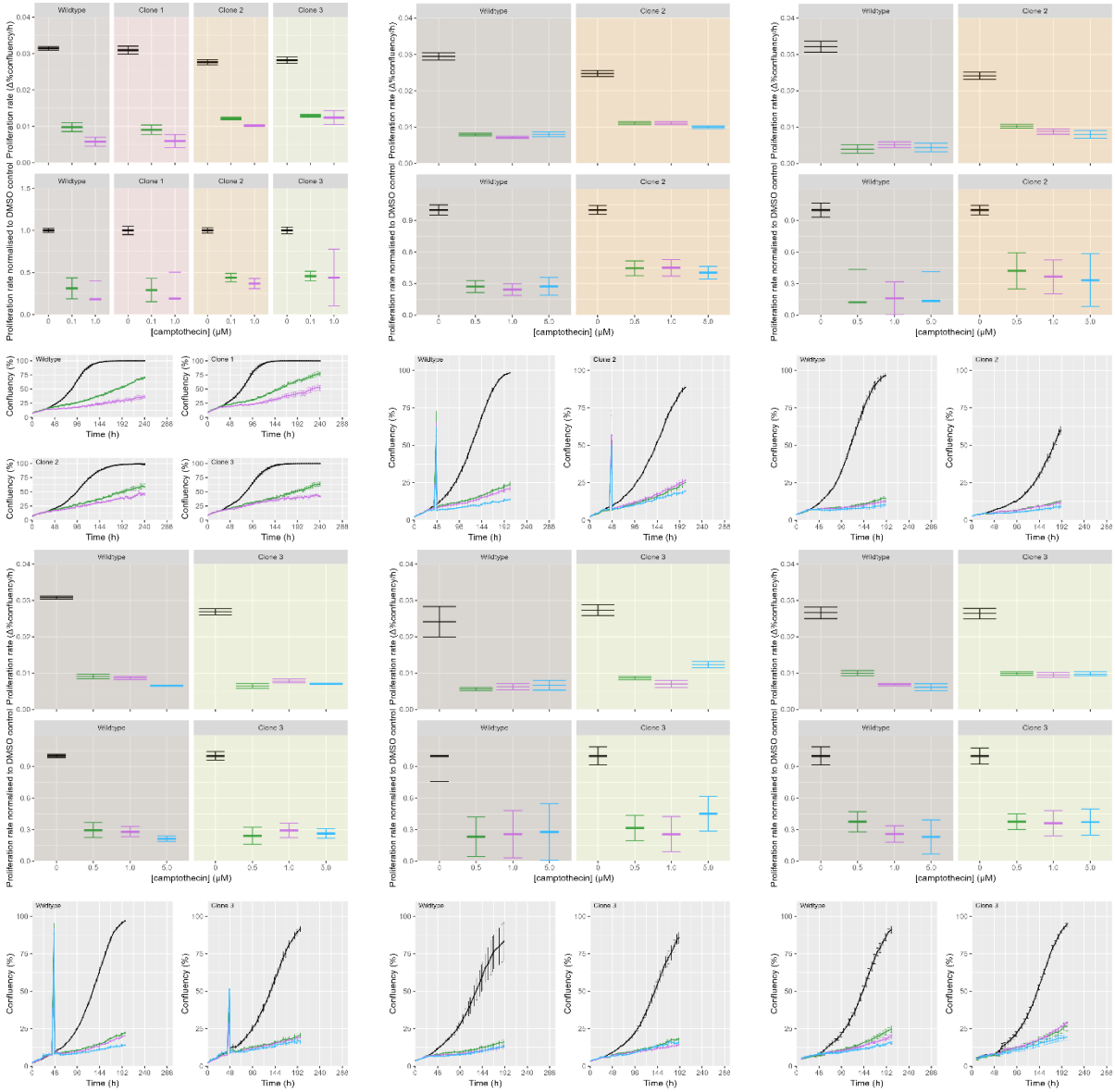
Primer dimers

4 PCR reactions were run in separate tubes simultaneously for each cell line. 1 product was run on the gel in Figure 2; the other 3 were stored at 4°C overnight then pooled and run on this gel.

Appendix 12 – metabolic activity calculations

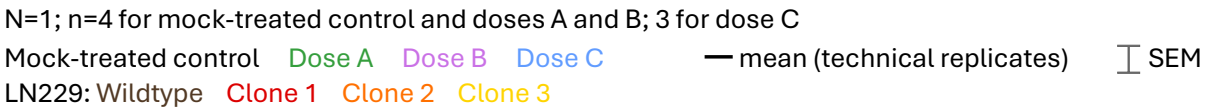


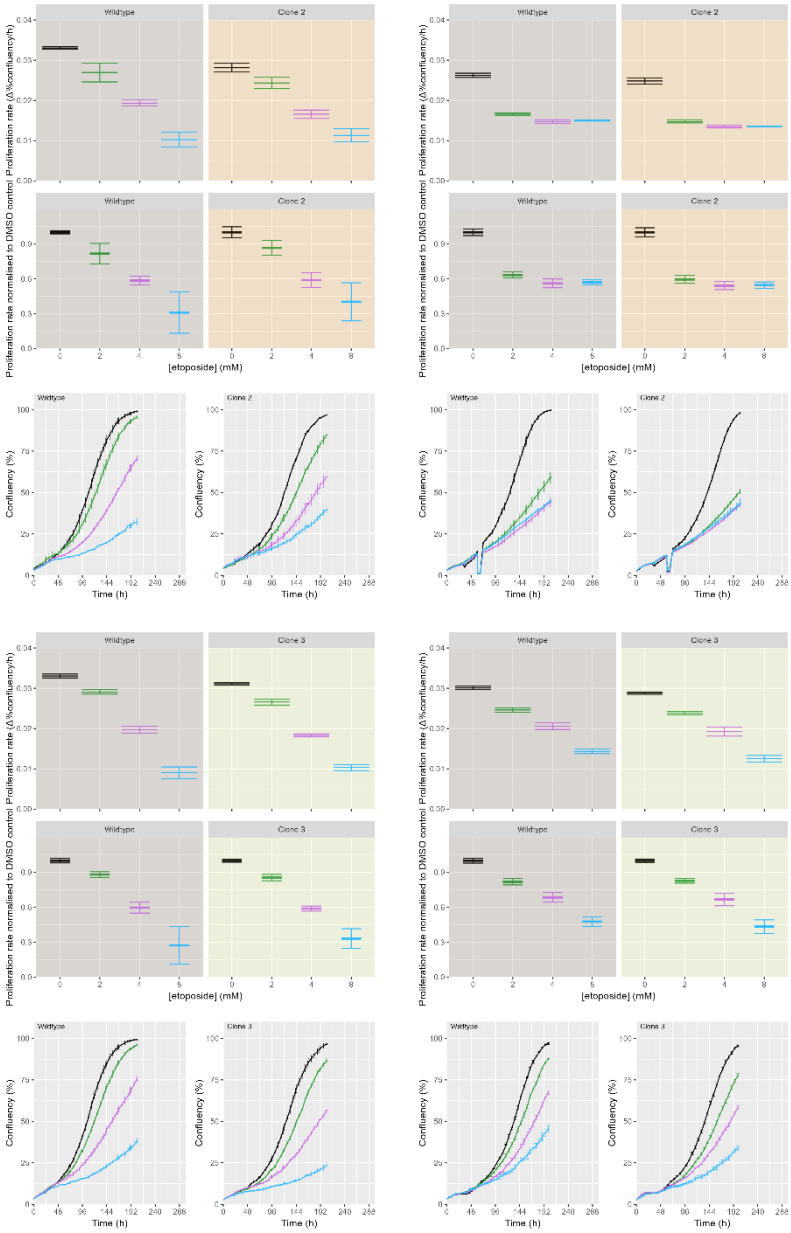
2 96-well plates were seeded at 4 different cell densities and incubated at 37°C, 5% CO_2 for ~2 days. Plates were imaged on an IncuCyte S3 at 10X magnification, then 10 µl/ml resazurin added for a further 3-h incubation at 37°C. Fluorescence was measured on a CLARIOstar Plus plate reader, and percentage confluency and cell counts were calculated using the cell-by-cell function of the IncuCyte analysis software. Line graphs show the mean and standard deviation of 4 technical replicates per seeding density. For bar graphs, all 16 replicates per cell line were combined and the highest 3 and lowest 3 values excluded prior to mean and standard deviation calculations. Statistical significance was calculated by one-way ANOVA with Dunnett's test in GraphPad Prism.
n = 4 per seeding density; ns = non-significant; $p<0.05$ = *; $p<0.01$ = **; $p<0.001$ = ***; $p<0.0001$ = ****
LN229: Wildtype Clone 1 Clone 2 Clone 3



Appendix 13 – proliferation after DNA damage

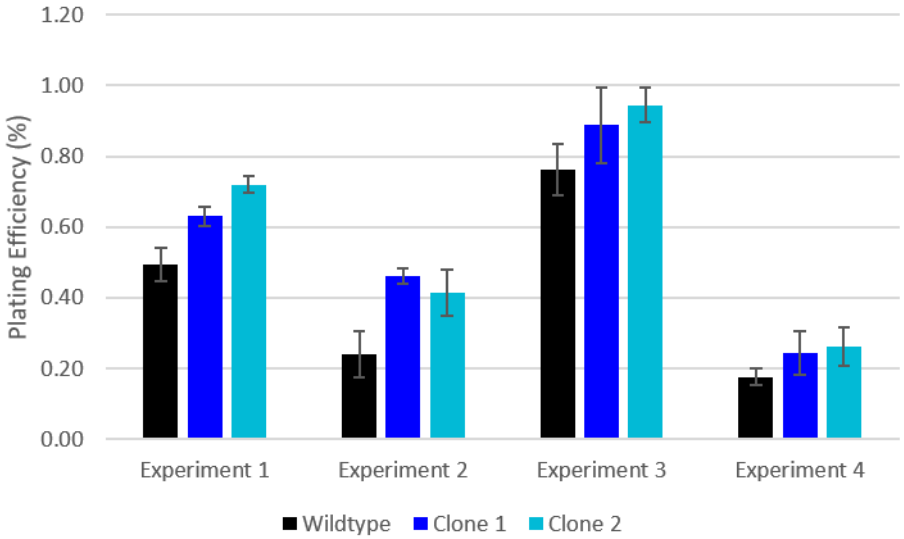
Additional experiments were run for camptothecin and etoposide, intended for analysis by normalisation to initial seeding density then untreated confluency at each timepoint. Higher seeding densities were used than in the main experiments, so the parameters used to isolate the linear region of the $\log_2$ graph had to be broadened to include sufficient data points (from 48 h instead of 72 h, and until 60% confluency in the untreated control instead of 50%). Clones 2 and 3 show a smaller change in proliferation rate after treatment with camptothecin, but since this was not reproduced in the main experiment, it is possible that this reflects a difference in the 24 h after the compound is removed, rather than a sustained effect on proliferation. It would nonetheless justify additional repeats of the main experiment, especially since the data in this appendix support the findings of the DNA damage screen by Olivieri et al. [2020]. Similarly, when the experiment was repeated with etoposide (same parameters as this camptothecin dataset), there was negligible difference in the relative treated proliferation rates between wildtype and HERC4 knockout populations.


N=1; n=4 for mock-treated control and doses A and B; 3 for dose C
Mock-treated control
Dose A
Dose B
Dose C
mean (technical replicates)
SEM
LN229: Wildtype
Clone 1
Clone 2
Clone 3


Wildtype
Clone 2
Clone 3
Proliferation rate normalised to DMSO control
Proliferation rate (Δ%confluency/h)
[etoposide] (mM)
Confluency (%)
Time (h)

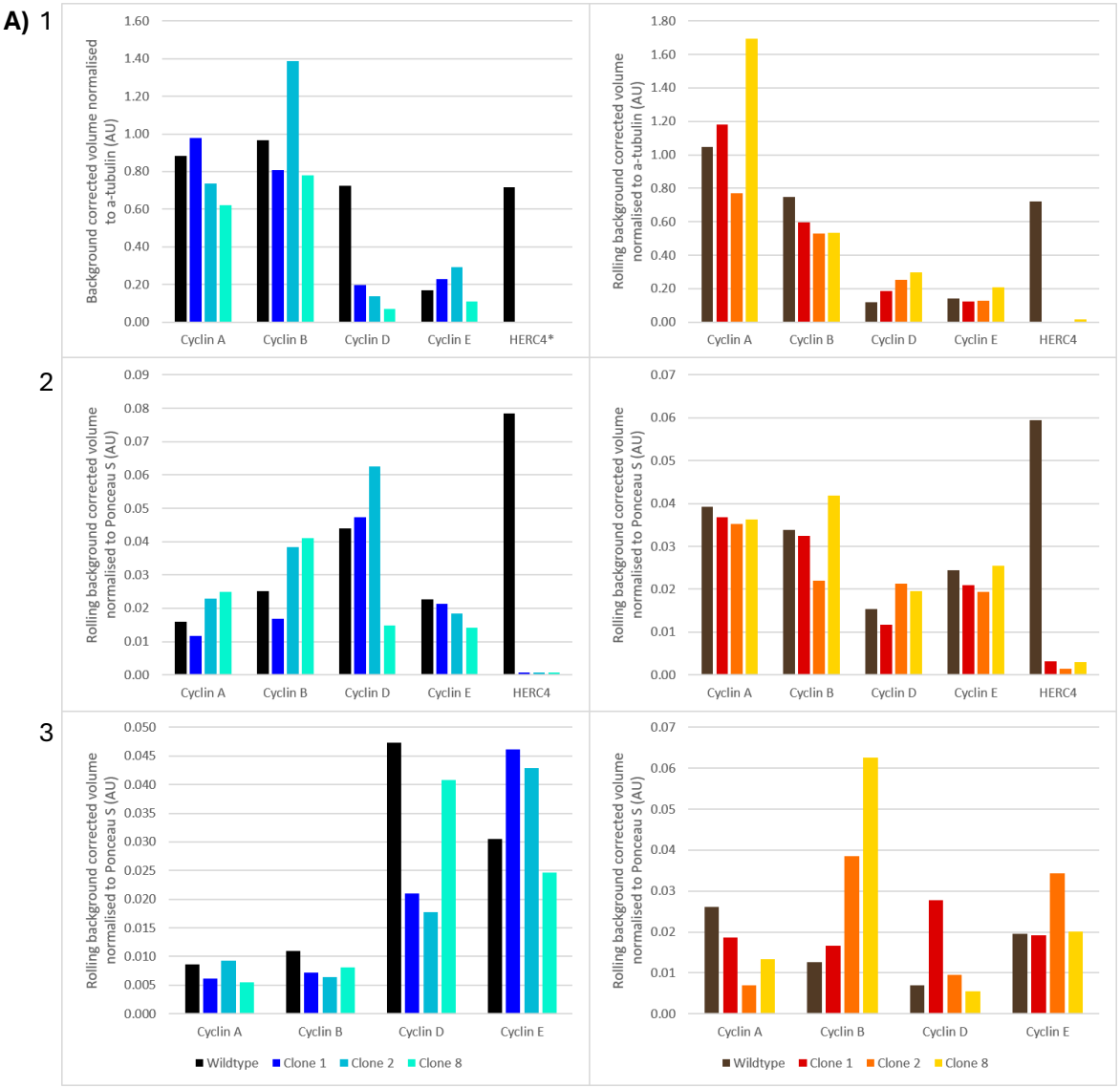
Appendix 14 – plating efficiencies for colony formation assays

	Experiment 1	Experiment 2	Experiment 3	Experiment 4
DBTRG WT	0.49 ±0.05	0.24 ±0.06	0.76 ±0.07	0.18 ±0.02
DBTRG Clone 1	0.63 ±0.03	0.46 ±0.02	0.89 ±0.11	0.24 ±0.06
DBTRG Clone 2	0.72 ±0.02	0.41 ±0.07	0.95 ±0.05	0.26 ±0.05



Plating efficiencies were calculated as the number of colonies counted for non-irradiated plates divided by the number of cells calculated to have been seeded into the well (100). The mean percentage for each cell line in each experiment is shown above with error limits of 1 standard deviation unit (calculated in Microsoft Excel as standard deviation of a population).

Appendix 15 – normalisation of western blots in Figure 9



A) Western blots were normalised using iBright analysis software and values for cyclins and HERC4 were normalised to those for α-tubulin (1) or Ponceau S (2 and 3). n=1 per graph

B) Ponceau S staining quantification may be misleading in the third repeat due to the low signal. The graph shown indicates values for Ponceau S staining in LN229 blot 3. There is a ~3-fold difference in the background-corrected measurements which would be expected to produce a more visible difference in the western blot (roughly equivalent to the difference between wildtype and Clone 2 in the cyclin D panel for DBTRG repeat 2).

3 – Proteomic changes associated with HERC4

3.1 – Introduction

There is reasonable evidence in the literature for HERC4 involvement in fertility and the immune response, and correlations between its expression and oncogenic processes such as enhanced proliferation, migration and invasion, and reduced apoptosis have been identified in multiple cancer types [Rodriguez and Stewart, 2007; Eslamloo et al., 2016; Xu et al., 2019; Zheng et al., 2017 – see Chapter 2 for more comprehensive references]. Mechanistic details for some of these models have been elucidated, and over a dozen putative interactors and substrates have been proposed (Table 1), but only 2 have been identified in multiple studies. SMO is the most frequently identified substrate, initially in *Drosophila* and subsequently in human cancer cells [Jiang et al., 2019; Sun et al., 2019; Zhu et al., 2024]. HERC4 loss exaggerates the wing phenotype generated by Smo overexpression in *Drosophila* by increasing Smo protein levels further. Smo interacts with both the RCC and HECT domains of Herc4, and Smo degradation in cycloheximide chase experiments is accelerated when Herc4 is overexpressed but delayed if a catalytically inactive Herc4 mutant is used. Smo phosphorylation inhibits Herc4-mediated ubiquitylation, suggesting that Herc4 may be involved in Smo turnover when the Hedgehog signalling pathway is inactive [Jiang et al., 2019]. These findings correlate with observations in both NSCLC and ovarian cancer. NSCLC tumours show decreased HERC4 and increased SMO expression compared to paratumour tissue, and the interaction between the two proteins was confirmed by IP. siRNA against HERC4 increased mRNA levels of Hedgehog target genes and accelerated cell proliferation [Sun et al., 2019]. Similarly, in ovarian cancer, tumour cells showed lower HERC4 levels compared to paratumour tissue. Higher HERC4 levels correlated with longer patient survival and HERC4 overexpression slowed tumour growth and reduced SMO levels in mouse

xenograft models [Zhu et al., 2024]. IP evidence for the interaction between HERC4 and SMO was replicated by Mutlu et al., who demonstrated that it is out-competed in the presence of AK59, a molecular glue that redirects HERC4 to STING [Mutlu et al., 2023].

The other HERC4 substrate identified by multiple studies is SAV1. Like SMO, it is marked for proteasomal degradation by HERC4-mediated ubiquitylation, which can be blocked by phosphorylation, in this case by Hippo signalling, or by Hippo binding. Sav1 binds to the RCC domain of Herc4, and Sav1 ubiquitylation is reduced though not completely abrogated based on a pull-down experiment with wildtype and catalytically inactive Herc4 [Aerne et al., 2015]. These experiments were done in fly models, but similar conclusions were drawn in human HCC cells [Huang et al., 2021]. Paired tumour and paratumour cells showed increased HERC4 and decreased SAV1 protein levels in the tumour populations, and the two proteins showed inverse correlations with patient survival. Patients classified as having low HERC4 had better prognosis than those with high HERC4 expression, while the opposite was true for SAV1. At a mechanistic level, IP experiments confirmed the interaction between SAV1 and HERC4, and that HERC4 overexpression could reverse the effects of SAV1 overexpression. SAV1 overexpression reduced tumour growth, suggesting a mechanism for the positive correlation between HERC4 expression and HCC cell proliferation shown in a different study, but the influence of HERC4 on tumour growth was not specifically tested [Huang et al., 2021; Zheng et al., 2017].

The effect of HERC4 on the wider Hippo signalling pathway has been explored in other studies. Unlike HERC3, it does not interact with $SCF^{\beta\text{-}TrCP}$, which marks YAP/TAZ, the transcription factors that regulate Hippo target genes, for degradation, and the same study suggested that HERC4 levels do not alter YAP/TAZ expression [Yuan et al., 2023]. However, it may indirectly influence YAP/TAZ levels in the context of EGFR signalling, since EGFR was found to bind to both HERC4 and SAV1 and promote their interaction with each other. EGRF overexpression increased SAV1 degradation, thereby relieving YAP/TAZ inhibition, allowing its translocation to the nucleus where

it is protected from proteasomal degradation. A role for HERC4 in this mechanism is of particular interest given that EGFR gene amplification is a defining feature of glioblastoma [Louis et al., 2021].

HERC4 has also been shown to interact with, ubiquitylate and cause degradation of LATS1 in breast cancer cells, an upstream mediator of YAP/TAZ phosphorylation [Xu et al., 2019]. This modification results in sequestration of the transcription factor in the cytosol and subsequent degradation, so by removing the proteins that promote this process, HERC4 may facilitate transcription of the pro-proliferation, anti-apoptosis genes targeted by the Hippo signalling pathway. This would explain the poorer prognosis associated with higher HERC4 levels in breast cancer [Huang et al., 2021].

These studies start to build a mechanistic model behind the phenotypes observed to correlate with HERC4 expression in cancer, namely changes to proliferation, apoptosis, migration and invasion. Increasing proliferation or apoptosis rates would explain the observation at the start of this project that HERC4 increases radiosensitivity, but neither proliferation rate nor cell cycle distribution was affected in the experiments presented in the previous chapter. Particularly given the variation between cell types already observed in the literature, it might therefore be expected that, in glioblastoma cells, HERC4 targets other areas of cell function. It is also possible that the published mechanisms are applicable in this context but are masked by other factors. Consequently, a broader approach was required, and one that does not rely on molecular details translating into phenotypic changes.

The ability of mass spectrometry to identify 1000s of peptides in a sample provides a suitable method for this unbiased exploration of proteins influenced by HERC4. Proteome characterisation after HERC4 knockout promises insight into the global effects of HERC4, including genes and pathways whose abundance and activity might be altered strongly but indirectly. If HERC4 influences protein expression, for example through changes in transcription,

mRNA or protein stability, or translation, these changes should be detected by comparison of HERC4 wildtype and knockout cells. Complementary to this, proximity labelling identifies proteins in the immediate vicinity of HERC4, including substrates and other interactors that might regulate its activity. Biotin ligases have been shown to identify known substrates of E3 ligases [Barroso-Gomila et al., 2023], and the TurboID enzyme has much greater activity than its predecessors, improving the sensitivity of the method [Cho et al., 2020]. Characterising the repertoire of proteins that interact with HERC4 should give insight into the pathways and processes affected by its activity, and confirmation of a published substrate or identification of a new one could lead on to exploring the ubiquitylation type and mechanism of HERC4.

While both the total proteome and proximity labelling methods are advantageous in their ability to generate extensive datasets, the volume of data can also be a challenge. If there are only a few proteins identified, or whose identification seems markedly more confident (either statistically or through larger changes in abundance between conditions), these can be individually pursued, but when the dataset is larger and more uniform, it is more practical to condense it into a series of trends to direct further investigation. Genes are annotated with terms related to their function and cellular location in a range of databases. For this study, the Kyoto Encyclopaedia of Genes and Genomes (KEGG) was used to collate identified proteins into pathways, and the Biological Process branch of the Gene Ontology database (GO-BP) was used to group proteins by their known or predicted functions [Kanehisa et al., 2021; Gene Ontology Consortium, 2004]. The main methods to identify enriched terms from these databases are over-representation analysis (ORA), gene set enrichment analysis (GSEA) and pathway topology (PT), which prioritise different factors and consequently have different strengths [Khatri et al., 2012]. ORA is arguably the simplest – it takes unranked lists of significantly differentially expressed genes and, for any given term, compares the proportion of the significant list linked to this term with the proportion of linked genes from a background list (any gene that might be expected in the samples tested). However, it requires the user to select which differentially expressed genes

are significant, giving largely arbitrary thresholds huge influence on the results. The sensitivity of the method is also limited, with performance declining substantially if the list length drops below 50. GSEA avoids the use of arbitrary thresholds by including all genes in the dataset and giving them a ranked score, usually based on their $-\log_{10}$(p-value) multiplied by the sign (+/-) of their $\log_2$(fold change) between conditions. This typically results in a larger useable dataset, avoiding the sensitivity issue encountered for smaller lists. While it addresses these limitations of ORA, it shares another disadvantage – it only considers which proteins belong to the same term, not interactions between these proteins. Pathway analysis incorporates this information, but therefore relies on its availability, which is a significant drawback for less well characterised processes. A combination of these methods with the breadth of data from mass spectrometry analysis offers a wider starting point than phenotypic experiments from which to narrow down potential roles for HERC4, including those that might influence radiosensitivity.

Protein	Interactor or substrate	Linkage type	Effect	Context	Reference
SAV1	Substrate		Degradation Higher HERC4 expression correlates with lower SAV1 levels and worse prognosis (increased cell proliferation, survival, invasion and migration)	*Drosophila* HCC	Aerne et al., 2015 Huang et al., 2021
SMO	Substrate		Degradation Inhibition of pro-growth Hedgehog signalling pathway	*Drosophila* NSCLC	Jiang et al., 2019 Sun et al., 2019 Zhu et al., 2024
c-MAF	Substrate	K48	Degradation. Slower tumour growth.	Multiple myeloma	Zhang et al., 2016
MafA	Substrate	K63	Inhibition (prevents stimulatory GSK3β-mediated phosphorylation)	Multiple myeloma	Zhang et al., 2023
PGR	Substrate		Degradation. Downregulation of fertility-linked genes.	Endometriosis	Huang et al., 2022
LATS1	Substrate		Degradation. Proliferation, survival and migration increase with HERC4 overexpression, but no rescue with LATS1 tested.	Breast cancer	Xu et al., 2019
DHODH	Substrate		Degradation. Relief of ferroptosis inhibition and increase in temozolomide sensitivity.	Glioblastoma	Miao et al., 2024
KRT19	Substrate		Degradation. Knockdown increases metastasis *in vivo*, and HERC4 overexpression reduces KRT19 levels and increases proliferation and migration.	Lung adenocarcinoma	Sun et al., 2026
METTL3	Interactor		m6A methylation on *HERC4* mRNA Knockdown reduces cell viability, proliferation and migration, EMT and angiogenesis. Role of interaction with HERC4 protein is unclear, but effects of knockdown reversed by HERC4 overexpression.	HCC	Sun et al., 2025
EGFR	Interactor		Facilitates HERC4 + SAV1 to relieve inhibition of Hippo pathway	Diabetic retinal fibrosis	Zhang et al., 2025
ZFTRAF1	Interactor		Unclear. Fibroblasts from patients with ZFTRAF1 mutations had higher levels of HERC4 than control fibroblasts.	Neurodevelopmental disorders	Asif et al., 2024
NEDD4	Interactor			HEK293FT cells, BioID	Barroso-Gomila et al., 2023
HPV E7	Interactor		Does not influence E7 levels	Cervical cancer	Huang et al., 2024
VmpA	Interactor			Insect cells	Canuto et al., 2023

Table 1: Published HERC4 interactors and substrates

3.2 – Methods

3.2.1 – Experiment Design

Mass spectrometry was selected as a complementary method to phenotypic experiments due to its ability to address the open question of what cellular processes might involve HERC4, rather than the specific hypotheses tested by the phenotypic experiments in the previous chapter. Given the E3 function of HERC4, it was expected that much of its activity would be directed to proteins, and that the majority of its phenotypic effects would be caused at the protein level too, suggesting that proteomic data held greater potential than other high-throughput 'omic' techniques for elucidating putative roles for HERC4.

The total proteome experiment was designed to probe indirect changes in protein levels as a result of HERC4 loss, on the basis that multiple changes clustered around the same function or pathway would indicate a role for HERC4 in this area. The inclusion of 2 clones was prioritised over 1 clone with and without IR on the basis that a broader exploration of HERC4 function could still yield the results needed to direct future experiments and therefore avoiding clonal effects was more important. LN229 cells were selected over DBTRG cells simply due to ease of culture – they grow more rapidly and more densely, making it easier to culture the numbers required for adequate protein extraction.

For proximity labelling, HEK293T cells were also chosen for practical reasons (easy transduction with TurboID-HERC4 and quick to grow). The method itself was chosen to probe more directly the proteins through which HERC4 might act, based on the hypothesis that, if these proteins had known functions, they would offer promising directions for investigating the role of HERC4 in a more targeted manner. Several proposed HERC4 substrates have already been shown to be degraded as a result of HERC4-mediated ubiquitylation, so inclusion of proteasome inhibitor

MG132 was included in place of IR in an attempt to separate substrates from interactors. Both experiments were limited to 3 conditions for financial reasons.

Together, the two proteomics methods were selected as a broader approach to characterising HERC4 function, in place of a more trial-and-error approach with phenotypic experiments. It was expected that the results would converge on a couple of pathways or processes, and that these would ideally support the data from the previous chapter. However, the exclusion of IR from either experiment extended the likely data beyond processes involved in IR sensitivity. This offered the benefit of highlighting putative areas of HERC4 involvement for further investigation even if involvement in radiosensitivity could not be confirmed, since the experiments for both results chapters were run in parallel.

3.2.2 - Preparation of total proteome samples

~10^6 wildtype cells or ~1.1 x 10^6 HERC4 knockout cells were seeded into 15-cm plates (3 per clone; 6 for wildtype) in ~20 ml D10- and incubated at 37°C, 5% CO_2 for 4 days until 70-80% confluent. Cells were harvested in the media by scraping, then centrifuged, washed in PBS, and frozen at -80°C.

Pellets were lysed in RIPA buffer with protease inhibitors on ice for ~10 minutes, then centrifuged and lysates isolated. Total protein concentration was measured by BCA assay and samples were diluted to the same concentration as the most dilute one. HERC4 levels were confirmed by western blot (same protocol as used in Chapter 2) and normalisation of total protein concentrations was confirmed by staining with Coomassie R-250 (0.1% in 50% methanol and 10% acetic acid).

3.2.3 – Processing of total proteome samples

Mass spectrometry processing and initial data analysis were conducted by Svenja Hester and Dr Iolanda Vendrell. Their analysis was limited to the steps outlined in this section. Samples were

digested using the S-Trap micro method then run on a Neo Vanquish liquid chromatography machine before mass spectrometry data was collected using data-independent acquisition.

Peptides were quantified from the raw data using DIA-NN v1.8.1 [Demichev et al., 2019] and the resultant data was processed further using Perseus v1.6.15.0 [Tyanova et al., 2016]. MaxLFQ was used for cross-run normalisation [Cox et al., 2014], and match between runs was disabled due to the use of knockout cell lines. Proteins were discarded if they were not detected in all 3 replicates for at least one cell line, resulting in 6317 confidently identified proteins out of an initial list of 6833 proteins.

0 or NA values were then replaced with values randomly selected from the lower end of the normal distribution for intensities in that sample. This imputation approach facilitates subsequent $\log_2$ transformation of the intensities and minimises the bias otherwise introduced by missing values. Since these values typically reflect a protein that was present but too scarce to be detected, replacing them with intensities from the lower end of the normal distribution does not interfere with data analysis.

A $\log_2$ transformation was applied to intensities, along with median normalisation, and each knockout clone was then compared to the wildtype cells and 2-sample t-tests with Benjamini-Hochberg truncation and a false discovery rate of 0.01 were used to determine statistical significance of the change in abundance of each protein in these comparisons. Subsequent analysis was conducted by the author.

3.2.4 – Preparation of proximity labelling samples

HEK293T cells expressing HERC4 with an N-terminal TurboID tag under the control of a doxycycline-inducible promoter were kindly provided by Dr Paul Smith. They were seeded into 15-cm plates in ~25 ml D10- and incubated at 37°C, 5% CO_2 until they reached 70-80% confluency. Doxycycline was then added to a final concentration of 1.3 µg/ml and the cells were incubated for a further 24 h. 3 plates were left untreated, biotin was added to the other 6 to a

final concentration of 50 µM, and MG132 was added to 3 of the biotin-treated plates to a final concentration of 10 µM. All plates were incubated for a further 3 hours at 37°C, 5% CO_2 before the cells were harvested in the treated media by scraping. Cells were pelleted by centrifugation and washed in PBS before the supernatant was removed and the pellets flash-frozen in liquid nitrogen. They were then stored at -80°C.

Pellets were resuspended in RIPA buffer with protease inhibitors and 0.5 µl/ml Benzonase, then incubated on ice for 30 minutes. They were centrifuged at 16,000 x g for 20 minutes at 4°C and the supernatant transferred to a clean Eppendorf. An aliquot of each lysate was reserved for western blot analysis.

1 ml 50% Streptavidin bead slurry was washed 3 times in HNN buffer (HEPES, NaCl and NaF; Appendix 2) and 3 times in RIPA buffer then aliquoted into 9 clean Eppendorf tubes. Residual buffer was removed and the lysates added. Samples were incubated on a rotating wheel at 4°C for ~1 h. The supernatant was then removed as the flow-through and the beads were washed 3 times in RIPA buffer then 3 times in HNN buffer. Residual supernatant was removed and for the mass spectrometry experiment, the remaining pellets were flash-frozen in liquid nitrogen then stored at -80°C. For the validation experiment, the beads were resuspended in 4X Laemmli buffer and heated to 90°C for a few minutes before being analysed, along with the input and flow-through aliquots, by western blot, using the protocol described in Chapter 2. 1%, 10% and 1% of the input, eluate and flow-through respectively was loaded into the gel. Antibody catalogue numbers are listed in Appendix 1.

3.2.5 – Processing of proximity labelling samples

On-bead digest using urea and Promega trypsin was performed by Dr Paul Smith. Sample processing and the preliminary data analysis described in this section was performed by Dr Iolanda Vendrell using DIA-NN (v1.8, library-free quantification against human UniProtSW) and Perseus. The same analysis parameters were used as for the total proteome experiment, namely

median centring for intensity normalisation, imputation of missing values based on a normal distribution, and removal of any peptides not present in all 3 replicates for at least one condition. Intensities were subject to $\log_2$ transformation, then compared by 2-sample t-test with a 1% false discovery rate. Subsequent analysis steps were conducted by the author.

3.2.6 – Analysis of both datasets

Results were imported into RStudio as $\log_2$(fold change) values and corresponding -$\log_{10}$(p-value) and HERC4 was removed from each dataset. For proximity labelling data, proteins that were significantly more abundant in the no-biotin control than in one or both of the biotin-treated conditions were assumed to bind to the beads through an interaction other than biotin-streptavidin, and were consequently removed from the datasets. Proteins with a negative $\log_2$(fold change) value for the -/+MG132 comparison were considered substrates. Those with a $\log_2$(fold change) value of 1 or more and a -$\log_{10}$(p-value) of at least 1.3 were considered significant, and these significance thresholds were applied to all datasets. The following lists were then analysed:

1. Interactors – proteins that were significantly less abundant in no-biotin samples than in either biotin-treated condition;
2. Substrates – proteins that were not significantly more abundant in no-biotin samples than in either biotin-treated sample, and were more abundant in MG132-treated than untreated samples;
3. Differentially expressed in Clone 1 – identified in wildtype and Clone 1 cells (not necessarily significantly different);
4. Differentially expressed in Clone 3 – identified in wildtype and Clone 3 cells (not necessarily significantly different);
5. Differentially expressed in either clone – present in list 3 and/or 4;
6. Differentially expressed in both clones – present in both list 3 and 4.

Where proteins were detected more than once in the same list, only the fold change with the highest $-\log_{10}$(p-value) was kept.

MSigDB gene collections were downloaded using the msigdbr library [Subramanian et al., 2005; Liberzon et al., 2011]. KEGG legacy pathways and Gene Ontology Biological Process (GO-BP) terms were selected for further analysis. Over-representation analysis was carried out using the clusterProfiler library. Proteins were split into significantly up- or downregulated based on whether they were more abundant in the control or treated samples, and the full dataset for the comparison, including non-significant proteins, was used as a background environment for the analysis. Minimum gene set size was set to 10, and enriched terms were considered significant if they contained at least 2 proteins and had an adjusted p-value of ≥0.05.

The clusterProfiler library was also used for GSEA analysis, along with AnnotationDbi to convert gene symbols to ENTREZ ID values for comparison with the KEGG database. 41 and 34 proteins were removed from the interactor and substrate lists respectively because they had no ENTREZ ID. These lists contained multiple protein names for some hits. These were reduced to the first name listed and duplicates were then removed, amounting to 247 and 248 respectively. For each protein, the row with the highest $-\log_{10}$(p-value) was kept (most statistically significant). Proteins were ranked by their $-\log_{10}$(p-value) multiplied by the sign of their $\log_2$(fold change) so that those closest to the top were the most significantly upregulated in wildtype cells, those closest to the bottom were the most significantly upregulated in knockout cells, and those nearer the middle were statistically insignificant. Default settings were used for gseKEGG and gseGO functions, and enriched terms with an adjusted p-value of ≥0.05 were considered significant.

For pathway analysis, significant hits were extracted from each dataset and passed to the run_pathfindR function from the pathFindR library, with the usual parameters for significance [Ulgen et al., 2019].

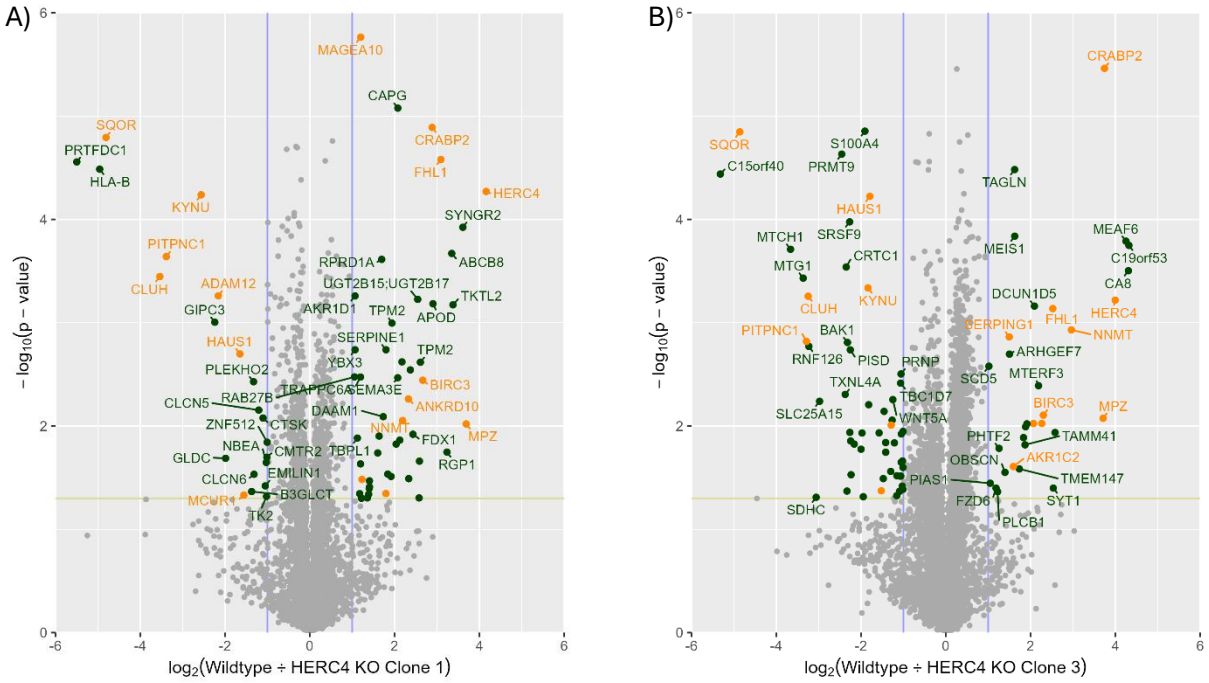
Terms were grouped manually and graphs were produced using ggplot2 and related libraries. Analysis code is in Appendix 2.

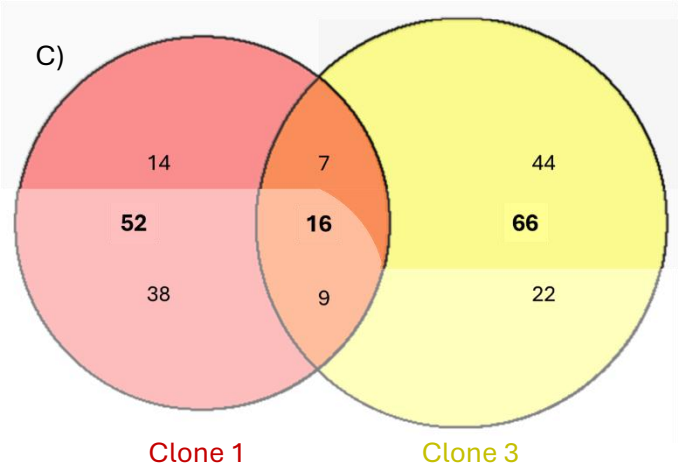
3.3 - Results

3.3.1 - Total Proteome

3.3.1.1 - Significant hits shared by both clones show tentative connection to metabolism, cell growth, development and the immune system

Whole-cell lysates from LN229 Clones 1 and 3 were used for total proteome analysis by mass spectrometry. Reassuringly, HERC4 was not detected in any replicates for either clone, but it was present in all 3 wildtype replicates (data not shown). Proteins that showed a ≥2-fold change in the clones compared to wildtype, with a $-\log_{10}$(p-value) of at least 1.3 ($p \approx 0.5$) were considered to show significant changes in expression after HERC4 loss (Figure 1A-B). There were 67 such proteins in Clone 1, of which 21 showed a negative correlation with HERC4 expression (more abundant in the knockout clone than in wildtype cells). For Clone 3, there were 82 differentially expressed proteins, of which 51 negatively correlated with HERC4 expression. Between the 2 clones, there were 16 common hits (Figure 1C-D), and each showed the same direction of change in both clones. Further analysis of these shared hits returned limited results. There were no significantly enriched KEGG and GO terms by ORA, GSEA or pathway analysis, and while STRING analysis did produce a few connections once two extra sets of nodes were added, only 2 networks contained more than 1 protein from the original dataset and 3 out of 5 connections had little validation in the literature (Figure 2). In light of this, the GO-BP terms for each protein were reviewed (only 6 of the proteins had KEGG annotations) and broader descriptors assigned (Table 2, Appendix 3). Cell cycle, muscle development and immune system applied to 2-3 proteins, but all other descriptors applied to only 1, so all descriptors were further grouped into 5 categories. 3 proteins were associated with mitochondrial activity, 3 to metabolism, 4 to cell growth, 4 to development and 8 to miscellaneous descriptors.

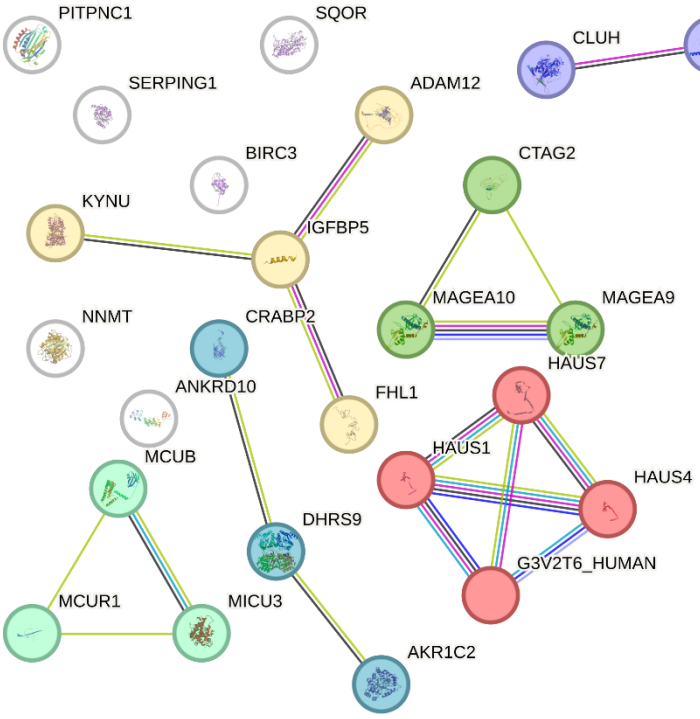




D)

Genes	Clone 1	Clone 3
MPZ	3.689773	3.711147
CRABP2	2.886755	3.74395
FHL1	3.09308	2.524722
NNMT	2.190676	2.962638
ANKRD10	2.326111	2.069914
BIRC3	2.665515	2.301484
MAGEA10	1.201423	2.265299
AKR1C2	1.795206	1.594355
SERPING1	1.230521	1.497836
MCUR1	-1.5557	-1.5222
HAUS1	-1.64896	-1.79141
ADAM12	-2.15948	-1.28843
KYNU	-2.56296	-1.83605
PITPNC1	-3.38585	-3.28732
CLUH	-3.53839	-3.24743
SQOR	-4.80859	-4.86021

Figure 1: Differentially expressed proteins in LN229 HERC4 knockout clones
Whole-cell lysates were prepared for Clones 1 and 3, then used for total proteome analysis by mass spectrometry. A and B) Differentially expressed proteins for Clone 1 and 3 respectively, with log2(fold change) values indicating correlation with HERC4 (negative values indicate higher abundance in the clone than in wildtype cells). Differential expression compared to wildtype was considered significant (green and orange points) if the fold change was greater than 2 (blue line) and had a -log10(p-value) of ≥1.3 (yellow line), and proteins differentially expressed in both clones are shown in orange. C) 52 and 66 proteins were differentially expressed in only one clone (1 and 3 respectively), and an additional 16 proteins were differentially expressed in both clones. Darker shades indicate higher abundance in clone than wildtype (negative correlation with wildtype), while lighter shades indicate the reverse. D) 16 proteins differentially expressed in both clones and their log2(fold change) values. All 16 had a -log10(p-value) of 1.3 or more.



Cluster	Gene count (from input)
HAUS complex	4 (1)
ADAM12, FHL1, IGFBP5, KYNU	4 (3)
Mixed	3 (1)
+ Calcium import into mitochondrion	3 (1)
+ Retinoic acid biosynthesis	3 (2)
Mixed	2 (1)

Figure 2: STRING analysis of common hits returns limited connections
Downloaded 29/11/25 from STRING v12. MPZ was excluded because neither "MPZ" nor "M0" was found in the database. 2 extra sets of nodes added to find connections. Only 2 networks included more than 1 gene from the common list (yellow and light blue), and of the connections in these, literature validation was found only for ADAM12-IGFBP5 [Loechel et al., 2000] and FHL2-IGFBP5 [Amaar et al., 2002].

Categories based on GO-BP terms	CLUH	MCUR1	SQOR	SERPING1	KYNU	NNMT	AKR1C2	HAUS1	BIRC3	FHL1	CRABP2	ADAM12	MPZ	MAGEA10	ANKRD10	PITPNC1
Mitochondrial organisation	■															
Calcium ion import into mitochondria		■														
Electron transport chain			*													
Metabolism							■									
Metabolism (Trp → NAD cofactors)					■											
Metabolism (carbohydrates and gluconeogenesis; protein)						■										
Cell growth											■					
Cell proliferation							■									
Cell cycle								■	■	■						
Development	■	■	■	■	■	■	■	■	■	■	■	■	■	■	■	■
Embryo development	■	■	■	■	■	■	■	■	■	■	■	■	■	■	■	■
Muscle development	■	■	■	■	■	■	■	■	■	■	■	■	■	■	■	■
Ion transport (muscle depolarisation)										■						
Vasculature development	■	■	■	■	■	■	■	■	■	■	■	■	■	■	■	■
Neuron development	■	■	■	■	■	■	■	■	■	■	■	■	■	■	■	■
Neuron signalling													■			
Cell differentiation	■	■	■	■	■	■	■	■	■	■	■	■	■	■	■	■
Cytoskeleton								■								
Cell adhesion													■			
Immune system									■							
Transcription														■		
Post-translational modification (Ub)									■							
Protein localisation															■	
Lipid localisation																■
Immune system				■	■											
Reproduction									■							

Table 2: Categorisation of GO-BP terms for differentially expressed proteins common to both clones
GO-BP terms for each protein were summarised into an overarching descriptor, and these descriptors were further grouped into 5 categories: mitochondria, metabolism, cell growth, development and other.

*Extrapolated from function – electron transport chain was not explicitly mentioned in linked GO-BP terms, but sulphide:quinone oxidoreductase activity is needed to prevent hydrogen sulphide-mediated inhibition of Complex IV.

3.3.1.2 - Combining significant hits from each clone produced more enriched terms, with some conflict between function and direction of change of proteins in the same term

Given the lack of significantly enriched terms in the 16 proteins differentially expressed in both clones, the analysis parameters were relaxed to look for additional suggestions for potential roles for HERC4, albeit more tentative ones. Proteins that were significantly altered in one or both clones compared to wildtype were included, giving an input of 130 proteins for subsequent analysis.[4] The resultant terms were then filtered for those containing hits from both clones (at least 1 gene from each clone, but not necessarily the same gene in both). Among the retained terms were several neurological diseases, metabolic or mitochondrial connections, and cell cycle processes, reflecting some of the functions suggested in the literature or explored in the data presented in Chapter 2 (Figure 3). It should be noted, however, that many of the top retained terms in the pathway analysis contained only 1 hit from Clone 1, NDUFB1, whose expression was positively correlated with HERC4 (downregulated in the knockout compared to the wildtype), while multiple proteins from the same pathway were identified in Clone 3, with negative correlation to HERC4 levels. All proteins listed from Clone 3 contribute positively to the term, and this contrast is particularly striking for NDUFB9, since both proteins contribute positively to Complex I in the mitochondrial respiratory chain, yet their abundance appears to change in opposite directions following the loss of HERC4.

Since a contrast of this nature might indicate that a pathway differs from the average wildtype population due to clonal variation rather than the effects of HERC4 loss, a scatter plot was created for each pathway (Figures 4-5). Most pathways had proteins that correlated positively and negatively with HERC4 expression, with some showing opposing changes on the pathway, such as BAK1 and BIRC3 for apoptosis, but others suggested conflicting effects. This highlighted

[4] 3 proteins were excluded despite being significant in one clone because the p-value was higher in the other clone, but the corresponding fold change was insignificant.

a key flaw in the analysis method, and one that is avoided by ORA and GSEA methods since enriched terms are identified by proteins with a common direction of change (Figures 4-5; Appendix 4). However, they do not rule out proteins with opposing effects on a term showing changes in the same direction, or that proteins with similar effects but opposite changes were present in the dataset but not highlighted by the analyses.

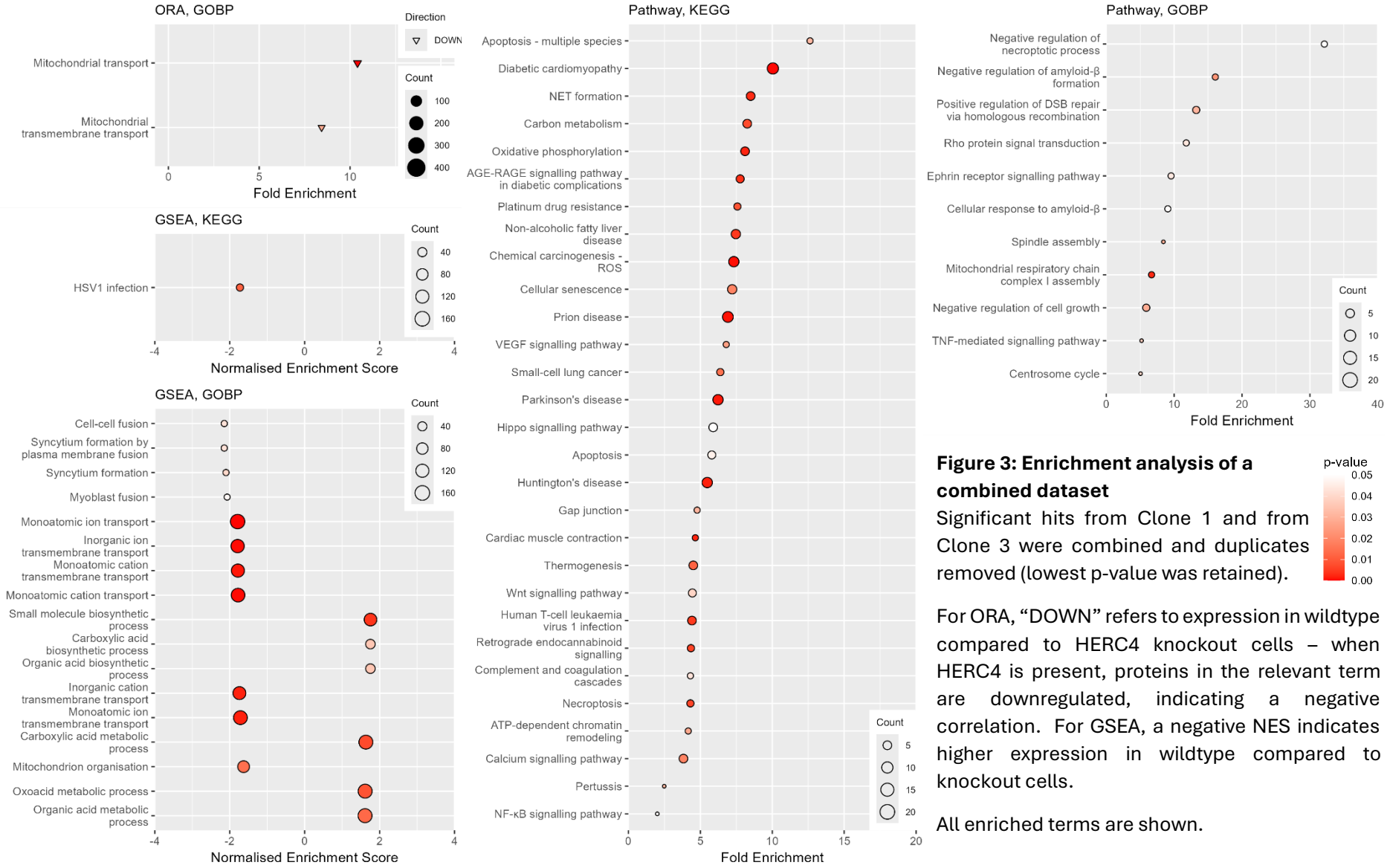


Figure 3: Enrichment analysis of a combined dataset

Significant hits from Clone 1 and from Clone 3 were combined and duplicates removed (lowest p-value was retained).

For ORA, "DOWN" refers to expression in wildtype compared to HERC4 knockout cells – when HERC4 is present, proteins in the relevant term are downregulated, indicating a negative correlation. For GSEA, a negative NES indicates higher expression in wildtype compared to knockout cells.

All enriched terms are shown.



Figure 4: Proteins contributing to enriched KEGG terms identified by pathway analysis of the combined total proteome dataset Genes contributing to each identified significant term were considered for their distribution between the two knockout clones and their direction of correlation with HERC4. Multiple terms related to the electron transport chain only had one gene from Clone 1, and this directly opposed the effect of genes identified from Clone 3, so these terms were discarded as inconsistent between the clones. Other terms, such as “Apoptosis” showed more consistency. ☆ Discarded terms

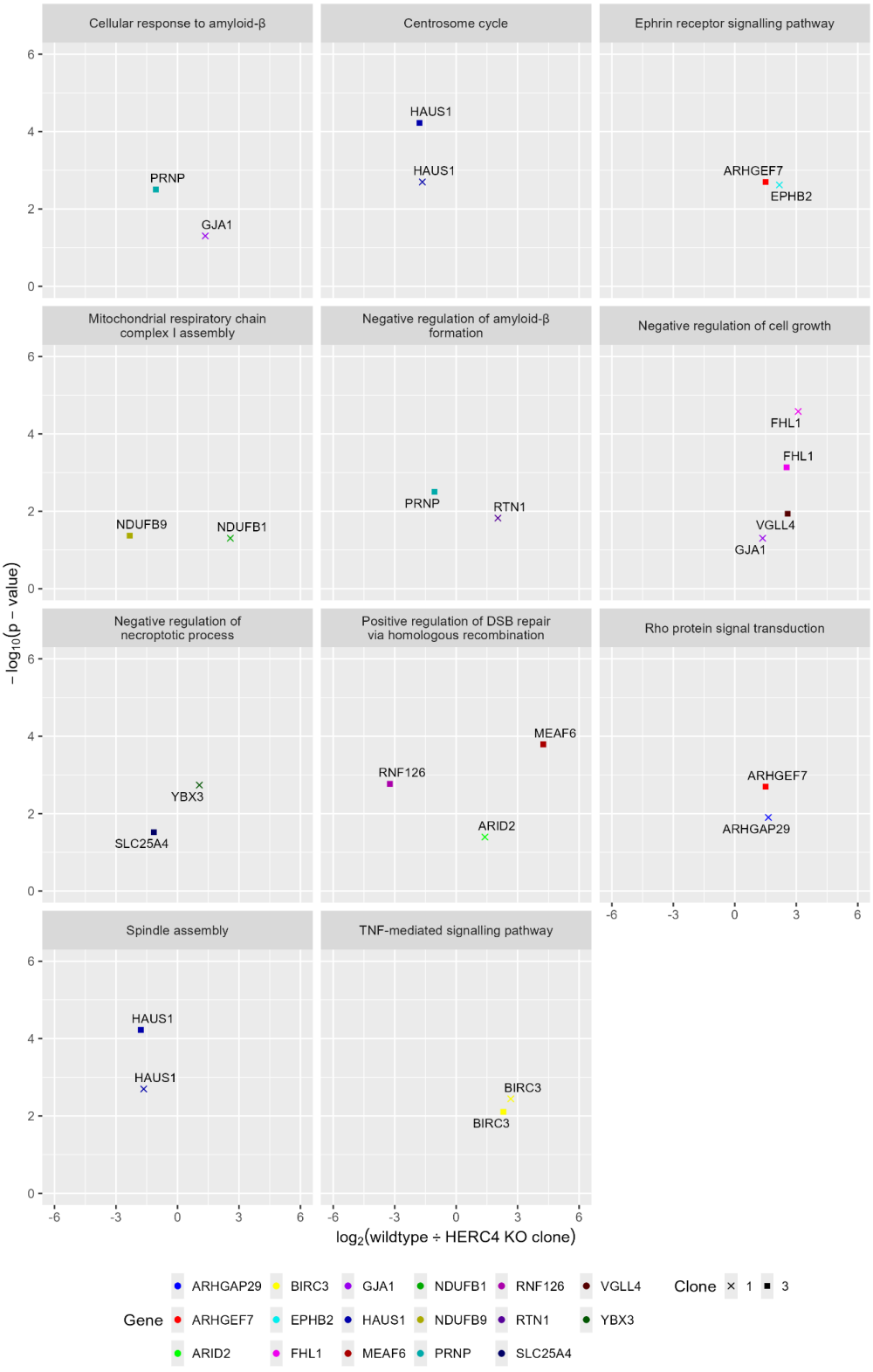


Figure 5: Proteins contributing to enriched GO-BP terms identified by pathway analysis of the combined total proteome dataset

Genes contributing to each identified significant term were considered for their distribution between the two knockout clones and their direction of correlation with HERC4.

3.3.1.3 - Differentially expressed proteins in Clone 3 show more similarity than those in Clone 1

To minimise the effect of the limitations of each analysis method, results from ORA, GSEA, pathway analysis (Figure 3) and STRING (Figure 6) were compared, on the basis that true positive findings would be identified by multiple methods. The only consistent theme across GO-BP terms was association with mitochondria, which was also highlighted in STRING analysis. However, as previously discussed for the top terms identified by pathway analysis, these terms are heavily biased towards Clone 3. Pathway terms relied on NDUFB1 from Clone 1, while the 1 and 2 terms identified by GSEA and ORA included only CLUH and MCUR1 from Clone 1 respectively. Notably, both CLUH and MCUR1 also show significantly different expression levels in Clone 3 compared to wildtype (CLUH was 11.6-fold and 9.51-fold higher than wildtype in Clone 1 and 3 respectively, and MCUR1 was 2.95- and 2.87-fold higher), and the identification of 3 separate proteins across the analysis types suggests there may be a connection that is too weak to be detected by these methods. STRING analysis also highlighted connection to the mitochondrial inner membrane as a unifying factor for many differentially expressed proteins, including 6 of the proteins identified in both clones and 18 from Clone 1. However, this is approximately half of the number from Clone 3 despite Clone 3 only having ~22% more significant hits overall, and STRING analysis on the clones separately only identifies this factor for Clone 3 (Appendix 5). It therefore seems that there is more similarity between proteins identified in Clone 3 than those identified in Clone 1, reinforced by the far fewer terms return by any analysis method for Clone 1 compared to Clone 3 (Figures 7 and 8).

Cluster	Gene count
Mitochondrion inner membrane	58
+ketosteroid monooxygenase activity	2
EFR3A, SEMA3E	2
DCUN1D5, FHL1	2
Deregulation of Rab and Rab effector genes in bladder cancer	2
RUNX3 regulates YAP1-mediated transcription	2

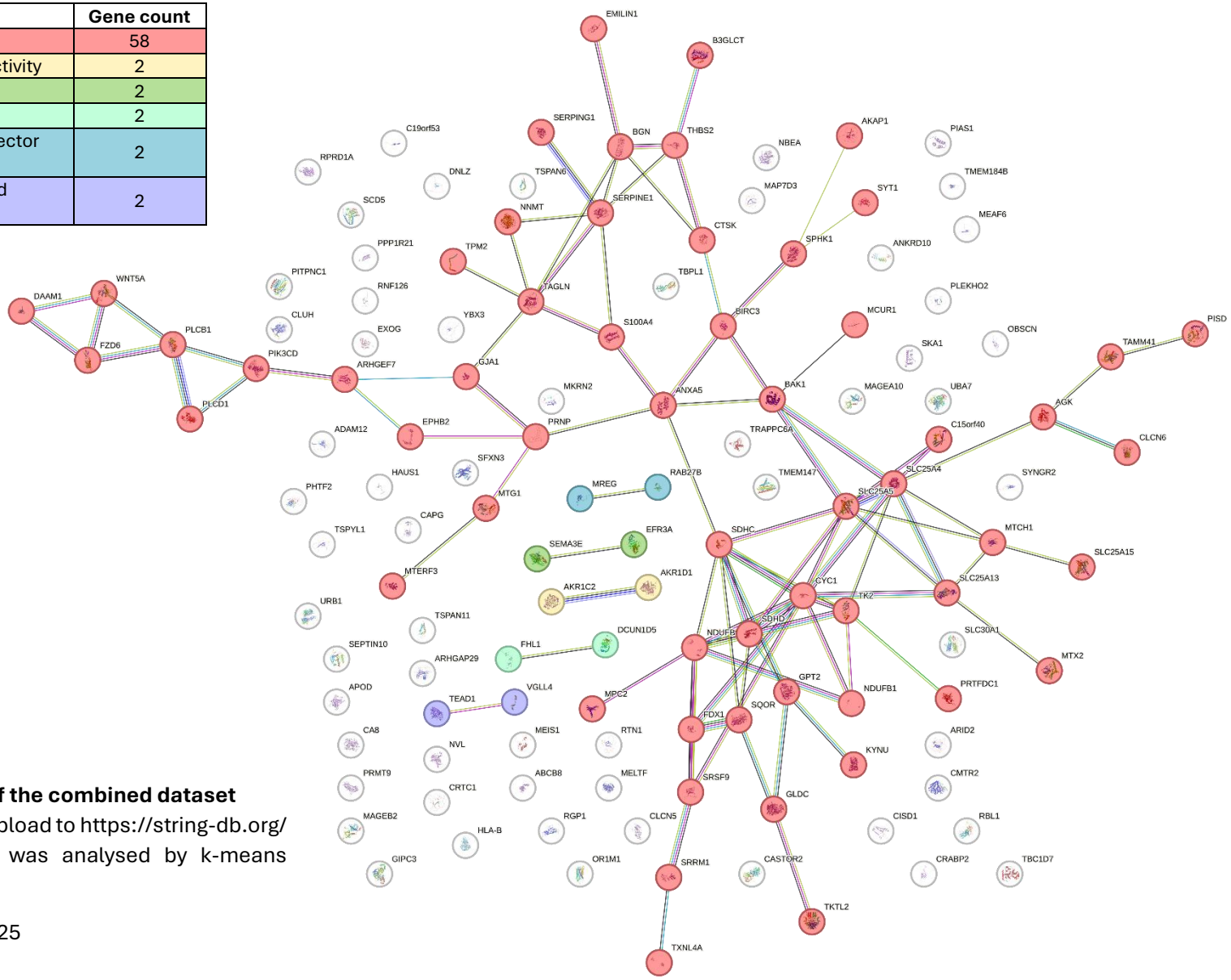


Figure 6: STRING analysis of the combined dataset
The combined dataset was upload to https://string-db.org/ and the resultant network was analysed by k-means clustering.

Network downloaded 28/11/25



Figure 7: Significantly enriched terms in Clone 1

Total proteome data was compared between wildtype and Clone 1 populations and ORA, GSEA and pathway analysis used to identify enriched KEGG and GO-BP terms. All significant terms are shown here – none were identified by ORA.

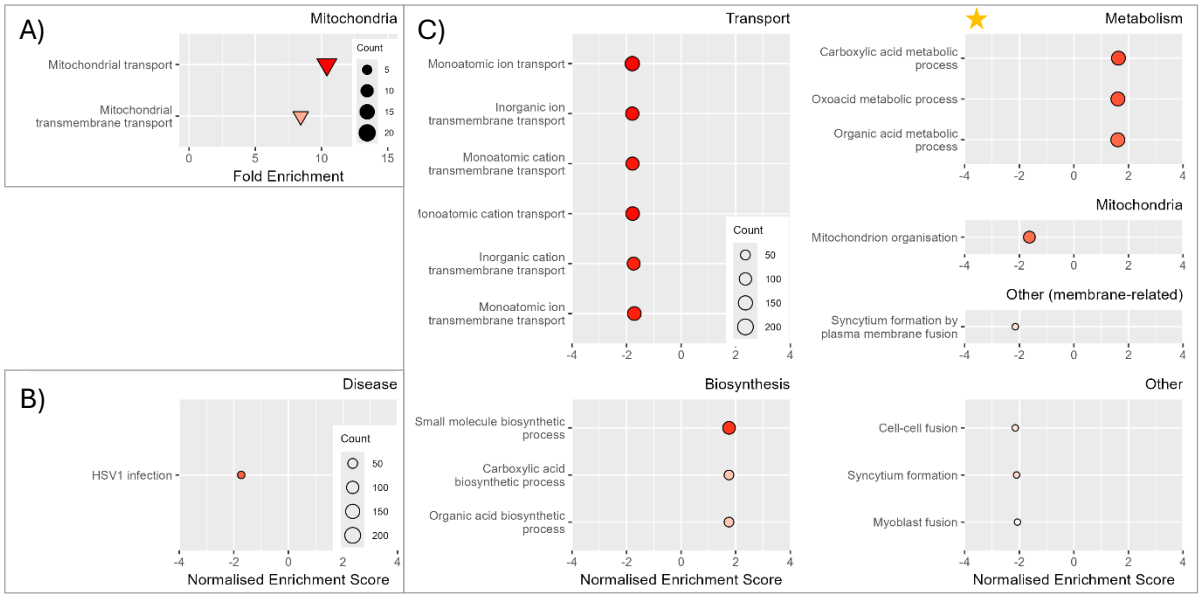


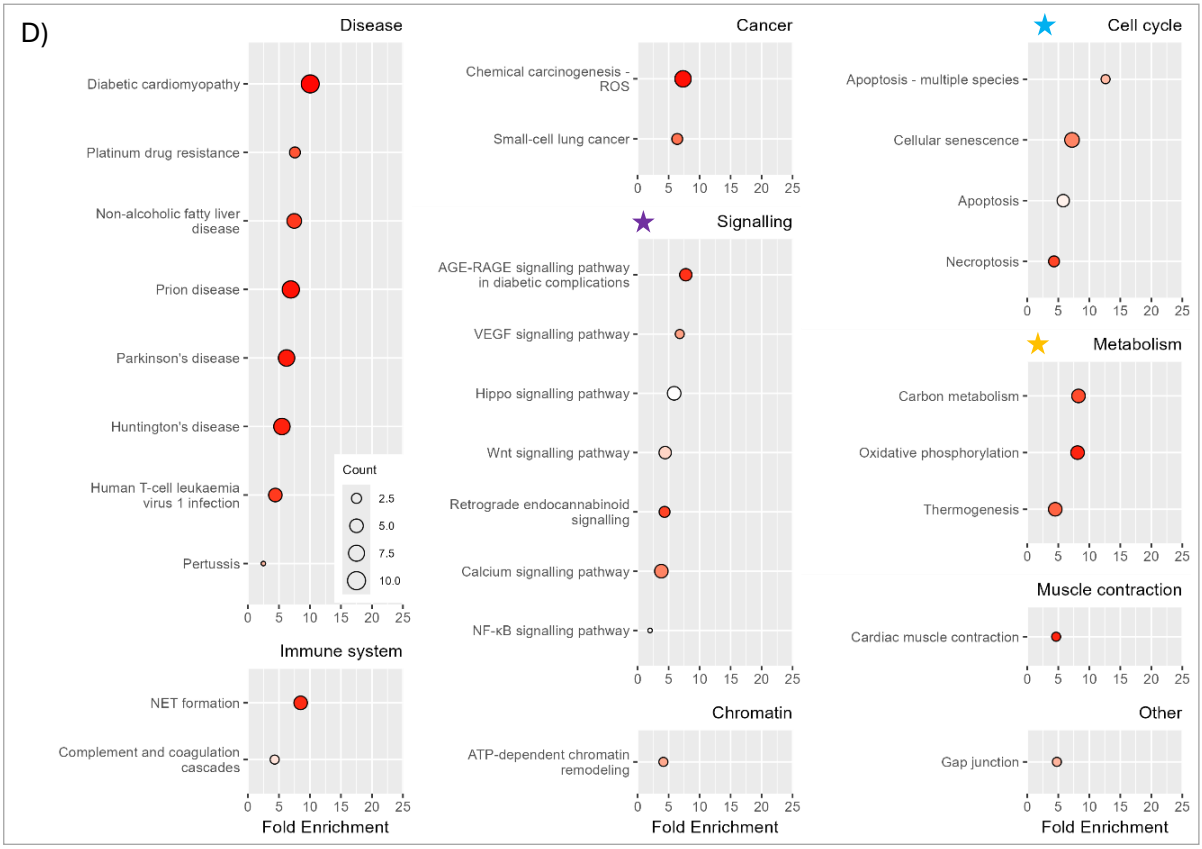
Figure 8: Significantly enriched terms in Clone 3

Total proteome data was compared between wildtype and Clone 1 populations and ORA, GSEA and pathway analysis used to identify enriched KEGG and GO-BP terms. Terms were ranked by their enrichment score, and the top 30 (or full dataset if fewer than 30 terms identified) are shown for each analysis.

3.3.1.4 - Terms in the combined dataset reinforce the putative role for HERC4 in cell proliferation and metabolism, and highlight several signalling pathways

Between the different analysis methods and databases, there was little consensus in terms with roughly comparable numbers of significant proteins from each clone. ORA analysis only returned terms from the GOBP database, both of which were discounted for having disproportionally few proteins from Clone 1 compared to Clone 3 (Figure 3). The single term identified from the KEGG database by GSEA was discounted for the same reason. Among the 3 remaining results sets (GSEA GOBP, and pathway KEGG and GOBP), there were 3 broad themes: metabolism, cell cycle and signalling (Figure 9).


A)
Mitochondria
Mitochondrial transport
Mitochondrial transmembrane transport
Count
5
10
15
20
0
5
10
15
Fold Enrichment
B)
Disease
HSV1 infection
Count
50
100
150
200
-4
-2
0
2
4
Normalised Enrichment Score
C)
Transport
Monoatomic ion transport
Inorganic ion transmembrane transport
Monoatomic cation transmembrane transport
Monoatomic cation transport
Inorganic cation transmembrane transport
Monoatomic ion transmembrane transport
Count
50
100
150
200
-4
-2
0
2
4
Biosynthesis
Small molecule biosynthetic process
Carboxylic acid biosynthetic process
Organic acid biosynthetic process
Normalised Enrichment Score
Metabolism
Carboxylic acid metabolic process
Oxoacid metabolic process
Organic acid metabolic process
Mitochondria
Mitochondrion organisation
Other (membrane-related)
Syncytium formation by plasma membrane fusion
Other
Cell-cell fusion
Syncytium formation
Myoblast fusion
Normalised Enrichment Score


D)
Disease
Diabetic cardiomyopathy
Platinum drug resistance
Non-alcoholic fatty liver disease
Prion disease
Parkinson's disease
Huntington's disease
Human T-cell leukaemia virus 1 infection
Pertussis
Count
2.5
5.0
7.5
10.0
0
5
10
15
20
25
Immune system
NET formation
Complement and coagulation cascades
Fold Enrichment
Cancer
Chemical carcinogenesis - ROS
Small-cell lung cancer
Signalling
AGE-RAGE signalling pathway in diabetic complications
VEGF signalling pathway
Hippo signalling pathway
Wnt signalling pathway
Retrograde endocannabinoid signalling
Calcium signalling pathway
NF-κB signalling pathway
Chromatin
ATP-dependent chromatin remodeling
Fold Enrichment
Cell cycle
Apoptosis - multiple species
Cellular senescence
Apoptosis
Necroptosis
Metabolism
Carbon metabolism
Oxidative phosphorylation
Thermogenesis
Muscle contraction
Cardiac muscle contraction
Other
Gap junction
Fold Enrichment

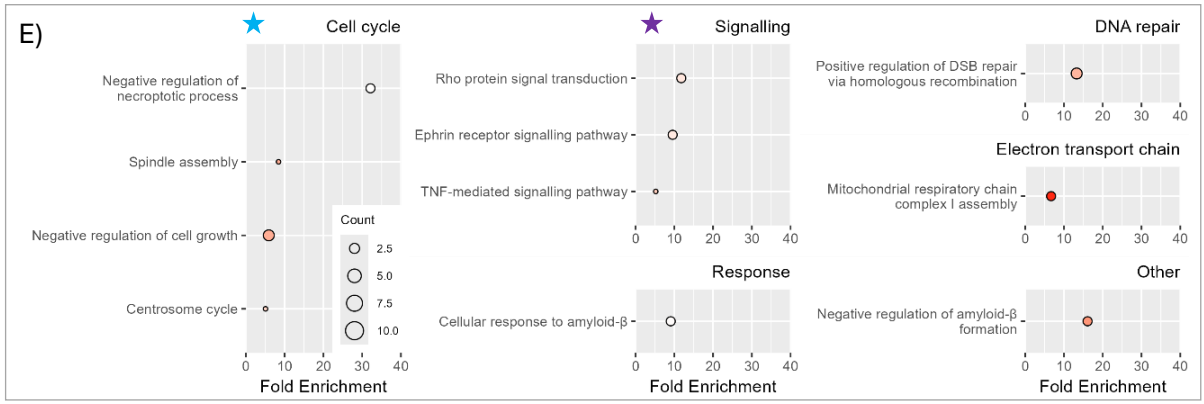

E)
Cell cycle
Negative regulation of necroptotic process
Spindle assembly
Negative regulation of cell growth
Centrosome cycle
Count
2.5
5.0
7.5
10.0
0
10
20
30
40
Fold Enrichment
Signalling
Rho protein signal transduction
Ephrin receptor signalling pathway
TNF-mediated signalling pathway
Response
Cellular response to amyloid-β
Fold Enrichment
DNA repair
Positive regulation of DSB repair via homologous recombination
Electron transport chain
Mitochondrial respiratory chain complex I assembly
Other
Negative regulation of amyloid-β formation
Fold Enrichment

Figure 9: Enrichment analysis of the combined dataset with terms grouped by theme
Significant hits from total proteomics data for each clone were combined and duplicates removed (lowest p-value was retained). ORA, GSEA or pathway analysis was used to identify significantly enriched terms, and these were manually split into themes. The terms in A and B were discarded as having disproportionately more proteins from Clone 3 than Clone 1. Of the remaining themes, only metabolism, cell cycle and signalling were identified in more than one analysis type, suggesting that these might have the strongest connection to HERC4 activity.

A) ORA, GO-BP; B) GSEA, KEGG; C) GSEA, GO-BP; D) Pathway, KEGG; E) Pathway, GO-BP

★ Metabolism ★ Cell cycle ★ Signalling

Metabolism

Metabolic terms were identified from the KEGG and GOBP databases by pathway analysis and GSEA respectively. Pathway analysis returned one relevant term – carbon metabolism – with multiple proteins from each clone (3 from Clone 1 and 2 from Clone 3), and it had the third highest enrichment score from this analysis (8.26). The 2 proteins from Clone 3, SDHC and D, plus GPT2 from Clone 1 have roles in the TCA cycle, while the other 2 proteins in Clone 1, GLDC and TKTL2, influence glycolysis. GPT2 and TKTL2 were more abundant in the wildtype cells, while the other 3 genes were more abundant in their respective knockout clones. GOBP terms identified by GSEA focused more specifically on carboxylic acid metabolism and the magnitude of their enrichment scores were among the lowest 4 identified by this analysis (1.61 or 1.63). The terms were centred around AKR1D1 and GPT2 from Clone 1, SCD5 from Clone 3, and CRABP2 and AKR1C2 that were significant in both clones, with all proteins showing positive correlation with HERC4 expression. This was the only set of terms across all analyses to contain more than one protein that was significant in both clones.

Cell cycle

Cell cycle terms were identified from both the KEGG and GOBP databases, but only by pathway analysis. From the KEGG database, apoptosis and cellular senescence were highlighted, each with proteins with positive and negative correlations with HERC4 expression. The terms had a fold enrichment of 5.79 and 7.21, placing them towards the lower end and middle of the group respectively. For apoptosis, anti-apoptotic BIRC3 was higher in wildtype cells, while pro-apoptotic CTSK and BAK1 were higher in the clones (approximately 2- and 4-fold higher in Clone 1 and 3 respectively), but PIK3CD was also more abundant after HERC4 loss (2.7-fold more abundant in Clone 3), despite its pro-survival effect. The combination of effect and correlation with HERC4 was far more mixed for cellular senescence proteins. Each clone contributed 1 protein that correlated positively with HERC4 and enhances senescence, Clone 3 had a further 2 such proteins repressing senescence, and Clone 1 had 2 proteins that negatively correlated

with HERC4 expression but 1 inhibits and the other promotes senescence. It therefore seems likely that the effect of changes in abundance of these proteins are not relevant to cellular senescence pathways, but that apoptotic mechanisms may be positively influenced by HERC4 loss.

A further repressive, broader term was identified from the GOBP database – negative regulation of cell growth – and for this, the combination of effect and HERC4 correlation was far simpler. All 3 genes (1 from each clone and 1 shared) were more abundant in wildtype than knockout cells, and all inhibit cell growth, although FHL1, the shared protein, also stimulates proliferation once phosphorylated. The other 2 cell cycle-related terms from the GOBP database (centrosome cycle and spindle assembly) rely solely on HAUS1, which was significantly more abundant in both clones compared to wildtype cells (~3.1- and 3.5-fold higher in each clone) and forms part of the augmin complex involved in mitotic spindle formation. Fold enrichment for spindle assembly was 8.42, placing close to the median of the results (5th out of 11; median of 9.06), but much lower than the top result of 32.13 (negative regulation of necroptotic process), and the other 2 cell cycle-related terms had the lowest fold enrichment of the set (5.89 and 5.05). However, the changes were statistically significant and together build a trend towards the changes in abundance of proteins associated with these 3 GOBP terms following HERC4 loss suggest a potential increase in proliferation in the knockouts, in potential conflict with those associated with apoptosis, which imply that HERC4 loss may increase cell death. On the other hand, elevation of both processes after HERC4 knockout would align the mass spectrometry data with the lack of significant difference in proliferation rate observed in Chapter 2.

Signalling pathways

There were no signalling pathways identified by GSEA, but 6 with roughly balanced genes from Clone 1 and 3 were highlighted from across the KEGG and GOBP databases by pathway analysis: Hippo, NF-κB, VEGF, Rho protein, Ephrin and TNF (fold enrichment of 5.89, 2.01, 6.80, 11.78, 9.55 and 5.20 respectively). Of these, only the Hippo signalling pathway had more than 2 proteins,

with 1 from Clone 1, 3 from Clone 3 and 1 from both, although its fold enrichment was in the middle of the group. Notably, 4 of these proteins cluster around the crossover with the Wnt pathway, which was also enriched but skewed towards Clone 3, but there was little consensus on how either pathway was influenced by loss of HERC4. WNT5A and TEAD1 abundance correlated negatively with that of HERC4, being 2.4- and 4.8-fold higher in Clone 3 than in wildtype cells, while SERPINE1, FZD6 and BIRC3 were less abundant in Clone 1 (3.5-fold), Clone 3 (2.3-fold) and both clones (6.4- and 4.9-fold) respectively, but all 5 proteins facilitate the signalling cascade or are upregulated by it. It is possible that increased levels of TEAD1 after HERC4 loss, perhaps driven by increased autocrine WNT5A signalling, would direct more of Hippo pathway protein YAP towards genes such as *BIRC3*, leaving less available for other binding partners that would direct it to genes such as *SERPINE1*. However, since BIRC3 and SERPINE1 were both less abundant after HERC4 loss, this model does not fully explain the dataset.

From the remaining 5 pathways, 2 (TNF and NF-κB) were enriched only by BIRC3 in both clones and the other 3 were identified through a different protein from each clone. For Rho protein signal transduction, these proteins were ARHGEF7 and ARHGAP29, and both were more abundant (2.8-fold and 3.1-fold) in wildtype cells than their respective clones. Since they have opposing effects on pathway activity, this suggests that the results are due to clonal differences rather than the loss of HERC4. ARHGEF7 was also highlighted as part of the Ephrin receptor signalling pathway for Clone 3, this time supported by EPHB2 from Clone 1, which, like ARHGEF7, facilitates signal transduction and was less abundant when HERC4 was absent. The other pathway with 2 proteins was VEGF signalling, with PIK3CD being 2.7-fold more abundant in Clone 3 and SPHK1 being 5.2-fold less abundant in Clone 1 than wildtype cells. This could be due to differing effects of HERC4 loss on different branches of the VEGF pathway, since PIK3CD transfers the signal to the PI3K-AKT pathway, regulating cell permeability, migration and survival while SPHK1 involves the MAPK pathway to regulate proliferation. Alternatively, these changes may also be reflective of clonal effect.

3.3.1.5 - Analysis of each clone in isolation highlighted terms connected to previously published roles for HERC4

Since no striking patterns were observed in the combined dataset, the clones were considered individually. GO terms, like proteins, are more convincing if identified in both clones, but it is possible that the effect of HERC4 knockout is masked in one or both clones by clonal differences from the wildtype population. Each clone was therefore analysed in isolation (Figures 7, 8,) and the results compared to both the literature and the lack of phenotype identified in Chapter 2 in case these sources could loosely replace the other clone in providing supporting evidence.

It should be noted that neither clone was particularly suitable for ORA since the only group with more than 50 proteins was those with a negative correlation with HERC4 expression in Clone 3. ORA is not powerful enough for smaller groups, so it was unsurprising that Clone 1 returned no enriched terms and Clone 3 produced substantially fewer than by either GSEA or pathway analysis (2 KEGG and 9 GO-BP terms compared to 41 and 106, and 103 and 32 for GSEA and pathway analysis respectively). The terms that were identified should be interpreted cautiously.

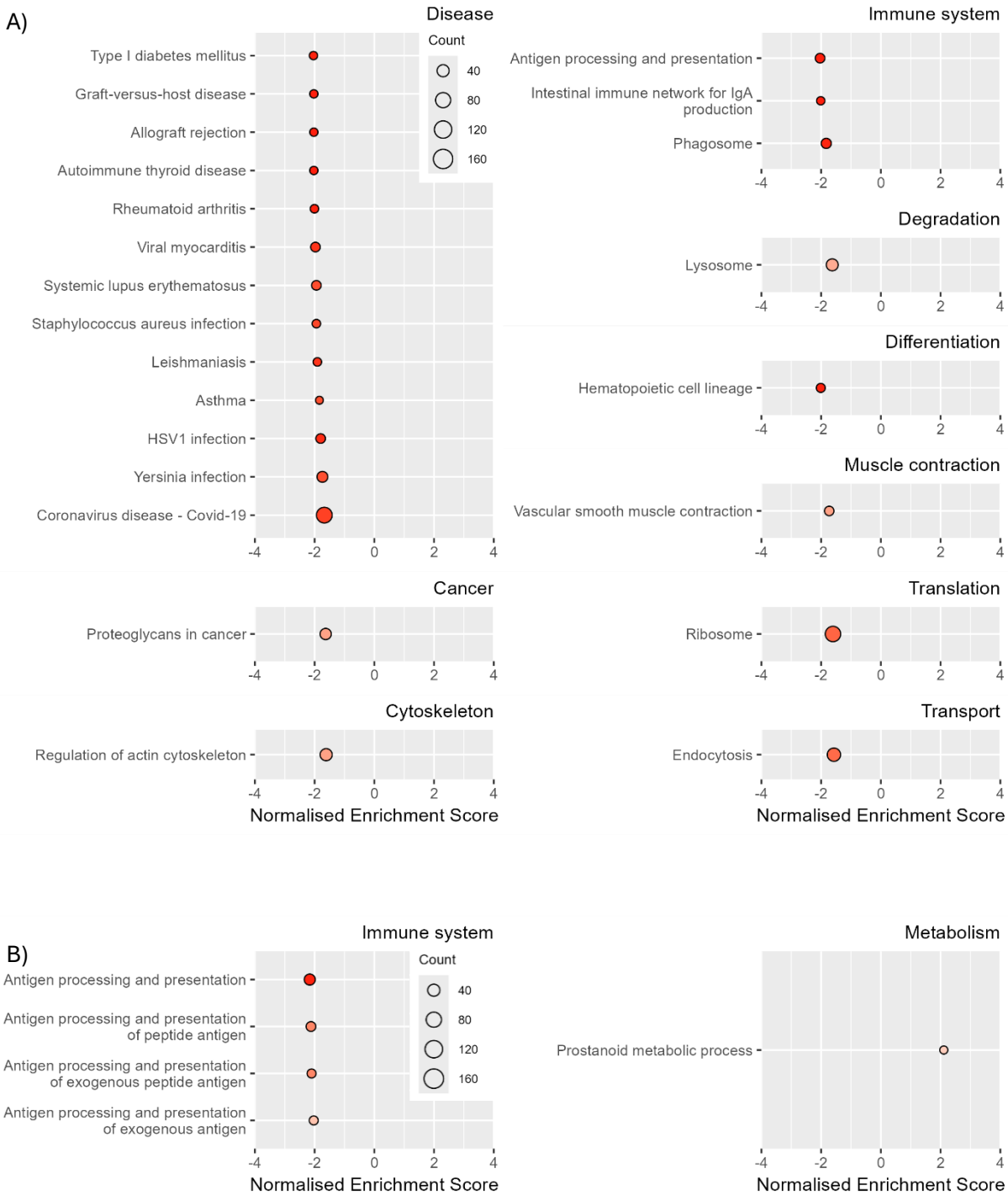


Figure 10: GSEA results for Clone 1, grouped by theme

GSEA analysis was used to identify significantly enriched terms for Clone 1 compared to wildtype cells, then these were manually split into themes.

A) KEGG terms; B) GO-BP terms

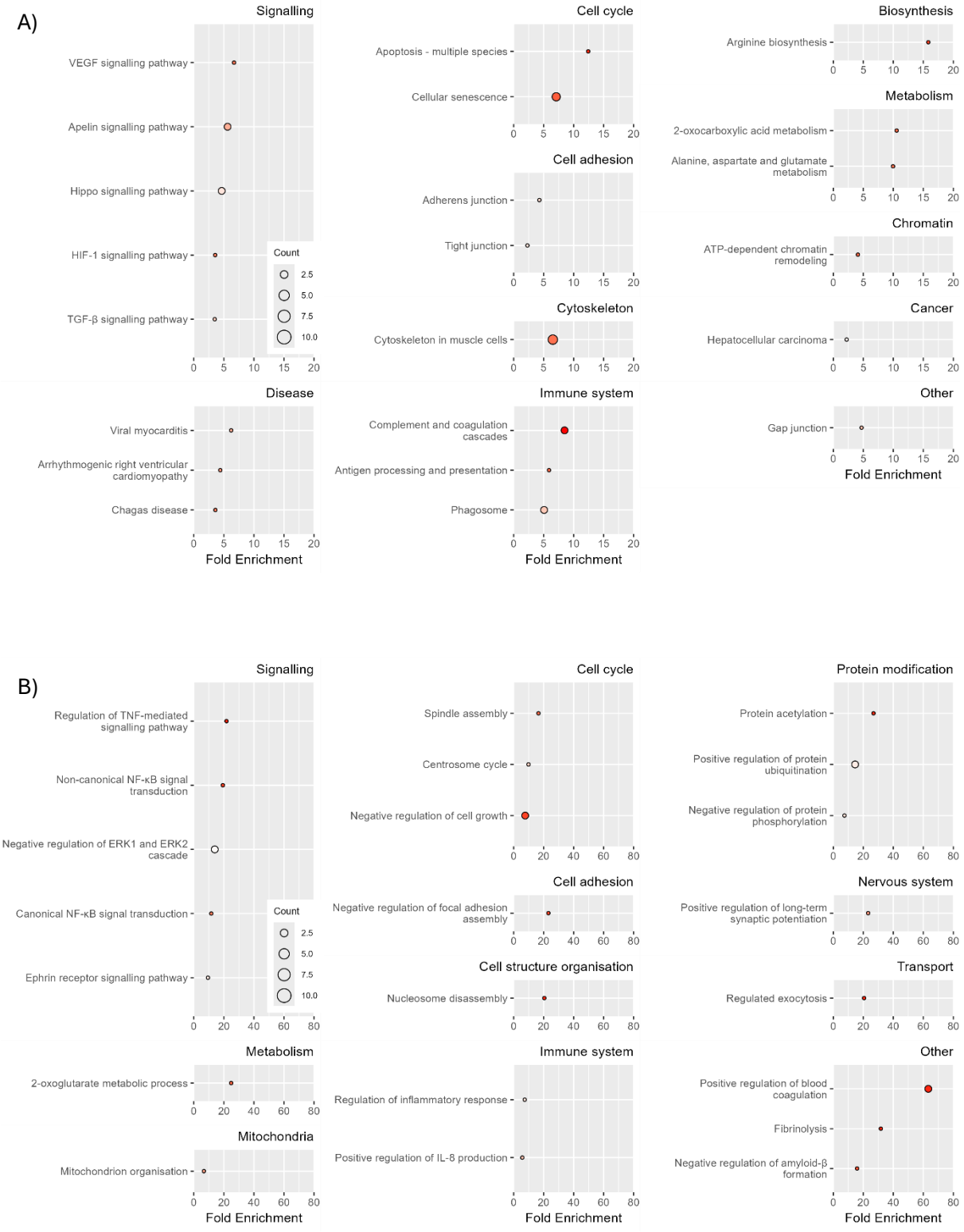


Figure 11: Pathway analysis results for Clone 1, grouped by theme

Pathway analysis was used to identify significantly enriched terms for Clone 1 compared to wildtype cells, then these were manually split into themes.

A) KEGG terms; B) GO-BP terms

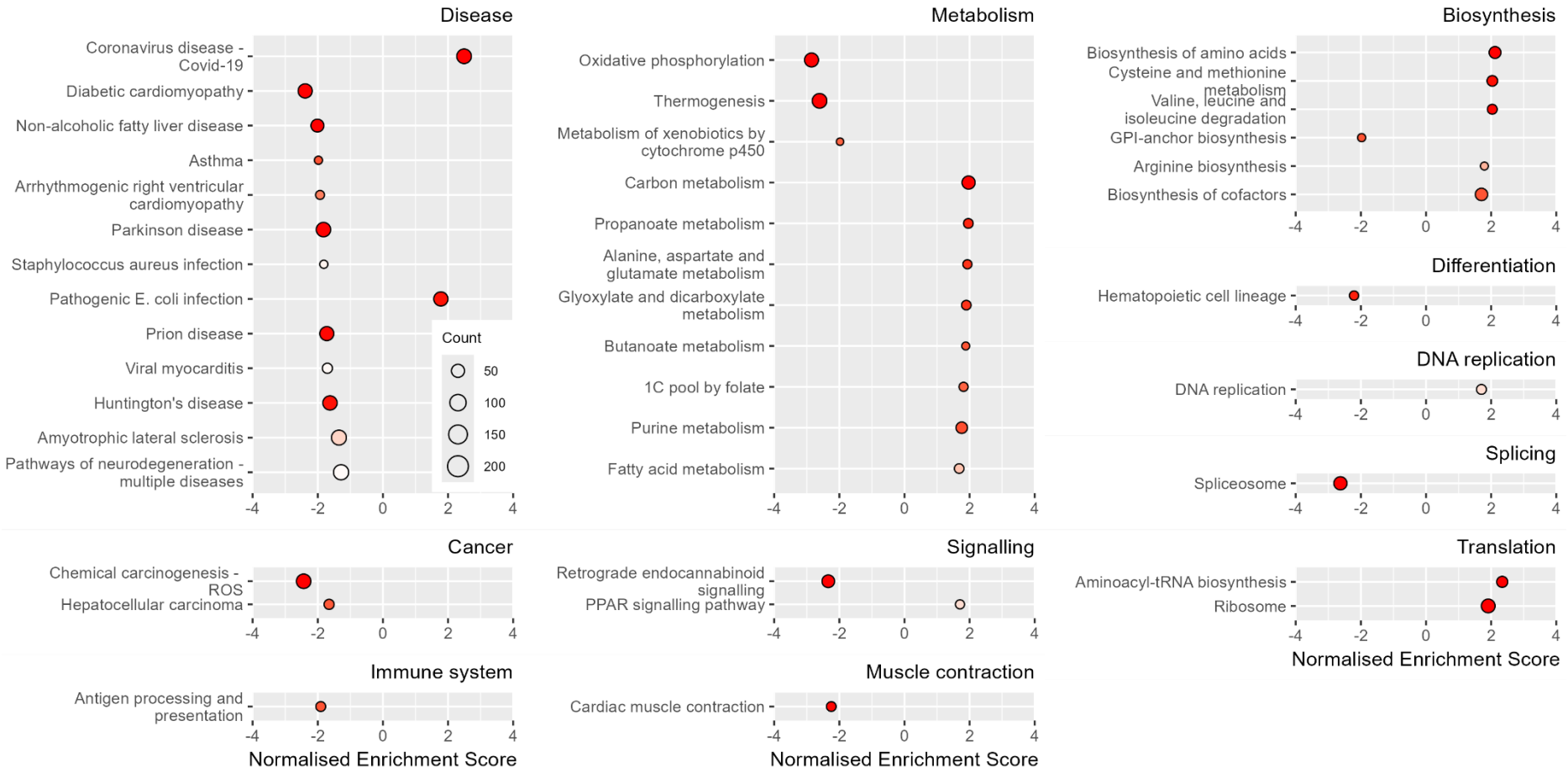


Figure 12: KEGG terms identified for Clone 3 by GSEA, grouped by theme

GSEA was used to identify significantly enriched terms for Clone 3 compared to wildtype cells, based on the KEGG database, then these terms were manually split into themes.

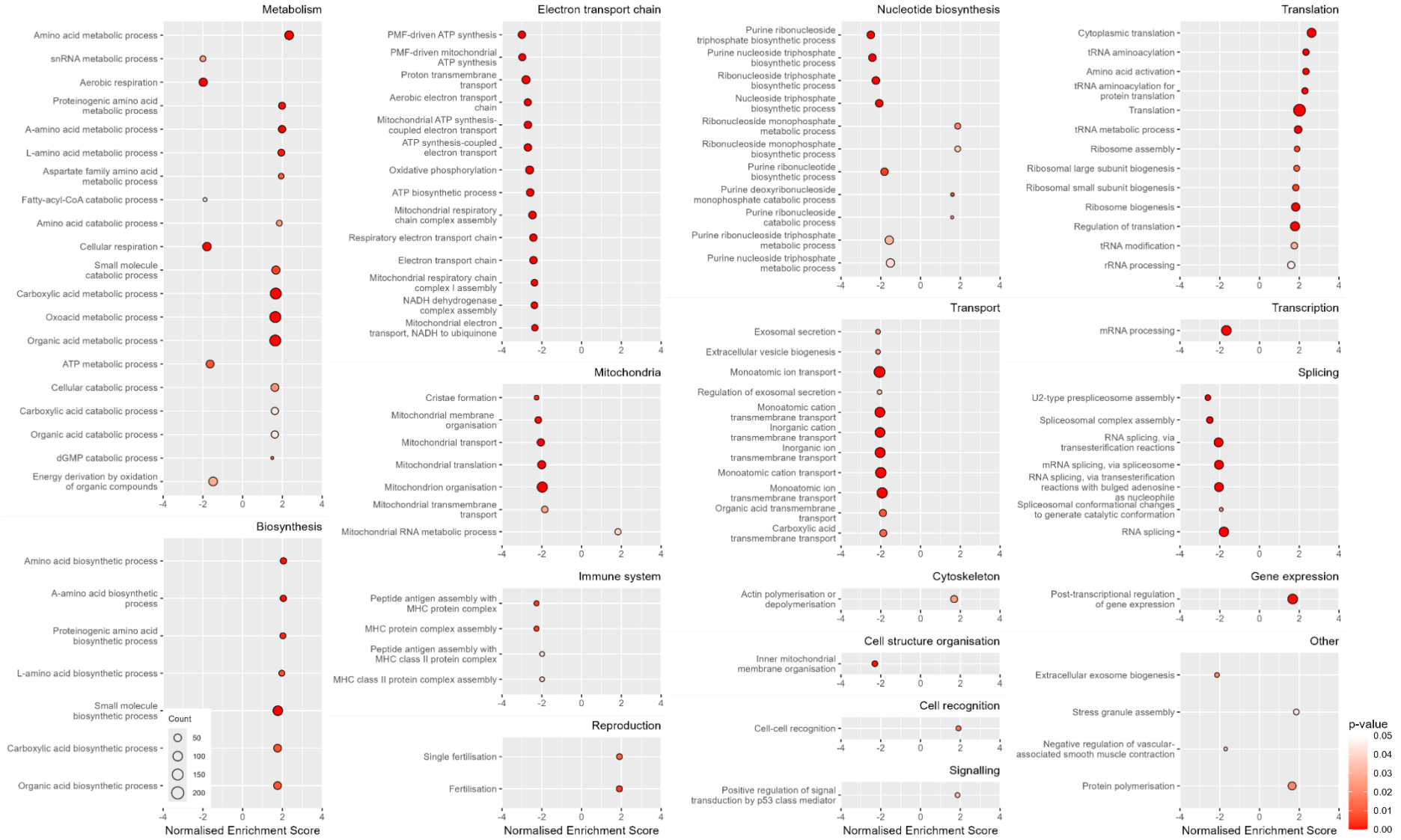


Figure 13: GO-BP terms identified for Clone 3 by GSEA, grouped by theme

GSEA was used to identify significantly enriched GO-BP terms for Clone 3 compared to wildtype cells, then these terms were manually split into themes.

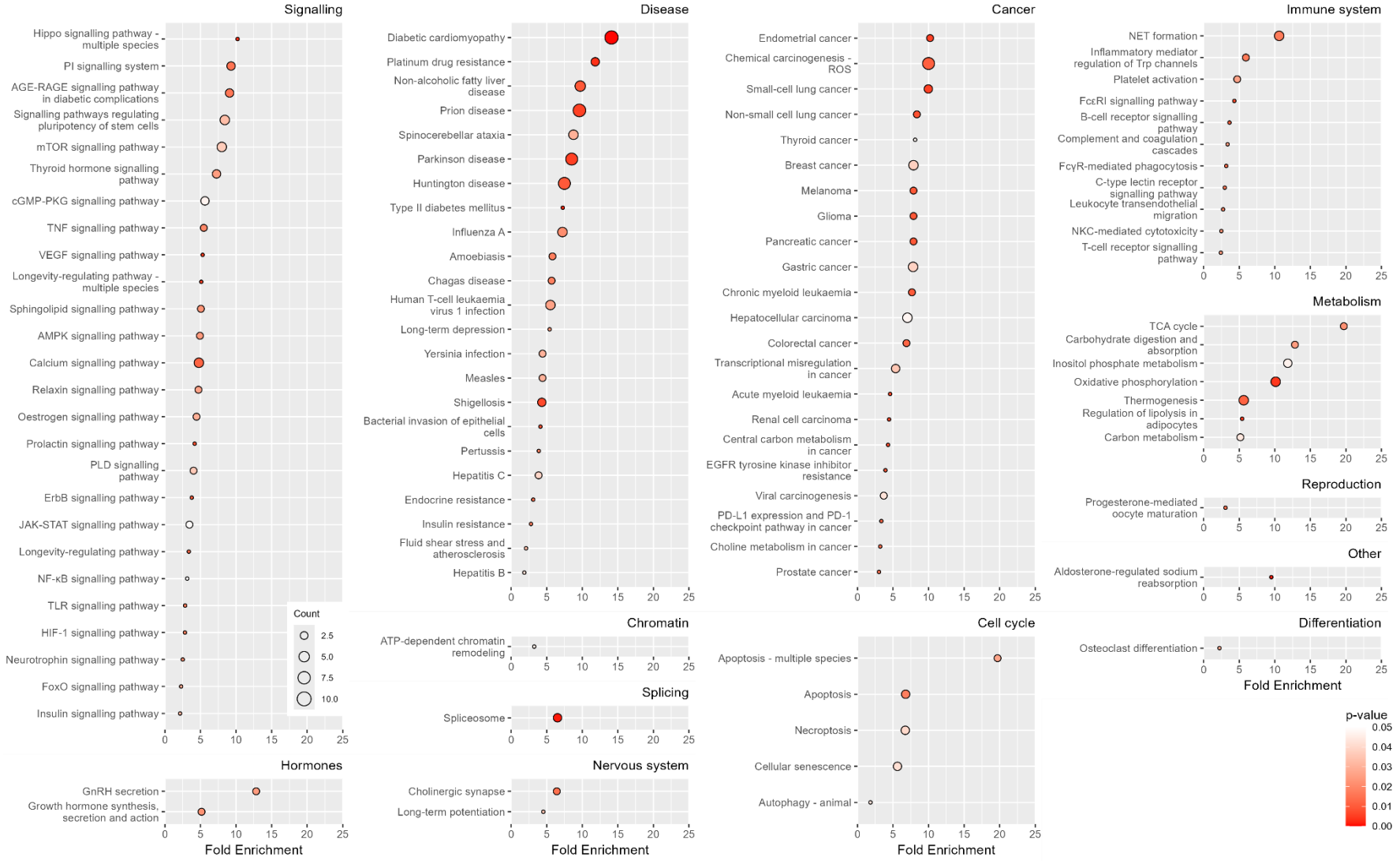


Figure 14: KEGG terms identified for Clone 3 by pathway analysis, grouped by theme

Pathway analysis was used to identify significantly enriched KEGG terms for Clone 3 compared to wildtype cells, then these terms were manually split into themes.

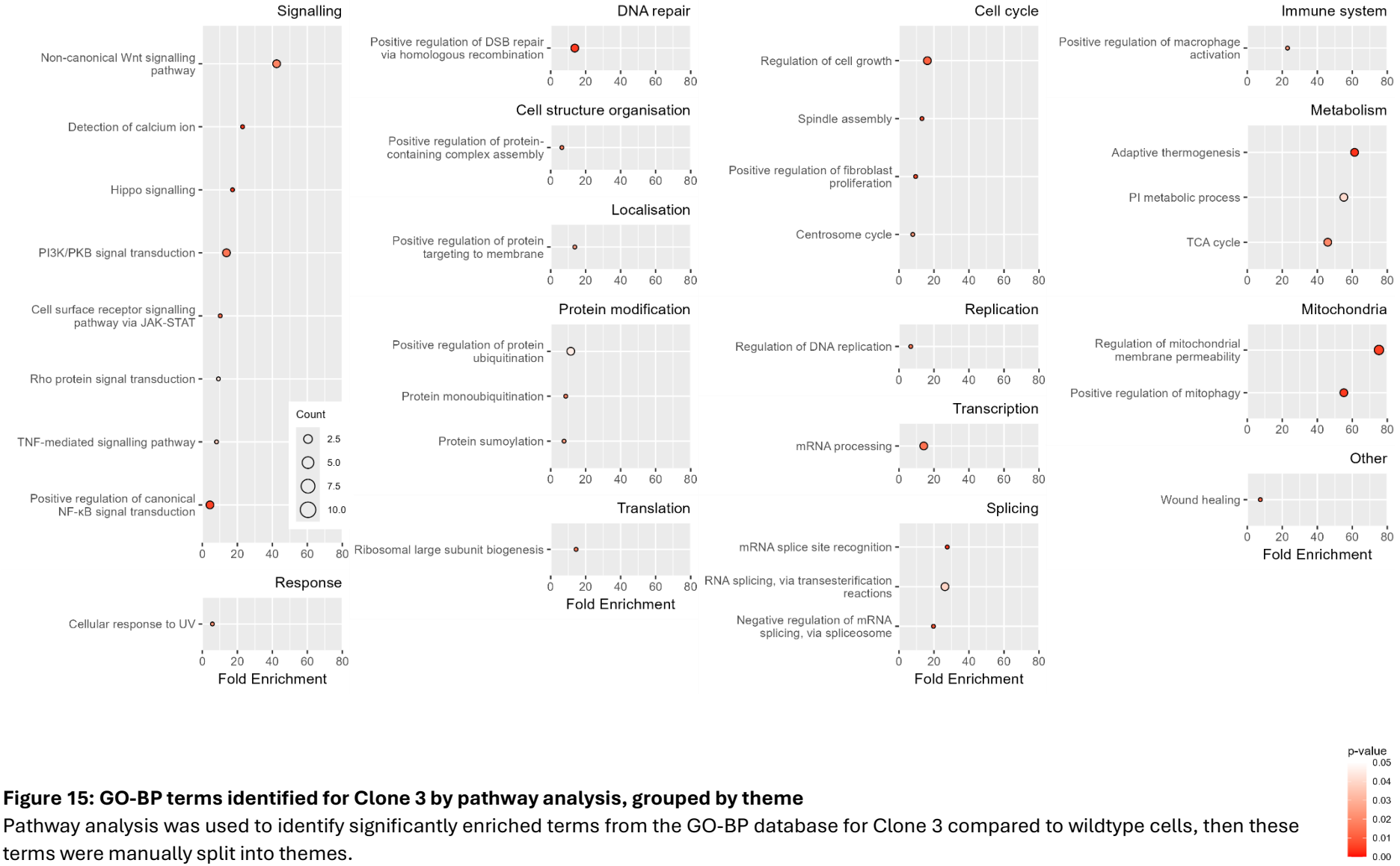


Figure 15: GO-BP terms identified for Clone 3 by pathway analysis, grouped by theme

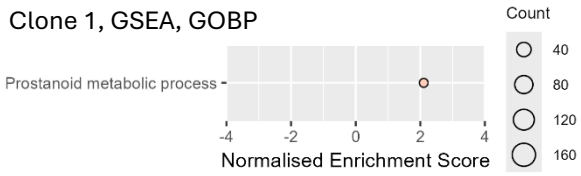
Pathway analysis was used to identify significantly enriched terms from the GO-BP database for Clone 3 compared to wildtype cells, then these terms were manually split into themes.

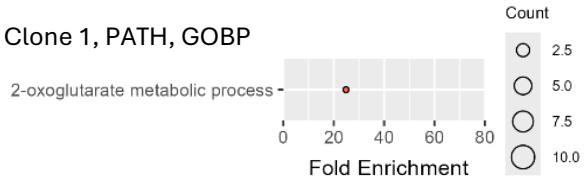
Metabolism

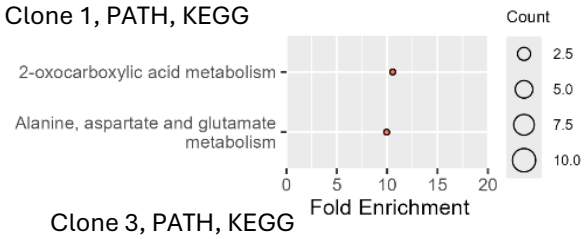
Despite resazurin assay data showing no significant change in aerobic respiration in Clone 3 compared to wildtype, many proteins linked to oxidative phosphorylation showed negative correlation with HERC4 loss, with increased abundance in the clone. Additionally, amino and carboxylic acid metabolism is higher in the wildtype cells than in Clone 3 (GSEA NES of 1.93 for alanine, aspartate and glutamate metabolism and 1.68 for fatty acid metabolism (KEGG terms), and ~2 or 1.8 for amino acid- or carboxylic acid-related GOBP terms), which could reflect a shift in dominant metabolic substrates.

Clone 1 has substantially fewer metabolic terms (Figure 16), and 3 out of the 4 terms were identified by pathway analysis because of 1 protein (GPT2), compared to predominantly GSEA and multiple proteins in Clone 3. The terms focused on amino acid metabolism, like some of those identified in Clone 3, and one term (alanine, aspartate and glutamate metabolism) appeared in both clones (pathway analysis fold enrichment of ~10 for Clone 1 and GSEA NES of ~2 in Clone 3). Although it is very weak evidence for a shared phenotype, it does undermine the hypothesis that the change in metabolic substrate possibly observed in Clone 3 is only due to clonal effect, supporting the conclusions drawn from the combined dataset.

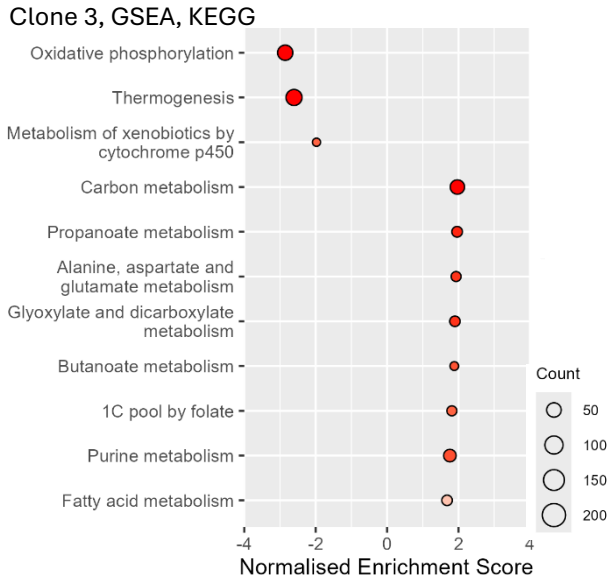
A)

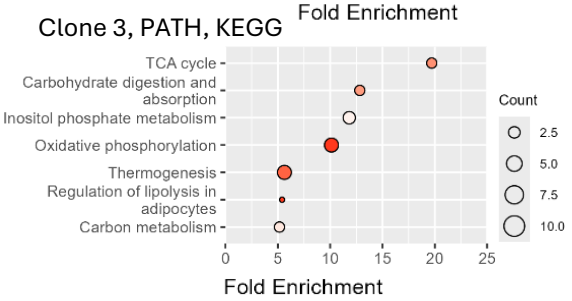


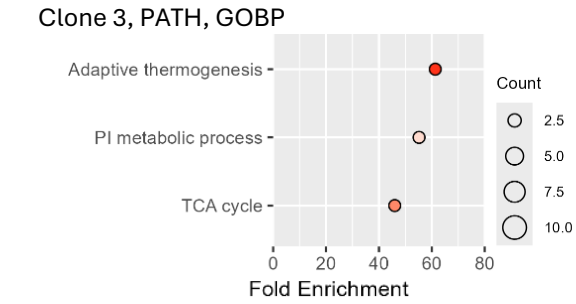




B)







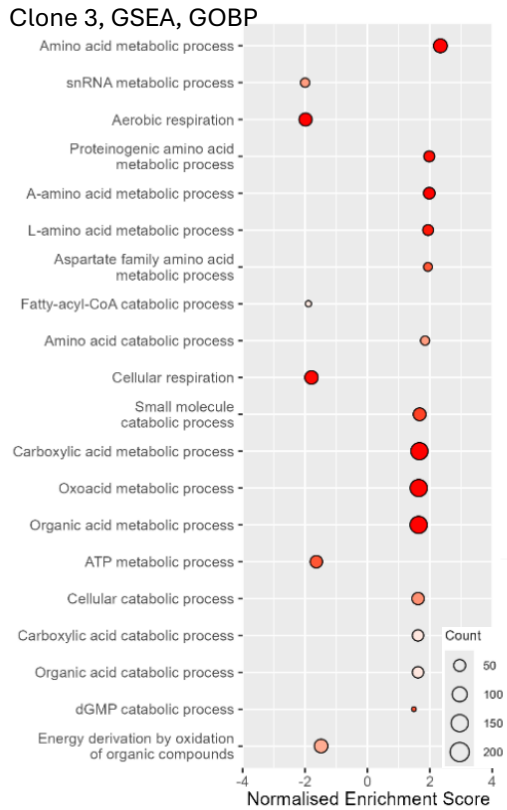
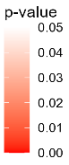


Figure 16: Metabolism-associated terms identified for each clone

Terms from each analysis related to metabolic activity (except the electron transport chain, since this was already identified as Clone 3-specific) were compared to identify common sub-themes between the clones.



Immune system

While data from Clone 3 produced many enriched metabolic terms, the dominant theme for Clone 1 terms was the immune system (Figure 17), a difference also reflected in the disease types identified from the KEGG database. For Clone 3, many of the proteins associated with the disease terms also appeared in the aerobic respiration terms, whereas for Clone 1, terms consist almost entirely of autoimmune diseases and bacterial or viral infections. The most frequently identified immune-related term is antigen presentation, which appeared in both GSEA and pathway analysis and from both KEGG and GOBP databases (Clone 1 GSEA NES ≈ -2 for KEGG and GOBP, and pathway analysis fold enrichment ≈ 6; Clone 3 GSEA NES ≈ -2 for KEGG). Similar terms were also identified for Clone 3, although these focused more specifically on MHC function (GSEA GOBP terms with NES of ~-2 or lower). In both clones, relevant proteins were more abundant in the knockout cells compared to wildtype ones. Despite the common theme across both clones, the only immune-related term to be identified in the combined dataset was Complement and coagulation cascades (~8- and 7-fold enrichment for clones 1 and 3 respectively, and ~4-fold in the combined analysis. All values produced by pathway analysis using KEGG terms.).

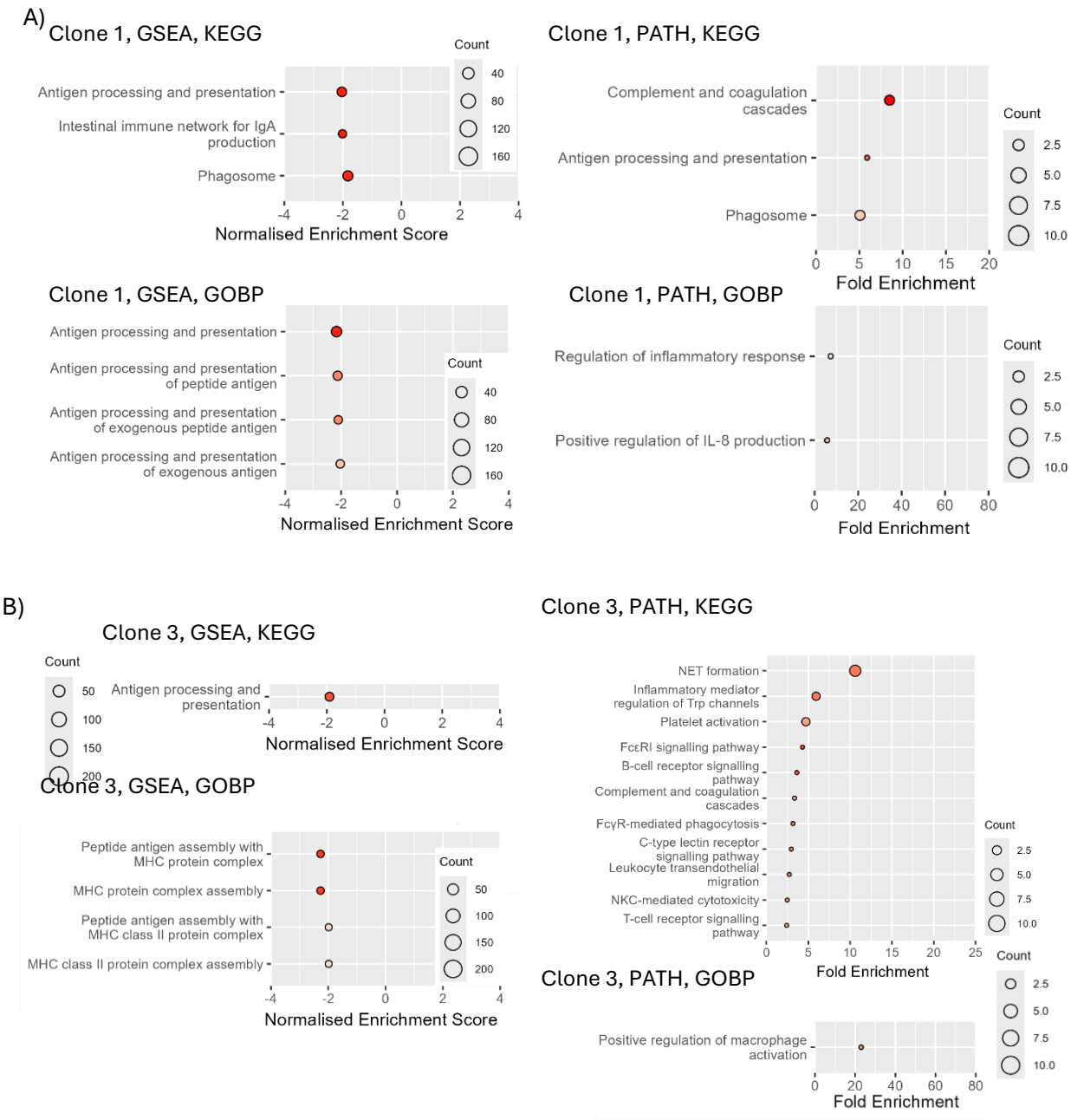


Figure 17: Immune system-associated terms identified for each clone
Terms from each analysis related to the immune system were compared to identify common sub-themes between the clones.

Other

The other theme shared between both clones was that of the cell cycle and proliferation, in support of the similar terms identified from the combined dataset (pathway analysis, fold enrichment mostly between 5 and 20). There were no other notable terms identified in Clone 1, but in Clone 3, fertilisation-linked proteins showed positive correlation with HERC4 expression (NES ~2), in line with the published role of HERC4 in sperm motility, although the only cell-specific term focused on oocyte maturation, not spermatozoa. Clone 3 also showed significant changes in abundance of 3 proteins involved in signalling cascades triggered by AGE (fold enrichment ~9; p-value 0.016), a class of protein and lipid products previously implicated in HERC4 expression, although it is unclear if it up- or downregulates HERC4 [Xie et al., 2024; Senavirathna et al., 2024]. 1 significant protein from Clone 1 was also annotated for this pathway, leading to its inclusion the enriched terms for the combined dataset, but it was insufficient for the term to be highlighted for Clone 1 in isolation.

3.3.2 - Proximity Labelling

Total proteome results tentatively indicate roles for HERC4 in metabolism, proliferation and the immune system, but fail to demonstrate any clear changes in protein expression following HERC4 loss. To explore HERC4 activity more directly, biotin-based proximity labelling was used to identify putative HERC4 interactors and substrates that are degraded after ubiquitylation. Control samples with no exogenous biotin were used to identify proteins binding non-specifically to streptavidin beads (those with higher abundance in the control than biotin-treated samples), and MG132 was used as a proteasome inhibitor to highlight potential substrates. Since HERC4 was overexpressed, it was assumed that the majority of proteins targeted to the proteasome would be HERC4 substrates. This approach does not, therefore, identify substrates whose ubiquitylation has implications other than proteasomal degradation, which will be indistinguishable from other interactors. In total, 1701 interactors and 515 substrates were identified, with an overlap of 416 proteins (Figure 18).

The same analysis protocols were used as for the total proteome data and the identified enriched terms were once again clustered into categories. Protein expression, processing and degradation were the most common categories and between them, they were identified by all analysis methods in both GO-BP and KEGG databases, for both interactors and substrates (12/12). The next most frequently highlighted cluster was localisation and transport, at least one of which was identified in all conditions except substrate analysis by ORA or GSEA using the KEGG database (10/12). Metabolism-associated terms were identified in 8/12 conditions, and the immune system, mitochondria and reproduction featured in 6/12. Telomeres were highlighted in 5/6 GO-BP analyses, and cell cycle, DNA repair and signalling terms were given additional consideration despite being largely confined to pathway analysis (4, 4 and 5/12 respectively) due to their connection to previous datasets and hypotheses.

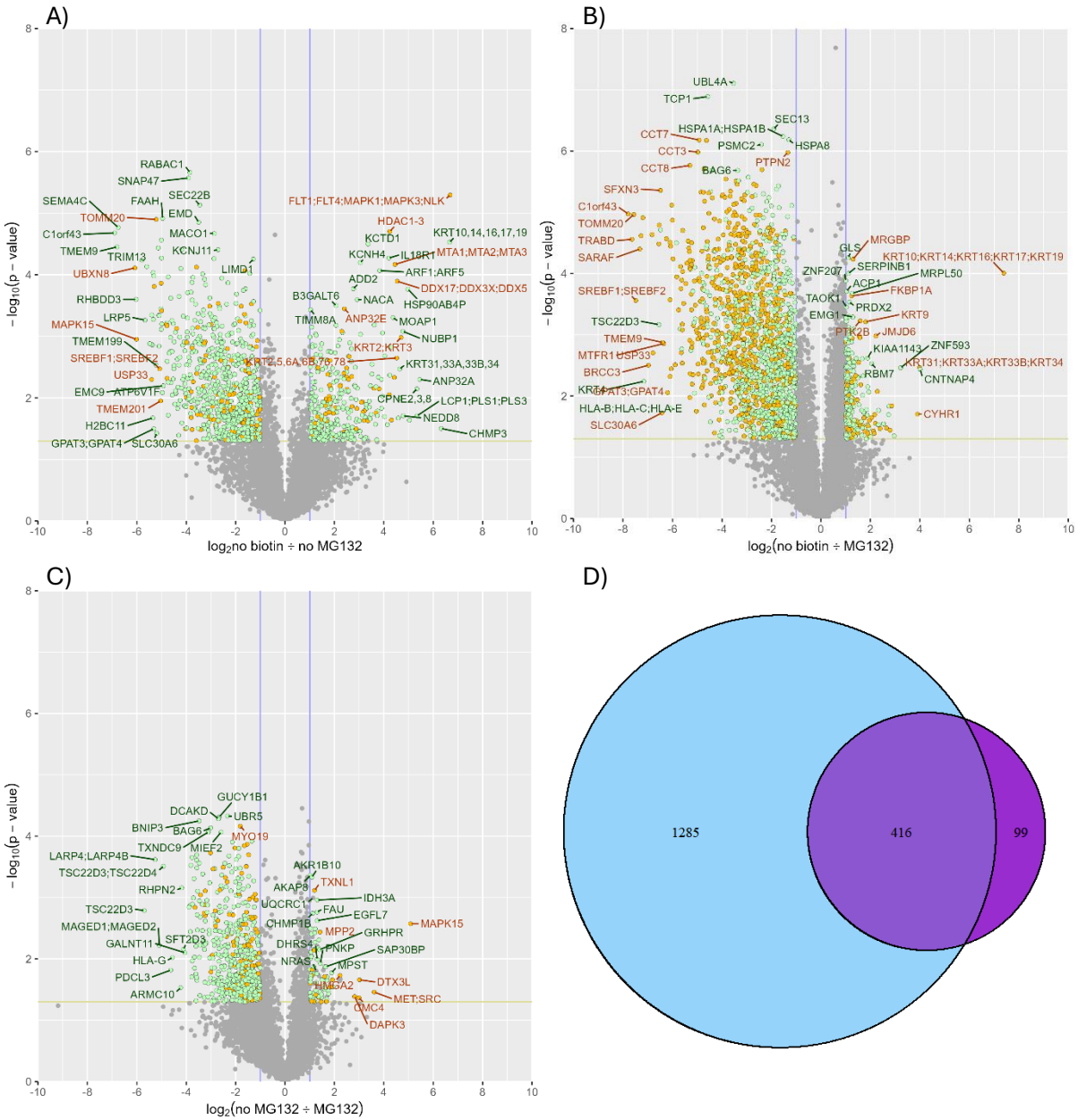


Figure 18: Proteins in close proximity to HERC4

HERC4 was tagged with TurboID to label nearby proteins with biotin. Biotinylated proteins were pulled down and identified by mass spectrometry.

A) Differential expression between samples treated with neither biotin nor MG132, and those treated with biotin only

B) Differential expression between samples treated with neither biotin nor MG132, and those treated with biotin and MG132

C) Differential expression between samples treated with biotin only, and those treated with biotin and MG132

D) Overlap of identified interactors (significantly more abundant in biotin-treated samples than in those without) and substrates (significantly more abundant in MG132-treated samples than MG132-untreated controls, and not significantly more abundant in samples without biotin than those with it).

Significant in graphed comparison

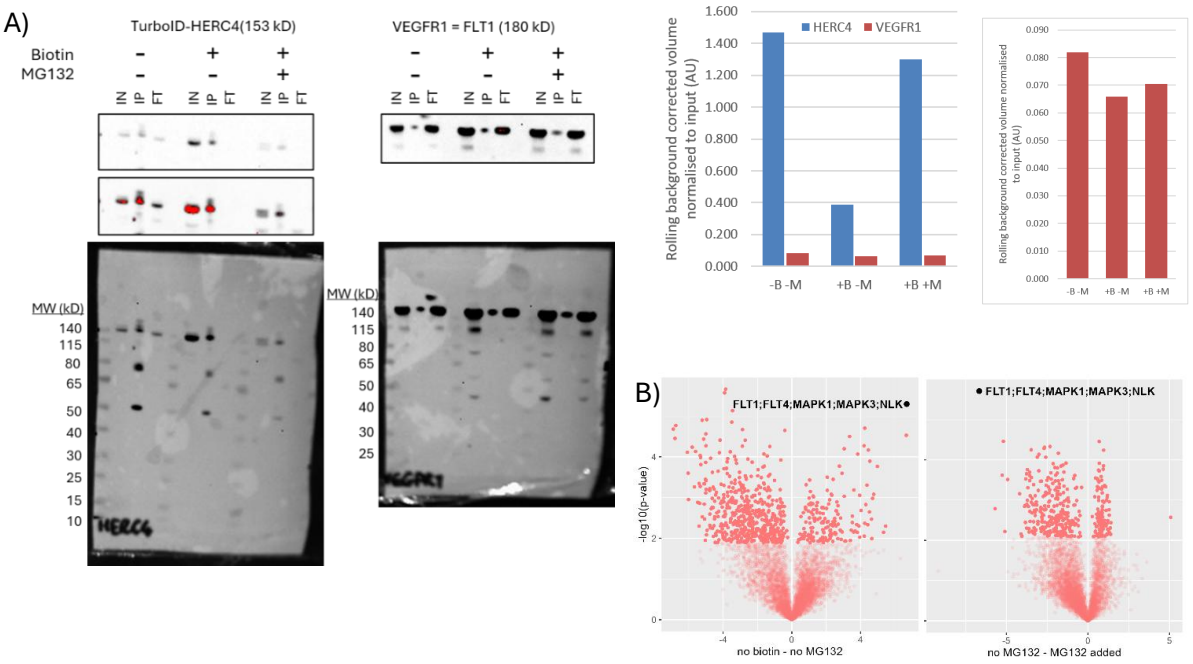
Significant in graphed comparison and -/+MG132 (A) or -/+biotin (B, C)

Interactors Substrates

3.3.2.1 – Validation

Validation by IP and western blot was limited by availability of suitable antibodies, and further optimisation is needed to determine appropriate loading concentrations, but preliminary results were encouraging. VEGFR (FLT1) was initially highlighted as the strongest candidate for a HERC4 substrate, since it was the hit with the biggest and most statistically significant fold change when MG132 was added (Figure 19a; ~100-fold change, p-value = $2x10^{-6}$). However, it was also more abundant in the no-biotin control than the biotin-treated, MG132-untreated condition (~100-fold change), suggesting that its interaction with the beads was not dependent on specific biotin-streptavidin binding. This was reinforced by its detection in IP eluate for all 3 conditions in the validation process, although it was not found in the biotin-treated, MG132-untreated mass spectrometry samples. Clearer normalisation of HERC4 levels between samples, and the addition of a control without TurboID-labelled HERC4 would provide stronger confirmation.

2 further proteins were successfully tested – USP11 and SAV1 (Figure 18C). USP11 was pulled down from the MG132-treated condition only, consistent with its classification as a substrate in the mass spectrometry results (2.7- and 2.8-fold higher in MG132-treated samples compared to no-biotin and no-MG132 samples respectively). SAV1 was just detectable in the same samples, which could explain the almost significant results in the mass spectrometry data (~6-fold higher in biotin-treated samples compared with untreated) and align with its annotation in the literature as a HERC4 substrate. However, the absence of a visible signal in the biotin-treated, MG132-untreated eluates prevents full consistency between the experiments since mass spectrometry found it to be similarly abundant in both conditions, and repeats with a more sensitive antibody are needed to make the data convincing. Additionally, quantification of input and IP signal shows a greater signal for the biotin-treated, MG132-untreated IP eluate relative to the input, compared to the same normalised value for the MG132-treated eluate, suggesting that some of the disparity may be due to differences in loading quantity, or high background imitating signal in the MG132-treated eluate (Figure 19C).


A)
TurboID-HERC4(153 kD)
VEGFR1 = FLT1 (180 kD)
Biotin
MG132
IN IP FT IN IP FT IN IP FT
MW (kD)
140
115
80
65
50
40
30
25
15
10
HERC4
Rolling background corrected volume normalised to input (AU)
HERC4 VEGFR1
-B -M
+B -M
+B +M
B)
FLT1;FLT4;MAPK1;MAPK3;NLK
-log10(p-value)
no biotin - no MG132
no MG132 - MG132 added

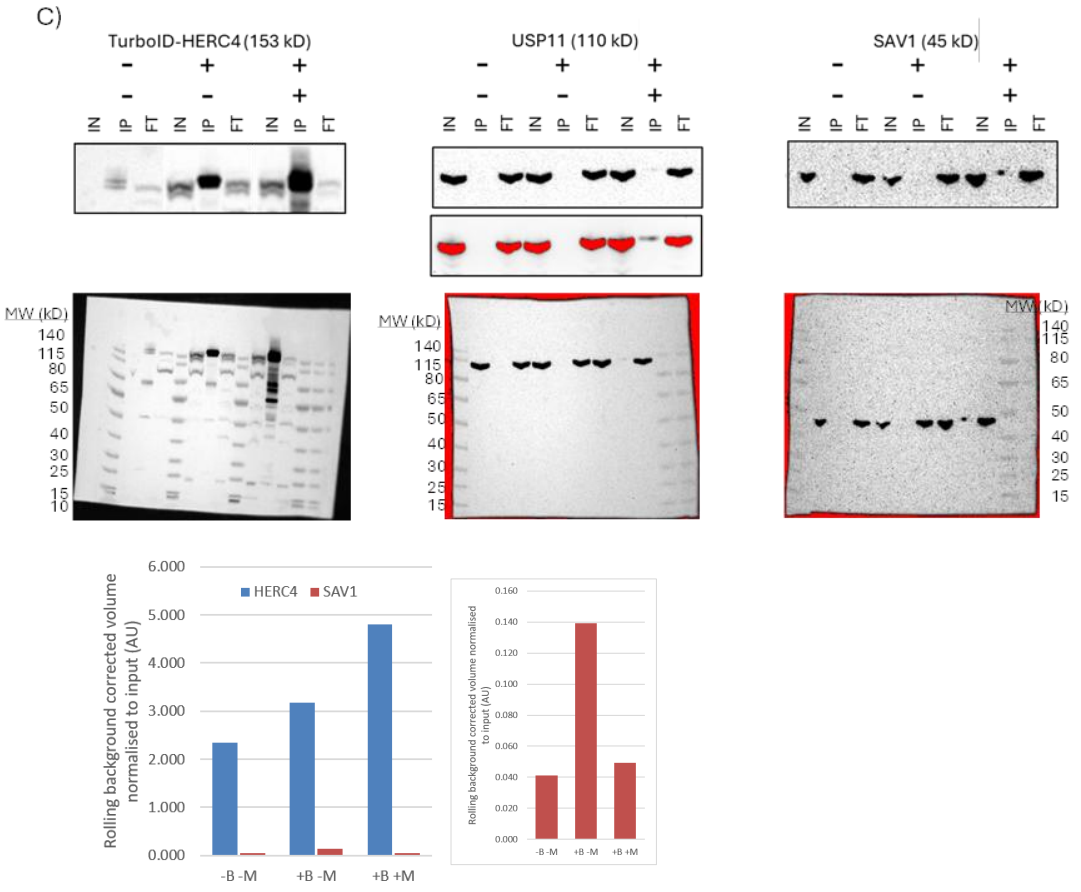

C)
TurboID-HERC4 (153 kD)
USP11 (110 kD)
SAV1 (45 kD)
IN IP FT IN IP FT IN IP FT
MW (kD)
140
115
80
65
50
40
30
25
15
10
Rolling background corrected volume normalised to input (AU)
HERC4 SAV1
-B -M
+B -M
+B +M

Figure 19: Validation of proximity-labelling mass spectrometry results

The biotin IP was repeated with fresh samples and the input (IN), eluates (IP) and flow-through (FT) were analysed by Western blot. 1%, 10% and 1% of each sample respectively was loaded into the gel.

A) VEGFR1 was pulled down in all conditions, including without exogenous biotin, suggesting it may be non-specific.

B) VEGFR1 pulldown data is consistent with its values in mass spectrometry dataset (pulled down more in no-biotin conditions than with biotin and without MG132), reinforcing the hypothesis that its interaction with the immunoprecipitation beads is non-specific.

C) USP11 was weakly detected in the MG132-treated sample but was not quantifiable in any IP samples. SAV1 may have been detected in the MG132-treated sample too, but repeats with a better antibody are required to confirm this.

Graphs in A and C show quantification of signal in IP samples relative to the signal for the same protein in the corresponding input samples. VEGFR and SAV1 values are shown relative to HERC4 values in the same experiment, and separately to account for being several orders of magnitude smaller. Quantification was done using iBright software. Total protein concentration was not measured.

3.3.2.2 - Protein processing

All 12 analyses (ORA, GSEA and pathway analysis of KEGG and GO-BP terms, for substrates and interactors) returned at least one term referencing the proteasome (Figure 20), and terms in 5 out of 6 interactor analyses referenced the endoplasmic reticulum (ER) in the context of protein processing, frequently including ER stress terms. For GSEA analysis, these terms had a normalised enrichment score between 1.5 and 2, and ORA analysis with GO-BP terms returned a fold enrichment of similar magnitude for ER stress and the ERAD pathway, or between 5 and 10 by pathway analysis. For substrates, protein degradation and processing terms related to the ER were far less abundant and were confined to pathway analysis (fold enrichment between 4 and 10). Only one of the 3 terms (Protein processing in the ER) placed in the top 30 terms ranked by fold enrichment (Appendix 6). "Proteasome" was notably the top KEGG term by both ORA and pathway analysis when the results were ranked by fold enrichment (7.04 and 33.02), but similar terms from the GO-BP database had the smallest enrichment levels by ORA. Pathway analysis also highlighted K11-, K27-, K48- and K63-linked ubiquitylation (Figure 21). K27 had the highest fold enrichment (~5) of the linkages identified when analysing the list of interactors, but it was not highlighted by substrate analyses. K11 had the highest fold enrichment for these (~10), followed by K48 and K63 in the same order as for the interactor dataset.

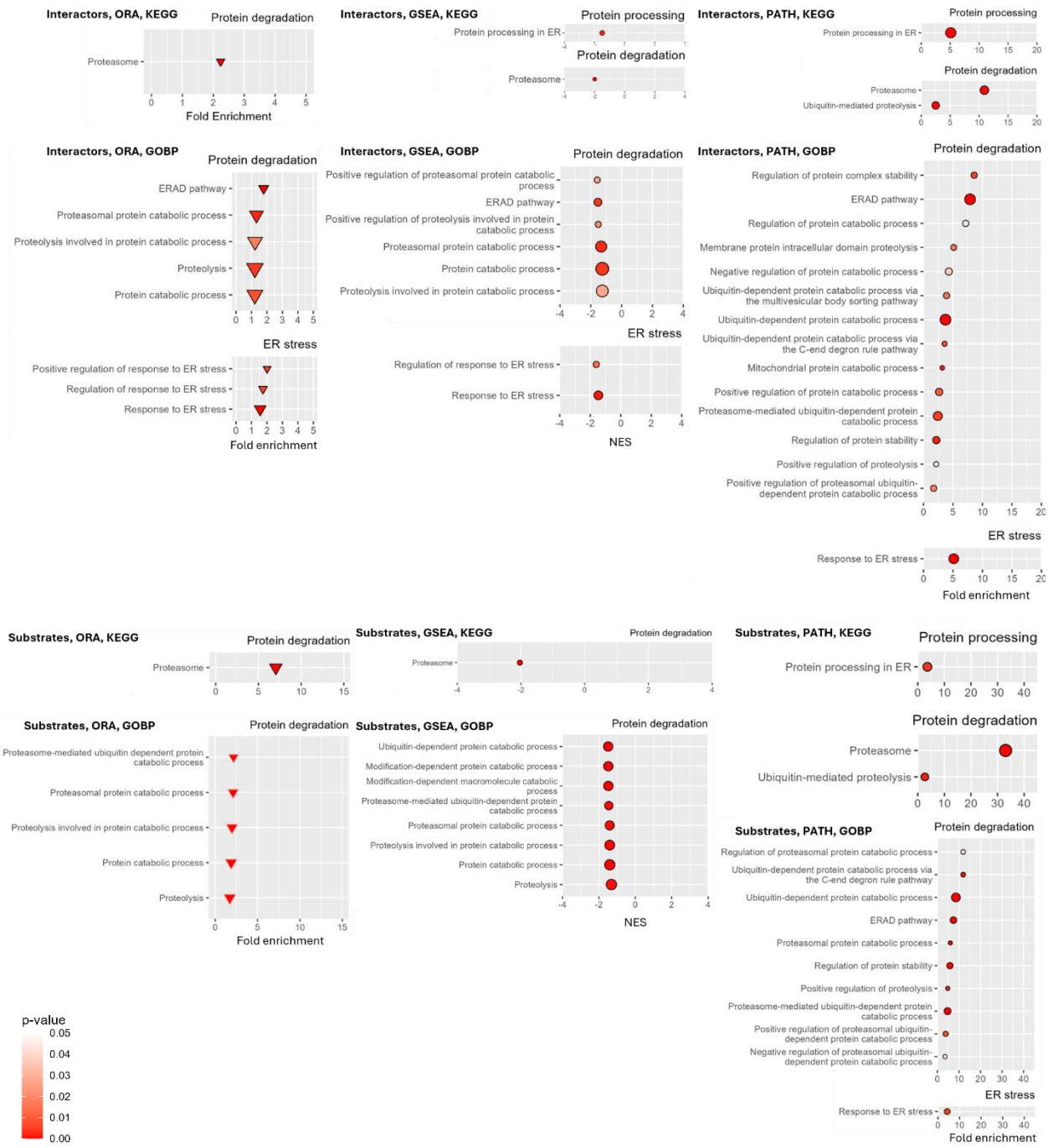


Figure 20: Protein processing-related terms enriched in interactor and substrate datasets
ORA, GSEA and pathway analysis were used to identify enriched KEGG and GO-BP terms from the list of interactors (significantly more abundant in biotin-treated samples than in those without) and substrates (significantly more abundant in MG132-treated samples than those without). Terms were ranked by their enrichment score then manually separated into themes. Protein degradation-related terms were present in all 3 analyses of both databases for both protein lists, and many of the interactor analyses also returned ER-related terms linked to protein processing and degradation.

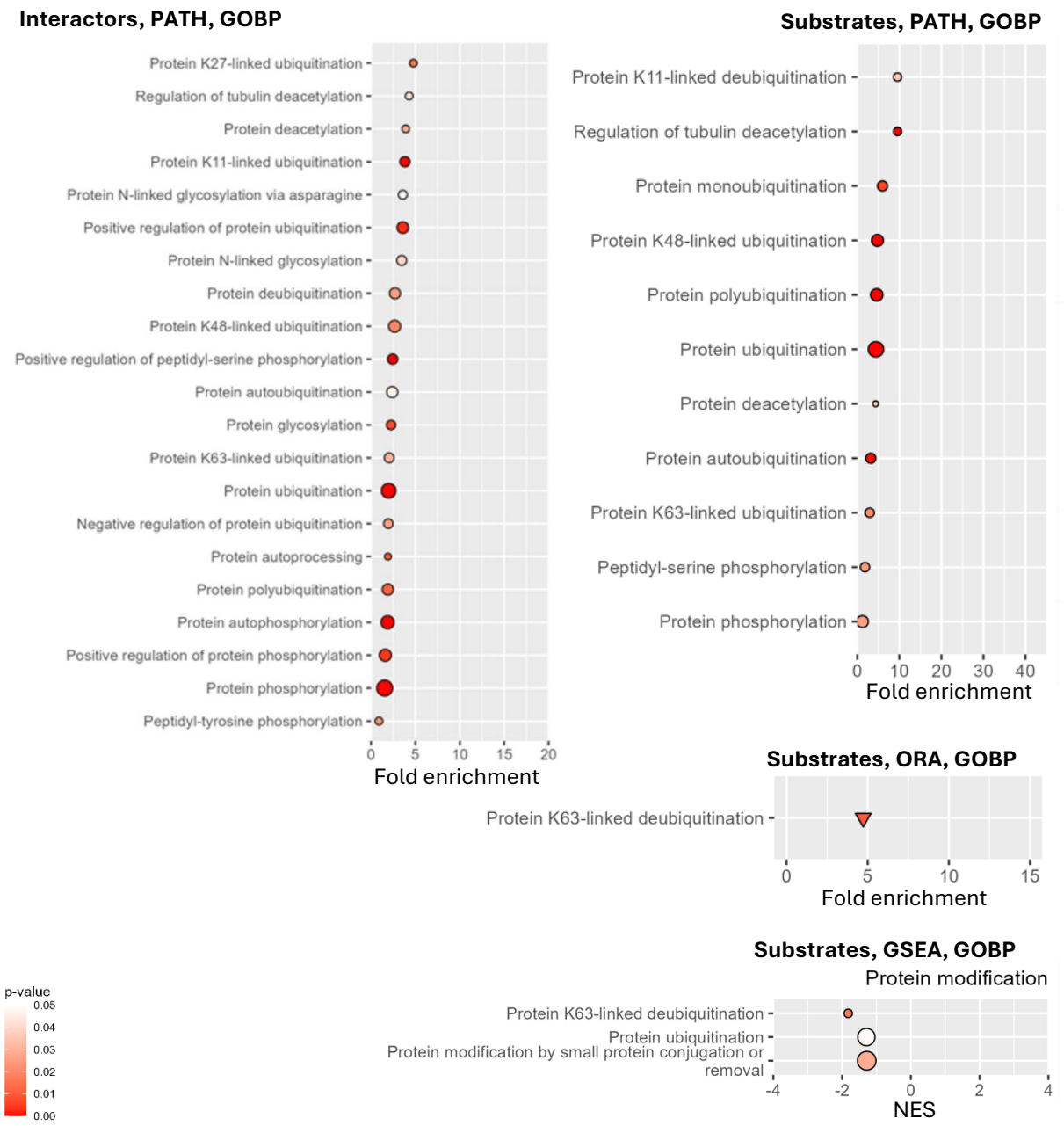


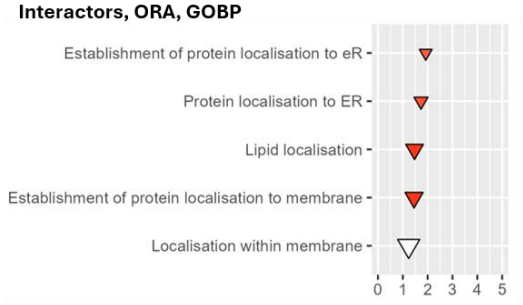
Figure 21: Ubiquitin-related terms enriched in interactor and substrate datasets
ORA, GSEA and pathway analysis were used to identify enriched KEGG and GO-BP terms from the list of interactors (significantly more abundant in biotin-treated samples than in those without) and substrates (significantly more abundant in MG132-treated samples than those without). Terms were ranked by their enrichment score then manually separated into themes. Protein ubiquitination was highlighted in 4 out of 12 analyses, and some of the relevant terms identified specific linkage types.

3.3.2.3 - Localisation and transport

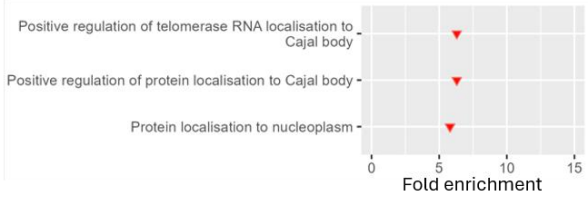
Localisation terms were identified solely from the GO-BP database and mostly relate to protein localisation to the plasma membrane, telomeres and Cajal bodies, or the ER (Figure 22). They were broadly similar between interactors and substrates Telomere-linked terms were particularly dominant, having the strongest enrichment of the relevant terms in 5 out of 6 analyses, and being the most abundant theme within localisation terms identified by GSEA. Notably, "positive regulation of establishment of protein localisation to telomere" was the third most enriched term by pathway analysis of interactors (fold enrichment of 11.45), and "regulation of telomerase RNA localisation to Cajal body" or "positive regulation of telomerase RNA localisation to Cajal body" had the strongest NES for GSEA analysis of interactors and substrates respectively (-2.21 and -2.05 while the majority of terms unrelated to telomeres had NES with a magnitude below 2).

In contrast, transport terms were distinct between the analysis sets. Vesicle transport, particularly around the ER and Golgi body, featured heavily in interactor analyses, while there were far fewer transport-related terms for substrates, primarily centred on protein export (Figure 23). Even in the interactor dataset, protein export featured strongly, producing the second highest enrichment factor for both GSEA and pathway analysis of GO-BP terms (-1.77 and 6.65 respectively).

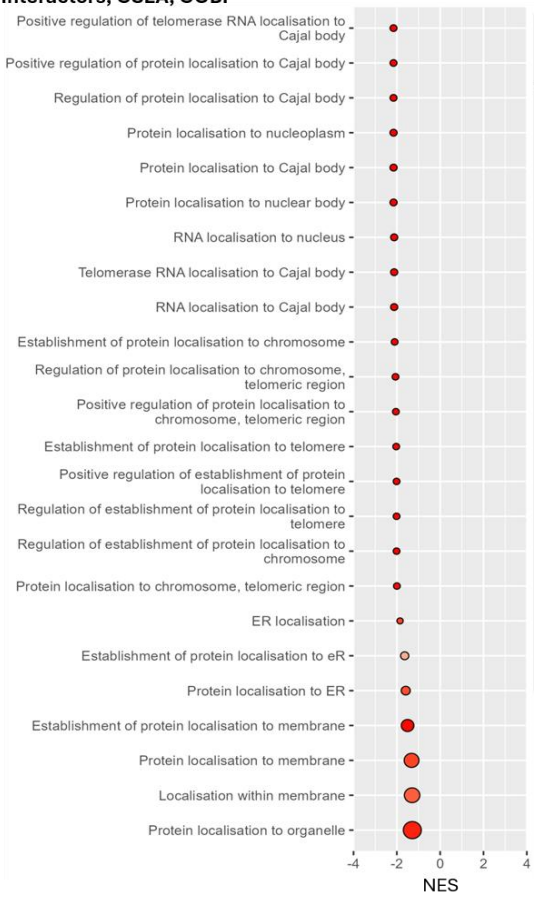
Interactors, ORA, GOBP



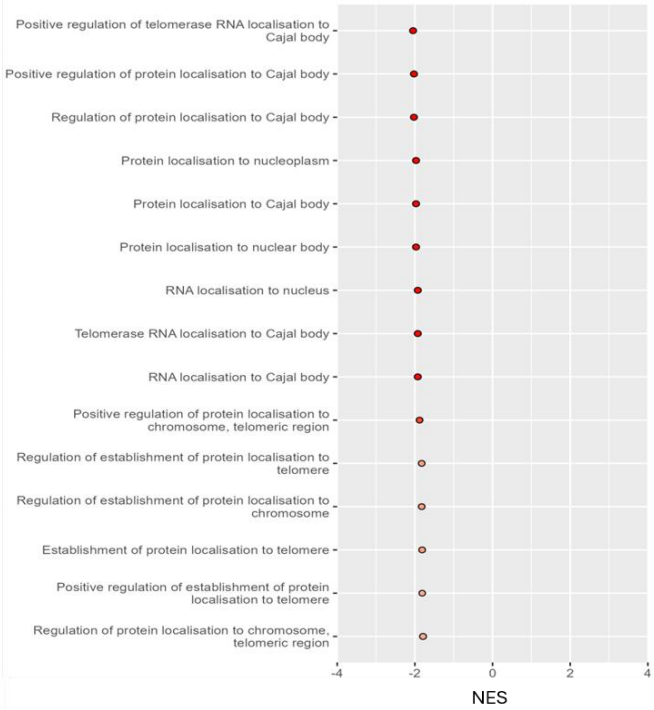
Substrates, ORA, GOBP



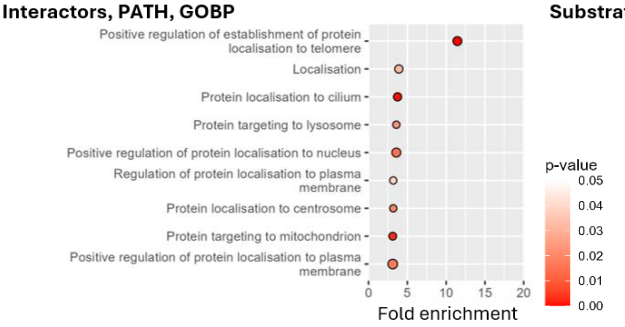
Interactors, GSEA, GOBP



Substrates, GSEA, GOBP



Interactors, PATH, GOBP



Substrates, PATH, GOBP

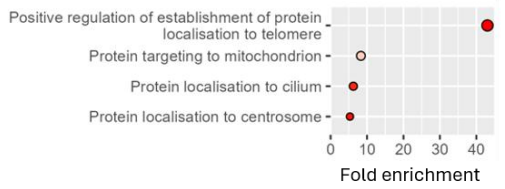


Figure 22: Localisation-related terms enriched in interactor and substrate datasets
ORA, GSEA and pathway analysis were used to identify enriched KEGG and GO-BP terms from the list of interactors (significantly more abundant in biotin-treated samples than in those without) and substrates (significantly more abundant in MG132-treated samples than those without). Terms were ranked by their enrichment score then manually separated into themes. Localisation terms were largely focused on the ER and telomeres.

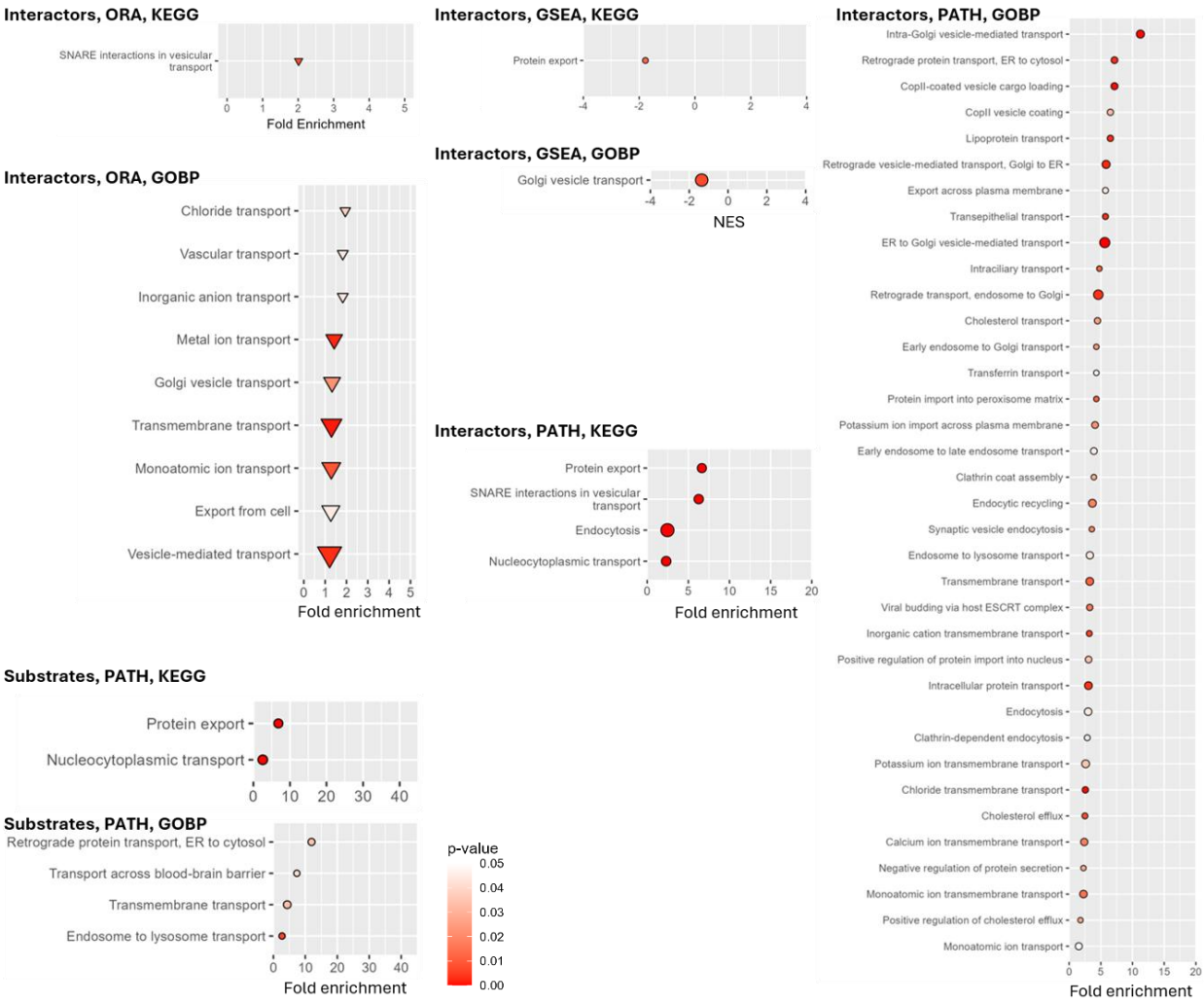


Figure 23: Transport-related terms enriched in interactor and substrate datasets
ORA, GSEA and pathway analysis were used to identify enriched KEGG and GO-BP terms from the list of interactors (significantly more abundant in biotin-treated samples than in those without) and substrates (significantly more abundant in MG132-treated samples than those without). Terms were ranked by their enrichment score then manually separated into themes, with transport-linked terms focusing on vesicle and protein transport.

3.3.2.4 - Metabolism and mitochondria

Based on the total proteome results, it was expected that there would be multiple terms linked to glycolysis and amino acid metabolism, but this was barely the case (Figure 24). All analysis methods returned terms relevant to metabolism for both interactors and substrates, although not always for both databases, but glycolysis was only referenced for substrates or interactors by pathway analysis of the GO-BP database. Substrate terms were very broad, and the glycolysis reference was limited to negative regulation of the process (fold enrichment: 4.35), while the results for interactors contained 3 terms, including "canonical glycolysis" and positive regulation of the process, with enrichment factors between 1 and 3. Other metabolic terms focused on lipid and folate metabolism, or simply "catabolic process". Mitochondria-related terms focused on mitophagy and organelle organisation, proving more relevant to cell cycle terms than to metabolism ones.

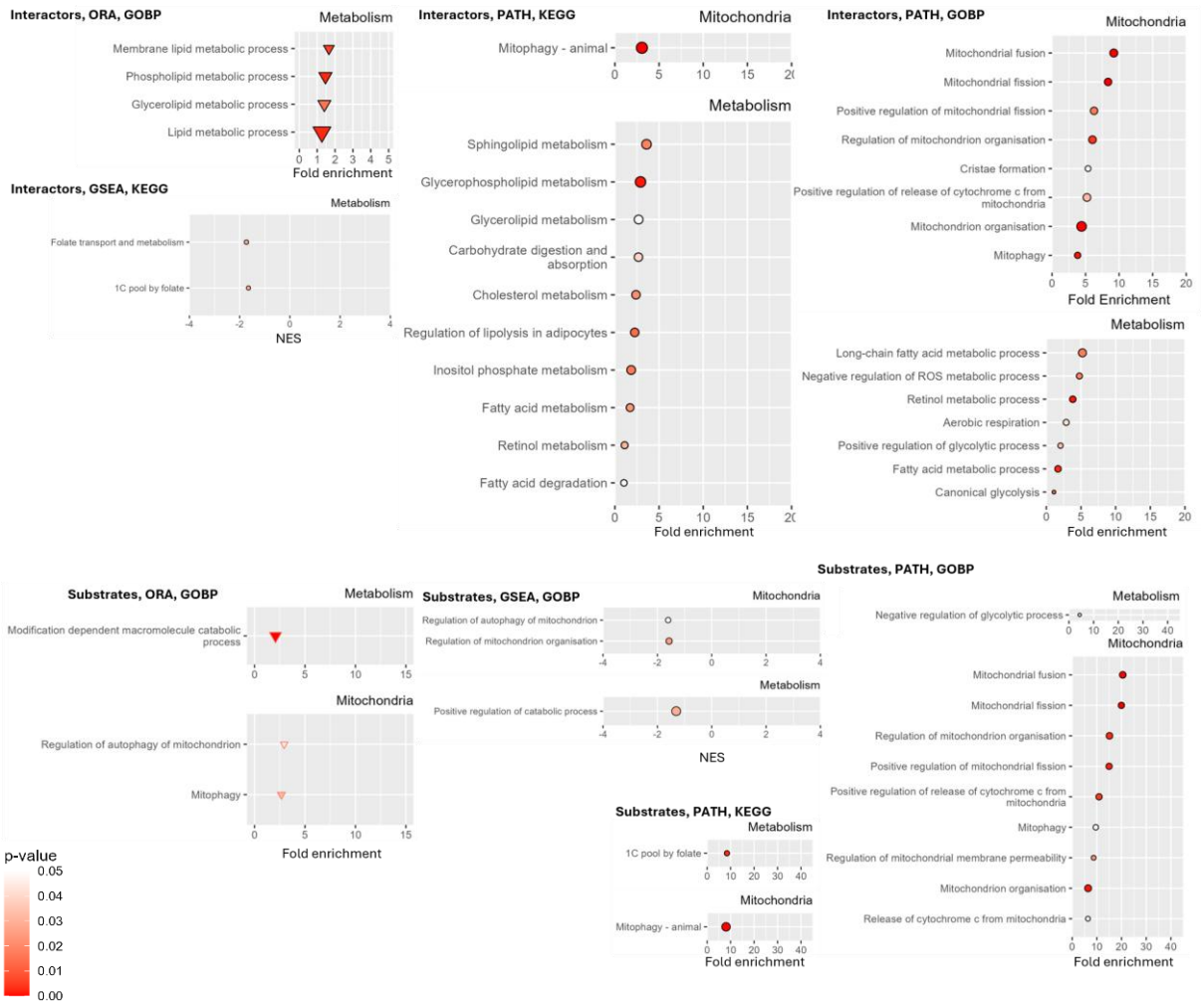


Figure 24: Mitochondria- and metabolism-related terms enriched in interactor and substrate datasets

ORA, GSEA and pathway analysis were used to identify enriched KEGG and GO-BP terms from the list of interactors (significantly more abundant in biotin-treated samples than in those without) and substrates (significantly more abundant in MG132-treated samples than those without). Terms were ranked by their enrichment score then manually separated into themes.

3.3.2.5 - Immune system

Compared to metabolic terms, those linked to the immune system showed greater correlation with the results from total proteome analysis, with 3 analyses identifying antigen presentation in some form (pathway analysis of the KEGG database for interactors and substrates with fold enrichment of ~3 and ~4 respectively, plus ORA analysis of the GO-BP database for substrates with a fold enrichment of ~5 for 2 very similar terms) (Figure 25). Other terms spanned various aspects of the immune responses, including pattern recognition and complement pathways from innate mechanisms, and T-cell and B-cell receptor signalling from the adaptive system, which suggests an emphasis on antigen recognition rather than presentation. However, all terms showed relatively low fold enrichment. For pathway analysis, for example, the term with the greatest enrichment was "positive regulation of T cell-mediated cytotoxicity" (substrates, GO-BP), but its value of ~10 was less than 25% of the most strongly enriched term for the same analysis ("Positive regulation of establishment of protein localisation to telomere", ~43).



Figure 25: Immune system-related terms enriched in interactor and substrate datasets
ORA, GSEA and pathway analysis were used to identify enriched KEGG and GO-BP terms from the list of interactors (significantly more abundant in biotin-treated samples than in those without) and substrates (significantly more abundant in MG132-treated samples than those without). Terms were ranked by their enrichment score then manually separated into themes. Antigen recognition, T and B cell-receptor signalling and pattern recognition receptors were particularly evident among immune system-related terms.

3.3.2.6 - Reproduction

Terms linked to reproduction were of particular interest (Figure 26), since involvement in this process is one of the most evidenced roles for HERC4 in the literature. 3 analyses for each dataset returned terms focused on gamete function. Both interactors and substrates were enriched with proteins linked to sperm-egg recognition and binding of sperm to the zona pellucida from the GO-BP database, based on GSEA (NES ≈ 2) and, for substrates, ORA (fold enrichment = 4.7), while KEGG terms identified for both datasets by pathway analysis focused on oocyte meiosis with potentially conflicting fold enrichment values of 2.2 and 0.81 for interactors and substrates respectively. The third analysis for interactors (PATH, GO-BP) identified only the broader term of "single fertilisation", which was also identified in substrates by GSEA (fold enrichment = 2.15 and NES = -1.80).

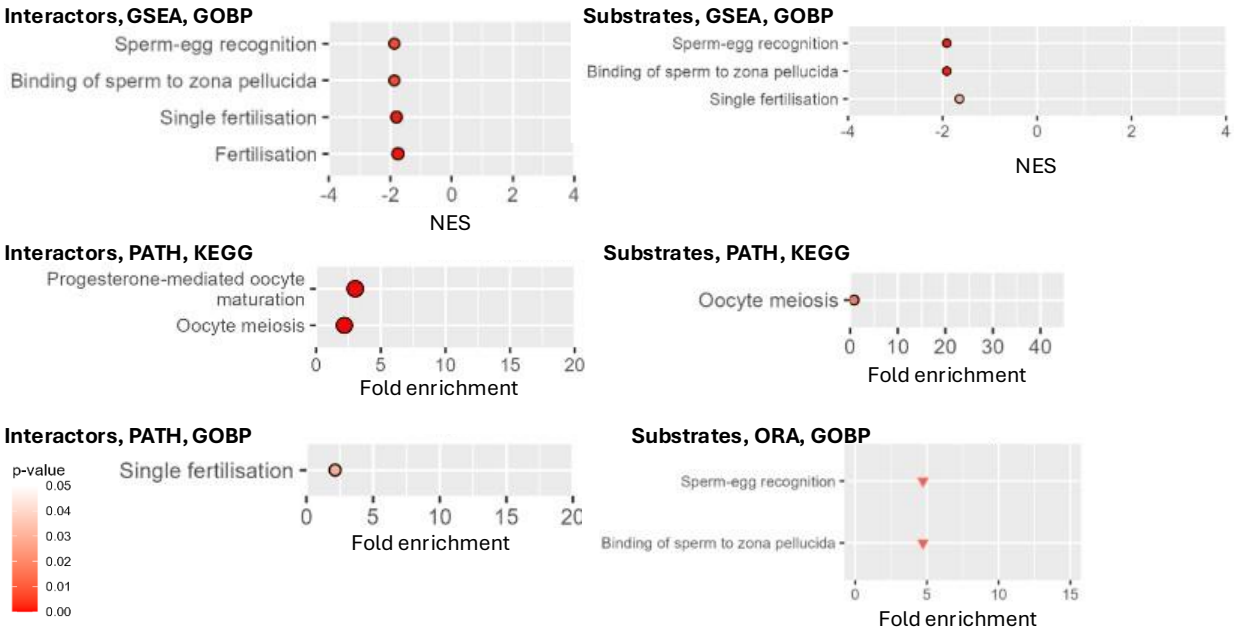


Figure 26: Reproduction-related terms enriched in interactor and substrate datasets
ORA, GSEA and pathway analysis were used to identify enriched KEGG and GO-BP terms from the list of interactors (significantly more abundant in biotin-treated samples than in those without) and substrates (significantly more abundant in MG132-treated samples than those without). Terms were ranked by their enrichment score then manually separated into themes. Fertilisation-linked terms mostly focused on sperm-egg interactions.

3.3.2.7 - Cell cycle and telomeres

Cell cycle terms were identified for both datasets using both databases, but only by pathway analysis (Figure 27). Terms from the KEGG database focused primarily on autophagy (fold enrichment of 3.8 for both interactors and substrates), cell death (fold enrichment of 1.75-3.07 in interactors; 2.33 (necroptosis) in substrates) and senescence (fold enrichment of 2.14 and 2.93 in interactors and substrates respectively), perhaps reflecting the frequency of terms connected to telomerase extension highlighted from the GO-BP database. These were selected by all 3 analysis methods for substrates, and by GSEA and pathway analysis for interactors, and their frequency fits with the prevalence of telomere-related localisation terms. If HERC4 ubiquitylates proteins involved in telomere extension, resulting in their degradation, this may shorten cellular life span, in keeping with the enrichment of anti-proliferation terms in this experiment and of pro-apoptotic terms in the total proteome data.

Other identified GO-BP terms highlighted spindle formation and the G2/M checkpoint for both interactors and substrates, suggesting potential involvement of HERC4 in the main cell cycle as well as exit from it. For pathway analysis of interactors, the 5 out of the top 6 cell cycle-related terms (fold enrichment between 3.58 and 5.45) referenced mitosis, G2, spindle assembly or a combination of these processes. 2 of these terms were also highlighted by the same analysis of substrates (spindle assembly, fold enrichment = 4.55; mitotic G2 DNA damage checkpoint signalling, fold enrichment = 7.97), and several other terms were present in both lists.


Interactors, PATH, GOBP
Cell cycle
Spindle assembly
Mitotic G2 DNA damage checkpoint signalling
Mitotic spindle assembly checkpoint signalling
Mitotic sister chromatid segregation
Centrosome cycle
Positive regulation of G2/M transition of mitotic cell cycle
Regulation of autophagy
Negative regulation of fibroblast proliferation
Autophagy
Regulation of mitotic cell cycle
Spindle organisation
Negative regulation of cellular senescence
Macroautophagy
Positive regulation of extrinsic apoptotic signalling pathway
Activation of Cys-type endopeptidase activity involved in apoptotic process
Regulation of cell division
Mitotic metaphase chromosome alignment
Positive regulation of autophagy
Centriole replication
Extrinsic apoptotic signalling pathway
Positive regulation of Cys-type endopeptidase activity involved in apoptotic process
Negative regulation of extrinsic apoptotic signalling pathway
Positive regulation of cell growth
Positive regulation of epithelial cell proliferation
Regulation of apoptotic process
Chromosome segregation
Regulation of cell cycle
Negative regulation of Cys-type endopeptidase activity involved in apoptotic process
MAPK cascade
Negative regulation of apoptotic signalling pathway
0 5 10 15 20
Interactors, PATH, KEGG
Autophagy - animal
Apoptosis - multiple species
Autophagy - other
Cell cycle
Cellular senescence
Apoptosis
Necroptosis
0 5 10 15 20
Substrates, PATH, GOBP
Regulation of chromosome segregation
Centrosome duplication
Negative regulation of fibroblast proliferation
Mitotic G2 DNA damage checkpoint signalling
Spindle organisation
Regulation of cell division
Spindle assembly
Regulation of cell cycle
Cell population proliferation
0 10 20 30 40
Fold enrichment
Interactors, GSEA, GOBP
Telomeres
Regulation of telomerase RNA localisation to Cajal body
Positive regulation of telomere maintenance via telomere lengthening
Positive regulation of telomere maintenance via telomerase
Telomerase RNA localisation
Regulation of telomere maintenance via telomere lengthening
Regulation of telomere maintenance via telomerase
Telomere maintenance via telomerase
Telomere maintenance via telomere lengthening
Positive regulation of telomere maintenance
-4 -2 0 2 4
NES
Substrates, ORA, GOBP
Regulation of telomerase RNA localisation to Cajal body
Telomerase RNA localisation
Positive regulation of telomere maintenance via telomere lengthening
Regulation of telomere maintenance via telomerase
Regulation of telomere maintenance via telomere lengthening
0 5 10 15
Fold enrichment
Substrates, GSEA, GOBP
Regulation of telomerase RNA localisation to Cajal body
Telomerase RNA localisation
Positive regulation of telomere maintenance via telomerase
Regulation of telomere maintenance via telomerase
Positive regulation of telomere maintenance via telomere lengthening
Regulation of telomere maintenance via telomere lengthening
Telomere maintenance via telomerase
Telomere maintenance via telomere lengthening
Positive regulation of telomere maintenance
-4 -2 0 2 4
NES
Interactors, PATH, GOBP
Positive regulation of telomere maintenance via telomerase
Regulation of telomere maintenance
Positive regulation of telomere capping
Positive regulation of telomerase activity
0 5 10 15 20
Substrates, PATH, GOBP
Positive regulation of telomere maintenance via telomerase
Positive regulation of telomerase activity
0 10 20 30 40
Fold enrichment
Substrates, PATH, KEGG
Cell cycle
Autophagy - animal
Cellular senescence
Necroptosis
Cell cycle
0 10 20 30 40
Fold enrichment
p-value
0.05
0.04
0.03
0.02
0.01
0.00

Figure 27: Cell cycle-related terms enriched in interactor and substrate datasets
ORA, GSEA and pathway analysis were used to identify enriched KEGG and GO-BP terms from the list of interactors (significantly more abundant in biotin-treated samples than in those without) and substrates (significantly more abundant in MG132-treated samples than those without). Terms were ranked by their enrichment score then manually separated into themes. There were multiple terms related to cell cycle exit through cell death or senescence, possibly related to the numerous terms referencing telomere maintenance. The other main themes centred on G2 and mitosis, and the spindle.

3.3.2.8 - DNA repair

DNA repair processes were only identified by pathway analysis (Figure 28), but they were reviewed further in case they gave molecular validation to the radioprotective effect seen in the original CRISPR screen that phenotypic experiments failed to recreate. In line with this, homologous recombination and mismatch repair were enriched from the KEGG database, plus DSB repair from the GO-BP database, for both interactors and substrates (fold enrichment: interactors = 2.32 (HR), 1.87 (MMR) and 2.08 (DSB repair); substrates = 5.17 (HR), 4.16 (MMR) and 4.35 (DSB repair)). The substrate dataset also highlighted "DSB processing" from the GO-BP database, along with "response to IR" (Appendix 6; fold enrichment = 6.83), reinforcing the original hypothesis that HERC4 may influence radiosensitivity, especially since the putative substrates promote DNA repair, indicating that HERC4 loss should reduce radiosensitivity.

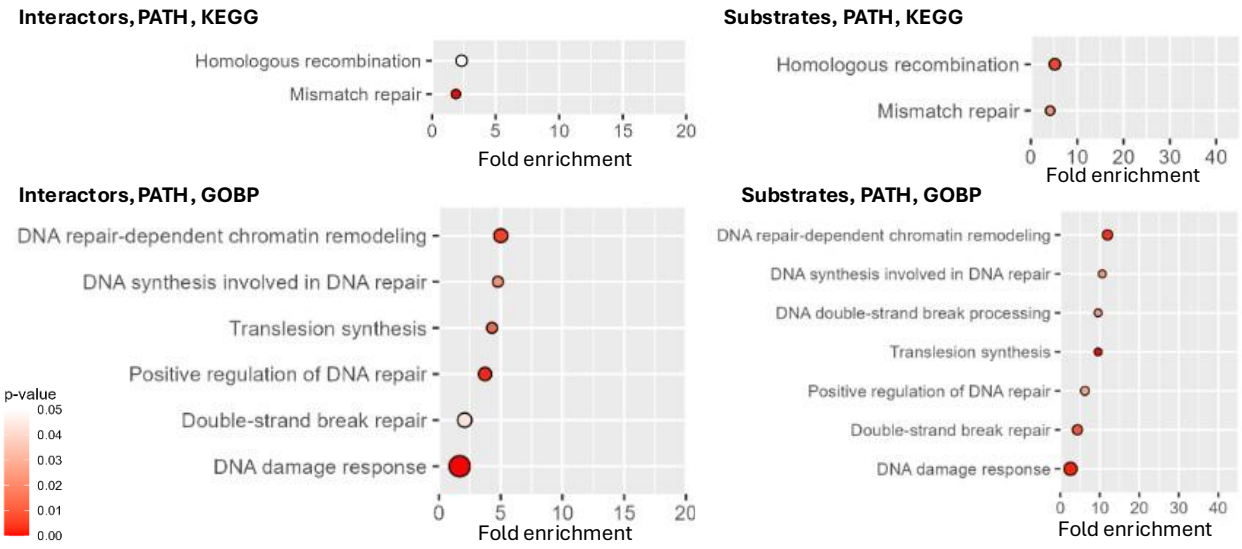


Figure 28: DNA repair-related terms enriched in interactor and substrate datasets
ORA, GSEA and pathway analysis were used to identify enriched KEGG and GO-BP terms from the list of interactors (significantly more abundant in biotin-treated samples than in those without) and substrates (significantly more abundant in MG132-treated samples than those without). Terms were ranked by their enrichment score then manually separated into themes. DNA repair terms were only identified by pathway analysis, but HR, MMR and DSB repair were highlighted for both interactors and substrates.

3.3.2.9 - Signalling

Signalling terms were also mostly identified by pathway analysis, except for 2 GO-BP terms found by GSEA to be enriched in the interactor dataset (Figure 29). NF-κB signalling was the most commonly referenced pathway and appeared in all 4 pathway analyses (fold enrichment of 1.14 and 1.80 for interactors; 1.63 and 1.99-2.64 for substrates (KEGG or GO-BP)). In support of the total proteome results, TNF signalling was identified for interactors in both databases (fold enrichment =1.42 (KEGG) and 2.68 (GO-BP)) and substrates in the KEGG database (fold enrichment = 1.89), and Hippo and VEGF pathways were also highlighted from both databases for interactors (Hippo: 1.04 and 1.06 (KEGG); 1.79 (GO-BP). VEGF: 1.10 (KEGG) and 2.56 (GO-BP)). AGE-RAGE signalling was also enriched, but only in interactors based on KEGG terms (fold enrichment = 1.10). Other notable enrichments were the Fanconi anaemia pathway (interactors and substrates, KEGG; fold enrichment = 2.05 and 3.90 respectively), given its implications for DNA damage responses, and Smoothened signalling, since SMO is one of the putative HERC4 substrates identified in the literature (fold enrichment = 3.98 (interactors) and 7.97 (substrates); both are GO-BP terms).

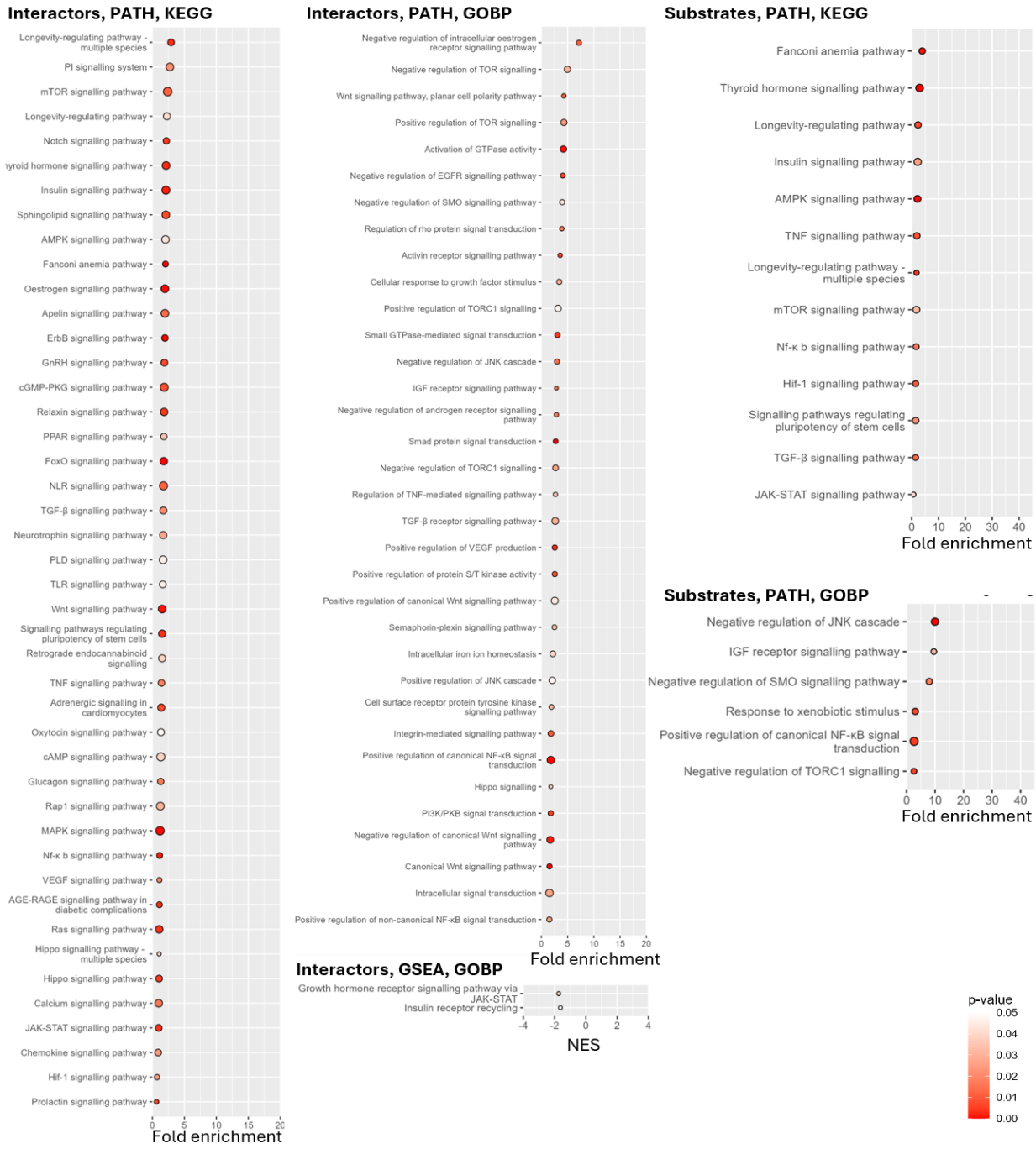


Figure 29: Cell signalling-related terms enriched in interactor and substrate datasets
ORA, GSEA and pathway analysis were used to identify enriched KEGG and GO-BP terms from the list of interactors (significantly more abundant in biotin-treated samples than in those without) and substrates (significantly more abundant in MG132-treated samples than those without). Terms were ranked by their enrichment score then manually separated into themes. Signalling terms were predominantly identified by pathway analysis, and NF-κB signalling was the most commonly identified pathway.

3.3.3 – Combined analysis

3.3.3.1 - Neither experiment confirmed published HERC4 substrates and interactors

8 substrates (DHODH, KRT19, LATS1, MAF-A, c-MAF, PGR, SAV1 and SMO) and 3 interactors (ZFTRAF1, EGFR and METTL3) were identified in an extensive literature review of HERC4, but the data presented here supported only one of these findings – that EGFR interacts with HERC4 (Figure 30A). As expected from the literature, EGFR was pulled down more in the mass spectrometry experiment after biotin treatment compared to the no-biotin control (Figure 30A, rows 3 and 4; 5.7- and 3.5-fold higher in MG132-untreated and -treated samples than no-biotin control), but showed no significant change between MG132 -treated and untreated samples, or in the knockout clones compared to wildtype cells (Figure 30A, row 5). It had a slightly bigger enrichment without MG132 than with the proteasome inhibitor, consistent with less competition from substrates for streptavidin binding, and its abundance was not significantly different between the knockout clones and wildtype population. The other substrates and interactors were all identified in at least one of the mass spectrometry experiments, but all failed to produce the results expected based on the literature.

ZFTRAF1 was only detected in the total proteome experiment, but while it was ~3-fold more abundant in Clone 3 than the wildtype cells, this comparison was statistically insignificant, and not reproduced in Clone 1, in which changes ZFTRAF1 levels were biologically and statistically insignificant (Figure 30C). The other interactor, METTL3, was detected in both experiments (Figure 30B). It was statistically significant for all 3 comparisons in the proximity labelling data, but it did not meet the 2-fold threshold required for a significant change in abundance for either comparison with the no-biotin control. It was in fact more abundant in the control than in the biotin-treated, no-MG132 samples, although not the MG132-treated ones, suggesting that it may show biotin-independent binding to the beads. The difference between MG132-treated and -

untreated samples, however, was biologically substantial (2.41 times more abundant in treated samples compared to untreated) as well as statistically significant, despite there being no published evidence of HERC4 causing degradation of METTL3 and the knockout clones showing only insubstantial changes METTL3 levels compared to the wildtype population.

Among the substrates, DHODH was the only one to be detected in the HERC4 knockout clones, but its abundance barely changed in either clone compared to the wildtype cells (~94% and ~110% of wildtype levels in Clones 1 and 3 respectively), with equally negligible p-values (Figure 31A). Its interactor, PRR11, by contrast, showed a substantial upregulation and almost reached significance in both clones (>400% of wildtype levels in both clones, with a $-\log_{10}$(p-value) of 1.10 and 1.01 respectively) (Figure 31B). Interestingly, PRR11 was a significant hit in the proximity labelling experiment, but only as a substrate; although it showed substantial upregulation without (6.71-fold) and especially with MG132 (24.36-fold) compared to the no-biotin control, neither difference was statistically significant. DHODH was not detected in this experiment.

Of the other 7 substrates, 4 were detected in the proximity labelling data – SMO, SAV1,LATS1 and KRT19 – but only SMO reached statistical significance in any of the 3 comparisons made (Figure 31C). Notably, its change in abundance with and without MG132 was insignificant (1.31-fold increase after MG132 treatment), suggesting that while it may interact with HERC4 (fold change of 7.54 and 9.86 for MG132-untreated and -treated samples compared to no-biotin control), it is not a substrate. However, an AlphaFold model of the interaction between the 2 proteins places the N-terminal methionine of SMO close to the catalytic cysteine, countering the results of the proximity labelling data (Figure 31D). SAV1 showed a similar pattern, almost reaching statistical significance in both comparisons with the no-biotin control, but falling decidedly short for the third comparison (Figure 31E). LATS1 was firmly insignificant, both statistically and biologically (Figure 31F), but KRT19 was more complex (Figure 31G). It was present in multiple hits (one unique and several encompassing at least 2 KRT proteins), many of which were significantly

enriched in the no-biotin control, suggesting that some KRT motifs may bind non-specifically to the IP beads. Of the peptides that were more abundant under biotin-treated conditions, none were significant. The KRT19-specific hit was statistically significant in the comparison of no-biotin and MG132-treated samples, but fell short of biological significance with a fold increase of 1.88 after treatment, and in the comparison of no-biotin and no-MG132 (+biotin) samples, its fold change was neither statistically nor biologically significant, with minimal values for both parameters. This suggests that KRT19 may interact weakly with HERC4, but does not support its annotation as a HERC4 substrate. There was no data for it in the total proteome experiment to confirm or disprove the annotation.

Considered together, these experiments suggest that HERC4 may well be involved in the pathways proposed by the literature, but they fail to validate the putative substrates in LN229 cells.

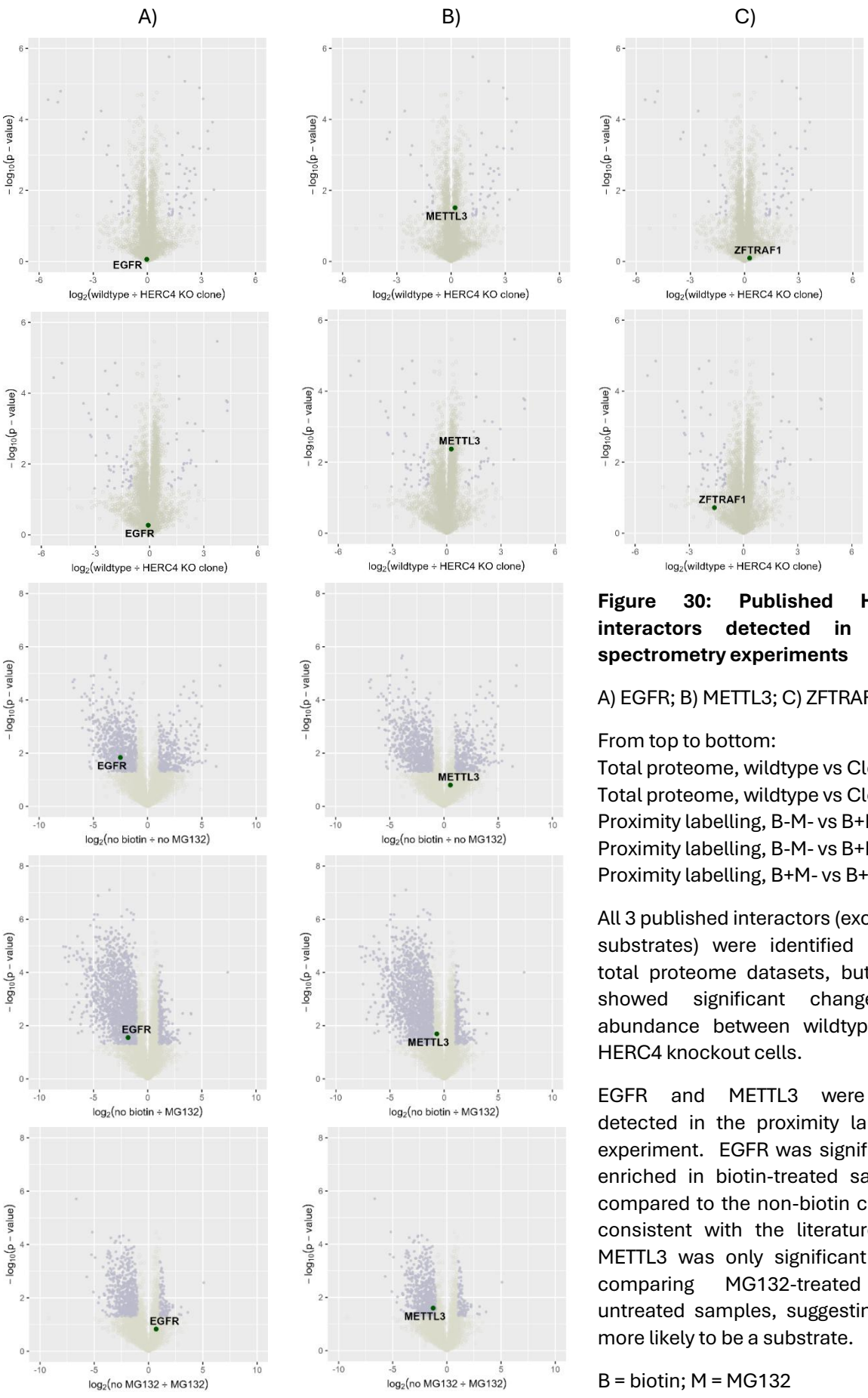


Figure 30: Published HERC4 interactors detected in mass spectrometry experiments

A) EGFR; B) METTL3; C) ZFTRAF1

From top to bottom:
Total proteome, wildtype vs Clone 1
Total proteome, wildtype vs Clone 3
Proximity labelling, B-M- vs B+M-
Proximity labelling, B-M- vs B+M+
Proximity labelling, B+M- vs B+M+

All 3 published interactors (excluding substrates) were identified in the total proteome datasets, but none showed significant changes in abundance between wildtype and HERC4 knockout cells.

EGFR and METTL3 were also detected in the proximity labelling experiment. EGFR was significantly enriched in biotin-treated samples compared to the non-biotin control, consistent with the literature, but METTL3 was only significant when comparing MG132-treated and untreated samples, suggesting it is more likely to be a substrate.

B = biotin; M = MG132

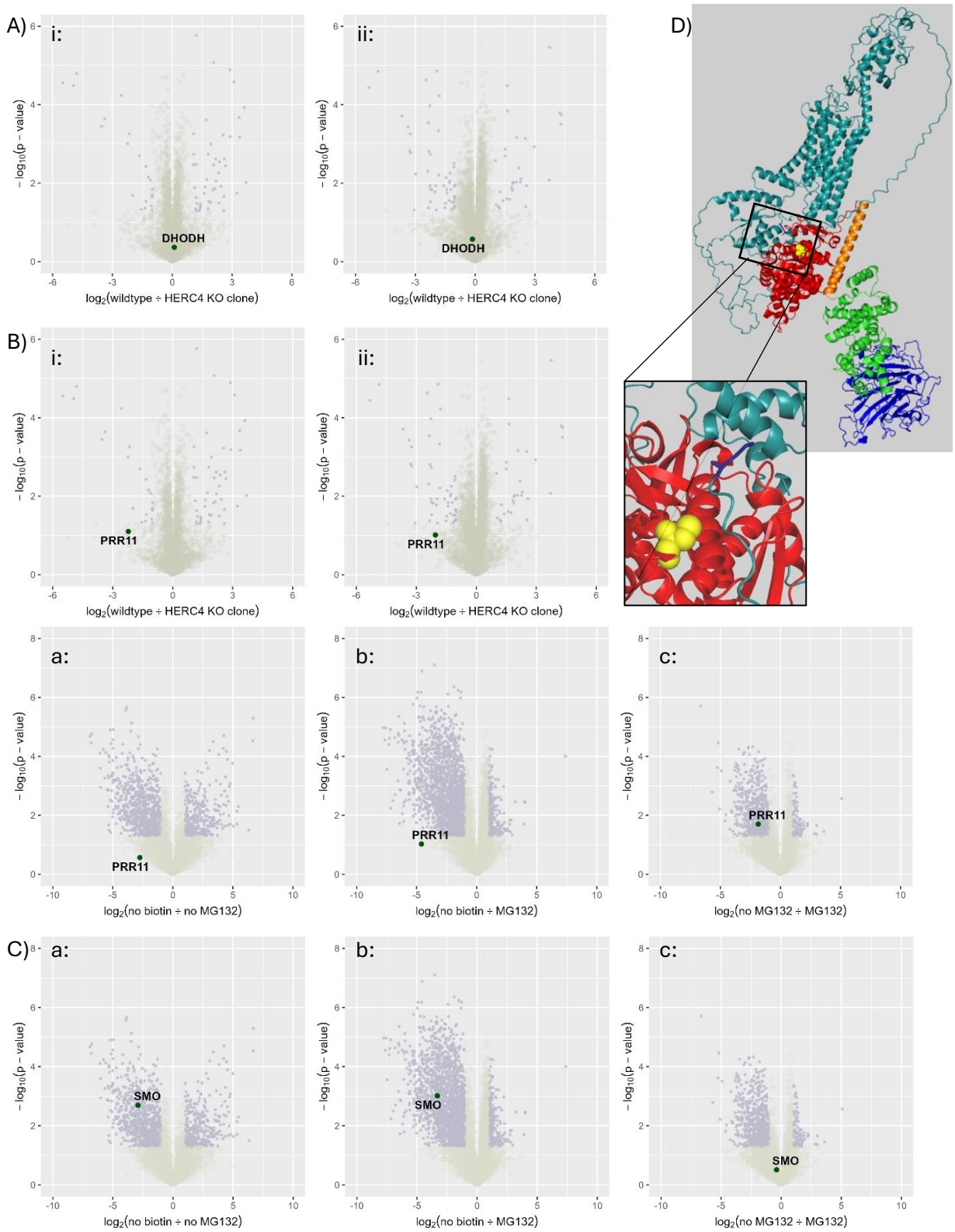


Figure 31a: Published HERC4 substrates detected in mass spectrometry experiments

A) DHODH; B) PRR11; C) SMO

D) AlphaFold model of SMO-HERC4 interaction (Analysis run using AlphaFold 3 on 13/07/25; ipTM = 0.2; pTM = 0.54 [Abramson et al., 2024]. Structures formatted in PyMOL [The PyMOL Molecular Graphics System, Version 3.0 Schrödinger, LLC])

Total proteome: i: wildtype vs Clone 1 ii: wildtype vs Clone 3

Proximity labelling : a: B-M- vs B+M- b: B-M- vs B+M+ c: B+M- vs B+M+

B = biotin; M = MG132

Continued overleaf

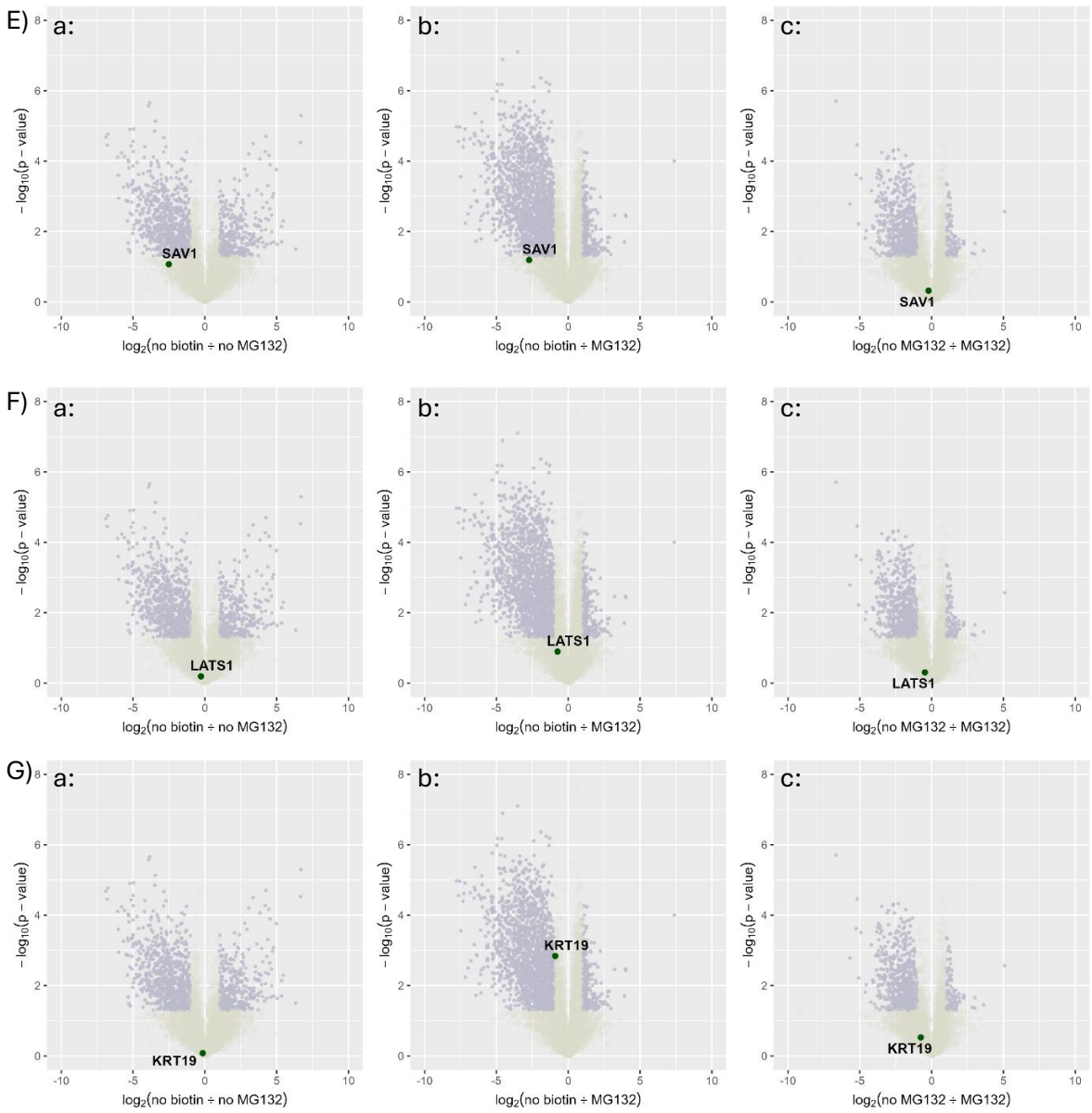


Figure 31b: Published HERC4 substrates detected in mass spectrometry experiments
E) SAV1; F) LATS1; G) KRT19
These 3 proteins were not detected in the total proteome experiment.
Proximity labelling : a: B-M- vs B+M- b: B-M- vs B+M+ c: B+M- vs B+M+
B = biotin; M = MG132

DHODH was only identified in the total proteome experiment, and showed no significant change in abundance after HERC4 loss. PRR11 was identified in both experiments, and was significantly enriched by MG132 treatment, consistent with its proposed role as an HERC4 substrate. Its increased abundance in the knockout clones did not reach statistical significance, but was biologically significant and close to the statistical threshold in both clones. SMO was convincingly identified as an interactor in both sets of biotin-treated samples compared to the untreated control, but was not significantly enriched by MG132 treatment, suggesting it may not be a substrate. SAV1 showed a similar pattern in the proximity labelling experiment, but fell just short of statistical significance in both +/- biotin comparisons. There was no biologically or statistically significant change in LATS1 abundance in any comparison, and while KRT19 comfortably exceeded the statistical threshold, its fold change was not considered biologically significant.

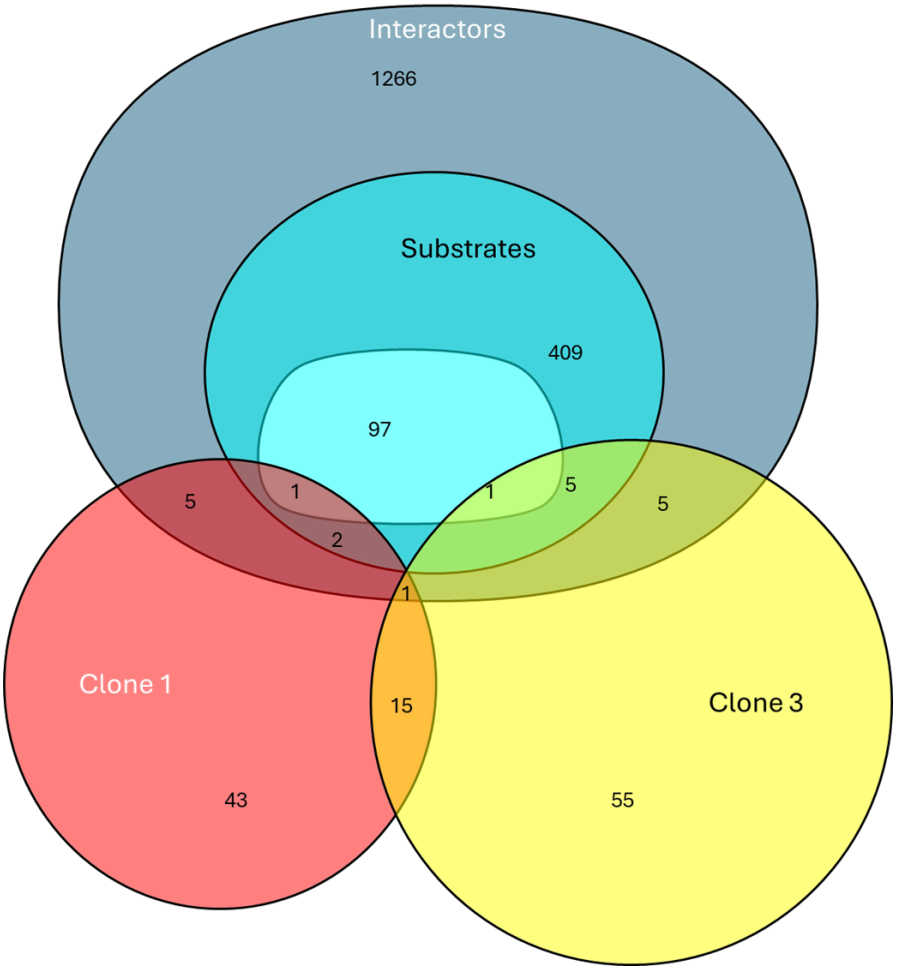
3.3.3.2 – Combined analysis identifies one shared hit between differentially expressed genes in both clones and putative HERC4 interactors

Comparison of the four sets of significant proteins (interactors, substrates, differentially expressed in Clone 1, and differentially expressed in Clone 3) showed very little overlap. The combined list had 1905 unique proteins, but only 20 of these were identified as significant in both experiments, and only 1 of these (HAUS1) was significant in both clones (Figure 32A). HAUS1 was significantly more abundant in both clones compared to the wildtype control (3.14- and 3.46-fold respectively), and it was considered an interactor based on its significant enrichment in MG132- treated conditions compared to the no-biotin control (3.16-fold more abundant after treatment). No substrates showed statistically significant changes in both clones. HAUS1 levels increased more than 2-fold following MG132 treatment, but the difference did not reach statistical significance, with a p-value of 0.13 (Figure 33A). However, since there was also limited increase in abundance in the MG132-untreated samples compared to the no-biotin controls, it is plausible that further work would override this lack of statistical significance and show HAUS1 to be a substrate of HERC4.

The proposed interaction between HERC4 and HAUS1 was modelled using AlphaFold 3 [Abramson et al., 2024] and at first, the model seemed promising (Figures 33B, 34A). The majority of the complex folded with a pIDDT score of >70 (confident or very highly so), and the pTM score for the complex is 0.62, above the threshold at which the fold is considered realistic. Additionally, HAUS1 appears to interact with both the β-barrel that is likely to facilitate interactor recognition and the catalytic HECT domain, strengthening the hypothesis that HAUS1 may be a substrate after all. Closer analysis revealed that, in this model, HAUS1 does not interact with the active site of HERC4, consistent with its identification as an interactor only and not a substrate (Figure 34B). At the other end of HERC4, no obvious hydrophobic interactions were observed and but some side chains are sufficiently close for hydrogen bonds to form between HAUS1 and the β-barrel of HERC4. A couple of putative donor-acceptor pairs were found to be separated by

approximately 3 Å, the expected length for hydrogen bonds between polypeptides, but others were more distant, in the range that indicates weak interaction [Jeffrey, 1997] (Figure 34C). The ipTM value of 0.16 is extremely low, suggesting that while the fold of each protein is likely to be correct, the model of their interaction is not. Overall, the AlphaFold model does not rule out an interaction between HERC4 and HAUS1, but nor does it build a strong model for this interaction, shifting the emphasis to empirical data for validation.

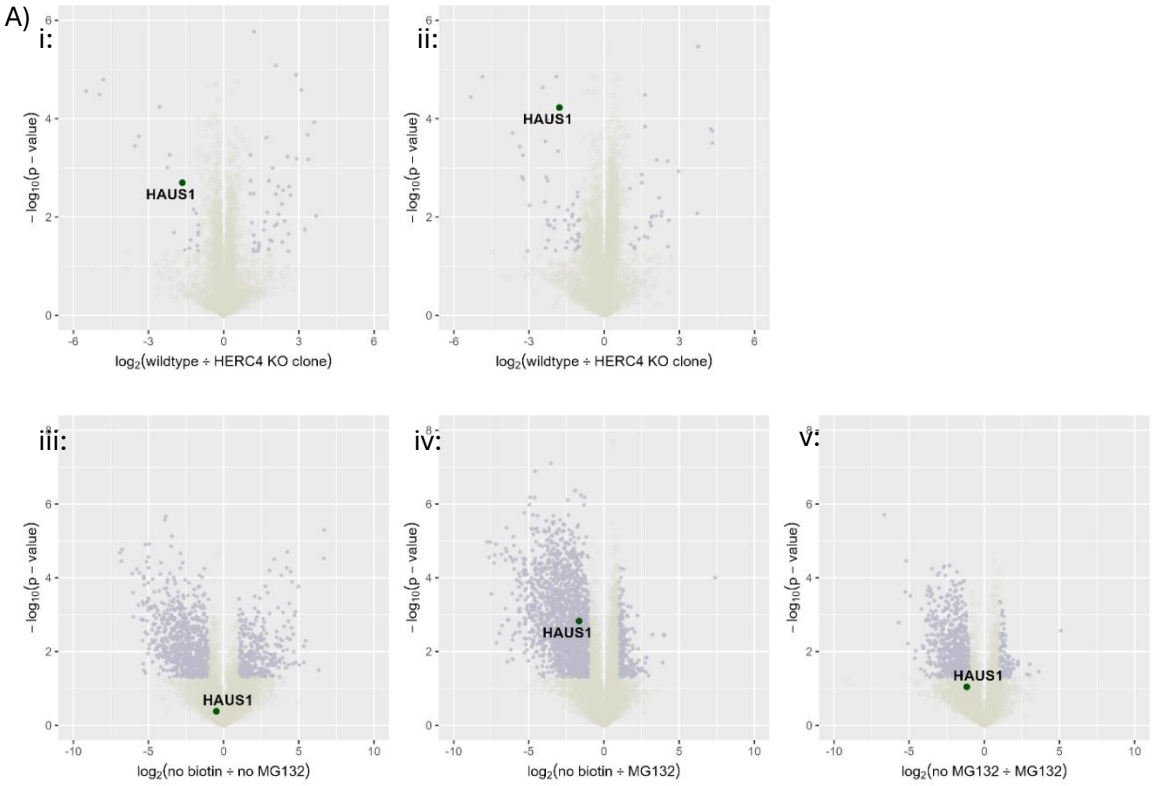
A)



B)

Group	Gene count
Interactors (only)	1701 (1266)
Substrates (only)	515 (97)
Clone 1 (only)	67 (43)
Clone 3 (only)	82 (55)
Interactor + substrate (only)	416 (409)
Interactor + clone 1 (only)	7 (5)
Interactor + clone 3 (only)	10 (5)
Interactor + clone 1 + clone 3	1
Interactor + substrate + clone 1	2
Interactor + substrate + clone 3	5
Substrate + clone 1 (only)	3 (1)
Substrate + clone 3 (only)	6 (1)
Substrate + clone 1 + clone 3	0
Interactor + substrate + clone 1 + clone 3	0

Figure 32: The number of proteins identified in each experiment and the overlap between them
The majority of, but not all, substrates were identified as interactors, and roughly a quarter of proteins identified in each clone were identified in the other, but there was minimal overlap between the 2 experiments. Of the 1905 unique proteins identified, only 20 were present in both total proteome and proximity labelling datasets, and only 1 of these was significant in both clones. This protein was only identified as an interactor – there were no substrates that were also identified in both clones.



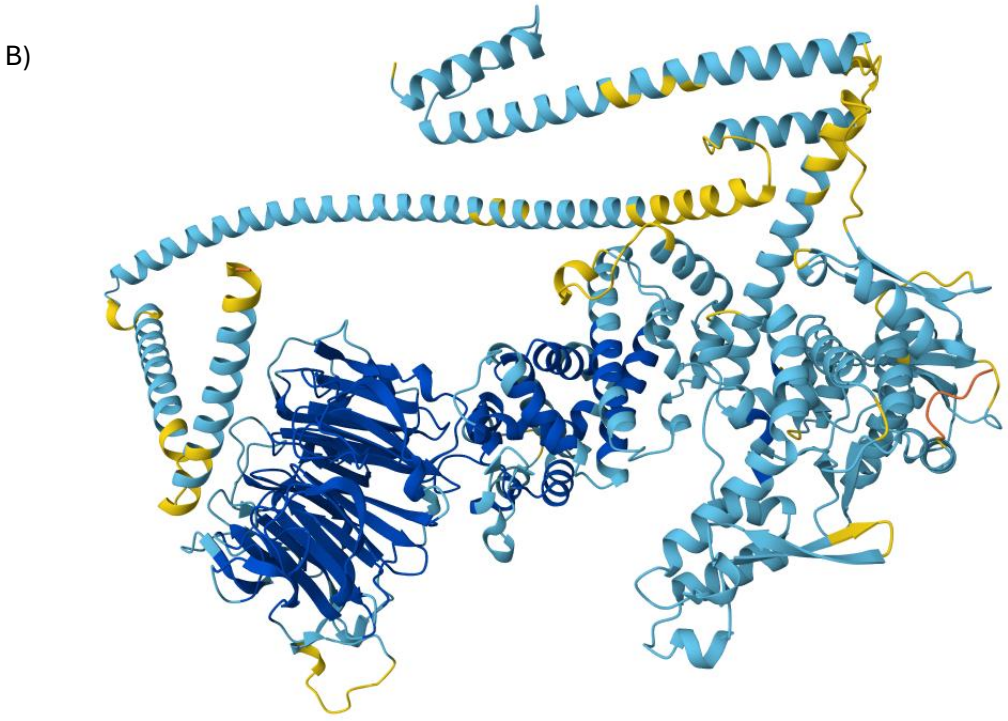
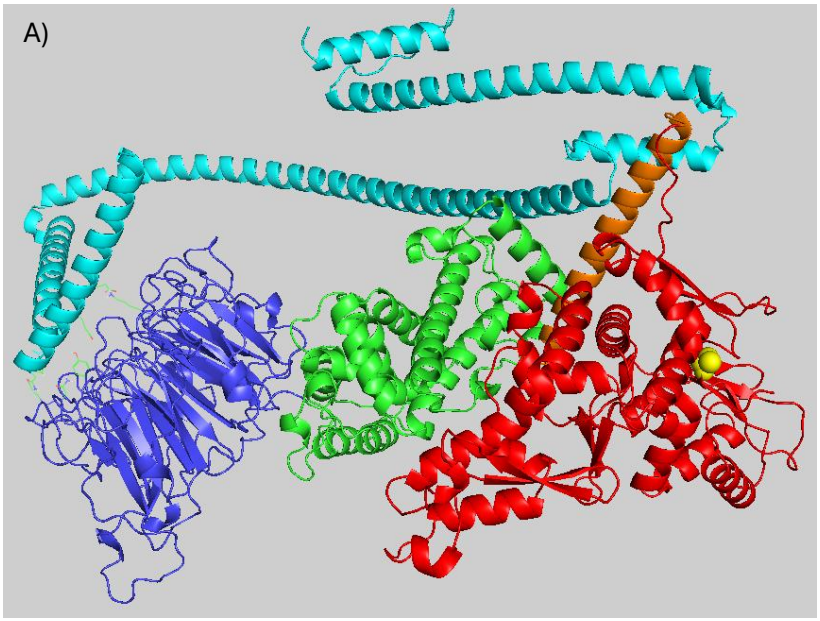


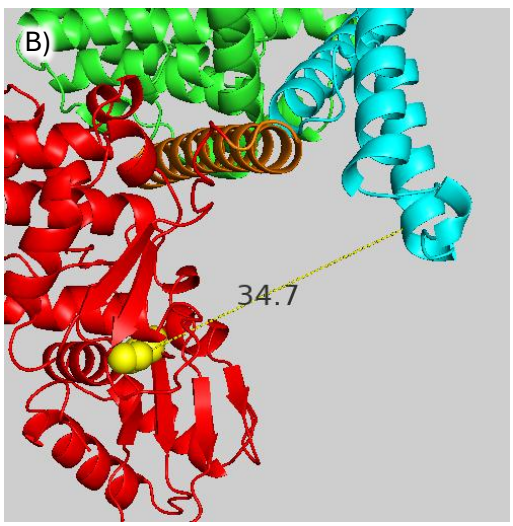
Figure 33: HAUS1 was identified as a significant interactor that was also more abundant in the HERC4 knockout clones than wildtype cells

A) Enrichment of HERC4 Total proteome: i: wildtype vs Clone 1 ii: wildtype vs Clone
Proximity labelling : iii: B-M- vs B+M- iv: B-M- vs B+M+ v: B+M- vs B+M+

B) AlphaFold model of HAUS1 interacting with HERC4. Analysis run 30/11/25; ipTM = 0.16; pTM = 0.62. [Abramson et al., 2024]

pIDDT > 90 (very high) 90 > pIDDT > 70 (confident) 70 > pIDDT > 50 (low) pIDDT < 50 (very low)





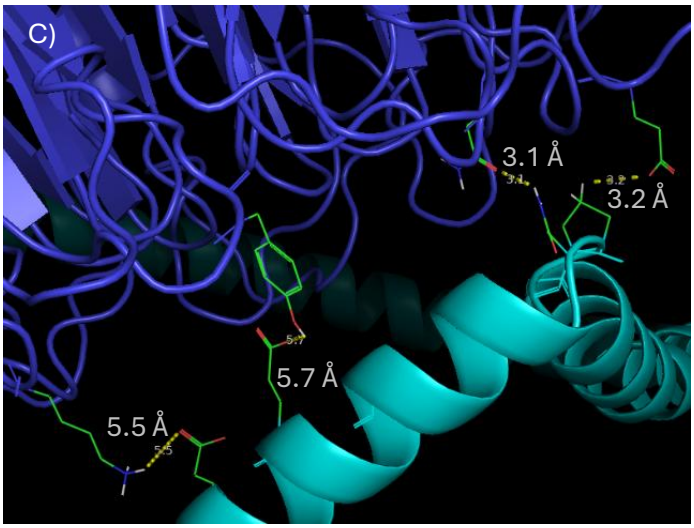


Figure 34: Predicted HERC4-HAUS1 interaction

A) Overall interaction model (HAUS1; HERC4 β-barrel, central domain, stabilising helix, HECT domain and catalytic cysteine) (Analysis run using AlphaFold 3 on 30/11/25; ipTM = 0.16; pTM = 0.62 [Abramson et al., 2024])

B) In this model, HAUS1 does not interact with the active site of HERC4.

C) In this model, HAUS1 is within hydrogen bonding distance of the HERC4 β-barrel.

Structures formatted in PyMOL [The PyMOL Molecular Graphics System, Version 3.0 Schrödinger, LLC]

3.4 - Discussion

The large volume of data generated by the mass spectrometry experiments presented here does not coalesce around a few strong themes or proteins in the way that was anticipated. Preliminary validation steps are inadequate to confirm the accuracy of the data, so the lack of dominant theme may indicate experiment design or execution issues. For example, the effects HERC4 loss might not be detectable by these methods, such as changes in protein activity rather than abundance, particularly since the downstream effects of HERC4-mediated ubiquitylation have not been extensively characterised and, consequently, might differ from the canonical induction of proteasomal degradation. HERC4 activity and therefore loss might also be significant only under certain conditions, suggesting that irradiated samples might be a useful supplement to the current dataset. Alternatively, the breadth of the dataset might in itself be key information. As the evolutionarily oldest member of the HERC family, HERC4 might span an array of functions that have since been divided between its potentially more specialised 'descendants'. The data should therefore be reviewed in the context of both the phenotypic data presented in the previous chapter and the results presented in the literature, which themselves span a range of putative functions and substrates. If, in the absence of a strong theme, some of the weaker trends are supported by multiple datasets and types, this gives credence to the suggestion that the range of patterns could be caused by HERC4 playing many roles. The most likely candidates for this are proliferation, apoptosis and the immune system, with HAUS1 being the strongest candidate for a mechanistic connection between HERC4 involvement in each of these pathways.

Proliferation

The literature on HERC4 identifies 11 putative binding partners, 2 areas of function, and involvement in multiple cancer types, predominantly influencing proliferation, apoptosis, migration and invasion [for example, Xu et al., 2019; Huang et al., 2021]. Of these 4 pathways, only the first 2 featured in the terms identified by the enrichment analyses presented here. Total proteome analysis indicated a loss of proliferation inhibition following HERC4 removal,

supporting the finding that HERC4 loss in ovarian cancer cells increases cyclin B1 expression and promotes cell growth [Zhu et al., 2024], HERC4 overexpression slows tumour growth in a mouse model of multiple myeloma (MM) [Zhang et al., 2016], and downregulation of HERC4 in NSCLC accelerates proliferation through increased SMO signalling [Sun et al., 2019]. However, it also contradicts the identification of HERC4 as a radiosensitiser in the CRISPR screen that initiated this project, since slower growth rates correlate with better survival after IR. This proposed phenotype better matches several other studies, which show a positive correlation between HERC4 levels and cell proliferation in breast cancer and hepatocellular carcinoma, suggesting that the role of HERC4 in proliferation may be complex or at least cell type-specific [Xu et al., 2019; Zheng et al., 2017; Huang et al., 2021; Sun et al., 2025]. It is notable that the cancer types in cells linked to published areas of HERC4 activity show one correlation (ovarian cancer and fertility; MM and the immune system), while 2 of the 3 without this link show another.

Apoptosis

It is also notable, however, that cell proliferation terms were scarce in the proximity labelling results, and cell cycle-related terms clustered instead around senescence and apoptosis. Both terms were also highlighted in the total proteome data, and while the proteins identified for senescence contradict each other in their function and direction of fold change, proteins from apoptotic pathways were more consistent in suggesting HERC4 knockout promotes apoptosis. In contrast to the cell proliferation terms aligning with the ovarian cancer and MM studies, these terms support the other studies, in which HERC4 upregulation promotes proliferation and inhibits apoptosis. If both sets of terms are true positive results, this would indicate an increase in cell turnover with no increase in population growth rate when HERC4 is lost, explaining the lack of change observed in proliferation experiments presented in the previous chapter, but once again failing to substantiate the hypothesis that HERC4 is a radiosensitiser.

Immune system

If HERC4 is unlikely to increase radiosensitivity by altering cell proliferation, it might instead increase the magnitude of immune response that is mounted in response to IR, although, short of localised cytokine signalling, this would not explain the phenotype observed in the monoculture conditions used for the initial CRISPR screen. Terms related to the immune system were enriched for both experiments, and antigen presentation was the most common theme within this. In the total proteome data, these terms focused on endogenous antigens, while proximity labelling data was skewed more towards exogenous ones. Minimising antigen presentation reduces display of cancer-specific neoantigens, making tumour cells less visible to the immune system, and correlating with the poor prognosis associated with increased HERC4 levels in many cancer types. It does not, however, reflect the positive correlation observed between HERC4 levels and MHC-related gene expression in melanoma and lung adenocarcinoma patients [Liu et al., 2024a]. On the other hand, Liu et al. also reported an increase in co-inhibitor molecules such as CD80/86 and CD274 (PD-L1) patients with higher HERC4 expression, the second of which was highlighted by pathway analysis of HERC4 interactors, and while HERC4 is also reportedly upregulated in response to viral infection in fish, this could be a control mechanism to dampen the immune response and prevent damage from excessive inflammation [Eslamloo et al., 2016; He et al., 2017; Gémez-Mata et al., 2021]. Upregulation of proteins that inhibit the second signal required for T-cell activation would complement downregulation of antigen-presenting proteins that provide the initial stimulatory signal, but fails to support the hypothesis that HERC4 increases radiosensitivity by facilitating an immune response to IR-induced damage. It is possible that the other immune-related terms identified by pathway analysis of putative HERC4 interactors offer a potential mechanism for this, but this seems doubtful given that, out of 6 analysis options, the terms were only identified by pathway analysis using the KEGG database, and such a function would be in opposition to the effects just discussed. Additionally, since the initial CRISPR screen was in *in vitro*,

immune responses cannot have contributed to the results, so any connection between HERC4 and the immune system cannot justify the initial hypothesis of HERC4 as a radio sensitiser.

HAUS1

Despite these limitations, the protein with the strongest connection to HERC4 in the mass spectrometry results may provide a mechanism to tie both themes together. HAUS1 was the only protein identified as significant in both knockout clones and in the HERC4 interactor dataset, and it combines the putative roles for HERC4 in both the cell cycle and the immune response. It was originally identified as a component of the human augmin complex involved in spindle and centrosome assembly [Lawo et al., 2009], and it has since been implicated in immune cell infiltration in several cancer types [Liu et al., 2024b; Wang et al., 2023; Yao et al., 2022; Tang et al., 2024]. It was found to be upregulated in glioma, including the TCGA glioblastoma dataset, and correlated with increased immune cell infiltration and worse prognosis. In one glioma study, T_H2 cells were among the specific types of infiltrating cell identified, which fits with the increased MHC class II expression observed here but does not directly explain the correlation with prognosis [Yao et al., 2022]. In HCC, higher HAUS1 levels were also associated with higher expression of immune checkpoint proteins [Tang et al., 2024], reinforcing the link between HERC4 and ICI sensitivity found by Liu et al. [Liu et al., 2024a]. However, the total proteome data presented here demonstrates elevated HAUS1 levels after HERC4 knockout, suggesting that the 2 proteins should have opposing effects on the immune response. The AlphaFold model gives poor evidence for a direct interaction between HERC4 and HAUS1, and proximity labelling data did not indicate HERC4-mediated degradation of HAUS1, so it is likely that the increased HAUS1 abundance after HERC4 loss is through an indirect mechanism. This creates scope for other influences on HAUS1 activity, potentially pushing it towards its function in the immune system and away from centrosomes and the cell cycle. This would also partly align the observations of Tang et al. with the data shown here – when HAUS1 was knocked down in the HCC model, apoptosis increased, matching the trends in enriched terms for both mass spectrometry

datasets. HAUS1 knockdown also reduced proliferation and caused a shift in cell cycle distribution, which was not evident in the cell cycle data in the previous chapter, but in glioblastoma stem cells, HAUS1 knockdown did not influence proliferation, so this may be a cell type-specific effect [Tang et al., 2024; Ding et al., 2017]. It is possible that HERC4 indirectly downregulates HAUS1 expression and facilitates sequestration of residual protein in complexes involved in immune responses rather than the cell cycle, but additional data would be required to add mechanistic detail and to reconcile this model fully with the phenotypic data presented previously.

It is similarly unclear how HAUS1 fits with previously published substrates, or other putative HERC4 interactors or targets identified here. The Hippo signalling pathway has the most opportunity to bridge the gap. It is the only process to contain multiple published substrates as well as proteins highlighted by both total proteome and proximity labelling data, and it is activated by the presence of extra centrosomes [Ganem et al., 2014]. MST1/2 are also implicated in correct centrosome detachment during mitosis, separately from their signalling role, and cells are twice as sensitive to HAUS1 loss when upstream activator TRIM69 is removed [Wang et al., 2023]. If HERC4 indirectly downregulates HAUS1, there may be greater reliance on MST1/2 use for centrosome segregation, drawing it away from the Hippo signalling pathway and reducing activation of its target, LATS1. Lower LATS1 activity would relieve inhibition of transcription factor YAP/TAZ and increase expression of Hippo target genes such as SERPINE1 and BIRC3, consistent with their downregulation in HERC4 knockout Clone 1 and both clones respectively. BIRC3 expression, however, is also reliant on TEAD, which was less abundant when HERC4 was present. It should also be noted that while degradation of the 2 published substrates in this pathway, SAV1 and LATS1/2, would reinforce the effects of less MST1/2 signalling activity, neither was identified even as an interactor, although SAV1 was close to statistical significance. The effect of HERC4 levels on the Wnt pathway needed for the third component of the complex involved in BIRC3 transcription is also contradictory, with WNT5A increasing and FZD6 decreasing after HERC4 loss despite both facilitating signal transduction, and further

information is needed to elucidate the influence of HERC4 on the interactors identified by proximity labelling. Consequently, there is a strong indication of HERC4 involvement in Hippo signalling, but the data is insufficient for more detailed conclusions.

3.5 – Conclusions and Future Directions

The data presented here supports some of the roles for HERC4 identified in the literature, particularly involvement in the immune system and cancer cell growth, as well as suggesting new areas for investigation such as DNA repair, many of which may influence radiosensitivity. However, the functions suggested by this data point towards a radioprotective effect rather than the radiosensitising phenotype observed in the CRISPR screen underpinning this project. These results also fail to identify a clear mechanistic basis for any of the putative functions. Out of 11 published interactors and substrates, only EGFR behaved as expected in the mass spectrometry data, and very few proteins changed consistently across these datasets. HAUS1 was the only protein to be significant in both HERC4 knockout clones and in the total proximity data, but it was only identified as an interactor, not a substrate, indicating that its change in abundance after HERC4 loss is likely to be indirect and unaffected by proteasome activity. A very tentative model suggests that HERC4 indirectly reduces HAUS1 expression, then directly prioritises its involvement in the immune system over centrosome segregation, but significant evidence would be required to substantiate this extrapolation of the current results.

The first step in gaining this evidence would be validation of HAUS1 as both an interactor of HERC4 and a target of its activity, albeit an indirect one, likely through additional IP experiments and analysis of HAUS1 levels and localisation after HERC4 loss and overexpression. Similarly, more rigorous validation of other proteins identified in one or both mass spectrometry datasets may give more certainty to their interpretation. It is also plausible that the lack of a standout theme in these results indicates a role in processes that require additional stimulation to be detected, such as signalling pathways or DNA damage responses, or that other proteins are compensating, although this should be less evident in an over-expression model. A HERC4 overexpression dataset might therefore be a valuable extension of the total proteome data presented here, and different

conditions (especially IR) or removal of other proteins may be needed in both experiments to shed more light on HERC4 interactors and effectors.

3.6 – References

Abramson, J., Adler, J., Dunger, J.; Evans, R.; Green, T.; Pritzel, A.; Ronneberger, O.; Willmore, L.; Ballard, A.J.; Bambrick, J.; Bodenstein, S.W.; Evans, D.A.; Hung, C.C.; O'Neill, M.; Reiman, D.; Tunyasuvunakool, K.; Wu, Z.; Žemgulytė, A.; Arvaniti, E.; Beattie, C.; Bertolli, O.; Bridgland, A.; Cherepanov, A.; Congreve, M.; Cowen-Rivers, A.I.; Cowie, A.; Figurnov, M.; Fuchs, F.B.; Gladman, H.; Jain, R.; Khan, Y.A.; Low, C.M.R.; Perlin, K.; Potapeno, Savy, P.; Singh, S.; Stecula, A.; Thillaisundaram, A.; Tong, C.; Yakneen, S.; Zhong, E.D.; Zielinski, M.; Žídek, A.; Bapst, V.; Kohli, P.; Jaderberg, M.; Hassabis, D. and Jumper, J.M. (2024) Accurate Structure Prediction of Biomolecular Interactions with AlphaFold 3 *Nature* 630:493-500

Aerne, B.L.; Gailite, I.; Sims, D. and Tapon, N. (2015) Hippo Stabilises Its Adaptor Salvador by Antagonising the HECT Ubiquitin Ligase Herc4 *PLOS One* 10(6):e0131113

Amaar, Y.G.; Thompson, G.R.; Linkhart, T.A.; Chen, S.T.; Baylink, D.J. and Mohan, S. (2002) Insulin-like Growth Factor-binding Protein 5 (IGFBP-5) Interacts with a Four and a Half LIM Protein 2 (FHL2) *Journal of Biological Chemistry* 277(14):12053-12060

Asif, M.; Khayyat, A.I.A.; Alawbathani, S.; Abdullah, U.; Sanner, A.; Georgomanolis, T.; Haasters, J.; Becker, K.; Budde, B.; Becker, C.; Thiele, H.; Baig, S.M.; Isidoro-García, M.; Winter, D.; Pogoda, H.M.; Muhammad, S.; Hammerschmidt, M.; Kraft, F.; Kurth, I.; Martin, H.G.; Wagner, M.; Nürnberg, P. and Hussain, M.S. (2024) Biallelic Loss-of-Function Variants of *ZFTRAF1* Cause Neurodevelopmental Disorder with Microcephaly and Hypotonia *Genetics in Medicine* 26(7):101143

Barroso-Gomila, O., Merino-Cacho, L., Muratore, V.; Perez, C.; Taibi, V.; Maspero, E.; Azkargorta, M.; Iloro, I.; Trulsson, F.; Vertegaal, A.C.O.; Mayor, U.; Elortza, F.; Polo, S.; Barrio, R. and Sutherland, J.D. BioE3 Identifies Specific Substrates of Ubiquitin E3 Ligases *Nature Communications* 14:7656

Canuto, F.; Duret, S.; Dubrana, M.P.; Claverol, S.; Malembic-Maher, S.; Foissac, X.and Arricau-Bouvery, N. (2023) A Knockdown Gene Approach Identifies an Insect Vector Membrane Protein with Leucin-Rich Repeats as One of the Receptors for the VmpA Adhesin of Flavescence Dorée Phytoplasma *Frontiers in Cellular and Infection Microbiology* 13:1289100

Cho, K.F.; Branon, T.C.; Udeshi, N.D.; Myers, S.A.; Carr, S.A. and Ting, A.Y. (2020) Proximity Labeling in Mammalian Cells with TurboID and Split-TurboID *Nature Protocols* 15(12):3971-3999

Cox, J.; Hein, M.Y.; Luber, C.A.; Paron, I.; Nagaraj, N. and Mann, M. (2014) Accurate Proteome-wide Label-free Quantification by Delayed Normalization and Maximal Peptide Ratio Extraction, Termed MaxLFQ *Technological Innovation and Resources* 13(9):2513-2526

Demichev, V.; Messner, C.B..; Vernardis, S.I.; Lilley, K.S. and Ralser, M. (2019) DIA-NN: Neural Networks and Interference Correction Enable Deep Proteome Coverage in High Throughput *Nature Methods* 17(1):41-44

Ding, Y.; Herman, J.A.; Toledo, C.M.; Lang, J.M.; Corrin, P.; Girard, E.J.; Basom, R.; Delrow, J.J.; Olson, J.M. and Paddison, P.J. (2017) ZNF131 Suppresses Centrosome Fragmentation in Glioblastoma Stem-Like Cells Through Regulation of HAUS5 *Oncotarget* 8(30):48545-48562

Eslamloo, K.; Xue, X.; Booman, M.; Smith, N.C. and Rise, M.L. (2016) Transcriptome Profiling of the Antiviral Immune Response in Atlantic Cod Macrophages *Developmental & Comparative Immunology* 63:187-205

Ganem, N.J.; Cornils, H.; Chiu, S.Y.; O'Rourke, K.P.; Arnaud, J.; Yimlamai, D.; Théry, M.; Camargo, F.D. and Pellman, D. (2014) Cytokinesis Failure Triggers Hippo Tumor Suppressor Pathway Activation *Cell* 158(4):833-848

Gémez-Mata, J.; Labella, A.M.; Bandín, I.; Borrego, J.J. and García-Rosado (2021) Immunogene Expression Analysis in Betanodavirus Infected-Senegalese Sole Using an OpenArray® Platform *Gene* 77:145430

Gene Ontology Consortium (2004) The Gene Ontology (GO) Database and Informatics Resource *Nucleic Acids Research* 32(suppl_1):D258-D261

He, L.; Zhang, A.; Xiong, L.; Li, Y.; Huang, R.; Liao, L.; Zhu, Z. and Wang, Y. (2017) Deep Circular RNA Sequencing Provides Insights into the Mechanism Underlying Grass Carp Reovirus Infection *International Journal Molecular Sciences* 18(9):1977

Huang, F.; Tang, X.; Sun, T.; Wang, G.; Ru, Q. and Zheng, Y. (2021) SAV1, Regulated by HERC4, Inhibits the Proliferation, Migration, and Invasion of Hepatocellular Carcinoma *Translational Cancer Research* 10(1):349-360

Huang, P.; Deng, W.; Bao, H.; Lin, Z.; Liu, M.; Wu, J.; Zhou, X.; Qiao, M.; Yang, Y.; Cai, H.; Rao, F.; Chen, J.; Chen, D.; Lu, J.; Wang ,H.; Qin, A. and Kong, S. (2022) SOX4 Facilitates PGR Protein Stability and FOXO1 Expression Conducive for Human Endometrial Decidualization *eLife* 11:e72073

Huang, X.; Huo, L.; Xiao, B.; Ouyang, Y.; Chen, F.; Li, J.; Zheng, X.; Wei, D.; Wu, Y.; Zhang, R.; Cao, X.; Kang, T. and Gao, Y. (2024) Activating STING/TBK1 Suppresses Tumor Growth via Degrading HPV16/18 E7 Oncoproteins in Cervical Cancer *Cell Death and Differentiation* 31:78-89

Jeffrey, G.A. (1997) An Introduction to Hydrogen Bonding *Oxford University Press*

Jiang, W.; Yao, X.; Shan, Z.; Li, W.; Gao, Y. and Zhang, Q. (2019) E3 Ligase Herc4 Regulates Hedgehog Signalling Through Promoting Smoothened Degradation *Journal of Molecular Cell Biology* 11(9):791-803

Kanehisa, M.; Furumichi, M.; Sato, Y.; Ishiguro-Watanabe, M. and Tanabe, M. (2021) KEGG: Integrating Viruses and Cellular Organisms *Nucleic Acids Research* 49(D1):D545-D551

Khatri, P.; Sirota, M. and Butte, A.J. (2012) Ten Years of Pathway Analysis: Current Approaches and Outstanding Challenges *PLoS Computational Biology* 8(2):e1002375

Lawo, S.; Bashkurov, M.; Mullin, M.; Ferreria, M.G.; Kittler, R.; Habermann, B.; Tagliaferro, A.; Poser, I.; Hutchins, J.R.A.; Hegemann, B.; Pinchev, D.; Buchholz, F.; Peters, J.M.; Hyman, A.A.; Gingras, A.C. and Pelletier, L. (2009) HAUS, the 8-Subunit Human Augmin Complex, Regulates Centrosome and Spindle Integrity *Current Biology* 19(10):816-826

Liberzon, A.; Subramanian, A.; Pinchback, R.; Thorvaldsdóttir, H.; Tamayo, P. and Mesirov, J.P. (2011) Molecular Signatures Database (MSigDB) 3.0 *Bioinformatics* 27(12):1739-1740

Liu, M.; Zhao, Z.; Wang, C.; Sang, S.; Cui, Y.; Lv, C.; Yang, X.; Zhang, N.; Xiong, K.; Chen, B.; Dong, Q.; Liu, K. and Gu, Y. (2024a) Harnessing Genetic Interactions for Prediction of Immune Checkpoint Inhibitors Response Signature in Cancer Cells *Cancer Letters* 594:216991

Liu, S.; Yu, Y.; Xu, J.; Wang, Y. and Li, D. (2024b) Single-Cell and Bulk RNA-Sequencing Reveals Mitosis-Involved Gene HAUS1 is a Promising Indicator for Predicting Prognosis and Immune Responses in Prostate Adenocarcinoma (PRAD) *Cell Biology International* 48(8):1169-1184

Loechel, F.; Fox, J.W.; Murphy, G.; Albrechtsen, R. and Wewer, U.M. (2000) ADAM 12-S Cleaves IGFBP-3 and IGFBP-5 and Is Inhibited by TIMP-3 *Biochemical and Biophysical Research Communications* 278(3):511-515

Louis, D.N.; Perry, A.; Wesseling, P.; Brat, D.J.; Cree, I.A.; Figarella-Branger, D.; Hawkins, C.; Ng, H.K.; Pfister, S.M.; Reifenberger, G.; Soffietti, R.; von Deimling, A.; Ellison, D.W (2021) The 2021 WHO Classification of Tumors of the Central Nervous System: a summary *Neuro-Oncology* 23(8) 1231-1251

Miao, Z.; Xu, L.; Gu, W.; Ren, Y.; Li, R.; Zhang, S.; Chen, C.; Wang, H.; Ji, J. and Chen, J. (2024) A Targetable PRR11-DHODH Axis Drives Ferroptosis- and Temozolomide-Resistance in Glioblastoma *Redox Biology* 73:103220

Mutlu, M.; Schmidt, I.; Morrison, A.I.; Goretzki, B.; Freuler, F.; Begue, D.; Simic, O.; Pythoud, N.; Ahrne, E.; Kapps, S.; Roest, S.; Bonenfant, D.; Jeanpierre, D.; Tran, T.T.T.; Maher, R.; An, S.; Rietsch, A.; Nigsch, F.; Hofmann, A.; Reece-Hoyes, J.; Parker, C.N. and Guerini, D. (2024) Small Molecule Induced STING Degradation Facilitated by the HECT Ligase HERC4 *Nature Communications* 15:4584

Rodriguez, C.I. and Stewart, C.L. (2007) Disruption of the Ubiquitin Ligase *HERC4* Causes Defects in Spermatozoon Maturation and Impaired Fertility *Developmental Biology* 312(2):501-508

Senavirathna, L.; Hasapes, C.; Chen, R. and Pan, S. (2024) Accumulation of Intracellular Protein Advanced Glycation End Products Alters Cellular Homeostasis for Protein Clearance in Pancreatic Ductal Epithelial Cells *Biochemistry* 63(14):1723-1729

Subramanian, A.; Tamayo, P.; Mootha, V.K.; Mukherjee, S.; Ebert, B.L.; Gillette, M.A.; Paulovich, A.; Pomeroy, S.L.; Golub, T.R.; Lander, E.S. and Mesirov, J.P. (2005) Gene Set Enrichment Analysis: A Knowledge-Based Approach for Interpreting Genome-Wide Expression Profiles *Proceedings of the National Academy of Sciences* 102(43):15545-15550

Sun, H.J.; Peng, M.H.; Feng, Z.Y.; Fu, H. and Liu, X.W. (2026) HERC4 Downregulates KRT19 to Promote Lung Adenocarcinoma, Migration, Invasion and EMT *Translational Oncology* 63:102593

Sun, T.; Geng, S.; Ru, Q. and Zheng, Y. (2025) METTL3 and HERC4: Elevated Expression and Impact on Hepatocellular Carcinoma Progression *Cancer Biotherapy and Radiopharmaceuticals* 40(3):173-184

Sun, X.; Sun, B.; Cui, M. and Zhou, Z. (2019) HERC4 Exerts an Anti-Tumor Role Through Destabilizing the Oncoprotein Smo *Biochemical and Biophysical Research Communications* 513(4):1013-1018

Tang, L.; Chen, Z.; Wei, C.; Liu, H.; Wang, B.; Yu, T.; Tao, X.; Yang, J.; Guan, J.; Yi, J.; Zhu, H.; Li, C.; Tang, P. and Wang, K. (2024) The Significance of HAUS1 and Its Relationship with Immune Microenvironment in Hepatocellular Carcinoma *Journal of Cancer* 15(5):1328-1341

Tyanova, S.; Temu, T.; Sinitcyn, P.; Carlson, A.; Hein, M.Y.; Geiger, T.; Mann, M. and Cox, J. (2016) The Perseus Computational Platform for Comprehensive Analysis of (Prote)Omics Data *Nature Methods* 13(9):731-740

Ulgen, E.; Ozisik, O. and Sezerman, O.U. (2019) pathfindR: An R Package for Comprehensive Identification of Enriched Pathways in Omics Data Through Active Subnetworks *Frontiers in Genetics* 10:858

Wang, Y.; Risteski, P.; Yang, Y.; Chen, H.; Droby, G.; Walens, A.; Jayaprakash, D.; Troester, M.; Herring, L.; Chernoff, J.; Tolić, I.M.; Bowser, J. and Vaziri, C. (2023) The TRIM69-MST2 Signaling Axis Regulates Centrosome Dynamics and Chromosome Segregation *Nucleic Acids Research* 51(19):10568-10589

Xie, F.; Liu, B.; Qiao, W.; He, J.Z.; Cheng, J.; Wang, Z.Y.; Hou, Y.M.; Zhang, X.; Xu, B.H.; Zhang, Y.; Chen, Y.G. and Zhang, M.X. (2024) Smooth Muscle NF90 Deficiency Ameliorates Diabetic Atherosclerotic Calcification in Male Mice via FBXW7-AGER1-AGEs Axis *Nature Communications* 15:4985

Xu, Y.; Ji, K.; Wu, M.; Hao, B.; Yao, K. and Xu, Y. (2019) A miRNA-HERC4 Pathway Promotes Breast Tumorigenesis by Inactivating Tumor Suppressor LATS1 *Protein & Cell* 10(8):595-605

Yao, Q.; Ge, X.; Lu, Z.; Shi, J.; Shen, J. and Chen, J. (2022) HAUS Augmin-Like Complex Subunit 1 Influences Tumour Microenvironment and Prognostic Outcomes in Glioma *Journal of Oncology* 2022:8027686

Yuan, B.; Liu, J.; Shi, A.; Cao, J.; Yu, Y.; Zhu, Y.; Zhang, C.; Qiu, Y.; Luo, H.; Shi, J.; Cao, X.; Xu, P.; Shen, L.; Liang, T.; Zhao, B. and Feng, X.H. (2023) HERC3 Promotes YAP/TAZ Stability and Tumorigenesis Independently of Its Ubiquitin Ligase Activity *The European Molecular Biology Organization Journal* 42(4):e111549

Zhang, W.; Zhang, X.; Chen, K. and Wang, Y. (2025) The Epidermal Growth Factor Receptor Regulates YAP Signalling and Promotes Diabetic Retinal Fibrosis by Modulating the Degradation SAV1 *Journal of Translation Medicine* 23:1319

Zhang, Z.; Li, M.; Lin, P.; Ren, Y.; He, Y.; Wang, S.; Xu, Y.; Cao, B.; Wang, G.; Moran, M.F. and Mao, X. (2023) The Ubiquitin Ligase HERC4 Suppresses MafA Transcriptional Activity Triggered by GSK3β in Myeloma by Atypical K63-Linked Polyubiquitination *Journal of Biological Chemistry* 299(5):104675

Zhang, Z.; Tong, J.; Tang, X.; Juan, J.; Cao, B.; Hurren, R.; Chen, G.; Taylor, P.; Xu, X.; Shi, C.X.; Du, J.; Hou, J.; Wang, G.; Wu, D.; Stewart, A.K.; Schimmer, A.D.; Moran, M.F. and Mao, X. (2016) The Ubiquitin Ligase HERC4 Mediates c-Maf Ubiquitination and Delays the Growth of Multiple Myeloma Xenografts in Nude Mice *Blood* 127(13):1676-1686

Zheng, Y.; Li, J.; Pan, C.; Zhou, G.; Zhuge, L.; Jin, L. and Fang, P. (2017) HERC4 Is Overexpressed in Hepatocellular Carcinoma and Contributes to the Proliferation and Migration of Hepatocellular Carcinoma Cells *DNA and Cell Biology* 36(6):490-500

Zhu, Q.; Yang, X. and Lv, Y. (2024) HERC4 Modulates Ovarian Cancer Cell Proliferation by Regulating SMO-Elicited Hedgehog Signaling *Biochimica et Biophysica Acta - General Subjects* 1868(4):130557

3.7 – Appendices

Appendix 1 – antibody catalogue numbers

Target protein	Dilution	Catalogue number
HERC4	1:1000	13691-1-AP
SMO	1:1000	sc-166685
SAV1	1:1000	sc-374366
VEGFR	1:1000	13687-1-AP
USP11	1:1000	sc-365528
Rabbit IgG	1:10,000 1:10,000	sc-2027 31460
Mouse IgG	1:10,000 1:5,000	sc-2025 31430

Appendix 2 – code for analysis of mass spectrometry data

Ferris_MS_Rscripts

Appendix 3 – GOBP terms for differentially expressed genes shared by both clones

Genes	$-\log_{10}$(p-value)	$\log_2$(fold change)	Most significant clone
ADAM12	3.260397	-2.15948	1
ANATOMICAL STRUCTURE FORMATION INVOLVED IN MORPHOGENESIS, BLOOD VESSEL MORPHOGENESIS, CELL ADHESION, CIRCULATORY SYSTEM DEVELOPMENT, MUSCLE CELL DIFFERENTIATION, MUSCLE STRUCTURE DEVELOPMENT, MYOBLAST FUSION, MYOTUBE DIFFERENTIATION, POSITIVE REGULATION OF DEVELOPMENTAL PROCESS, POSITIVE REGULATION OF MULTICELLULAR ORGANISMAL PROCESS, POSITIVE REGULATION OF VASCULATURE DEVELOPMENT, PROTEOLYSIS, REGULATION OF ANATOMICAL STRUCTURE MORPHOGENESIS, REGULATION OF MULTICELLULAR ORGANISMAL DEVELOPMENT, REGULATION OF VASCULATURE DEVELOPMENT, STRIATED MUSCLE CELL DIFFERENTIATION, SYNCYTIUM FORMATION, TUBE DEVELOPMENT, TUBE MORPHOGENESIS, VASCULATURE DEVELOPMENT			
AKR1C2	1.607601	1.594355	3
ALCOHOL METABOLIC PROCESS, AMINOGLYCOSIDE ANTIBIOTIC METABOLIC PROCESS, C21 STEROID HORMONE METABOLIC PROCESS, CARBOHYDRATE DERIVATIVE METABOLIC PROCESS, CELLULAR RESPONSE TO ALCOHOL, CELLULAR RESPONSE TO ENDOGENOUS STIMULUS, CELLULAR RESPONSE TO FATTY ACID, CELLULAR RESPONSE TO HORMONE STIMULUS, CELLULAR RESPONSE TO KETONE, CELLULAR RESPONSE TO LIPID, CELLULAR RESPONSE TO OXYGEN CONTAINING COMPOUND, CELLULAR RESPONSE TO PROSTAGLANDIN STIMULUS, DIGESTION, EPITHELIAL CELL DIFFERENTIATION, EPITHELIUM DEVELOPMENT, FATTY ACID METABOLIC PROCESS, GLYCOSIDE METABOLIC PROCESS, GLYCOSYL COMPOUND METABOLIC PROCESS, G PROTEIN COUPLED RECEPTOR SIGNALLING PATHWAY, HORMONE METABOLIC PROCESS, ICOSANOID METABOLIC PROCESS, KETONE METABOLIC PROCESS, LIPID METABOLIC PROCESS, MONOCARBOXYLIC ACID METABOLIC PROCESS, OLEFINIC COMPOUND METABOLIC PROCESS, ORGANIC ACID METABOLIC PROCESS, PHOSPHATIDYLINOSITOL 3 KINASE PROTEIN KINASE B SIGNAL TRANSDUCTION, POLYKETIDE METABOLIC PROCESS, POSITIVE REGULATION OF CELL POPULATION PROLIFERATION, POSITIVE REGULATION OF INTRACELLULAR SIGNAL TRANSDUCTION, POSITIVE REGULATION OF PHOSPHATIDYLINOSITOL 3 KINASE PROTEIN KINASE B SIGNAL TRANSDUCTION, POSITIVE REGULATION OF SIGNALLING, PRIMARY ALCOHOL METABOLIC PROCESS, PROGESTERONE METABOLIC PROCESS, PROSTANOID METABOLIC PROCESS, REGULATION OF CELL POPULATION PROLIFERATION, REGULATION OF HORMONE LEVELS, RESPONSE TO ALCOHOL, RESPONSE TO ENDOGENOUS STIMULUS, RESPONSE TO FATTY ACID, RESPONSE TO HORMONE, RESPONSE TO KETONE, RESPONSE TO LIPID, RESPONSE TO OXYGEN CONTAINING COMPOUND, RESPONSE TO PROSTAGLANDIN, RESPONSE TO PROSTAGLANDIN D, SECONDARY METABOLIC PROCESS, SMALL MOLECULE METABOLIC PROCESS, STEROID METABOLIC PROCESS, TERTIARY ALCOHOL METABOLIC PROCESS, UNSATURATED FATTY ACID METABOLIC PROCESS			
ANKRD10	2.261915	2.326111	1
ESTABLISHMENT OF PROTEIN LOCALISATION, ESTABLISHMENT OF PROTEIN LOCALISATION TO ORGANELLE, PROTEIN LOCALISATION TO ORGANELLE, PROTEIN TARGETING			
BIRC3	2.443451	2.665515	1
ACTIVATION OF IMMUNE RESPONSE, ACTIVATION OF INNATE IMMUNE RESPONSE, APOPTOTIC PROCESS, BIOLOGICAL PROCESS INVOLVED IN INTERSPECIES INTERACTION BETWEEN ORGANISMS, CANONICAL NF KAPPAB SIGNAL TRANSDUCTION, CELL CYCLE, CYTOKINE MEDIATED SIGNALLING PATHWAY, CYTOPLASMIC PATTERN RECOGNITION RECEPTOR SIGNALLING PATHWAY, DEFENSE RESPONSE TO OTHER ORGANISM, DEFENSE RESPONSE TO SYMBIONT, DEVELOPMENTAL PROCESS INVOLVED IN REPRODUCTION, GAMETE GENERATION, IMMUNE RESPONSE REGULATING SIGNALLING PATHWAY, INFLAMMATORY RESPONSE, INTRACELLULAR RECEPTOR SIGNALLING PATHWAY, MALE GAMETE GENERATION, MULTICELLULAR ORGANISMAL REPRODUCTIVE PROCESS, NECROPTOTIC PROCESS, NEGATIVE REGULATION OF PROGRAMMED CELL DEATH, NEGATIVE REGULATION OF PROGRAMMED NECROTIC CELL DEATH, NON CANONICAL NF KAPPAB SIGNAL TRANSDUCTION, NUCLEOTIDE BINDING DOMAIN LEUCINE RICH REPEAT CONTAINING RECEPTOR SIGNALLING PATHWAY, POSITIVE REGULATION OF CANONICAL NF KAPPAB SIGNAL TRANSDUCTION, POSITIVE REGULATION OF DEFENSE RESPONSE, POSITIVE REGULATION OF IMMUNE RESPONSE, POSITIVE REGULATION OF IMMUNE SYSTEM PROCESS, POSITIVE REGULATION OF INTRACELLULAR SIGNAL TRANSDUCTION, POSITIVE REGULATION OF POST TRANSLATIONAL PROTEIN MODIFICATION, POSITIVE REGULATION OF PROTEIN METABOLIC PROCESS, POSITIVE REGULATION OF PROTEIN MODIFICATION PROCESS, POSITIVE REGULATION OF PROTEIN UBIQUITINATION, POSITIVE REGULATION OF RESPONSE TO BIOTIC STIMULUS, POSITIVE REGULATION OF RESPONSE TO EXTERNAL STIMULUS, POSITIVE REGULATION OF SIGNALLING, POST TRANSLATIONAL PROTEIN MODIFICATION, PROGRAMMED NECROTIC CELL			

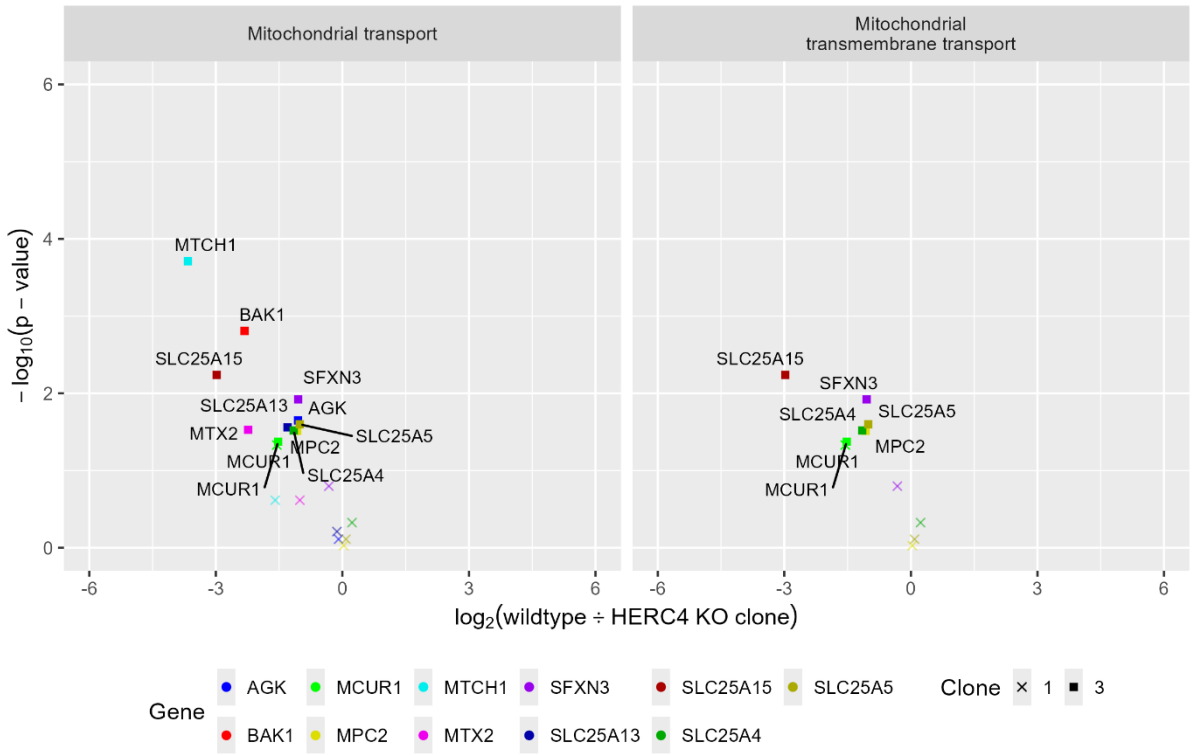
DEATH, PROTEIN MODIFICATION BY SMALL PROTEIN CONJUGATION, REGULATION OF CELL CYCLE, REGULATION OF CYTOPLASMIC PATTERN RECOGNITION RECEPTOR SIGNALLING PATHWAY, REGULATION OF DEFENSE RESPONSE, REGULATION OF IMMUNE RESPONSE, REGULATION OF IMMUNE SYSTEM PROCESS, REGULATION OF INFLAMMATORY RESPONSE, REGULATION OF INNATE IMMUNE RESPONSE, REGULATION OF NUCLEOTIDE BINDING DOMAIN LEUCINE RICH REPEAT CONTAINING RECEPTOR SIGNALLING PATHWAY, REGULATION OF PATTERN RECOGNITION RECEPTOR SIGNALLING PATHWAY, REGULATION OF POST TRANSLATIONAL PROTEIN MODIFICATION, REGULATION OF PROGRAMMED CELL DEATH, REGULATION OF PROGRAMMED NECROTIC CELL DEATH, REGULATION OF PROTEIN METABOLIC PROCESS, REGULATION OF PROTEIN MODIFICATION PROCESS, REGULATION OF PROTEIN UBIQUITINATION, REGULATION OF RESPONSE TO BIOTIC STIMULUS, REGULATION OF RESPONSE TO EXTERNAL STIMULUS, REGULATION OF RESPONSE TO STRESS, REGULATION OF RIG I SIGNALLING PATHWAY, REGULATION OF TOLL LIKE RECEPTOR SIGNALLING PATHWAY, REPRODUCTIVE PROCESS, RESPONSE TO PEPTIDE, RESPONSE TO TUMOUR NECROSIS FACTOR, RIG I SIGNALLING PATHWAY, SEXUAL REPRODUCTION, TOLL LIKE RECEPTOR SIGNALLING PATHWAY, TUMOUR NECROSIS FACTOR MEDIATED SIGNALLING PATHWAY			
CLUH	3.447429	-3.53839	1
INTRACELLULAR DISTRIBUTION OF MITOCHONDRIA, MITOCHONDRION DISTRIBUTION, MITOCHONDRION LOCALISATION, MITOCHONDRION ORGANISATION, ORGANELLE LOCALISATION			
CRABP2	5.462445	3.74395	3
APPENDAGE DEVELOPMENT, APPENDAGE MORPHOGENESIS, AXON DEVELOPMENT, CELL GROWTH, CELL MORPHOGENESIS, CELL MORPHOGENESIS INVOLVED IN NEURON DIFFERENTIATION, CELL PROJECTION MORPHOGENESIS, CELL PROJECTION ORGANISATION, COLLATERAL SPROUTING, DEVELOPMENTAL CELL GROWTH, DEVELOPMENTAL GROWTH, DEVELOPMENTAL GROWTH INVOLVED IN MORPHOGENESIS, EMBRYONIC APPENDAGE MORPHOGENESIS, EMBRYONIC FORELIMB MORPHOGENESIS, EMBRYONIC MORPHOGENESIS, EMBRYO DEVELOPMENT, EPIDERMIS DEVELOPMENT, FATTY ACID TRANSPORT, FORELIMB MORPHOGENESIS, GENERATION OF NEURONS, GROWTH, HORMONE METABOLIC PROCESS, ISOPRENOID METABOLIC PROCESS, LIPID LOCALISATION, LIPID METABOLIC PROCESS, MONOCARBOXYLIC ACID METABOLIC PROCESS, MONOCARBOXYLIC ACID TRANSPORT, NEUROGENESIS, NEURON DEVELOPMENT, ORGANIC ACID METABOLIC PROCESS, ORGANIC ACID TRANSPORT, ORGANIC ANION TRANSPORT, POSITIVE REGULATION OF AXONOGENESIS, POSITIVE REGULATION OF CELLULAR COMPONENT ORGANISATION, POSITIVE REGULATION OF CELL DEVELOPMENT, POSITIVE REGULATION OF CELL DIFFERENTIATION, POSITIVE REGULATION OF CELL GROWTH, POSITIVE REGULATION OF CELL PROJECTION ORGANISATION, POSITIVE REGULATION OF COLLATERAL SPROUTING, POSITIVE REGULATION OF DEVELOPMENTAL GROWTH, POSITIVE REGULATION OF DEVELOPMENTAL PROCESS, POSITIVE REGULATION OF GROWTH, POSITIVE REGULATION OF MULTICELLULAR ORGANISMAL PROCESS, POSITIVE REGULATION OF NERVOUS SYSTEM DEVELOPMENT, POSITIVE REGULATION OF NEUROGENESIS, REGULATION OF ANATOMICAL STRUCTURE MORPHOGENESIS, REGULATION OF ANATOMICAL STRUCTURE SIZE, REGULATION OF AXONOGENESIS, REGULATION OF CELLULAR COMPONENT SIZE, REGULATION OF CELL DEVELOPMENT, REGULATION OF CELL DIFFERENTIATION, REGULATION OF CELL GROWTH, REGULATION OF CELL PROJECTION ORGANISATION, REGULATION OF CELL SIZE, REGULATION OF COLLATERAL SPROUTING, REGULATION OF DEVELOPMENTAL GROWTH, REGULATION OF EXTENT OF CELL GROWTH, REGULATION OF GROWTH, REGULATION OF HORMONE LEVELS, REGULATION OF MULTICELLULAR ORGANISMAL DEVELOPMENT, REGULATION OF NERVOUS SYSTEM DEVELOPMENT, REGULATION OF NEUROGENESIS, REGULATION OF NEURON PROJECTION DEVELOPMENT, RETINOIC ACID METABOLIC PROCESS, SMALL MOLECULE METABOLIC PROCESS, TERPENOID METABOLIC PROCESS			
FHL1	4.580013	3.09308	1
ANIMAL ORGAN MORPHOGENESIS, CELL CYCLE, CELL CYCLE G1 S PHASE TRANSITION, CELL CYCLE G2 M PHASE TRANSITION, CELL CYCLE PHASE TRANSITION, CELL CYCLE PROCESS, CELL GROWTH, GROWTH, MEMBRANE DEPOLARISATION, METAL ION TRANSPORT, MITOTIC CELL CYCLE, MITOTIC CELL CYCLE PHASE TRANSITION, MITOTIC CELL CYCLE PROCESS, MONOATOMIC CATION TRANSMEMBRANE TRANSPORT, MONOATOMIC CATION TRANSPORT, MONOATOMIC ION TRANSMEMBRANE TRANSPORT, MONOATOMIC ION TRANSPORT, MUSCLE ORGAN DEVELOPMENT, MUSCLE STRUCTURE DEVELOPMENT, NEGATIVE REGULATION OF CELL CYCLE, NEGATIVE REGULATION OF CELL CYCLE G1 S PHASE TRANSITION, NEGATIVE REGULATION OF CELL CYCLE G2 M PHASE TRANSITION, NEGATIVE REGULATION OF CELL CYCLE PROCESS, NEGATIVE REGULATION OF CELL GROWTH, NEGATIVE REGULATION OF GROWTH, NEGATIVE REGULATION OF MITOTIC CELL CYCLE, NEGATIVE REGULATION OF MITOTIC CELL CYCLE PHASE TRANSITION, POSITIVE REGULATION OF MONOATOMIC ION TRANSMEMBRANE TRANSPORT, POSITIVE REGULATION OF MONOATOMIC ION TRANSPORT, POSITIVE REGULATION OF POTASSIUM ION TRANSMEMBRANE TRANSPORT, POSITIVE REGULATION OF POTASSIUM ION TRANSPORT, POSITIVE REGULATION OF TRANSMEMBRANE TRANSPORT, POSITIVE REGULATION OF TRANSPORT, POTASSIUM ION TRANSPORT, REGULATION OF ATRIAL CARDIAC MUSCLE CELL MEMBRANE DEPOLARISATION, REGULATION OF CELL CYCLE, REGULATION OF CELL CYCLE G1 S PHASE TRANSITION, REGULATION OF CELL CYCLE G2 M PHASE TRANSITION, REGULATION OF CELL			

CYCLE PHASE TRANSITION, REGULATION OF CELL CYCLE PROCESS, REGULATION OF CELL GROWTH, REGULATION OF GROWTH, REGULATION OF MEMBRANE DEPOLARISATION, REGULATION OF MEMBRANE POTENTIAL, REGULATION OF MITOTIC CELL CYCLE, REGULATION OF MITOTIC CELL CYCLE PHASE TRANSITION, REGULATION OF MONOATOMIC ION TRANSMEMBRANE TRANSPORT, REGULATION OF MONOATOMIC ION TRANSPORT, REGULATION OF POTASSIUM ION TRANSMEMBRANE TRANSPORT, REGULATION OF POTASSIUM ION TRANSPORT, REGULATION OF TRANSMEMBRANE TRANSPORT, REGULATION OF TRANSPORT, TRANSMEMBRANE TRANSPORT			
HAUS1	4.223518	-1.79141	3
CELL CYCLE, CELL CYCLE PROCESS, CELL DIVISION, CHROMOSOME SEGREGATION, CYTOSKELETON ORGANISATION, MEMBRANELESS ORGANELLE ASSEMBLY, MICROTUBULE BASED PROCESS, MICROTUBULE CYTOSKELETON ORGANISATION, MICROTUBULE NUCLEATION, MICROTUBULE ORGANIZING CENTER ORGANISATION, MICROTUBULE POLYMERISATION, MICROTUBULE POLYMERISATION OR DEPOLYMERISATION, ORGANELLE ASSEMBLY, PROTEIN CONTAINING COMPLEX ORGANISATION, PROTEIN POLYMERISATION, REGULATION OF CELLULAR COMPONENT BIOGENESIS, REGULATION OF CYTOSKELETON ORGANISATION, REGULATION OF MICROTUBULE BASED PROCESS, REGULATION OF MICROTUBULE CYTOSKELETON ORGANISATION, REGULATION OF MICROTUBULE NUCLEATION, REGULATION OF MICROTUBULE POLYMERISATION, REGULATION OF MICROTUBULE POLYMERISATION OR DEPOLYMERISATION, REGULATION OF ORGANELLE ORGANISATION, REGULATION OF PROTEIN CONTAINING COMPLEX ASSEMBLY, REGULATION OF PROTEIN POLYMERISATION, REGULATION OF SUPRAMOLECULAR FIBER ORGANISATION, SPINDLE ASSEMBLY, SPINDLE ORGANISATION, SUPRAMOLECULAR FIBER ORGANISATION			
KYNU	4.238009	-2.56296	1
ALPHA AMINO ACID METABOLIC PROCESS, AMINE METABOLIC PROCESS, AMINO ACID CATABOLIC PROCESS, AMINO ACID METABOLIC PROCESS, AROMATIC AMINO ACID FAMILY CATABOLIC PROCESS, AROMATIC AMINO ACID METABOLIC PROCESS, BENZENE CONTAINING COMPOUND METABOLIC PROCESS, BIOLOGICAL PROCESS INVOLVED IN INTERSPECIES INTERACTION BETWEEN ORGANISMS, DEFENSE RESPONSE TO OTHER ORGANISM, DEFENSE RESPONSE TO SYMBIONT, DE NOVO NAD BIOSYNTHETIC PROCESS FROM L TRYPTOPHAN, DICARBOXYLIC ACID BIOSYNTHETIC PROCESS, DICARBOXYLIC ACID METABOLIC PROCESS, ERYTHROSE 4 PHOSPHATE PHOSPHOENOLPYRUVATE FAMILY AMINO ACID CATABOLIC PROCESS, ERYTHROSE 4 PHOSPHATE PHOSPHOENOLPYRUVATE FAMILY AMINO ACID METABOLIC PROCESS, INDOLALKYLAMINE METABOLIC PROCESS, INDOLE CONTAINING COMPOUND CATABOLIC PROCESS, INDOLE CONTAINING COMPOUND METABOLIC PROCESS, KETONE CATABOLIC PROCESS, KETONE METABOLIC PROCESS, KYNURENINE METABOLIC PROCESS, L AMINO ACID CATABOLIC PROCESS, L KYNURENINE METABOLIC PROCESS, L TRYPTOPHAN CATABOLIC PROCESS TO KYNURENINE, MONOCARBOXYLIC ACID METABOLIC PROCESS, NAD BIOSYNTHETIC PROCESS, NAD METABOLIC PROCESS, NON PROTEINOGENIC AMINO ACID CATABOLIC PROCESS, NON PROTEINOGENIC AMINO ACID METABOLIC PROCESS, NUCLEOBASE CONTAINING SMALL MOLECULE METABOLIC PROCESS, NUCLEOSIDE PHOSPHATE BIOSYNTHETIC PROCESS, NUCLEOTIDE BIOSYNTHETIC PROCESS, NUCLEOTIDE METABOLIC PROCESS, ORGANIC ACID BIOSYNTHETIC PROCESS, ORGANIC ACID CATABOLIC PROCESS, ORGANIC ACID METABOLIC PROCESS, ORGANOPHOSPHATE BIOSYNTHETIC PROCESS, ORGANOPHOSPHATE METABOLIC PROCESS, PHOSPHORUS METABOLIC PROCESS, PROTEINOGENIC AMINO ACID METABOLIC PROCESS, PURINE CONTAINING COMPOUND BIOSYNTHETIC PROCESS, PURINE CONTAINING COMPOUND METABOLIC PROCESS, PURINE NUCLEOTIDE BIOSYNTHETIC PROCESS, PYRIDINE CONTAINING COMPOUND BIOSYNTHETIC PROCESS, PYRIDINE CONTAINING COMPOUND METABOLIC PROCESS, QUINOLINATE BIOSYNTHETIC PROCESS, QUINOLINATE METABOLIC PROCESS, RESPONSE TO NITROGEN COMPOUND, RESPONSE TO NUTRIENT, RESPONSE TO NUTRIENT LEVELS, RESPONSE TO OXYGEN CONTAINING COMPOUND, RESPONSE TO PEPTIDE, RESPONSE TO TYPE II INTERFERON, RESPONSE TO VITAMIN, SMALL MOLECULE BIOSYNTHETIC PROCESS, SMALL MOLECULE CATABOLIC PROCESS, SMALL MOLECULE METABOLIC PROCESS			
MAGEA10	5.764384	1.201423	1
NEGATIVE REGULATION OF NUCLEOBASE CONTAINING COMPOUND METABOLIC PROCESS, NEGATIVE REGULATION OF RNA METABOLIC PROCESS, NEGATIVE REGULATION OF TRANSCRIPTION BY RNA POLYMERASE II			
MCUR1	1.372937	-1.5222	3
CALCIUM IMPORT INTO THE MITOCHONDRION, CALCIUM ION HOMEOSTASIS, CALCIUM ION IMPORT, CALCIUM ION TRANSMEMBRANE TRANSPORT, CALCIUM ION TRANSPORT, CELLULAR HOMEOSTASIS, CHEMICAL HOMEOSTASIS, HOMEOSTATIC PROCESS, IMPORT INTO THE MITOCHONDRION, INORGANIC ION HOMEOSTASIS, INTRACELLULAR MONOATOMIC ION HOMEOSTASIS, METAL ION TRANSPORT, MITOCHONDRIAL CALCIUM ION HOMEOSTASIS, MITOCHONDRIAL CALCIUM ION TRANSMEMBRANE TRANSPORT, MITOCHONDRIAL TRANSMEMBRANE TRANSPORT, MITOCHONDRIAL TRANSPORT, MONOATOMIC CATION TRANSMEMBRANE TRANSPORT, MONOATOMIC CATION TRANSPORT, MONOATOMIC ION HOMEOSTASIS, MONOATOMIC ION TRANSMEMBRANE TRANSPORT, MONOATOMIC			

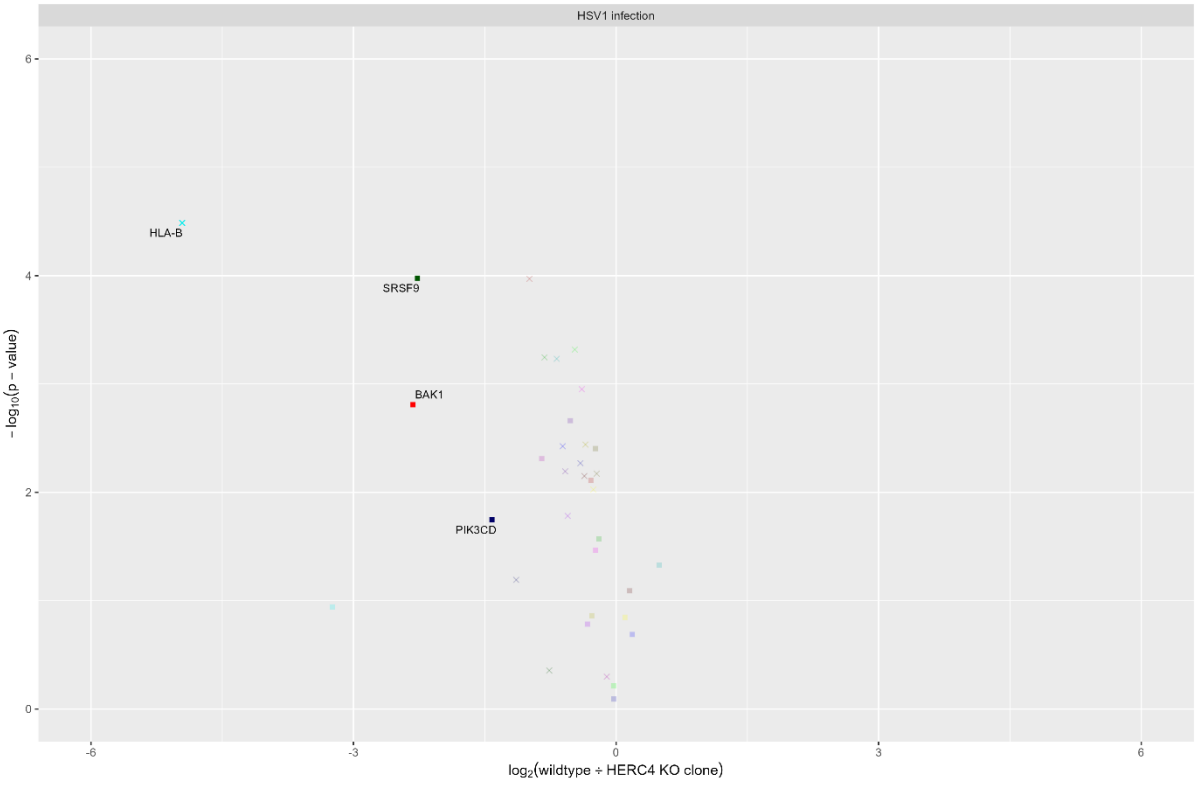
ION TRANSPORT, POSITIVE REGULATION OF MITOCHONDRIAL CALCIUM ION CONCENTRATION, TRANSMEMBRANE TRANSPORT			
MPZ	2.074678	3.711147	3
CELL ADHESION, CELL AGGREGATION, CELL-CELL ADHESION, CELL-CELL ADHESION VIA PLASMA MEMBRANE ADHESION MOLECULES, CELL-CELL SIGNALLING, ENSHEATHMENT OF NEURONS, SYNAPTIC SIGNALLING			
NNMT	2.93034	2.962638	3
ALKALOID METABOLIC PROCESS, AMIDE METABOLIC PROCESS, CARBOHYDRATE BIOSYNTHETIC PROCESS, CARBOHYDRATE METABOLIC PROCESS, GLUCOSE METABOLIC PROCESS, MACROMOLECULE DEACYLATION, METHYLATION, MONOSACCHARIDE BIOSYNTHETIC PROCESS, MONOSACCHARIDE METABOLIC PROCESS, POSITIVE REGULATION OF CARBOHYDRATE METABOLIC PROCESS, POSITIVE REGULATION OF GLUCONEOGENESIS, POSITIVE REGULATION OF GLUCOSE METABOLIC PROCESS, POSITIVE REGULATION OF PROTEIN METABOLIC PROCESS, POSITIVE REGULATION OF PROTEIN MODIFICATION PROCESS, POSITIVE REGULATION OF SMALL MOLECULE METABOLIC PROCESS, PROTEIN DEACETYLATION, PROTEIN DEACYLATION, PYRIDINE CONTAINING COMPOUND METABOLIC PROCESS, REGULATION OF CARBOHYDRATE BIOSYNTHETIC PROCESS, REGULATION OF CARBOHYDRATE METABOLIC PROCESS, REGULATION OF GLUCONEOGENESIS, REGULATION OF GLUCOSE METABOLIC PROCESS, REGULATION OF PROTEIN DEACETYLATION, REGULATION OF PROTEIN METABOLIC PROCESS, REGULATION OF PROTEIN MODIFICATION PROCESS, REGULATION OF SMALL MOLECULE METABOLIC PROCESS, SMALL MOLECULE BIOSYNTHETIC PROCESS, SMALL MOLECULE METABOLIC PROCESS, VITAMIN METABOLIC PROCESS, WATER SOLUBLE VITAMIN METABOLIC PROCESS			
PITPNC1	3.640029	-3.38585	1
INTERMEMBRANE LIPID TRANSFER, LIPID LOCALISATION, MEMBRANE ORGANISATION, ORGANOPHOSPHATE ESTER TRANSPORT, PHOSPHOLIPID TRANSPORT			
SERPING1	2.862837	1.497836	3
ACTIVATION OF IMMUNE RESPONSE, ADAPTIVE IMMUNE RESPONSE, ADAPTIVE IMMUNE RESPONSE BASED ON SOMATIC RECOMBINATION OF IMMUNE RECEPTORS BUILT FROM IMMUNOGLOBULIN SUPERFAMILY DOMAINS, BIOLOGICAL PROCESS INVOLVED IN INTERSPECIES INTERACTION BETWEEN ORGANISMS, B CELL MEDIATED IMMUNITY, CIRCULATORY SYSTEM PROCESS, COMPLEMENT ACTIVATION, COMPLEMENT ACTIVATION CLASSICAL PATHWAY, COMPLEMENT ACTIVATION LECTIN PATHWAY, DEFENSE RESPONSE TO OTHER ORGANISM, DEFENSE RESPONSE TO SYMBIONT, FIBRINOLYSIS, HEMOSTASIS, HUMORAL IMMUNE RESPONSE, HUMORAL IMMUNE RESPONSE MEDIATED BY CIRCULATING IMMUNOGLOBULIN, IMMUNE EFFECTOR PROCESS, LEUKOCYTE MEDIATED IMMUNITY, LYMPHOCYTE MEDIATED IMMUNITY, NEGATIVE REGULATION OF COAGULATION, NEGATIVE REGULATION OF COMPLEMENT ACTIVATION, NEGATIVE REGULATION OF DEFENSE RESPONSE, NEGATIVE REGULATION OF HUMORAL IMMUNE RESPONSE, NEGATIVE REGULATION OF IMMUNE EFFECTOR PROCESS, NEGATIVE REGULATION OF IMMUNE RESPONSE, NEGATIVE REGULATION OF IMMUNE SYSTEM PROCESS, NEGATIVE REGULATION OF INNATE IMMUNE RESPONSE, NEGATIVE REGULATION OF MULTICELLULAR ORGANISMAL PROCESS, NEGATIVE REGULATION OF RESPONSE TO BIOTIC STIMULUS, NEGATIVE REGULATION OF RESPONSE TO EXTERNAL STIMULUS, NEGATIVE REGULATION OF RESPONSE TO STIMULUS, NEGATIVE REGULATION OF RESPONSE TO WOUNDING, NEGATIVE REGULATION OF WOUND HEALING, POSITIVE REGULATION OF IMMUNE RESPONSE, POSITIVE REGULATION OF IMMUNE SYSTEM PROCESS, REGULATION OF BODY FLUID LEVELS, REGULATION OF COAGULATION, REGULATION OF COMPLEMENT ACTIVATION, REGULATION OF DEFENSE RESPONSE, REGULATION OF HUMORAL IMMUNE RESPONSE, REGULATION OF IMMUNE EFFECTOR PROCESS, REGULATION OF IMMUNE RESPONSE, REGULATION OF IMMUNE SYSTEM PROCESS, REGULATION OF INNATE IMMUNE RESPONSE, REGULATION OF RESPONSE TO BIOTIC STIMULUS, REGULATION OF RESPONSE TO EXTERNAL STIMULUS, REGULATION OF RESPONSE TO STRESS, REGULATION OF RESPONSE TO WOUNDING, REGULATION OF WOUND HEALING, RESPONSE TO WOUNDING, WOUND HEALING			
SQOR	4.847965	-4.86021	3
SULPHUR COMPOUND METABOLIC PROCESS			

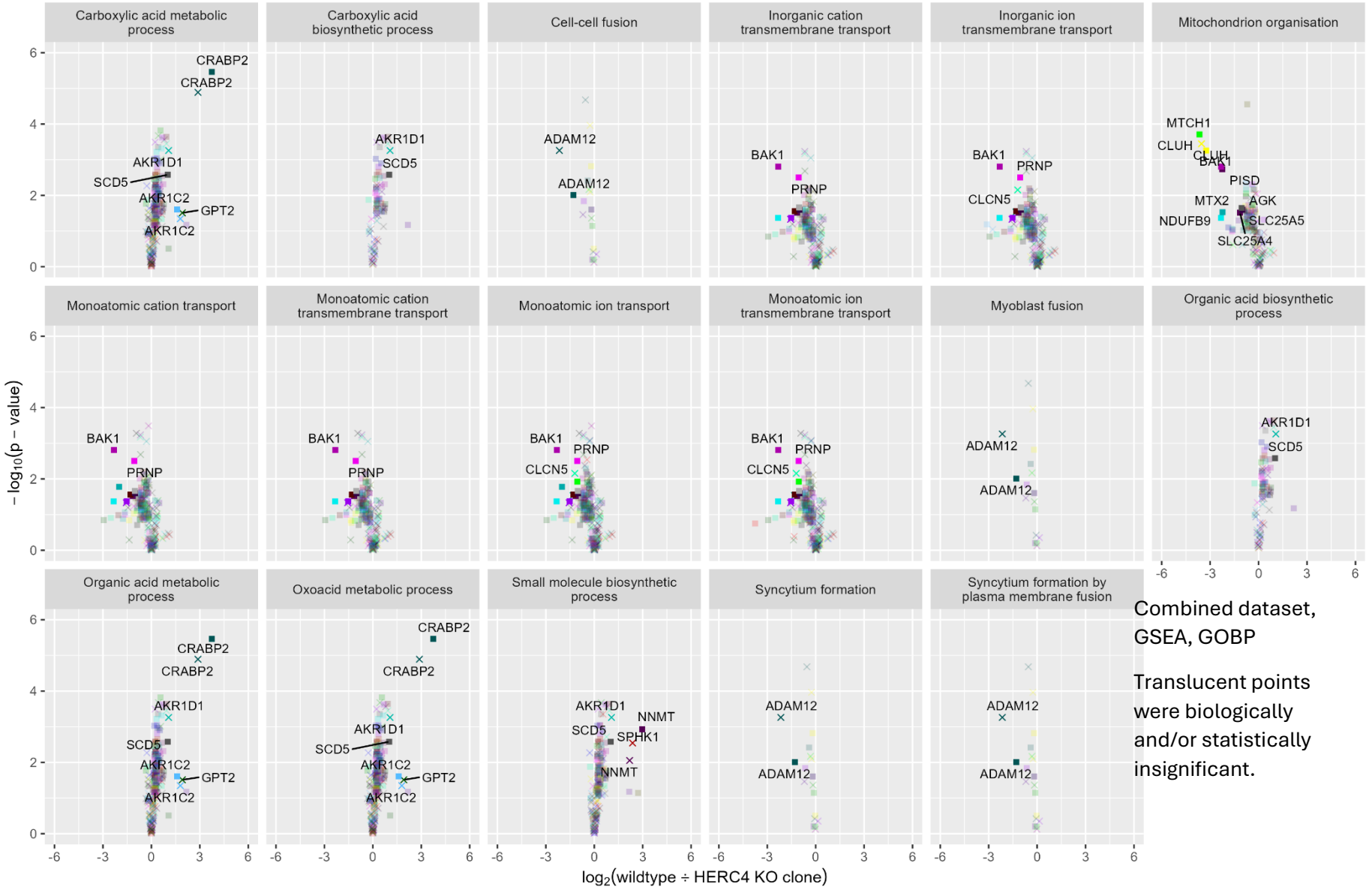
Appendix 4 – volcano plots for pathway analysis

Combined dataset, ORA, GOBP



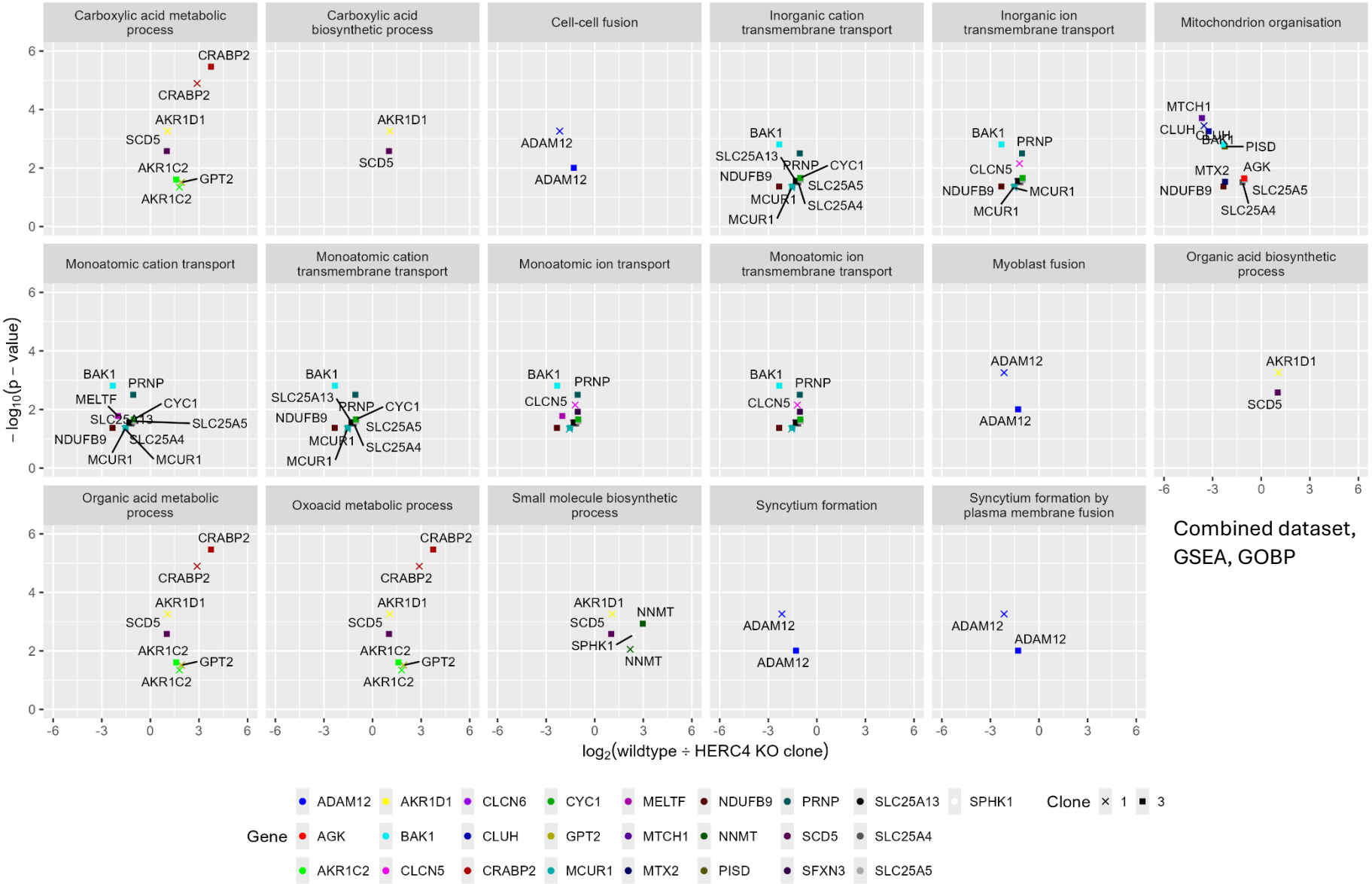
Combined dataset, GSEA, KEGG





Combined dataset, GSEA, GOBP

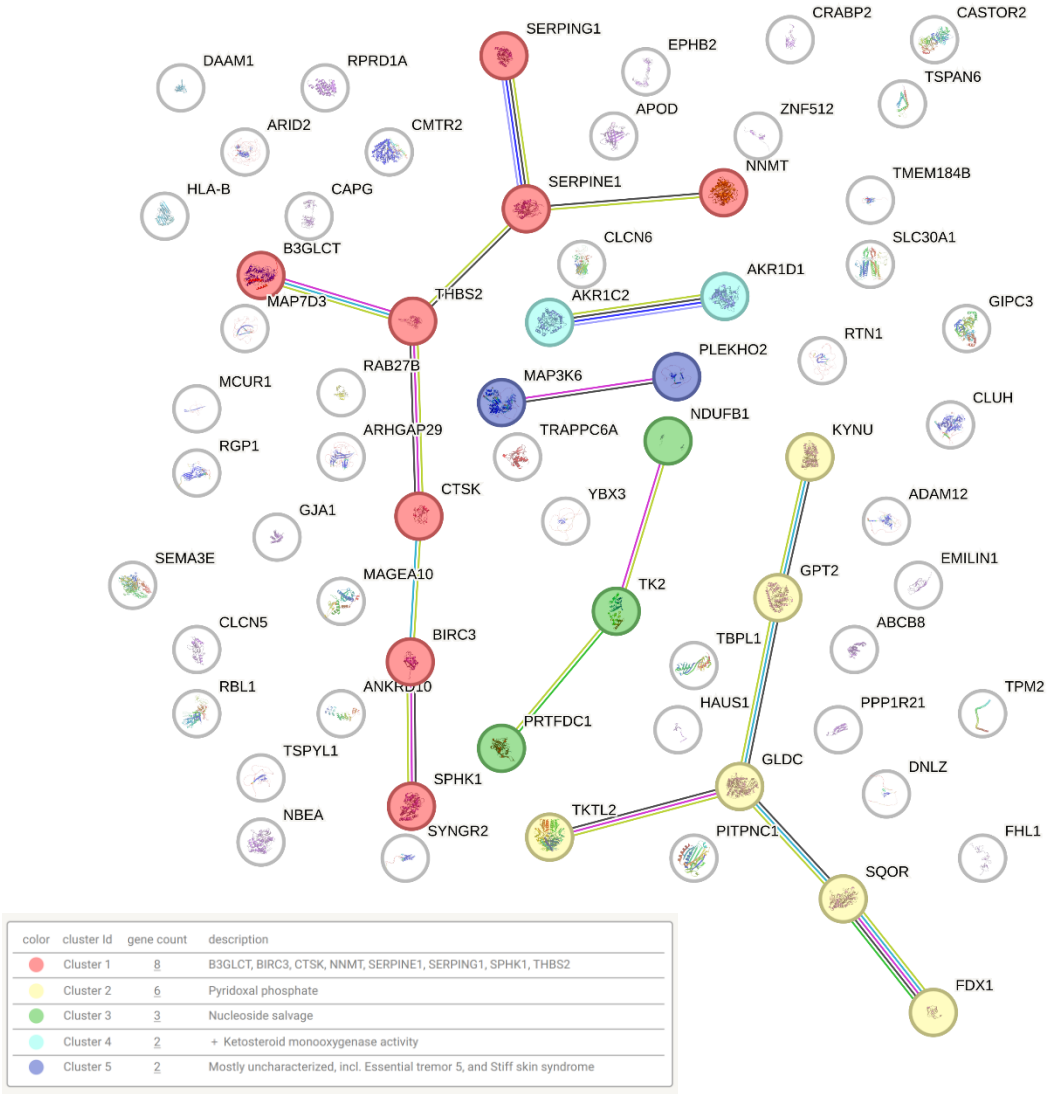
Translucent points were biologically and/or statistically insignificant.



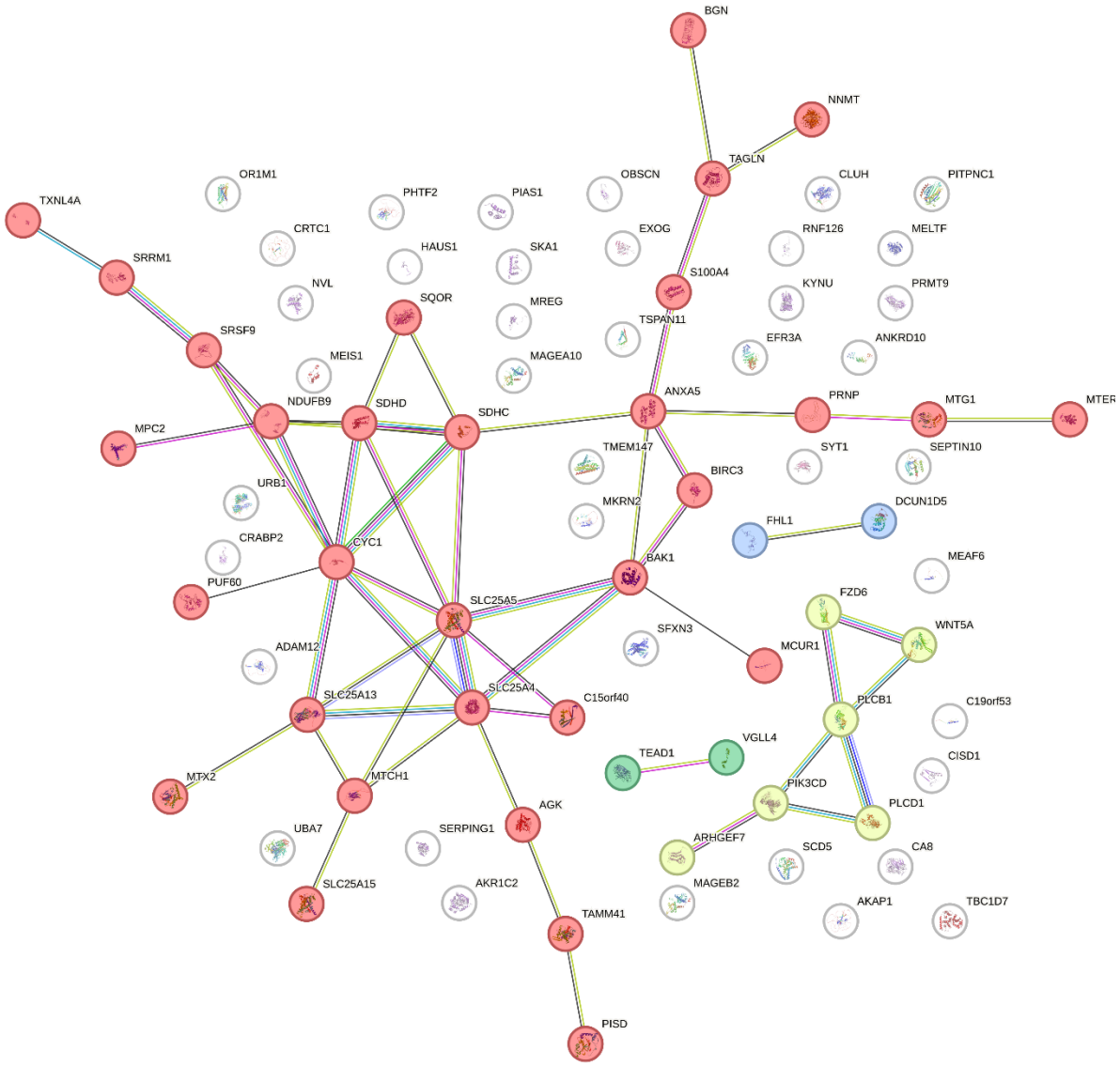
Combined dataset, GSEA, GOBP

Appendix 5 – STRING networks for Clone 1 and Clone 3 separately

Clone 1 – downloaded 3rd December 2025



color	cluster Id	gene count	description
	Cluster 1	8	B3GLCT, BIRC3, CTSK, NNMT, SERPINE1, SERPING1, SPHK1, THBS2
	Cluster 2	6	Pyridoxal phosphate
	Cluster 3	3	Nucleoside salvage
	Cluster 4	2	+ Ketosteroid monooxygenase activity
	Cluster 5	2	Mostly uncharacterized, incl. Essential tremor 5, and Stiff skin syndrome



color	cluster Id	gene count	description
	Cluster 1	31	Mitochondrion inner membrane
	Cluster 2	6	+ Ca2+ pathway
	Cluster 3	2	RUNX3 regulates YAP1-mediated transcription
	Cluster 4	2	DCUN1D5, FHL1

Clone 3 – downloaded 3rd December 2025 (STRING v12.0)

Appendix 6 – proximity labelling analysis results

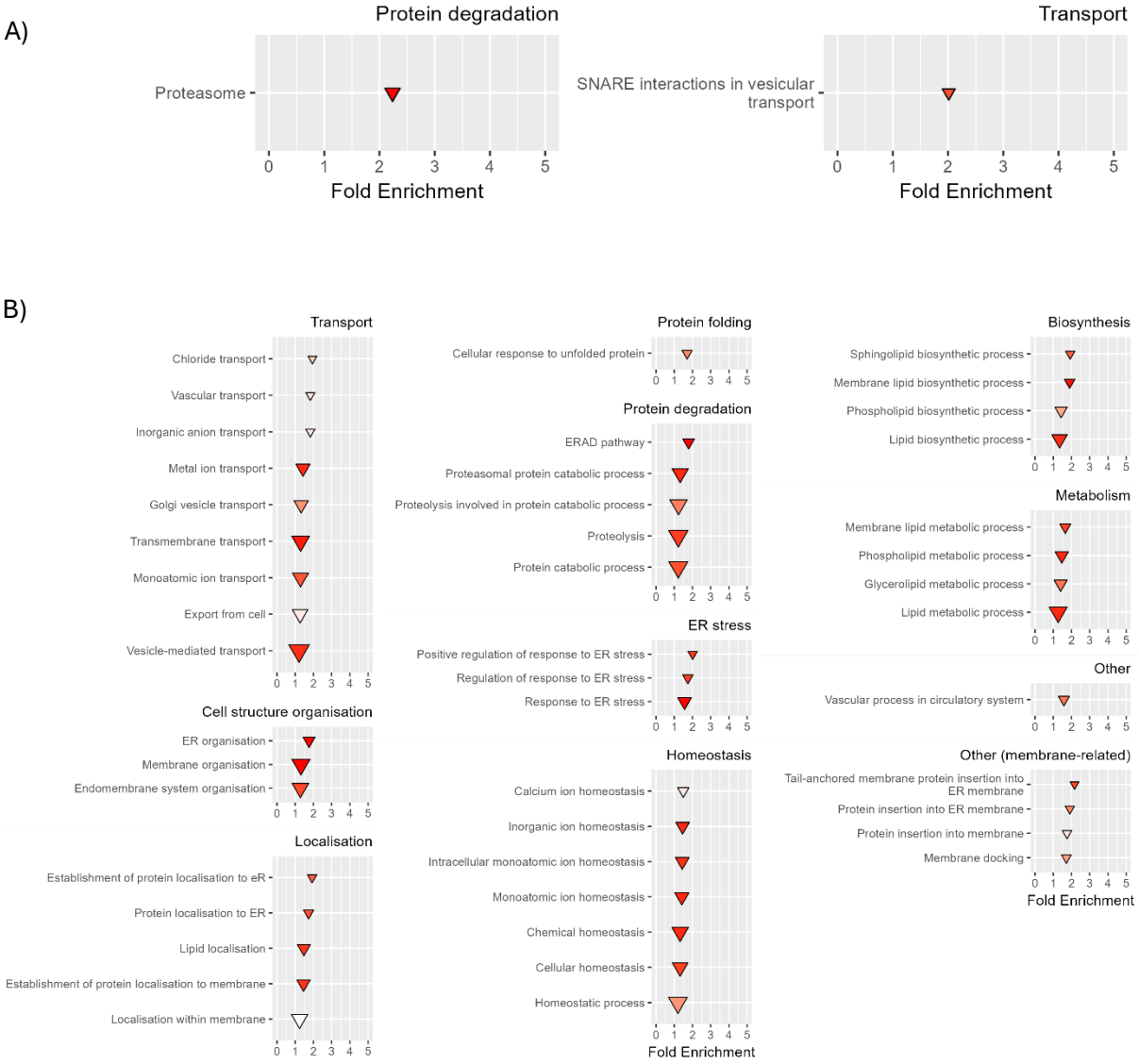


Figure A: Terms identified for interactors by ORA, grouped by theme
ORA was used to identify significantly enriched terms for interactors, based on the KEGG (A) and GO-BP (B) databases, then these terms were manually split into themes. Very few KEGG terms were identified, but one was associated with protein degradation, which was also highlighted by GO-BP terms.

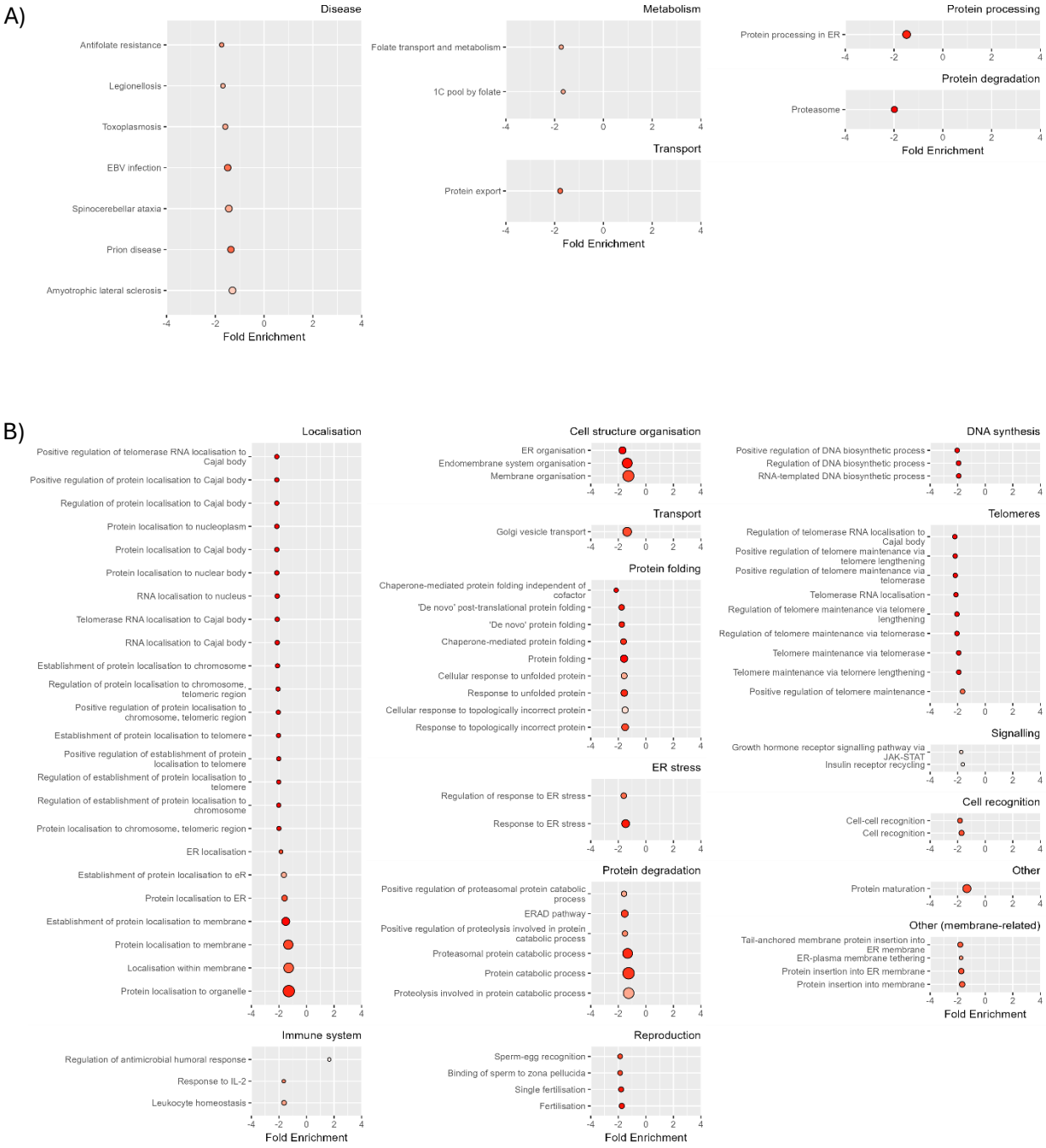


Figure B: Terms identified for interactors by GSEA, grouped by theme

GSEA was used to identify significantly enriched terms for interactors, based on the KEGG (A) and GO-BP (B) databases, then these terms were manually split into themes. The most common theme was localization, particularly to telomeres, while protein degradation was the only theme identified in both databases.

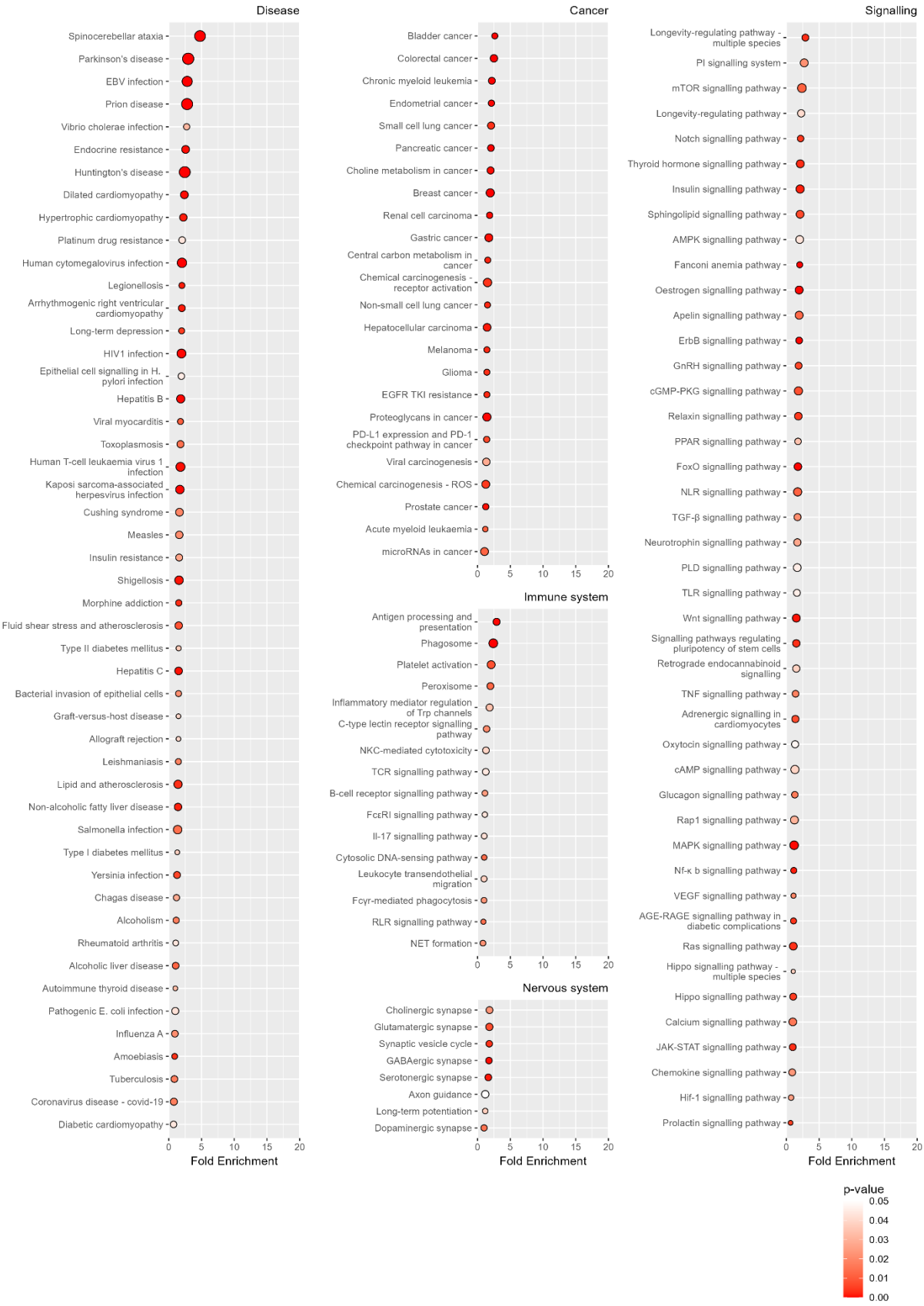

Disease
Spinocerebellar ataxia
Parkinson's disease
EBV infection
Prion disease
Vibrio cholerae infection
Endocrine resistance
Huntington's disease
Dilated cardiomyopathy
Hypertrophic cardiomyopathy
Platinum drug resistance
Human cytomegalovirus infection
Legionellosis
Arrhythmogenic right ventricular cardiomyopathy
Long-term depression
HIV1 infection
Epithelial cell signalling in H. pylori infection
Hepatitis B
Viral myocarditis
Toxoplasmosis
Human T-cell leukaemia virus 1 infection
Kaposi sarcoma-associated herpesvirus infection
Cushing syndrome
Measles
Insulin resistance
Shigellosis
Morphine addiction
Fluid shear stress and atherosclerosis
Type II diabetes mellitus
Hepatitis C
Bacterial invasion of epithelial cells
Graft-versus-host disease
Allograft rejection
Leishmaniasis
Lipid and atherosclerosis
Non-alcoholic fatty liver disease
Salmonella infection
Type I diabetes mellitus
Yersinia infection
Chagas disease
Alcoholism
Rheumatoid arthritis
Alcoholic liver disease
Autoimmune thyroid disease
Pathogenic E. coli infection
Influenza A
Amoebiasis
Tuberculosis
Coronavirus disease - covid-19
Diabetic cardiomyopathy
0 5 10 15 20
Fold Enrichment
Cancer
Bladder cancer
Colorectal cancer
Chronic myeloid leukemia
Endometrial cancer
Small cell lung cancer
Pancreatic cancer
Choline metabolism in cancer
Breast cancer
Renal cell carcinoma
Gastric cancer
Central carbon metabolism in cancer
Chemical carcinogenesis - receptor activation
Non-small cell lung cancer
Hepatocellular carcinoma
Melanoma
Glioma
EGFR TKI resistance
Proteoglycans in cancer
PD-L1 expression and PD-1 checkpoint pathway in cancer
Viral carcinogenesis
Chemical carcinogenesis - ROS
Prostate cancer
Acute myeloid leukaemia
microRNAs in cancer
0 5 10 15 20
Immune system
Antigen processing and presentation
Phagosome
Platelet activation
Peroxisome
Inflammatory mediator regulation of Trp channels
C-type lectin receptor signalling pathway
NKC-mediated cytotoxicity
TCR signalling pathway
B-cell receptor signalling pathway
FcεRI signalling pathway
Il-17 signalling pathway
Cytosolic DNA-sensing pathway
Leukocyte transendothelial migration
Fcγr-mediated phagocytosis
RLR signalling pathway
NET formation
0 5 10 15 20
Nervous system
Cholinergic synapse
Glutamatergic synapse
Synaptic vesicle cycle
GABAergic synapse
Serotonergic synapse
Axon guidance
Long-term potentiation
Dopaminergic synapse
0 5 10 15 20
Fold Enrichment
Signalling
Longevity-regulating pathway - multiple species
PI signalling system
mTOR signalling pathway
Longevity-regulating pathway
Notch signalling pathway
Thyroid hormone signalling pathway
Insulin signalling pathway
Sphingolipid signalling pathway
AMPK signalling pathway
Fanconi anemia pathway
Oestrogen signalling pathway
Apelin signalling pathway
ErbB signalling pathway
GnRH signalling pathway
cGMP-PKG signalling pathway
Relaxin signalling pathway
PPAR signalling pathway
FoxO signalling pathway
NLR signalling pathway
TGF-β signalling pathway
Neurotrophin signalling pathway
PLD signalling pathway
TLR signalling pathway
Wnt signalling pathway
Signalling pathways regulating pluripotency of stem cells
Retrograde endocannabinoid signalling
TNF signalling pathway
Adrenergic signalling in cardiomyocytes
Oxytocin signalling pathway
cAMP signalling pathway
Glucagon signalling pathway
Rap1 signalling pathway
MAPK signalling pathway
Nf-κ b signalling pathway
VEGF signalling pathway
AGE-RAGE signalling pathway in diabetic complications
Ras signalling pathway
Hippo signalling pathway - multiple species
Hippo signalling pathway
Calcium signalling pathway
JAK-STAT signalling pathway
Chemokine signalling pathway
Hif-1 signalling pathway
Prolactin signalling pathway
0 5 10 15 20
Fold Enrichment
p-value
0.05
0.04
0.03
0.02
0.01
0.00

Figure Ci: KEGG terms identified for interactors by pathway analysis, grouped by theme
Pathway analysis was used to identify significantly enriched terms for interactors, based on the KEGG database, then these terms were manually split into themes. The most common themes were disease, cancer, signalling and the immune system. Less abundant themes are displayed on the next page.

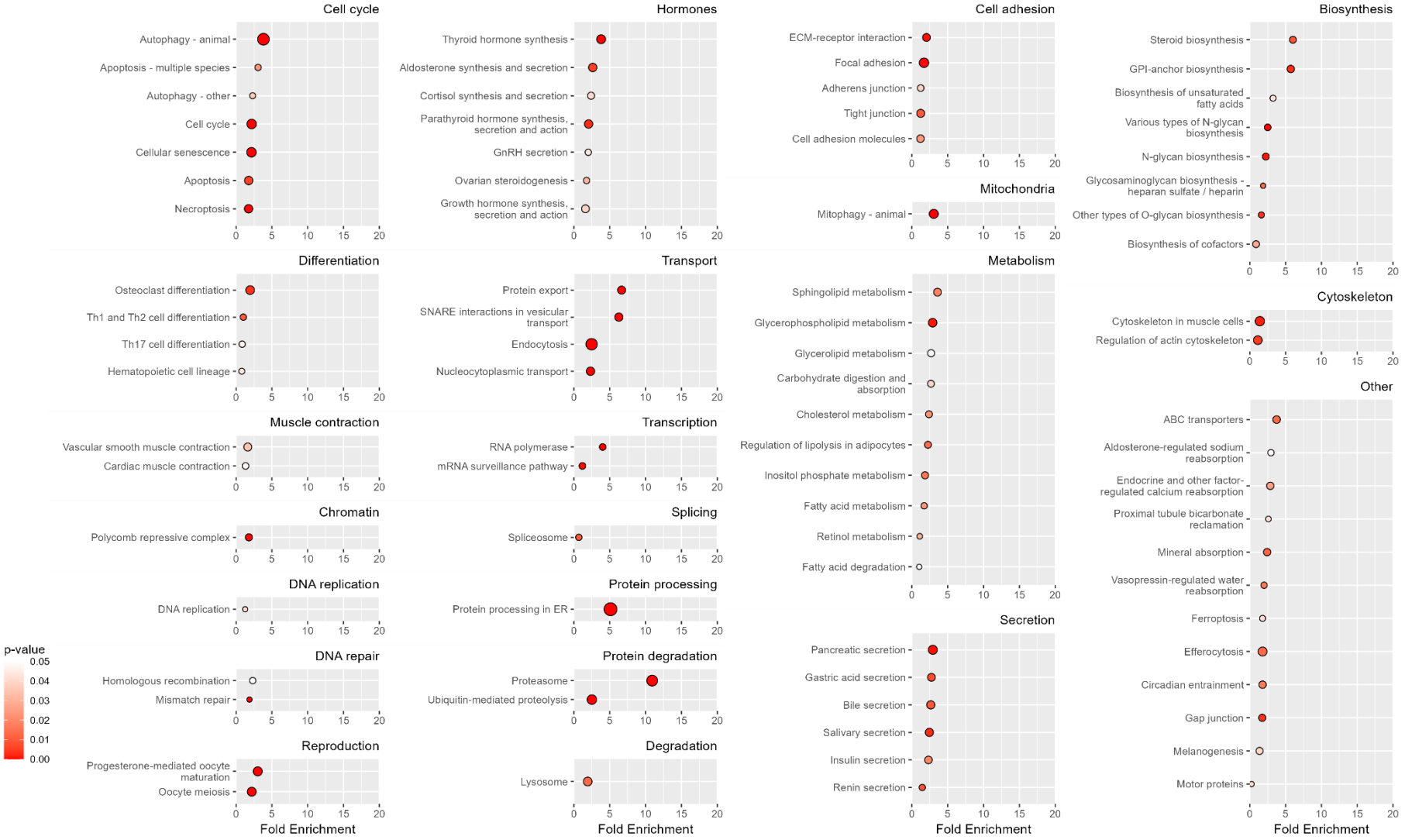

Cell cycle
Autophagy - animal
Apoptosis - multiple species
Autophagy - other
Cell cycle
Cellular senescence
Apoptosis
Necroptosis
Hormones
Thyroid hormone synthesis
Aldosterone synthesis and secretion
Cortisol synthesis and secretion
Parathyroid hormone synthesis, secretion and action
GnRH secretion
Ovarian steroidogenesis
Growth hormone synthesis, secretion and action
Cell adhesion
ECM-receptor interaction
Focal adhesion
Adherens junction
Tight junction
Cell adhesion molecules
Mitochondria
Mitophagy - animal
Biosynthesis
Steroid biosynthesis
GPI-anchor biosynthesis
Biosynthesis of unsaturated fatty acids
Various types of N-glycan biosynthesis
N-glycan biosynthesis
Glycosaminoglycan biosynthesis - heparan sulfate / heparin
Other types of O-glycan biosynthesis
Biosynthesis of cofactors
Differentiation
Osteoclast differentiation
Th1 and Th2 cell differentiation
Th17 cell differentiation
Hematopoietic cell lineage
Transport
Protein export
SNARE interactions in vesicular transport
Endocytosis
Nucleocytoplasmic transport
Metabolism
Sphingolipid metabolism
Glycerophospholipid metabolism
Glycerolipid metabolism
Carbohydrate digestion and absorption
Cholesterol metabolism
Regulation of lipolysis in adipocytes
Inositol phosphate metabolism
Fatty acid metabolism
Retinol metabolism
Fatty acid degradation
Cytoskeleton
Cytoskeleton in muscle cells
Regulation of actin cytoskeleton
Muscle contraction
Vascular smooth muscle contraction
Cardiac muscle contraction
Transcription
RNA polymerase
mRNA surveillance pathway
Chromatin
Polycomb repressive complex
Splicing
Spliceosome
Secretion
Pancreatic secretion
Gastric acid secretion
Bile secretion
Salivary secretion
Insulin secretion
Renin secretion
Other
ABC transporters
Aldosterone-regulated sodium reabsorption
Endocrine and other factor-regulated calcium reabsorption
Proximal tubule bicarbonate reclamation
Mineral absorption
Vasopressin-regulated water reabsorption
Ferroptosis
Efferocytosis
Circadian entrainment
Gap junction
Melanogenesis
Motor proteins
DNA replication
DNA replication
Protein processing
Protein processing in ER
DNA repair
Homologous recombination
Mismatch repair
Protein degradation
Proteasome
Ubiquitin-mediated proteolysis
Reproduction
Progesterone-mediated oocyte maturation
Oocyte meiosis
Degradation
Lysosome
0 5 10 15 20
Fold Enrichment
p-value
0.05
0.04
0.03
0.02
0.01
0.00

Figure Cii: KEGG terms identified for interactors by pathway analysis, grouped by theme
Pathway analysis was used to identify significantly enriched terms for interactors, based on the KEGG database, then these terms were manually split into themes. Of those shown here, metabolism and


Signalling
Negative regulation of intracellular oestrogen receptor signalling pathway
Negative regulation of TOR signalling
Wnt signalling pathway, planar cell polarity pathway
Positive regulation of TOR signalling
Activation of GTPase activity
Negative regulation of EGFR signalling pathway
Negative regulation of SMO signalling pathway
Regulation of rho protein signal transduction
Activin receptor signalling pathway
Cellular response to growth factor stimulus
Positive regulation of TORC1 signalling
Small GTPase-mediated signal transduction
Negative regulation of JNK cascade
IGF receptor signalling pathway
Negative regulation of androgen receptor signalling pathway
Smad protein signal transduction
Negative regulation of TORC1 signalling
Regulation of TNF-mediated signalling pathway
TGF-β receptor signalling pathway
Positive regulation of VEGF production
Positive regulation of protein S/T kinase activity
Positive regulation of canonical Wnt signalling pathway
Semaphorin-plexin signalling pathway
Intracellular iron ion homeostasis
Positive regulation of JNK cascade
Cell surface receptor protein tyrosine kinase signalling pathway
Integrin-mediated signalling pathway
Positive regulation of canonical NF-κB signal transduction
Hippo signalling
PI3K/PKB signal transduction
Negative regulation of canonical Wnt signalling pathway
Canonical Wnt signalling pathway
Intracellular signal transduction
Positive regulation of non-canonical NF-κB signal transduction
0 5 10 15 20
Cell cycle
Spindle assembly
Mitotic G2 DNA damage checkpoint signalling
Mitotic spindle assembly checkpoint signalling
Mitotic sister chromatid segregation
Centrosome cycle
Positive regulation of G2/M transition of mitotic cell cycle
Regulation of autophagy
Negative regulation of fibroblast proliferation
Autophagy
Regulation of mitotic cell cycle
Spindle organisation
Negative regulation of cellular senescence
Macroautophagy
Positive regulation of extrinsic apoptotic signalling pathway
Activation of Cys-type endopeptidase activity involved in apoptotic process
Regulation of cell division
Mitotic metaphase chromosome alignment
Positive regulation of autophagy
Centriole replication
Extrinsic apoptotic signalling pathway
Positive regulation of Cys-type endopeptidase activity involved in apoptotic process
Negative regulation of extrinsic apoptotic signalling pathway
Positive regulation of cell growth
Positive regulation of epithelial cell proliferation
Regulation of apoptotic process
Chromosome segregation
Regulation of cell cycle
Negative regulation of Cys-type endopeptidase activity involved in apoptotic process
MAPK cascade
Negative regulation of apoptotic signalling pathway
0 5 10 15 20
Development
Neural tube closure
Regulation of embryonic development
0 5 10 15 20
Differentiation
Negative regulation of fat cell differentiation
0 5 10 15 20
Chromatin
Heterochromatin formation
DNA methylation-dependent heterochromatin formation
Chromatin remodeling
0 5 10 15 20
Replication
Positive regulation of DNA replication
0 5 10 15 20
DNA repair
DNA repair-dependent chromatin remodeling
DNA synthesis involved in DNA repair
Translesion synthesis
Positive regulation of DNA repair
Double-strand break repair
DNA damage response
0 5 10 15 20
Telomeres
Positive regulation of telomere maintenance via telomerase
Regulation of telomere maintenance
Positive regulation of telomere capping
Positive regulation of telomerase activity
0 5 10 15 20
Gene expression
RISC complex assembly
Negative regulation of gene expression via chromosomal CpG island methylation
Regulatory ncRNA-mediated gene silencing
mRNA export from nucleus
Circadian regulation of gene expression
Negative regulation of gene expression
0 5 10 15 20
Transcription
Positive regulation of nuclear-transcribed mRNA poly(A) tail shortening
Positive regulation of nuclear-transcribed mRNA catabolic process, deadenylation-dependent decay
mRNA 3'-end processing
Negative regulation of miRNA transcription
Nuclear-transcribed mRNA catabolic process, nonsense-mediated decay
Positive regulation of miRNA transcription
Regulation of transcription by RNA polymerase II
Positive regulation of NF-κB transcription factor activity
Negative regulation of nf-κb transcription factor activity
Regulation of DNA-templated transcription
Positive regulation of DNA-binding transcription factor activity
0 5 10 15 20
Splicing
mRNA splicing, via spliceosome
0 5 10 15 20
Response
Response to bacterium
Response to insulin
Cellular response to steroid hormone stimulus
Cellular response to oxidative stress
Cellular response to starvation
Response to UV
Response to hypoxia
Cellular response to hypoxia
Cellular response to insulin stimulus
Vasculogenesis
0 5 10 15 20
Hormones
Response to progesterone
0 5 10 15 20
Fold Enrichment
Cytoskeleton
Regulation of cytokinesis
0 5 10 15 20
Cell adhesion
Cell adhesion mediated by integrin
Cell-substrate adhesion
Negative regulation of anoikis
Heterotypic cell-cell adhesion
Cell-matrix adhesion
Substrate adhesion-dependent cell spreading
Cell adhesion
0 5 10 15 20
Other (membrane-related)
Tail-anchored membrane protein insertion into ER membrane
Protein insertion into ER membrane by stop-transfer membrane-anchor sequence
Membrane fusion
0 5 10 15 20
Fold Enrichment
Reproduction
Single fertilisation
0 5 10 15 20
Other
Glycosylation
Lysosomal lumen acidification
Cell communication by electrical coupling involved in cardiac conduction
Protein stabilisation
Negative regulation of amyloid-β formation
Regulation of protein-containing complex assembly
Amyloid fibril formation
Blood coagulation
Negative regulation of amyloid fibril formation
Cell migration
Negative regulation of protein-containing complex assembly
Positive regulation of cell migration
0 5 10 15 20
Fold Enrichment
p-value
0.05
0.04
0.03
0.02
0.01
0.00

Figure Di: GO-BP terms identified for interactors by pathway analysis, grouped by theme
Pathway analysis was used to identify significantly enriched terms for interactors, based on the GO-BP database, then these terms were manually split into themes. Of those shown here, transport, protein modification and degradation, and the immune system were the most abundant.


Transport
Intra-Golgi vesicle-mediated transport
Retrograde protein transport, ER to cytosol
CopII-coated vesicle cargo loading
CopII vesicle coating
Lipoprotein transport
Retrograde vesicle-mediated transport, Golgi to ER
Export across plasma membrane
Transepithelial transport
ER to Golgi vesicle-mediated transport
Intraciliary transport
Retrograde transport, endosome to Golgi
Cholesterol transport
Early endosome to Golgi transport
Transferrin transport
Protein import into peroxisome matrix
Potassium ion import across plasma membrane
Early endosome to late endosome transport
Clathrin coat assembly
Endocytic recycling
Synaptic vesicle endocytosis
Endosome to lysosome transport
Transmembrane transport
Viral budding via host ESCRT complex
Inorganic cation transmembrane transport
Positive regulation of protein import into nucleus
Intracellular protein transport
Endocytosis
Clathrin-dependent endocytosis
Potassium ion transmembrane transport
Chloride transmembrane transport
Cholesterol efflux
Calcium ion transmembrane transport
Negative regulation of protein secretion
Monoatomic ion transmembrane transport
Positive regulation of cholesterol efflux
Monoatomic ion transport
0 5 10 15 20
Localisation
Positive regulation of establishment of protein localisation to telomere
Localisation
Protein localisation to cilium
Protein targeting to lysosome
Positive regulation of protein localisation to nucleus
Regulation of protein localisation to plasma membrane
Protein localisation to centrosome
Protein targeting to mitochondrion
Positive regulation of protein localisation to plasma membrane
0 5 10 15 20
Metabolism
Long-chain fatty acid metabolic process
Negative regulation of ROS metabolic process
Retinol metabolic process
Aerobic respiration
Positive regulation of glycolytic process
Fatty acid metabolic process
Canonical glycolysis
0 5 10 15 20
Electron transport chain
Mitochondrial respiratory chain complex I assembly
0 5 10 15 20
Fold Enrichment
Translation
Ribosome disassembly
Rescue of stalled ribosome
miRNA-mediated gene silencing by inhibition of translation
rRNA processing
0 5 10 15 20
Protein folding
Positive regulation of ERAD pathway
Protein folding in ER
ER unfolded protein response
Chaperone-mediated protein folding
Protein folding
Protein quality control for misfolded or incompletely synthesised proteins
Chaperone cofactor-dependent protein refolding
Protein refolding
0 5 10 15 20
Protein modification
Protein K27-linked ubiquitination
Regulation of tubulin deacetylation
Protein deacetylation
Protein K11-linked ubiquitination
Protein N-linked glycosylation via asparagine
Positive regulation of protein ubiquitination
Protein N-linked glycosylation
Protein deubiquitination
Protein K48-linked ubiquitination
Positive regulation of peptidyl-serine phosphorylation
Protein autoubiquitination
Protein glycosylation
Protein K63-linked ubiquitination
Protein ubiquitination
Negative regulation of protein ubiquitination
Protein autoprocessing
Protein polyubiquitination
Protein autophosphorylation
Positive regulation of protein phosphorylation
Protein phosphorylation
Peptidyl-tyrosine phosphorylation
0 5 10 15 20
Secretion
Positive regulation of exosomal secretion
0 5 10 15 20
Cell structure organisation
ER organisation
Membrane organisation
Nuclear pore complex assembly
Negative regulation of cilium assembly
Peroxisome organisation
Golgi organisation
Multivesicular body assembly
Positive regulation of cilium assembly
Cilium assembly
Cell-cell junction organisation
0 5 10 15 20
Mitochondria
Mitochondrial fusion
Mitochondrial fission
Positive regulation of mitochondrial fission
Regulation of mitochondrion organisation
Cristae formation
Positive regulation of release of cytochrome c from mitochondria
Mitochondrion organisation
Mitophagy
0 5 10 15 20
Fold Enrichment
Protein degradation
Regulation of protein complex stability
ERAD pathway
Regulation of protein catabolic process
Membrane protein intracellular domain proteolysis
Negative regulation of protein catabolic process
Ubiquitin-dependent protein catabolic process via the multivesicular body sorting pathway
Ubiquitin-dependent protein catabolic process
Ubiquitin-dependent protein catabolic process via the C-end degron rule pathway
Mitochondrial protein catabolic process
Positive regulation of protein catabolic process
Proteasome-mediated ubiquitin-dependent protein catabolic process
Regulation of protein stability
Positive regulation of proteolysis
Positive regulation of proteasomal ubiquitin-dependent protein catabolic process
0 5 10 15 20
ER stress
Response to ER stress
0 5 10 15 20
Immune system
Positive regulation of autophagosome assembly
Negative regulation of autophagosome assembly
Negative regulation of viral transcription
Positive regulation of T cell-mediated cytotoxicity
Positive regulation of neutrophil chemotaxis
Autophagosome maturation
Cellular response to exogenous dsRNA
Positive regulation of macroautophagy
IL-1-mediated signalling pathway
Myd88-dependent TLR signalling pathway
Autophagosome assembly
Negative regulation of cGAS/STING signalling pathway
Response to IL-1
Positive regulation of type I interferon production
Cytoplasmic PRR signalling pathway
Innate immune response
TCR signalling pathway
Defense response to bacterium
0 5 10 15 20
Nervous system
Microglial cell activation
Neuron projection development
0 5 10 15 20
Homeostasis
ER calcium ion homeostasis
Cell volume homeostasis
Intracellular glucose homeostasis
Intracellular sodium ion homeostasis
Calcium ion homeostasis
Intracellular calcium ion homeostasis
Insulin receptor signalling pathway
Cholesterol homeostasis
0 5 10 15 20
Biosynthesis
Sphingolipid biosynthetic process
Bile acid biosynthetic process
GPI anchor biosynthetic process
Ceramide biosynthetic process
Phosphatidic acid biosynthetic process
Cholesterol biosynthetic process
Negative regulation of fatty acid biosynthetic process
Phosphatidylinositol biosynthetic process
0 5 10 15 20
Fold Enrichment
p-value
0.05
0.04
0.03
0.02
0.01
0.00

Figure Dii: GO-BP terms identified for interactors by pathway analysis, grouped by theme
Pathway analysis was used to identify significantly enriched terms for interactors, based on the GO-BP database, then these terms were manually split into themes. Of those shown here, signalling and the cell cycle were the most abundant themes, and DNA repair was also notable in the context of IR sensitivity.

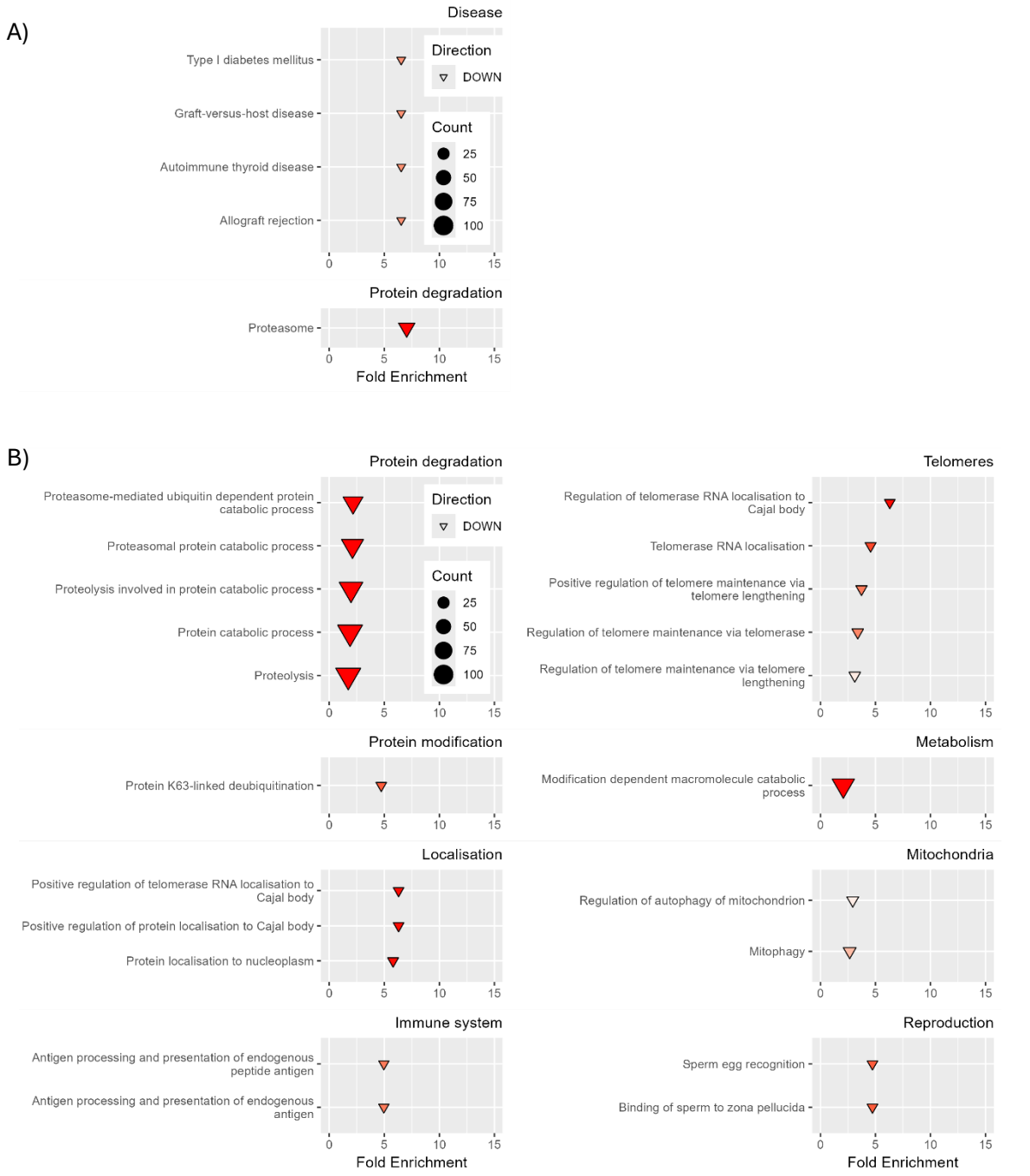


Figure E: Terms identified for substrates by ORA, grouped by theme

ORA was used to identify significantly enriched terms for substrates, based on the KEGG (A) and GO-BP (B) databases, then these terms were manually split into themes. Few terms were identified, especially from the KEGG database, but the theme of protein degradation was common to both analyses. Amongst the GO-BP terms, several terms referred to telomeres, mirroring the enrichment of this theme in the interactor dataset, while 2 terms were associated with each of the immune system and reproduction, reflecting 2 themes from published studies on HERC4.

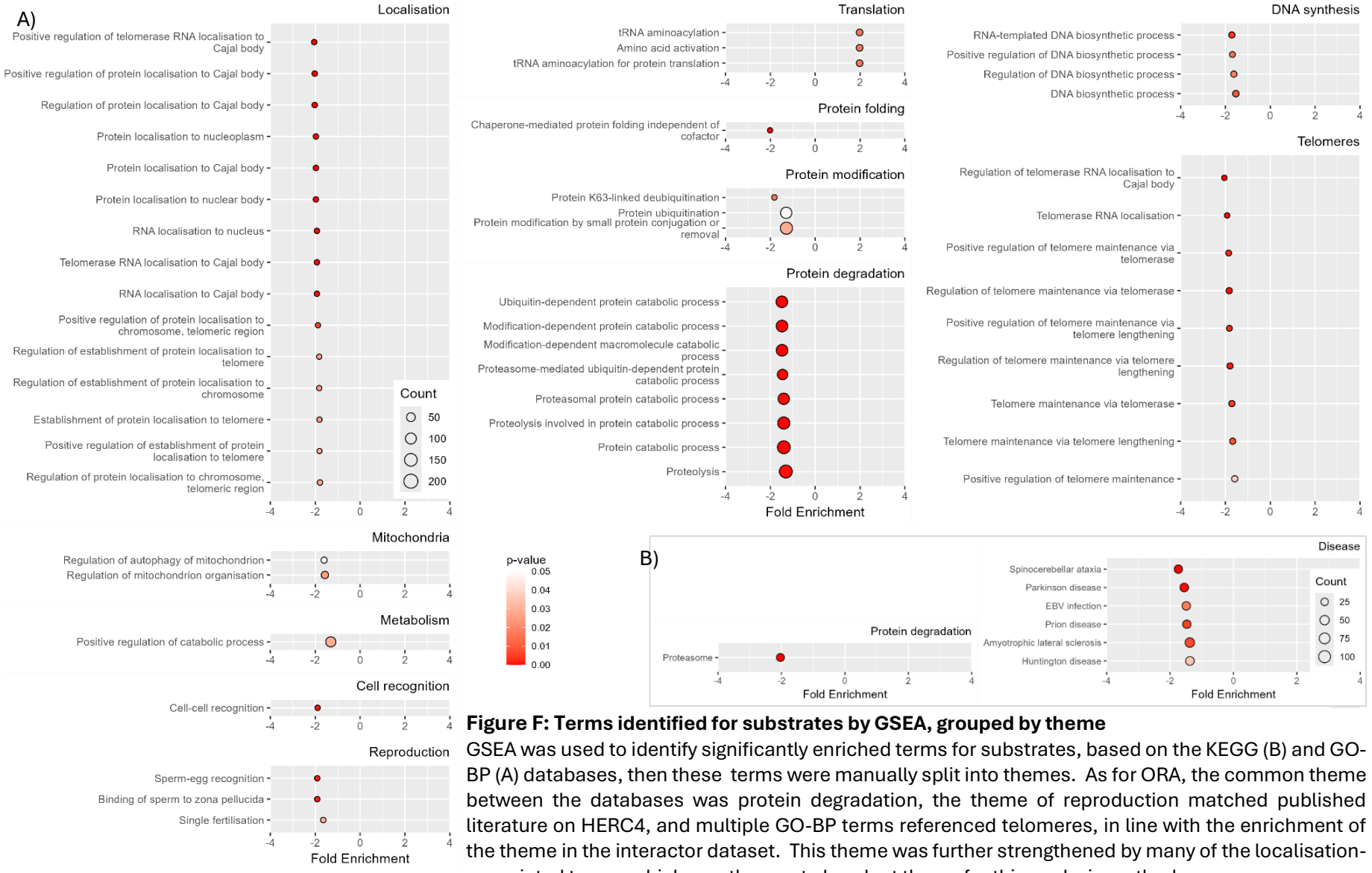


Figure F: Terms identified for substrates by GSEA, grouped by theme

GSEA was used to identify significantly enriched terms for substrates, based on the KEGG (B) and GO-BP (A) databases, then these terms were manually split into themes. As for ORA, the common theme between the databases was protein degradation, the theme of reproduction matched published literature on HERC4, and multiple GO-BP terms referenced telomeres, in line with the enrichment of the theme in the interactor dataset. This theme was further strengthened by many of the localisation-associated terms, which was the most abundant theme for this analysis method.



Figure G: KEGG terms identified for substrates by pathway analysis, grouped by theme
Pathway analysis was used to identify significantly enriched terms for substrates, based on the KEGG database, then these terms were manually split into themes, of which the most commonly identified were disease, cancer and signalling.

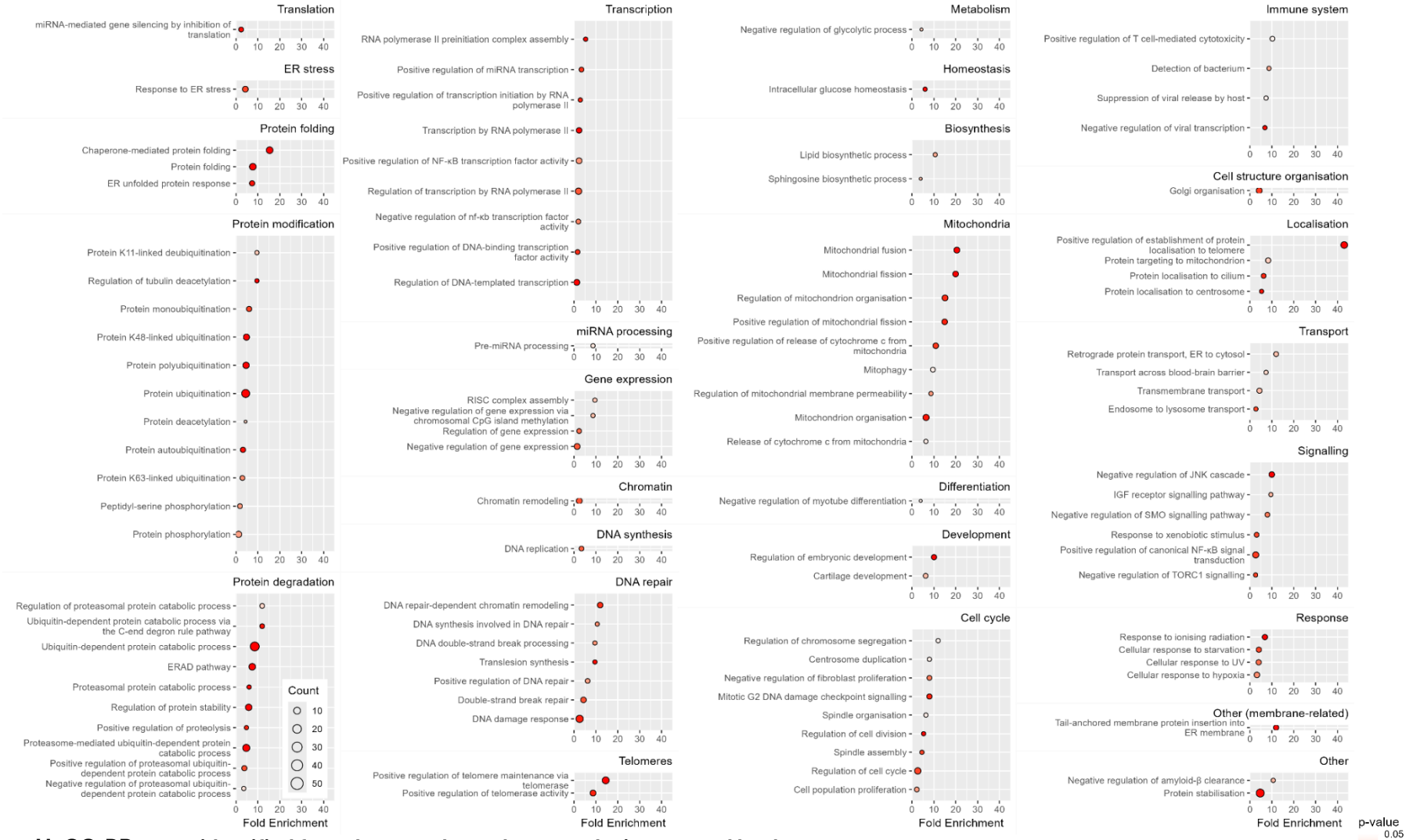


Figure H: GO-BP terms identified for substrates by pathway analysis, grouped by theme

Pathway analysis was used to identify significantly enriched terms for substrates, based on the GO-BP database, then these terms were manually split into themes. Unlike other analyses, there were no dominant themes, but protein degradation and modification, DNA repair, the cell cycle and the immune system were present, all of which were highlighted as particularly notable in the context of HERC4 as a radiosensitising E3 ligase.

4 – Discussion

A CRISPR screen conducted by Dr Hongbin Yang to identify E3 ligases involved in survival after IR highlighted HERC4 as a strong candidate for a radiosensitiser, since knocking it out produced the highest positive (improved survival) z-score of any non-essential gene tested. Initial validation supported this result, and in a separate DNA damage screen by Olivieri et al., HERC4 was associated with a set of 27 genes that were enriched for DSB repair and mitotic regulation [Olivieri et al., 2020; analysis using tool built by Ge et al., 2020], further reinforcing the hypothesis that it may influence cell survival after exposure to IR.

However, this hypothesis proved difficult to confirm through phenotypic experiments. HERC4 knockout clones were generated in 2 glioblastoma cell lines, DBTRG and LN229, but neither cell line showed a change in post-IR proliferation rates. 3 clones from each cell line were tested at 4 Gy (the dose used in the initial CRISPR screen) and 10 Gy, and the only result to achieve statistical significance was the third DBTRG clone at 10 Gy, which showed a substantially worse growth rate compared to the wildtype control. Nonetheless, additional experiments were conducted to explore factors commonly associated with radiosensitivity, in case the proliferation assay was misleading. The outcomes and appropriate next steps are outlined in Table 1.

Experiment	Outcome	Strengths and limitations	Next steps
Knockout clones	HERC4 is not essential	✓ Stable knockout with full HERC4 loss ✓ No sustained Cas9 expression × Cells may adjust over time to lack of HERC4	Inducible system (e.g. doxycycline-induced expression of sgRNA [Snijders et al., 2019])
Proliferation assay	HERC4 loss may slow proliferation but does not affect change in proliferation rate after IR or chemically-induced DNA damage	✓ Cells are grown under standard culture conditions, not in isolation as in colony formation assays.	Assess recovery time - image cells more frequently until expected proliferation achieved. Single-cell tracking on IncuCyte to assess number of surviving and proliferating cells
Resazurin assay	HERC4 loss has no significant effect on aerobic respiration rate	✓ IncuCyte images allow more confident normalisation of resazurin reduction to cell number compared to counting cells when seeding × Resazurin is an indirect measurement and confined to the oxidative stages of respiration	Seahorse assays (e.g. ATP production rate or glycolytic rate) Glucose uptake assay + GLUT1 western blot L-lactate assay (Increased glucose consumption and lactate production are indicative of the Warburg effect)
Cell cycle assays	HERC4 loss does not affect distribution through the cell cycle	✓ Consistent conclusions from 2 experiment types × Only tested under NIR conditions	Repeat flow cytometry and western blot analysis after IR with a particular focus on checkpoints and proportion of cells in relatively radiosensitive phases. Synchronise cells and compare time taken for population to be redistributed through the cell cycle Apoptosis assays (e.g. TUNEL assay or cytochrome c release)
Colony formation assay	DBTRG cells are not suitable for this method	✓ Gold standard for assessing survival after IR	Repeat with alternative cell lines, particularly LN229
DNA damage western blot	HERC4 loss may influence DNA damage signalling	× Only 1 repeat per cell line and DNA damage agent × Inconsistent results for these 2 experiments × Only 2 DNA damage markers assessed and unmodified versions not analysed	More repeats with more markers spanning more DNA repair pathways (e.g. pRPA for HR, pDNA-PKcs for NHEJ)
Total proteome mass spectrometry	There were no strong trends for either dataset, but proliferation, apoptosis and the immune system featured notably in both datasets, and HAUS1 was the only protein to be significant in both clones and as a HERC4 interactor.	✓ Selected pathways identified by multiple analysis methods × Effect of IR not tested × Limited to changes in protein abundance, not activity	Repeat with a knockout population instead of clones, and include a set of irradiated samples. Use tandem ubiquitin binding entities to extract ubiquitylated proteins (identify changes in abundance of modified proteins)
Proximity labelling mass spectrometry		✓ Selected pathways identified by multiple analysis methods × Effect of IR not tested × Does not identify substrates whose ubiquitylation does not cause proteasomal degradation	Replace MG132 samples with irradiated samples

Table 1: Summary of and next steps for experiments presented in previous chapters

4.1 - DNA repair

The first "R of radiobiology" is repair – the ability to undo the DNA damage caused by IR. Pathway analysis of putative HERC4 substrates identified in a proximity labelling mass spectrometry experiment highlighted an enrichment of DNA repair-related proteins, including terms for DSB repair and homologous recombination, the latter of which was also highlighted in the interactor dataset from the same experiment, and in the combined analysis of the total proteomes from LN229 Clones 1 and 3. This supports the data from the CRISPR screens by Yang and Olivieri, but phenotypic results were less clear. γH2Ax and pATM were probed by western blot as markers of DSBs, the dominant cytotoxic IR-induced lesion, and in DBTRG cells treated with 10 Gy, γH2Ax was increased in the 2 knockout clones tested, while pATM levels were similar or slightly lower compared to the wildtype. In LN229 cells treated with camptothecin to induce replication-associated DBSs, however, the opposite trends were observed, with less γH2Ax but elevated pATM levels compared to the wildtype. There are 2 obvious differences between the experiments, namely p53 status of the cell lines (DBTRG expresses wildtype p53 while LN229 has a homozygous loss-of-function mutation) and the DNA damage agent. IR causes damage at any point in the cell cycle, although cells are more sensitive in mitosis and less so in S phase, while camptothecin-induced DSBs occur only in S phase. The reliance of camptothecin-induced DSBs on DNA replication may result in ATR being the dominant H2A kinase, in place of ATM, perhaps explaining the seemingly contradictory effect of HERC4 loss on DNA damage signalling in LN229 cells. p53 may regulate a mechanism that modifies or counteracts the effect of HERC4 to explain the opposing changes in γH2Ax levels in DBTRG compared to LN229 cells, but otherwise, neither difference offers an obvious explanation for the western blot results. Interpretation of these datasets is further limited by the lack of repeats and because levels of unmodified ATM and H2Ax were not probed, so it is unclear if the changes observed are due to changes in modification rates or protein availability. A more complete dataset, including markers from other aspects of DNA

damage signalling and repair, may shed more light on the preliminary findings that HERC4 influences this process, albeit in an inconsistent manner.

The proximity labelling data also revealed an unexpected connection to DNA damage and repair through the extensive enrichment of telomere-related GO-BP terms across all 3 analysis methods for both substrates and interactors, with the exception of interactors by ORA. Telomeres, and specifically their length, are well-established as a factor in senescence, a process whose potential contribution to HERC4-mediated radiosensitivity is discussed below, but, when improperly maintained, they also impair processing of IR-induced DNA damage [Mirjolet et al., 2015]. One suggested explanation for this is that shortened telomeres fuse with IR-induced breaks elsewhere in the genome, blocking repair and reducing chromosome stability to sensitise cells to IR [Latre et al., 2003]. Another is that telomere shortening induces chromatin compaction, limiting access of pATM activated by DNA damage to its chromatin-associated substrates. This includes γH2Ax, and Drissi et al. found that its phosphorylation was delayed in cells with shorter telomeres [2011], providing a possible explanation for the reduced γH2Ax levels seen here in camptothecin-treated LN229 clones despite the simultaneous increase in pATM levels. If HERC4 loss suppresses telomere maintenance, indirectly causing chromatin compaction, it might increase the magnitude of DNA damage signalling, hence elevated pATM, while blocking transmission of this signal, indicated in this dataset by lower γH2Ax. This would be particularly interesting in the context of glioblastoma given the activating mutations characteristically found the *TERT* promoter. A longer time course for the experiment shown here is needed to validate this hypothesis, plus investigation of the effect of proteins such as telomerase on the results, but this model would conflate a strong, seemingly outlying result from the proximity labelling data with the apparently contradictory result from the western blot. It should also be considered, however, that this model is based on DNA damage induced by camptothecin, not IR and may be compounded by camptothecin-mediated telomerase inhibition [Rembiałkowska et al., 2025]. This limitation is particularly strong given that the same

trends in pATM and γH2Ax levels were not replicated in irradiated DBTRG cells. Nevertheless, it would be prudent to include later time points in future replicates of both western blot experiments. The dataset could also be strengthened by the inclusion of additional markers more specific to particular DNA repair pathways, such as phospho-DNA-PKcs for NHEJ and phospho-RPA for HR.

4.2 - Cell cycle

The role of the cell cycle in IR survival was also considered more directly by western blot analysis of cyclin levels. Zhu et al. observed a negative correlation between HERC4 and cyclin B1 expression in ovarian cancer [Zhu et al., 2024], while Wei et al. found that cyclin D1 expression declined after HERC4 silencing in a cervical cancer cell line [Wei et al., 2016]. In a multiple myeloma model, HERC4 was shown to ubiquitylate c-MAF, whose target genes include cyclin D2 [Zhang et al., 2016], providing further evidence of a cell cycle function for HERC4. However, the work presented here failed to confirm these changes. 1 repeat in DBTRG cells showed downregulation of cyclin D1 in all clones, consistent with the literature, and interestingly, 1 repeat in LN229 cells showed the inverse trend, but neither observation was reproducible. Similarly for cyclin B1, LN229 clones showed a subtle decrease in expression compared to the wildtype control, but this was not seen in other repeats in either cell line. The changes in cyclins D1 and B1 were not observed in the same experiment, and there were no compensatory changes in other cyclins, further undermining the relevance of these observations. This was supported by the consistent cell cycle distribution observed by DAPI and EdU staining. 2 out of 3 LN229 HERC4 knockout clones showed a marked but statistically insignificant increase in cells in replicating S phase, and all 3 showed a similarly distinct but insignificant decrease in cells in non-standard phases, but this was not reproduced in DBTRG cells, whose only slight and once again statistically insignificant trend was towards slightly more cells in G1 after HERC4 loss. It is notable, however, that these experiments were done without IR or alternative treatment, so it is

plausible that HERC4 influences cell cycle progression only when the cells are challenged with DNA damage. It would also be useful to extend the western blot experiment to include senescence and apoptotic markers, since these were the most frequently enriched cell cycle-related terms in either the proximity labelling or the total proteome mass spectrometry experiments. It seems unlikely, based on the data shown here, that HERC4 affects radiosensitivity by altering the proportion of cells in relatively radiosensitive or -resistant phases, but it may influence the speed at which damaged cells move through cell cycle checkpoints and therefore the time available for successful repair (the G2/M DNA damage checkpoint and regulation of this transition were among the most enriched cell cycle terms for interactors, as assessed by pathway analysis using the GO-BP database), or the number of cells that enter senescence, with the same effect. It would be particularly interesting to explore the effect of HERC4 loss on the spindle checkpoint and mitotic catastrophe, given its potential interaction with and downregulation of HAUS1. Additionally, in line with the re-assortment principle in the 6 Rs of Radiobiology, it would also be valuable to measure the time taken for synchronised cells to redistribute themselves through the cell cycle, in case HERC4 increases variation in cell cycle progression but not the average distribution.

4.3 - Proliferation

The other growth-related R is repopulation – the ability to replace cells killed by IR and the speed with which this is achieved. Each cell line had one knockout clone that grow significantly more slowly than the wildtype control, another that was substantially, but statistically significantly, slower and one that was noticeably but not significantly faster than wildtype cells. This was borne out anecdotally by the time taken to reach confluency by cells from each line in routine culture. While slower proliferation often corresponds to increased radioresistance due to cells having more time to complete DNA repair processes, a stronger difference might be expected if this phenotype was responsible for the initial survival advantage of HERC4 depletion observed in

the IR CRISPR screen, and there was little evidence in the mass spectrometry experiments for HERC4 influencing proliferation rates.

4.4 - Hypoxia and reoxygenation

No phenotypic experiments were conducted to explore the effect of HERC4 on hypoxia-induced radioresistance, but several relevant terms were identified by pathway analysis of the mass spectrometry data - response to hypoxia and HIF-1 signalling were among the enriched terms for both interactors and substrates. The same method also highlighted HIF-1 and VEGF signalling for both clones, but only from the KEGG database. While Clone 1 displayed lower levels of SPHK1 (VEGF pathway) and SERPINE1 (HIF-1 pathway), the first of which contributes to HIF-1 activation and the second is upregulated by HIF-1, in Clone 3, both pathways were enriched solely through the increased expression of PI3KCD, which facilitates signal transmission from the VEGF receptor (VEGFR) to HIF-1. The VEGF receptor was a seemingly strong hit in the proximity labelling data, but it was discounted as binding to the streptavidin beads independently of its biotinylation, and in combination with the conflicting results between the clones, this provides very poor evidence for HERC4 involvement in hypoxia responses. There is also limited evidence in the literature to implicate it in tumour reoxygenation. Sun et al. show increased angiogenesis when HERC4 is overexpressed, perhaps mediated by its ubiquitylation of KRT19, leading to its proteasomal degradation [Sun et al., 2026], and a different Sun et al. group found that HERC4 overexpression can reverse VEGF and FGF downregulation caused by its interactor METTL3 [Sun et al., 2025]. This is sufficient to demonstrate a potential connection between HERC4 and tumour reoxygenation, despite the discouraging mass spectrometry results, but it also leaves plenty of scope for further enquiry. However, oxygen levels were not manipulated in the initial IR CRISPR screen, so validation of this result is unlikely to depend on such a role for HERC4, implying that any involvement in hypoxia or reoxygenation pathways is in addition to the mechanism underlying the initial result.

4.5 - Metabolism

Of the miscellaneous mechanisms included in the Radiosensitivity R of Radiobiology, the themes of metabolism and ER stress were the most relevant. Mitochondrial activity was assessed by the extent of resazurin reduction, but the only notable difference demonstrated was that Clone 2 had greater activity per cell, consistent with its cells being larger than those of other clones or the wildtype population, as determined by phase microscopy. Accordingly, the difference was lost when resazurin reduction was normalised to confluency instead of cell count. However, the main metabolic shift associated with both tumorigenesis and radioresistance is an increase in glycolysis, which would not have been detected by this method if not accompanied by a drop in the oxidative stages of respiration. A Seahorse ATP assay would be better suited to analysing both overall respiratory activity and the relative contributions of glycolysis and oxidative phosphorylation. More targeted analysis of glucose consumption, expression of glycolysis pathway components, or lactate production would also provide more certainty as indicators of the extent of the Warburg effect. Several proteins involved in glucose metabolism were differentially expressed in LN229 knockout clones, but these were primarily centred on the TCA cycle and carboxylic acid metabolism and were inconsistent in their direction of change following HERC4 knockout, suggesting that the differences may be particular to the clones, not their genetic alteration. Proximity labelling data contained very few terms related to glucose metabolism. Pathway analysis of the interactor dataset returned 2 glycolysis-related terms plus “aerobic respiration”, so HERC4 involvement in the Warburg effect cannot be completely discounted, but lipid metabolism was a more consistent reference for metabolic terms. This is not inconsistent with the references to mitochondria highlighting apoptotic and cell death mechanisms, rather than respiratory ones, since lipid signalling often contributes to these pathways. While this gives little support to a hypothetical role of HERC4 in respiratory substrate and pathway selection, it fits well with the earlier proposal that HERC4 may influence cell cycle exit towards cell death or senescence.

4.6 - ER stress

The other notable pathway in this category is that of ER stress, which is known to increase radiosensitivity, likely by increasing cell death signalling so that cells are closer to the threshold required to effect this process. All 3 analysis methods highlighted ER stress, unfolded protein response, and ERAD terms for interactors, and pathway analysis highlighted ERAD and ER stress for substrates too. Protein folding and ER activity were also common themes by pathway analysis and GSEA of both datasets, but all 5 themes were notably absent from the total proteome data, suggesting that any involvement of HERC4 in these processes is directed at a downstream outcome, not simply ER function.

4.7 - Reactive oxygen species

ROS provide a third radiosensitising mechanism, and there were relevant terms in both mass spectrometry experiments, but it was not a frequently observed theme. However, in light of the reasonably abundant mitochondria-related terms that focus on mitophagy and apoptosis, ROS generation and protection against their deleterious effects warrants further exploration. ROS availability has been shown to be essential for HIF-1-mediated upregulation of SERPINE1 [Zhang et al., 2023], connecting this topic to the tentative hypoxia links in the mass spectrometry data, and it might also prove relevant to investigation of any role HERC4 might play in DNA damage.

4.8 - Immune responses

The last of the 6 Rs of Radiobiology is reactivation of the immune system, and this was considered only in the mass spectrometry experiments. Antigen presentation was a particularly common theme in both total proteome and proximity labelling data, especially if the innate immune system equivalent (damage- or pathogen-associated molecular pattern recognition) is also considered. A role in antigen presentation could be particularly pertinent to glioblastoma treatment, since it is renowned as an immunologically cold tumour. This protects it from

immunotherapies and can be counteracted by treatments that increase display of neoantigens [Ma et al., 2022]. T-cell activation assays or profiling the repertoire of antigens presented, for example, would allow this putative role to be investigated further. Altering these pathways would allow HERC4 to influence radiosensitivity *in vivo* by modifying the strength of immune cell-mediated tumour recognition, but their intercellular effects are unlikely to have contributed to the result of the IR CRISPR screen given its *in vitro* setting. There were, however, several terms referencing cytokine production, which could affect tumour cells as well as those in the immune system. For example, IL-6 treatment increases the radioresistance of oral squamous cell carcinoma cells grown and irradiated *in vitro*, and radioresistant oesophageal cancer cells have been shown to increase the resistance of co-culture relatively radiosensitive cells through IL-6 secretion [Matsuoka et al., 2016; Xie et al., 2023]. In the context of the wider immune response, cytokine repertoires influence the types of cells recruited and the phenotypes they adopt, and the mass spectrometry analyses highlighted several terms related to T helper cell differentiation, suggesting another possible role for HERC4 in tumour- or IR-induced immune responses. Further exploration of this should involve characterisation of the HERC4-HAUS1 interaction proposed by the mass spectrometry data, alongside its influence on immune signalling, since HAUS1 has been implicated in immune cell infiltration in various cancer types (references in Chapter 3).

4.9 - References

Drissi, R.; Wu, J.; Hu, Y.; Bockhold, C. and Dome, J.S. (2011) Telomere Shortening Alters the Kinetics of the DNA Damage Response After Ionizing Radiation in Human Cells *Cancer Prevention Research (Philadelphia)* 4(12):1973-1981

Ge, S.X.; Jung, D. and Yao, R. (2020) ShinyGo: a Graphical Gene-Set Enrichment Tool for Animals and Plants *Bioinformatics* 36(8):2628-2629

Latre, L.; Tusell, L.; Martin, M.; Miró, R.; Egozcue, J.; Blasco, M.A. and Genescà, A. (2003) Shortened Telomeres Join to DNA Breaks Interfering with Their Correct Repair *Experimental Cell Research* 287(2):282-288

Ma, R.; Rei, M.; Woodhouse, I.; Ferris, K.; Kirschner, S.; Chandran, A.; Gileadi, U.; Chen, J.L.; Pinho, M.P.; Ariosa-Morejon, Y.; Kriaucionis, S.; Ternette, N.; Koohy, H.; Ansorge, O.; Ogg, G.; Plaha, P. and Cerundolo, V. (2022) Decitabine Increases Neoantigen and Cancer Testis Antigen Expression to Enhance T-Cell-Mediated Toxicity Against Glioblastoma *Neuro-Oncology* 24(12):2093-2106

Matsuoka, Y.; Nakayama, H.; Yoshida, R.; Hirosue, A.; Nagata, M.; Tanaka, T.; Kawahara, K.; Sakata, J.; Arita, H.; Nakashima, H.; Shinriki, S.; Fukuma, D.; Ogi, H.; Hiraki, A.; Shinohara, M.; Toya, R. and Murakami, R. (2016) IL-6 Controls Resistance to Radiation by Suppressing Oxidative Stress via the Nrf2-Antioxidant Pathway in Oral Squamous Cell Carcinoma *British Journal of Cancer* 115:1234-1244

Mirjolet, C.; Boidot, R.; Saliques, S.; Ghiringhelli, F.; Maingon, P. and Créhange, G. (2015) The Role of Telomeres in Predicting Individual Radiosensitivity of Patients with Cancer in the Era of Personalized Radiotherapy *Cancer Treatment Reviews* 41(4):354-360

Olivieri, M.; Cho, T.; Álvarez-Quilón, A.; Li, K.; Schellenberg, M.J.; Zimmermann, M.; Hustedt, N.; Rossi, S.E.; Adam, S.; Melo, H.; Heijink, A.M.; Sastre-Moreno, G.; Moatti, N.; Szilard, R.K.; McEwan, A.; Ling, A.K.; Serrano-Benitez, A.; Ubhi, T.; Feng, Su.; Pawling, J.; Delgado-Sainz, I.; Ferguson, M.W.; Dennis, J.W.; Brown, G.W.; Cortés-Ledesma, F.; Williams, R.S.; Martin, A.; Xu, D. and Durocher, D. (2020) A Genetic Map of the Response to DNA Damage in Human Cells *Cell* 182(2):481-496

Rembiałkowska, N.; Sędzik, M.; Kisielewska, M.; Łuniewska, W.; Sebastianka, K.; Molik, K.; Skinderowicz, K.; Kuźnicki, J.; Tunikowska, J. and Kulbacka, J. (2025) Telomere Maintenance and DNA Repair: A Bidirectional Relationship in Cancer Biology and Therapy *Cancers* 17(14):2284

Snijders, K.E.; Cooper, J.D.; Vallier, L. and Bertero, A. (2019) Conditional Gene Knockout in Human Cells with Inducible CRISPR/Cas9 *Methods in Molecular Biology* 1961:185-209

Sun, H.J.; Peng, M.H.; Feng, Z.Y.; Fu, H. and Liu, X.W. (2026) HERC4 Downregulates KRT19 to Promote Lung Adenocarcinoma, Migration, Invasion and EMT *Translational Oncology* 63:102593

Sun, T.; Geng, S.; Ru, Q. and Zheng, Y. (2025) METTL3 and HERC4: Elevated Expression and Impact on Hepatocellular Carcinoma Progression *Cancer Biotherapy and Radiopharmaceuticals* 40(3):173-184

Wei, M.; Zhang, Y.L.; Chen, L.; Cai, C.X. and Wang, H.D. (2016) RNA Interference of HERC4 Inhibits Proliferation, Apoptosis and Migration of Cervical Cancer Hela Cells *Journal of Southern Medical University* 37(2):232-237

Xie, C.; Chen, X.; Chen, Y.; Wang, X.; Zuo, J.; Zheng, A.; Luo, Z.; Cheng, X.; Zhong, S.; Jiang, J.; Du, J.; Zhao, Y.; Jiang, P.; Zhang, W.; Chen, D.; Pan, H.; Shen, L.; Zhu, B.; Zhou, Q.; Xu, Y. and Tang, K.F. (2023) Mutual Communication Between Radiosensitive and Radioresistant Esophageal Cancer Cells Modulates Their Radiosensitivity *Cell Death and Disease* 14:846

Zhang, L.; Cao, Y.; Guo, X.; Wang, X.; Han, X.; Kanwore, K.; Hong, X.; Zhou, H. and Gao, D. (2023) Hypoxia-Induced ROS Aggravate Tumor Progression Through HIF-1α-SERPINE1 Signaling in Glioblastoma *Journal of Zhejian University. Science. B.* 24(1):32-49

Zhang, Z.; Tong, J.; Tang, X.; Juan, J.; Cao, B.; Hurren, R.; Chen, G.; Taylor, P.; Xu, X.; Shi, C.X.; Du, J.; Hou, J.; Wang, G.; Wu, D.; Stewart, A.K.; Schimmer, A.D.; Moran, M.F. and Mao, X. (2016) The Ubiquitin Ligase HERC4 Mediates c-Maf Ubiquitination and Delays the Growth of Multiple Myeloma Xenografts in Nude Mice *Blood* 127(13):1676-1686

Zhu, Q.; Yang, X. and Lv, Y. (2024) HERC4 Modulates Ovarian Cancer Cell Proliferation by Regulating SMO-Elicited Hedgehog Signaling *Biochimica et Biophysica Acta - General Subjects* 1868(4):130557

5 - Conclusion and Future Directions

The data presented here is at best inconclusive with regards to the hypothesis that HERC4 is a radiosensitiser. There was no clear phenotypic evidence of HERC4 loss altering characteristics typically associated with radiosensitivity, but nor did the results categorically refute the hypothesis, and the mass spectrometry data in particular highlighted several relevant pathways whose components either interact with HERC4 or are differentially expressed when it is removed. Overall, this set of experiments provides justification for further investigation of HERC4 in the context of IR responses. Key to this would be repetition of the proliferation and colony formation assays presented here with a knockout population (instead of clones) and clear positive controls to confirm the sensitivity of these assays. Should HERC4 prove to be involved in radiosensitivity, cell cycle work should be extended to include changes in distribution after treatment and the probability of cells undergoing mitosis or entering senescence. Analysis of the extent to which HERC4 knockout cells rely on glycolysis, compared to their wildtype equivalents, might also prove valuable, and protocols such as T-cell activation assays or enzyme-linked immunosorbent assays to characterise cytokine repertoires with and without HERC4 expression might reveal a role for the ligase in a whole-organism setting.

In pursuing the role of HERC4, in radiosensitivity or other contexts, it would be valuable to consider the limitations of the approaches taken here, particularly the use of knockout cell lines in a disease already shown to delete the chromosome on which HERC4 is found. Glioblastoma already shows loss of Chromosome 10 compared to the average ploidy of its cells, which could indicate that the remaining copies of the genes on this chromosome are essential, hence their retention, or that they are of little importance altogether, hence the loss of the other copies. In light of the data presented here, it seems probable that HERC4 falls into the second category and that overexpression models might yield more substantial phenotypic results. Similarly, the knockout cells may have compensated for HERC4 loss during continued culture, so repeating

the irradiated proliferation assay with siRNA-mediated or inducible HERC4 knockdown may provide the validation of the initial CRISPR screen that has so far remained elusive. This would also eliminate the ambiguity of clonal differences, ensuring that any observed changes are likely attributable solely to HERC4 levels.

A second improvement would be to increase the challenge to the cells in each experiment. No change in cell cycle activity under normal conditions does not necessarily rule out a change in cell cycle activity after irradiation, for example. This could be extended to additional factors such as hypoxia or generation of double knockouts to include genes that might display synthetic lethality with HERC4. Just as the knockout clones here may have adjusted to the loss of HERC4, so too might cells have evolved to use the other, very similar HERC proteins in place of HERC4, regardless of its availability, so these would be one group of candidates for synthetic lethality work. In addition, Álvarez-Quilón et al. identified HERC4 in a synthetic lethality screen with the *APEX2* gene [2020]. APE2, the protein product of this gene, is a nuclease that can process the 3' end of DNA breaks when the phosphate group binding to both the 2' and 3' carbon of the deoxyribose moiety, a modification that otherwise stalls repair, suggesting that HERC4 may have a complementary function in DNA damage pathways [Álvarez-Quilón et al., 2020]. The addition of hypoxic conditions throughout irradiation experiments would increase the clinical relevance of the conclusions, given the importance of oxygen levels in radiosensitivity and their tendency in glioblastoma to be below normal physiological, much less atmospheric values. 1% oxygen would conform with much of the literature, although values as low as 0.1% would be relevant [Musah-Eroje & Watson, 2019; Evans et al., 2004; Beppu et al., 2002; Chédeville & Madureira, 2021].

Perhaps the strongest conclusion that can be drawn from this project is that although HERC4 showed great potential as a radiosensitiser, the data collected to date does not reflect this promise. A more comprehensive investigation of HERC4 activity in different contexts, such as hypoxia (0.1-1% oxygen) or synthetic lethality backgrounds, may better characterise its function in IR sensitivity or other cellular mechanisms.

5.1 – References

Álvarez-Quilón, A.; Wojtaszek, J.L.; Mathieu, M.C.; Patel, T.; Appel, C.D.; Hustedt, N.; Rossi, S.E.; Wallace, B.D.; Setiaputra, D.; Adam, S.; Ohashi, Y.; Melo, H.; Cho, T.; Gervais, C.; Muñoz, I.M.; Grazzini, E.; Young, J.T.F.; Rouse, J.; Zinda, M.; Williams, R.S. and Durocher, D. (2020) Endogenous DNA 3' Blocks Are Vulnerabilities for BRCA1 and BRCA2 Deficiency and Are Reversed by the APE2 Nuclease *Molecular Cell* 78(6):1152-1165

Beppu, T.; Kamada, K.; Yoshida, Y.; Arai, H.; Ogasawara, K. and Ogawa, A. (2002) Change of Oxygen Pressure in Glioblastoma Tissue under Various Conditions *Journal of Neuro-Oncology* 58:47-52

Chédeville, A.L. and Madureira, P.A. (2021) The Role of Hypoxia in Glioblastoma Radiotherapy Resistance *Cancers* 13(3):542

Evans, S.M.; Judy, K.D.; Dunphy, I.; Jenkins, W.T.; Hwang, W.T.; Nelson, P.T.; Lustig, R.A.; Jenkins, K.; Magarelli, D.P.; Hahn, S.A.; Collins, R.A.; Grady, M.S. and Koch, C.J. (2004) Hypoxia is Important in the Biology and Aggression of Human Brain Tumours *Clinical Cancer Research* 10(24):8177-8184

Musah-Eroje, A. and Watson, S. (2019) Adaptive Changes of Glioblastoma Cells Following Exposure to Hypoxic (1% Oxygen) Tumour Microenvironment *Internation Journal of Molecular Sciences* 20(9):2091

Appendix 1 – catalogue numbers

4% PFA	Santa Cruz Biotechnology	sc-281692
X2 PageRuler™ Prestained Protein	Fisher Scientific	11812124
Acetic acid	Sigma Aldrich	695084
Agarose	Thermo Scientific	17850
Alexa fluor 647 azide	Thermo Scientific	A10277
BCA Reagent A	Thermo Scientifc	23221
BCA Reagent B (also used as $CuSO_4$ stock)	Thermo Scientifc	23224
Benzonase	EMD Millipore	70664-4
Biotin	Sigma-Aldrich	B4501
Bleomycin	Alfa Aesar	J60727.MA
BSA	Sigma-Aldrich	A7906-100G
Camptothecin	MP Biomedicals	0215973225
CellBind 6-well plates	Corning	3335
Coomassie R-250	Thermo Scientific	20278
Countess cell counting slides	Life Technologies	C10283
Crystal violet	Alfa Aesar	B21932
DAPI	Merck Life Science	D9542
DMEM	Merck Life Science	D6429
DMSO	MP Biomedicals	0219605580
Doxycycline	MP Biomedicals	0219895505
EDTA	Fisher Scientific	443885J
EdU	Thermo Scientific	A10044
Ethanol	Sigma-Aldrich	32221
Ethidium bromide	Sigma	E1510
Etoposide	Alfa Aesar	A1971-APE
FBS	Merck Life Science	F9665
GeneRuler 1 kb DNA ladder	Thermo Scientific	SM0312
Glycine	Sigma-Aldrich	G8898
HEPES	Thermo Scientific	15630080
siRNA (HERC4)	Santa Cruz Biotechnology	sc-90436
siRNA (Control B)	Santa Cruz Biotechnology	sc-44230
Laemmli buffer (4X)	Invitrogen	NP0007
Lowry Reagent A	Bio-Rad Laboratories	5000113
Lowry Reagent B	Bio-Rad Laboratories	5000114
Lowry Reagent S	Bio-Rad Laboratories	5000115
Methanol	Fisher Scientific	10674862
MG132	Merck Life Science	C2211
Milk powder	Sigma-Aldrich	70166
20X MOPS buffer	Life Technologies	NP000102
NuPAGE™ Bis-Tris 4-12% gels	Life Technologies	WG1403BOX NW04125BOX
Olaparib	Stratech Scientific	A4154-APE
PBS	Life Technologies	10010056
Pen-Strep	Gibco	15140122
Ponceau S	MP Biomedicals	151942
Protease inhibitors	Thermo Scientific Sigma	78441 P8340

PVDF	Sigma-Aldrich	IPFL00010
Q5 high-fidelity 2X master mix	New England Biolabs	M0492S
Qiagen DNeasy Blood and Tissue kit	Qiagen	69504
QIAquick Gel Extraction kit	Qiagen	28706
Resazurin	Sigma	R7017
SDS	Santa Cruz Biotechnology	sc-24950
siRNA transfection medium	Santa Cruz Biotechnology	sc-36868
siRNA transfection reagent	Santa Cruz Biotechnology	sc-29528
Sodium ascorbate	Sigma	A7631
Sodium azide	G Biosciences	786-299
Sodium chloride	Sigma-Aldrich	S7653
Sodium fluoride	Sigma-Aldrich	S7920
Strep-tactin® Sepharose beads	Fisher Scientific	12723074
SuperSignal™ West Pico PLUS Chemiluminescent Substrate	Thermo Scientific	34578
TAE buffer	Thermo Scientific	B49
Tris base	Sigma-Aldrich	93352
Tris-HCl, pH 8	Thermo Scientific	J62726.K2
Triton™ X-100	Sigma-Aldrich	T8787
Trypan blue (from Vi-CELL™ reagent pack)	Beckman Coulter	383198
TrypLE	Life Technologies	12604013
Tween	Fisher Scientific	10485733
Zeocin	Invitrogen	46-0509

Appendix 2 – buffers

RIPA buffer: 50 mM Tris-HCl, pH 8; 150 mM NaCl, 1% Triton, 1 mM EDTA, 1% SDS

HNN buffer: 50 mM HEPES, 50 mM NaF, pH8; 0.15 M NaCl

Transfer buffer: 25 mM Tris base, 192 mM glycine, 10% methanol